



**EVALUATION OF DE-ICING CHEMICAL AND  
MOISTURE MASS TRANSFER IN FREEZING  
SOILS**

A thesis submitted for the degree of Doctor of Philosophy

By

Assel Sarsembayeva

College of Engineering, Design and Physical Sciences

Brunel University London

March 2017

## **Abstract**

Highway subsoils in cold countries are subject to increased thermal conductivity, disruption of natural moisture circulation as well as dynamic loading and application of de-icing chemicals in the winter months. In this work, the moisture mass transfer in a state of vapour flow and the de-icing chemical migration were considered during unidirectional freezing. The moisture mass transfer in a gaseous state was previously widely neglected in the exploration of frost heave.

To conduct freeze-thaw cycles with increased lengths of soil samples and a modified slow freezing technique, an environmental chamber of nine samples capacity was designed. Supplying the non-saline samples with either 11 or 22 g/L sodium chloride solution signified chemical mass transport over the sample length and a significant change in temperature-moisture distribution when compared to deionised water supplied test results.

The presented conceptual model with vapour mass transfer was based on the thermodynamic equilibrium of vapour density with temperature change and the phase transition to ice during thermal energy withdrawal. Compared to the widely used coupled heat-mass models, the vapour flow based model clearly explained the driving forces and presented a much easier algorithm for calculation. The de-icing chemical displacement was explained as the migration of the dissolved ions together with hygroscopic water transport, which in turn, was driven by cryosuction forces. The reduction of hydraulic conductivity during the secondary salinisation with sodium chloride was caused by chemical osmosis, which tended to equalise the solute concentration in pore water over the sample length.

The research outcomes indicate a significant contribution to the future perspectives on frost heave modelling and prognosis. Further research could extend this work by inclusion of the vapour mass transfer in quantitative analysis for soil freezing. The effect of secondary salinisation should be also foreseen in the long term prognosis for highway subsoils exploitation.

# List of Content

<b>Abstract</b> .....	ii
<b>List of Content</b> .....	iii
<b>Acknowledgments</b> .....	vi
<b>Abbreviations and glossary</b> .....	vii
<b>Nomenclature</b> .....	viii
<b>List of Figures</b> .....	xiii
<b>List of Tables</b> .....	xvii
<b>1 INTRODUCTION</b>	
1.1 Area of study.....	3
1.2 Research aims .....	5
1.3 Research methods.....	6
1.4 Limitations.....	7
1.5 Practical value.....	7
1.6 The structure of the work.....	8
<b>2 LITERATURE REVIEW</b>	
2.1 Temperature distribution in the highway subsoils during the winter period.....	9
2.2 The site area.....	11
2.3 Accepted knowledge in frost heave study.....	12
2.3.1 Frost heave testing methods .....	13
2.3.2 Moisture redistribution during the soil freezing and existing approaches to frost heave study.....	21
2.3.3 Current understanding of frost heave.....	29
2.4 Study of deformation-strength characteristics of soils during freeze-thaw cycles .....	33
2.4.1 Engineering properties of soils during thaw weakening.....	35
2.5 Deposition and distribution of de-icing chemicals in the road soil area.....	37
2.5.1 Impact of the salinity on the freezing point.....	39

2.5.2 Chemical and moisture mass transfer in the soil induced by temperature gradient.....	44
2.5.3 Variations of engineering properties in subsoils affected by de-icing chemicals and freeze-thaw cycles.....	46
2.6 Phase equilibrium and the Gibbs' phase rule.....	48
2.6.1 Phase equilibrium for a single substance system. Clausius-Clayperon equation.....	49
2.7 Summary .....	50
<b>3 METHODS AND MATERIALS</b>	
3.1 Introduction.....	53
3.2 Environmental chamber design.....	54
3.3 Soil modelling and classification tests.....	59
3.4 Sample preparation.....	67
3.5 Initial density parameters of the soil samples before testing.....	70
3.6 Freeze-thaw cycles procedure.....	74
3.6.1 Temperature monitoring of the freeze-thaw cycles.....	76
3.6.2 Vertical linear movement observation during the test.....	76
3.6.3 Post freeze-thaw sampling and testing.....	76
3.6.4 Determination of the moisture content.....	78
3.6.5 Obtaining the sodium chloride content.....	79
3.6.6 Tests for mechanical and thermo- hydro- dynamical properties...	81
3.7 Summary.....	85
<b>4 RESULTS</b>	
4.1 Introduction.....	87
4.2 Temperature field change.....	87
4.3 Moisture content change.....	93
4.4 Frost heave observations .....	104
4.5 Chemical content change .....	110
4.6 Density and structure change.....	115
4.7 Strength-deformation properties change.....	120
4.7.1 Cohesion and angle of internal friction change.....	121
4.7.2 California bearing ratio.....	122
4.7.3 Permeability and compressibility characteristics.....	123
4.8 Heat conductivity.....	126

4.9 Summary.....	127
<b>5 DISCUSSIONS</b>	
5.1 Discussion of the obtained results.....	130
5.2 Evaluation of moisture mass transfer theory.....	132
5.2.1 Energy balance during vapour mass transfer.....	138
5.2.2. Moisture mass transfer in the highway subsoils application.....	139
5.3 Calculation of the vapour mass transfer in unsaturated freezing soils.....	141
5.3.1 The algorithm of vapour mass transfer calculations in unsaturated soils.....	141
5.3.2 Calculation of vapour flow on example of Test 3 .....	144
5.3.3 Limitations of the mass transfer calculation in the above example.....	151
5.3.4 Interaction and comparison with other approaches to vapour mass transport calculation.....	152
5.4 Chemical mass transfer.....	153
5.5 Summary.....	156
<b>6 CONCLUSIONS AND RECOMMENDATIONS FOR FUTURE WORK</b>	
6.1 General overview.....	159
6.2 Key findings of the work.....	161
6.3 Key limitations.....	161
6.4 Further research.....	162
6.4.1 Moisture mass transfer perspectives.....	162
6.4.2 De-icing chemicals mass transfer perspectives.....	163
<b>LIST OF REFERENCES</b> .....	164
<b>Appendix A</b> .....	176
<b>Appendix B</b> .....	181
<b>Appendix C</b> .....	206
<b>Appendix D</b> .....	208
<b>Appendix E</b> .....	211

## **Acknowledgements**

This work has been undertaken in recognition of the greatness of God and admiration of the harmony in nature and universe, in general. My inspiration in science was constantly supported by my principal supervisor Dr Philip Collins, whose personal accomplishments and experience in the field are reputable. I express my deepest gratitude to him for supporting me in challenges, for his professionalism and tolerance in scientific approaches, as well as empathy in hard times and cherished understanding when I had to suspend my studies at short notice in order to raise a family.

I would like to acknowledge the industrial consultant in this project, Mr Peter Reading, for supporting me with his vast knowledge and experience in geotechnics. My grateful thanks to Mr Neil Macfadyen, who puts his technical support at the forefront of his work and who shared my enthusiasm from the beginning until the end of the project. My great appreciation goes to all of the technician team: Mr Simon Le Geyt, Mr Paul Szadorski, Mr Gerald Edwardson, Mr Richard Parish and Mr Malcolm Austin. And special thanks to Mr Costas Xanthos for his technical support with the refrigeration and temperature control equipment.

The academics in the Civil Engineering department are also greatly acknowledged, in particular, my second supervisor Dr Xiangming Zhou, Professor John Bull, Dr Nuhu Braimah, Dr Evina Katsou, Professor Mizi Fan, among others, for being open to discussing any issues that arose during my study journey.

I want to thank my sponsor, the JSC “Centre for International Programs “Bolashak” and the government of Kazakhstan for providing with me a full scholarship to gain a PhD. Thanks for those who believed and waited for me in my motherland.

Special thanks to those who have read or are going to review my work to make it better and therefore, more meaningful.

And at last, but not the least I would like to express my profound thanks to my husband Bayandy, our children, our parents and our new baby, born during my PhD studies and to all the colleagues and friends, whose names I wasn't able to note here.

## Abbreviations and glossary

ASTM Standard	American Society for Testing and Materials Standard
BS	British Standard
GERI	Geotechnical Research Engineering Institute
CBR	California bearing ratio
Freezing front	The advancing boundary between frozen and unfrozen parts of soil
Frost shattering	The mechanical disintegration of soil because of pressure of freezing water
Frozen fringe	The zone between the warmest isotherms where the ice lens are growing and ice lens exist
MP	Migration potential
meq	Millequivalents
‘Open’ system	The system with free access to water supply
RTD	Resistance temperature detector
SFCC	Soil freezing characteristics curve
SP	Segregation potential
TDR	Time domain reflectometer
COMSOL	Multiphysics software

## Nomenclature

$A_{air\ voids}$	Cumulative air voids channel cross section
$A_w$	Cumulative water channel cross section
$a_w$	Water activity
$C$	Specific heat
$c$	Cohesion
$C_u$	Coefficient of uniformity
$C_c$	Coefficient of curvature
$C_R$	Load ring calibration
$c_v$	Coefficient of consolidation
$e$	Voids ratio
$e_0$	Initial voids ratio
$D$	Soil water diffusivity
$D_a$	Vapour diffusivity in soil
$D_{sal}$	Degree of salinity
$E_W$	equivalent weight
$f$	Intensive degrees of freedom
$G_s$	Specific gravity
$\Delta G_c$	Free energy variation in crystal
$\Delta G_s$	Free energy variation in surface
$\Delta G_v$	Free energy variation in volume
$\Delta G_{i-l}$	Free energy of the ice-liquid interface
$g$	Gravitational acceleration
$H$	Height of the specimen
$H_r$	Relative humidity



$h_p$	Pore water pressure head
$k$	Coefficient of permeability
$k_f$	Hydraulic conductivity in freezing soils
$k_h$	Unsaturated hydraulic conductivity
$k_l$	Hydraulic conductivity
$k_{lh}$	Isothermal hydraulic conductivity for liquid water
$k_{lT}$	Thermal hydraulic conductivity for liquid water
$k_{vh}$	Isothermal vapour conductivity
$k_{vT}$	Thermal vapour conductivity
$L$	Latent heat
$L_{wi}$	Latent heat of freezing
$L_0$	Initial length of the specimen
$L_S$	Linear shrinkage
$L_D$	length of oven-dry specimen
$M$	Molar mass
$m_v$	Coefficient of compressibility
$m_i$	Mass of ice
$m_{vapour}$	Mass of vapour
$m_s$	Mass of solids
$m_w$	Mass of water
$N_A$	Avogadro's number
$n$	Porosity
$n_{max}$	Maximum porosity
$P$	Pressure
$P_w$	Water pressure

$P_{sw}$	Saturated vapour pressure over water
$P_{si}$	Saturated vapour pressure over ice
$PI$	Plasticity index
$p$	number of phases
$R$	Universal gas constant
$Q$	Heat
$Q_s$	Heat loss for solids
$Q_w$	Heat loss for water
$Q_i$	Heat loss for ice
$Q_v$	Heat loss for vapour
$q_v$	Flux density of the vapour part
$q_l$	Flux density of the liquid part
$R$	Reading of the loading ring
$r_0$	Initial radius
$SP_o$	Segregation potential at zero overburden pressure
$S_r$	Degree of saturation
$t$	Time
$t_f$	Time to failure
$T_0$	Absolut temperature
$T$	Temperature
$T_f$	Freezing temperature
$T_f^*$	Freezing point of pure water at the absolute temperature
$T_{f-sal.soil}$	Freezing temperature of saline soil
$\Delta T_{f-solution}$	Freezing temperature suppression caused by the solution
$T_s$	Segregation freezing temperature

$T_{pw}$	Pore water freezing temperature
$\Delta T$	Temperature change
$\Delta T_{\gamma}$	Temperature depression, when free energy of the ice-liquid interface is counteracted
$V$	Volume of the soil
$V_a$	Volume of air
$V_i$	Volume of ice
$V_v$	Volume of voids
$V_{vapour}$	Volume of vapour
$V_w$	Volume of water
$V_{M,w}$	Molar volume of water
$V_{M,i}$	Molar volume of ice crystal
$\bar{V}$	Specific volume
$\alpha_G$	Gardener's exponent for the moisture characteristics
$\alpha_w$	Gardener's multiplier for the moisture characteristics
$\beta$	Gardener's exponent multiplier for hydraulic conductivity
$\epsilon$	Gardener's empirical factor
$\pi$	Pi number = 3.14159
$\pi_l$	Osmotic pressure of liquid water
$v$	Speed of flow, velocity
$W$	Moisture content
$W_p$	Plasticity limit
$\Omega$	Volume of a single ice crystal molecule
$\varphi$	Angle of internal friction
$\gamma_{sf}$	Surface tension between ice embryo and water
$\sigma_n$	Normal stress

$\tau$	Shear stress
$\rho$	Bulk density
$\rho_{dry}$	Dry density
$\rho_s$	Particle density
$\rho_{vs}$	Saturated vapour density
$\rho_{vapour}$	Vapour density
$\rho_w$	Density of water
$\theta$	The volumetric sum of unfrozen water and ice
$\theta_i$	Volumetric ice content
$\theta_l$	Volumetric liquid (unfrozen) water content
$\theta_{tW}$	Total volumetric water content
$\lambda$	Thermal conductivity
$\mu$	Molar mass of vapour
$\eta$	Enhancement factor, coefficient (Cass <i>et al.</i> , 1984)
$\Delta g_v$	Decrease in volume of a single molecule of the Gibbs free energy
$M_W$	Molecular weight of water

## List of Figures

- Figure 1.1 – Mass transfer sketch under a highway pavement
- Figure 1.2 – Map of Kazakhstan from [www.geographicguide.com](http://www.geographicguide.com)
- Figure 2.1 – Monthly frost depth across of road section after Chunpeng *et al.* (2010)
- Figure 2.2 – Seasonal freezing depth of soils in Kazakhstan. (Teltayev and Suppes, 2014)
- Figure 2.3 - Piston cylinder model of ice growth and “capillary theory” after Everett (1961)
- Figure 2.4 – The phenomenon of ‘regelation’ after O'Neill and Miller (1985)
- Figure 2.5 – Regelation of ice within the soils
- Figure 2.6 – A proportionality between ice lens formation and temperature gradient according to ‘segregation potential’ theory
- Figure 2.7 – ‘Porosity rate function’ according to thermodynamic model after Michalowski and Zhu (2006)
- Figure 2.8 - A mathematical model FROSTB to simulate a coupled heat-moisture transfer
- Figure 2.9 - Accumulation of de-icing chemicals in the road soil area
- Figure 2.10 – Stability diagram for the most common de-icing chemicals in Kazakhstan highway exploitation (Sarsembayeva, 2005)
- Figure 2.11 – Temperature boundary between firmly frozen and plastic frozen soils according to: 1- initial freezing temperature; 2 – unfrozen water content; 3 – modulus of deformation; cohesion (by Aksenov, 2008).
- Figure 2.12– Phase diagram for a single substance system according to Gibbs’ phase equilibrium
- Figure 3.1 - Environmental chamber for freeze-thaw cycles with nine soil sample capacity
- Figure 3.2 – Environmental chamber for freeze-thaw cycles with a capacity of nine 1m length soil columns
- Figure 3.3 - Experimental settings for 50 cm length samples with variable density

Figure 3.4 – Preparation of the experiment: a - perforation of a plastic mold for thermocouple insertion, b – surcharge sliding inside the chilling collar, c – cooling system control manifolds.

Figure 3.5 – Temperature control unit with a glycol reservoir

Figure 3.6 – Particle size analysis of the sand part in the modelled soils, determined by dry sieving

Figure 3.7 - Dry density – moisture content curves for sandy clay with 2.5 kg rammer compaction test

Figure 3.8 – Direct shear result for 17.2 % sandy clay soils with particle size less than 2 mm

Figure 3.9 - California bearing ratio test on the triaxial machine rig

Figure 3.10 – Load-penetration curve for CBR pertaining to a moisture content of  $W=17.6\%$

Figure 3.11–CBR - moisture content relationship curve

Figure 3.12 - Specific gravity test by small pycnometer method: a – filled with a sample and de-ionised water, b – in a desiccation camera

Figure 3.13 – Linear shrinkage

Figure 3.14 – Sample preparation

Figure 3.15 – Testing for leaks before assembling the mould

Figure 3.16 – Sample weighing

Figure 3.17 – Example of the cooling unit set temperature and the corresponding temperature on the soil surface in Test 2

Figure 3.18 – Soil column positioning over the sampling immediately after the removing from the environmental chamber

Figure 3.19 – Sampling after freeze-thaw cycles

Figure 3.20 – Preparation of the remaining sample material for ultrasound testing

Figure 3.21 – Sampling for moisture content determination

Figure 3.22 – Oven dried samples were used for chemical content determination

Figure 3.23 – Electrical conductivity meter for sodium chloride measurements

Figure 3.24 - Calibration chart for the sodium chloride - electrical conductivity relation

Figure 3.25 - Log-pressure –voids ratio curve for the soil sample with freeze-thaw cycle parameters

- Figure 3.26 – Triaxial test
- Figure 3.27 – Mohr circles for a sandy clay soil sample
- Figure 3.28 – Thermal conductivity measurements
- Figure 4.1 – Temperature field distribution in Test 1 for the example of column #1
- Figure 4.2 - Temperature field distribution in Test 2 for the example of column #1
- Figure 4.3 – Temperature distribution in columns #1 and #9 in Test 3, with de-ionised water introduced to the column bases of various soil densities
- Figure 4.4 - Temperature distribution in columns #1 and #9 in Test 4, with 11,000 mg/litre sodium chloride solution supply and various soil densities
- Figure 4.5 – Temperature field distribution in Test 5 with 22,000 mg/litre sodium chloride supply and various soil densities
- Figure 4.6 – Moisture intake during the Test 1 (a) and Test 2 (b) with maximum dry density and 1 m soil sample height
- Figure 4.7 – Moisture redistribution by the sample length in Test 1 with a deionised water supply: a- in columns #1-3 after two freeze-thaw cycles, b – in all nine columns terminated after: first freezing cycle (columns #7-9), first thawed cycle (columns #4-6) and second freezing cycle (columns #1-3)
- Figure 4.8 – Moisture distribution in Test 2 after two freeze-thaw cycles with 11,000mg/litre de-icing chemicals solution supply
- Figure 4.9 - Moisture intake during the freeze-thaw cycles of the soils in Test 3 with deionised water supply and various densities, as presented in Table 4.2
- Figure 4.10 - Moisture intake during the freeze-thaw cycles of the soils in Test 4 with 11,000 mg-litre sodium chloride solution supply and various densities
- Figure 4.11 - Moisture distribution for Test 3 after two freeze-thaw cycles using samples with deionised water supply
- Figure 4.12 – Moisture distribution for Test 4 after two freeze-thaw cycles using samples with various dry density and 11,000mg/litre sodium chloride solution supply
- Figure 4.13 – Moisture intake during the freeze-thaw cycles in Test 5
- Figure 4.14 – Dry density - moisture content redistribution relationships after the freeze-thaw cycles in Test 5
- Figure 4.15 – Moisture redistribution in soil samples after freeze-thaw cycles in Test

Figure 4.16 – Relationship between the surface temperature and frost heave by time, h: a – for samples supplied with deionised water in Test 1; and b - for samples supplied at the base with 11,000 mg/litre NaCl solution in Test 2 (Sarsembayeva and Collins, 2017)

Figure 4.17 - Relation between the frost heave and temperature 5 cm distance from the soil surface in Test 1. The black line represents the average polynomial relationship

Figure 4.18 – Frost heave in the samples with varied density in Test 3

Figure 4.19 – Frost heave in the samples with varied density in Test 4

Figure 4.20 – Frost heave in the samples with varied density, supplied with 22 g/L NaCl solution, in Test 5

Figure 4.21 – The percentage of sodium chloride to oven dried soil by weight, on average, after freeze-thaw cycles for Test 2

Figure 4.22 – Sodium chloride ratio in variable density samples after Test 4, in % to oven dried soil mass

Figure 4.23 – Sodium chloride ratio in variable density samples after Test 5, in % to oven dried soil mass

Figure 4.24 - Dry density distribution through the length of the sample after Test 1

Figure 4.25 - Dry density distribution through the length of the sample after Test 2

Figure 4.26 – General density change in the samples with variable dry density for Test 3

Figure 4.27 – Dry density change during the freeze-thaw cycles in Test 4

Figure 4.28 – Horizontal stratified structure of ice lenses at the top 10 cm layer of the sample supplied by deionised water for Test 1 (the sample is lying on its side)

Figure 4.29 – Structure of the soil sample after freeze-thaw cycles supplied with 11,000 mg/l sodium chloride solution in Test 4 (the sample is lying on its side)

Figure 4.30 – Triaxial test for the soil sample with  $W=19.5\%$

Figure 4.31 – Dry density-moisture relation according to the CBR test

Figure 4.32 – Effect of disturbance of the soil samples with different moisture content

Figure 4.33 – Heat conductivity results within the moisture content range

Figure 4.34 – Dry density-heat conductivity relation



Figure 5.1 – Soil sample structure at the different stages of freezing: a - unfrozen equilibrium; b - beginning of the freezing of ice lenses segregation; c - further freezing of frost penetration; and d - frost shattering and frost heave stage

Figure 5.2 – Ice lenses formation in the freezing soil

Figure 5.3 – Energy balance of moisture mass transfer during freezing in soils

Figure 5.4 – Dynamic load effect on moisture mass transport under the highways: a - static condition; b – application of the short-term dynamic load and c – frost heave thickness expansion

Figure 5.5 – Algorithm of vapour mass transfer calculation

Figure 5.6 – Cumulative air voids channel cross section

Figure 5.7 – Calculation of the vapour rate passing through the cumulative air voids channel in the mould section over time  $t$

Figure 5.8 - Conceptual model of chemical mass transfer

Figure 5.9 – Mass transfer and impact strength diagram

## List of Tables

- Table 1.1 – Climatic parameters for the cold season in Astana and Almaty cities according to SNIP RK2.04-01-2010 (2010)
- Table 1.2 – Technical classification of highways in Kazakhstan according to SNIP RK 3.03-09-2006 (2006)
- Table 2.1 – Examples of freeze-thaw cyclical testing in laboratory conditions
- Table 2.2 – De-icing chemicals commonly used on highways
- Table 2.3 – Soil types by the degree of salinity  $D_{sal}$  according to Russian Federation and Kazakhstan standards for construction
- Table 2.4 – Freezing temperature for the saline soils by Yarkin (1990)
- Table 3.1 – Environmental chamber equipped elements
- Table 3.2 – California Bearing Ratio test results when moisture content is  $W=17.6\%$
- Table 3.3 – Initial soil characteristics and soil tests following the procedures in BS1377-1:1990
- Table 3.4 – Soils characteristics before freeze-thaw cycles in test 1
- Table 3.5 – Soil characteristics before freeze-thaw cycles in test 2
- Table 3.6 – Variable density distribution within the soil samples in test 3
- Table 3.7 – Variable density distribution within the soil samples in test 4
- Table 3.8 – Variable density distribution within the soil samples in test 5
- Table 3.9 – Freeze-thaw test characteristics
- Table 3.10 – Oedometer consolidation test results for the sample with a moisture content of 17.2%
- Table 3.11 – Triaxial test results
- Table 4.1 - Temperature distribution within the soil samples in Test 3
- Table 4.2 – Moisture-density change in Test 5
- Table 4.3 – Calculation of sodium chloride content: the average for nine columns after freeze-thaw cycles for Test 2
- Table 4.4 – Sodium chloride content for column #1 with density  $\rho=1.51 \text{ g/cm}^3$  (Test 4 with 11 g/L NaCl supply from the base)
- Table 4.5 – Moisture –density change before and after the freeze-thaw cycles with deionised water supply in Test 1
- Table 4.6 - Moisture –density change before and after the freeze-thaw cycles with 11,000 mg/litre sodium chloride feeding in Test 2

Table 4.7 – Triaxial test results

Table 4.8 – California bearing ratio

Table 4.9 – Oedometer consolidation test results of the sample with  $W=20.82\%$

Table 4.10 – Oedometer consolidation test results of the sample with  $W=23.25\%$

Table 5.1 – Soil sample parameters before and after the freeze-thaw cycles with deionised water supply: Test 3

Table 5.2 – Calculation of soil parameters at 590-614 h time interval of the Test 3 for the example of sample #1

Table 5.3a - Calculation of the moisture mass transfer in the soils for the example of Test 3, sample #1

Table 5.3b - Calculation of the moisture mass transfer in the soils for the example of Test 3, sample #1(continuation of Table 5.3a)

Table 5.4 – Calculation of soil parameters for the 590-614 h time interval for Test 3 for the example of sample #5

Table 5.5a - Calculation of the moisture mass transfer in the soils for the example of Test 3, sample #5

Table 5.5b - Calculation of the moisture mass transfer in the soils for the example of Test 3, sample #5 (continuation of Table 5.5a)

# 1 INTRODUCTION

This thesis explores the processes of moisture and de-icing chemical mass transfer in soils during unidirectional downward freezing. These transfers have been simulated in the laboratory via cyclical freeze-thaw tests with non-saline soil samples that were supplied with sodium chloride solution from the base, in order to simulate the highway subsoils that have been treated with de-icing chemicals during the winter period.

Global warming during the last few decades has led to serious changes in the moisture-temperature regime of the soils at both high and low latitudes (Bockheim *et al.*, 2013; Dioliuti *et al.*, 2011; Harris *et al.*, 2007). In areas characterised by low winter temperatures, this has an influence on the seasonal migration of moisture within the active layers (Murton *et al.*, 2016; Matsuoka 2011). In particular, global warming entails a change in water-ice ratio over the world and as a consequence enlarges the zones with flooded or saturated soils. Another important problem is the impact of ice-water phase change on the bearing capacity of foundations and the engineering properties of subsoils forming the foundations of constructed infrastructure, such as highways and bridges (Harris *et al.*, 2007). According to the literature (Szymanski *et al.*, 2015; Horvath *et al.*, 2005) the patterned soil structures in polar area, which have been affected with the strong freezing, caused the forming of the contraction cracks and cryoturbation of loose and initially unsorted soft sediment soils, while the moisture transport contributed the formation of ice lenses and ice needles.

To provide a safe level of friction on highway pavements in the cold countries of the northern hemisphere, like Canada, Norway, Finland, Russia, Kazakhstan, Mongolia and others, a range of different methods of ice removal are used: de-icing chemicals, sand and other abrasive materials application, heating etc. Of these, the application of de-icing chemicals is the most effective and cheap method. De-icing chemicals are used in liquid, solid dry and pre-wetted forms. Natural reserves of magnesium chloride hexahydrate, halite or industrial wastes can be used as raw materials for the de-icing chemicals. Liquid chlorides, such as highly concentrated solutions of sodium calcium, and magnesium chloride are suitable for this purpose. The salts can be used both individually or mixed together in various proportions. The best effect is achieved when using “saturated solutions”, i.e. the solutions that are close to the maximum possible concentration for the particular salt (Kiyalbayev, 2003; Lee, 2017). As a result of their hygroscopic nature, ions of de-icing chemicals attract solvent molecules and create new chemical compounds - hydrates. The resulting solution has a lower freezing point than water. This benefits the

pavement surface ice removal, but significantly changes the chemical composition of the environment.

Wide application of de-icing chemicals leads to their long term accumulation in roadside areas, noticeably changing the chemical content of the ground water (Blomqvist and Johansson, 1999; Lundmark and Olofsson, 2007) and potentially affecting the hydro-thermal regime of the roadside soils. Moreover, it might change the designed engineering characteristics of the subsoils under the highways due to gradual salinisation and depression of the freezing point of the ground water (Yarkin, 1990; Arenson and Segó, 2006; Torrance and Schellekens, 2006; Sinitsyn and Løset, 2011). It is hypothesised that de-icing chemicals migrate with ground water towards the freezing front, which in turns might cause a secondary salinisation (Figure 1.1). Due to the higher density of pavement materials and their high thermal conductivity, the temperature field under highways significantly differs from the natural unpaved ground (Arenson *et al.*, 2006; Han Chunpeng *et al.*, 2010; Junwei *et al.*, 2013).

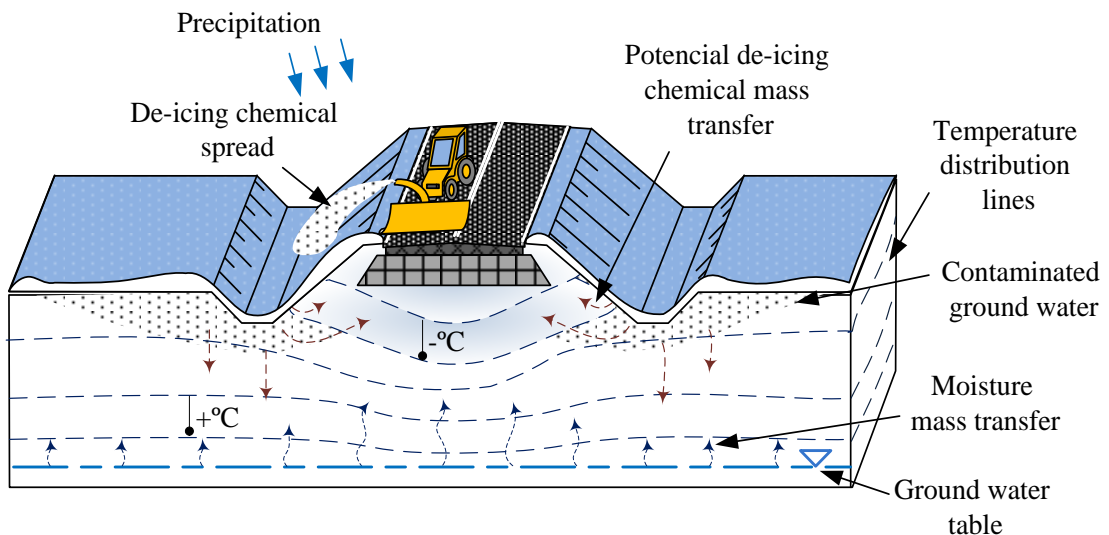


Figure 1.1 – Mass transfer sketch under a highway pavement

After infiltrating the soils, the solution of de-icing chemicals decreases the freezing temperature of the ground water, depending on the concentration. The part of the ground water which has been contaminated with de-icing chemicals remains unfrozen until it reaches the eutectic cooling temperature. At the same time, the part of the soil located right under the pavement remains in the previous non-saline condition, assuming that pavements are impermeable or have very low hydraulic conductivity. Moreover, the temperature depression under the road is much greater than the roadside soils due to increased thermal conductivity of the denser layers. It is hypothesised that moisture mass

transfer occurs laterally from the salinised soils and also vertically from the water table to the top. The de-icing chemicals mass transfer may occur through chemical potential as well as with moisture mass transfer due to the temperature gradient. Gradual salinisation of the soil under the highway pavement might significantly change the temperature profile and bearing capacity not only in winter months, but also in spring time, during the thaw weakening period.

Previous similar studies have had contradictory results regarding chemical migration under temperature drop (Brouchkov, 2000; Bing and He, 2008; Vidyapin and Cheverev, 2008). Consequently, it was decided to explore the process of de-icing chemicals' mass transfer by an experimental study with freeze-thaw cycles. Great interest has also been generated regarding moisture migration within unsaturated and saturated freezing soils at temperatures below zero degrees and the role of vapour in them. Constructed highway subsoils are often designed to have limited drainage and hence, the soils beneath the roads might be in an unsaturated condition. Vapour convection has been widely underestimated in geotechnics up to the present day and its calculation has been generally neglected in moisture transfer modelling. To fill this gap in knowledge it was decided to conduct a cyclical freeze-thaw experiment with a modified testing method, which was adapted to allow for the close examination of mass transfer in the freezing subsoils of highways.

### 1.1 Area of study

In this work, the laboratory based approach has been approximated to Kazakhstan's climatic and geological conditions. According to the local standard (SNIP RK 2.04-01-2010, 2010), the Astana region is classified as being in III Climate zone with a minimum day temperature of -41 °C in winter and a record low temperature of -52 °C. The annual average humidity is 59% (Table 1.1).

Table 1.1 – Climatic parameters for the cold season in Astana and Almaty cities, according to SNIP RK2.04-01-2010 (2010).

City	Minimum day temperature °C	Average temperature for the coldest 5 days in a year, °C	Average humidity for the most cold month, %	Precipitation during the November – March period, mm	Maximum wind speed from the average by rumbas in January, m/s
Astana	-41	-36	80	88	5.9
Almaty	-30	-23	75	213	1.3



Figure 1.2 – Map of Kazakhstan from [www.geographicguide.com](http://www.geographicguide.com)

With a relatively low density of railways and waterways, Kazakhstan has an extensive highway network and in many regions this is the only means of transportation. The total length of the highways is up to 128 thousand kilometres. Of these, 85,214 km are public roads, including 23,011 km - republican; and 62,203 km - of local importance, with the remainder being departmental and municipal roads. 80% of all freight transport is made via highway links, which is severely complicated by the weather conditions in winter time. The roads in Kazakhstan are divided into five categories, based on road network capacity and traffic congestion (Table 1.2). Highway design in this setting includes calculation of the thickness of flexible pavements considering the deformation criteria: elastic deflection, resistance to the shear and stretching during the layers bending (SNIP RK 3.03-09-2006, 2006). In order to provide the flow capacity and safety requirements on the urban highways and countryside roads in the winter period, around 30-35,000 m<sup>3</sup> of de-icing chemicals and sand mix are used annually in Kazakhstan (KazPravda, 2016). There is not much information about the contamination of roadside soils from the de-icing chemicals application in the local area and hence, the chemical concentration of ground water was assessed based on a world-wide literature review.

Sodium chloride concentration of 11- 22 g/L was accepted as the level of contamination, corresponding to those values observed by Pedersen *et al.* (2000) at 1—10 metres distance from the road.

Table 1.2 – Technical classification of highways in Kazakhstan according to SNIP RK 3.03-09-2006 (2006)

Road category	Estimated road network capacity		National economic and administrative purposes of the road
	Converted to a car, unit/day	In transport units per day	
I-a	More than 14000	More than 9000	Highways of international and republican importance
I-b	More than 14000	More than 7000	Highways of international and republican importance (Not assigned to category I-a)
II	6000 - 14000	3000 - 7000	Highways of international and republican importance (Not assigned to category I-a or I-b)
III	2000 - 6000	1000 - 3000	Highways of republican or local significance (Not assigned to category I-b or II)
IV	200 - 2000	100 - 1000	Highways of republican or local significance (Not assigned to category I-b, II or III)
V	Less than 200	Less than 100	Highways of republican or local significance (Not assigned to category III or IV)

The geotechnical characteristics of soil samples were synthesised in a manner similar to Astana soils, according to the geological report of Karaganda GIIZ (Tulebekova *et al.*, 2012; Zhussupbekov *et al.*, 2016).

## 1.2 Research aims

The research detailed here examines the heat and mass transfer in highway subsoils during the winter period by simulating soil samples with freeze-thaw cycles and simultaneously supplying them with deionised water or brine from the base. To contribute a deep understanding of moisture/chemical mass transfer within the soils induced by temperature gradient, the following subtasks were pursued:

1. Design of a laboratory test to simulate the freezing rate of highway subsoils in conditions close to natural ones.
2. Testing the hypothesis that chemical mass transfer occurs, when induced by temperature gradient and possibly because of the chemical osmosis phenomena.



3. Observation of the moisture mass transfer when supplied with deionised water or sodium chloride solution. Establishing the correlation with temperature distribution in relation to the soil sample length, frost heave and mass transfer with time, when supplied with deionised water or a de-icing chemical solution from the base.
4. A study of moisture mass transfer and the role of vapour flow in it. Assessing the driving forces in unidirectional freezing of soils and consideration of the calculation.

Means of further ideas that have been tested in the research are:

- ❖ The use a significantly modified freeze-thaw cycle method developed using increased soil sample lengths and a slow freezing technique in an environmental chamber.
- ❖ Understanding of the relation between freezing rate, frost heave, chemical and moisture mass transfer observed and analysed in various density soils over the sample length.
- ❖ The development of a conceptual model for frost heave, using the differential calculation approaches including the vapour mass transfer in unsaturated soils and the hygroscopic moisture mass transfer in saturated soils, where the vapour flow was dominant at temperatures below 0 °C. The driving force for the vapour flow was identified as a saturated vapour difference, reflecting the actual soil temperature and sample length.
- ❖ The presentation of an example vapour mass transfer calculation based on the cyclical freezing and thawing test results of soil samples compacted to different dry densities. The proposed calculation method was based on thermodynamic equilibrium principals and excluded the usage of adapted or empirical parameters.
- ❖ An understanding of the process of chemical mass transfer induced by temperature gradient and chemical potential, observed in all samples with various densities and length. The driving force for the chemical mass transfer is explained as being due to the liquid water migration and diffusion phenomena.

### **1.3 Research methods**

For this study a combined approach, including a literature review, field data from previous studies in Kazakhstan, laboratory testing and theoretical data and analytical techniques were used. The laboratory testing included the design of an environmental

chamber for freeze-thaw cycles, slow unidirectional freezing techniques, the supply of deionised water or de-icing chemical solution from the base along with observation of the temperature, moisture, frost heave and chemical content. It also included classification tests before freezing as well as tests for engineering characteristics and chemical content change after it. In the theoretical study, the empirical observations were developed from the first principles of phase equilibrium, the theory of thermodynamics, mass transfer, and chemical osmosis. For further data analyses and graph charts production, Excel, Visio and Matlab tools were used. Some parameters required supplemental calibration and conversion to be understood correctly.

#### **1.4 Limitations**

Because of the impossibility of transporting representative samples from Kazakhstan, the geotechnical characteristics were synthesised using remoulded soil samples. The simplification of natural conditions, included: step freezing and day-night fluctuations of the temperature, free access of all the soil samples to the base water supply and the limitation of the freezing and thawing cycles to two, according to the recommendations of the majority of existing standards for freeze-thaw testing (BS 812-124:2009, ASTM D 5918-06, GOST 28622-2012 and BS EN 64 1997-2:2007, section 5, 5.5.10 Frost susceptibility). The mentioned limitations did not diminish the presented method and had very little effect on the obtained results.

#### **1.5 Practical value**

The practical value of the research includes the calculation algorithm for moisture mass transfer in unsaturated soils and possible prediction using a quantity simulation method. The improved conceptual model for ice lens formation gives a good understanding of mass transfer processes in the freezing soils and also has a good correlation with vapour transfer theory in unsaturated soils. The established chemical mass transfer induced by temperature gradient implies the secondary salinisation of highway subsoils during pavement treatment with de-icing chemicals. A key recommendation for highway engineers is that the transfer of de-icing chemicals into the road sub-structure, and the potential impact on the road's mechanical performance should be considered at the design stage. That is, the anticipated contamination of the ground with de-icing chemicals and change of bearing capacity over time necessitate having

foresight regarding these at the design stage. The main findings of the work have been presented at major geotechnical conferences, namely, IAEG-AGMEP 2014, Turin, Italy and XVI ECMGE 2015, Edinburgh, UK as well as having been published in the “Cold Regions Sciences and Technology” Journal, 2017 (Sarsembayeva and Collins, 2015; Sarsembayeva and Collins, 2017).

## **1.6 The structure of the work**

The thesis includes this introduction, six main chapters, a list of references and four appendices. The introduction has presented the relevance of the study, background information of the research area, research objectives and has provided some conceptions about the proposed outcomes and their practical value.

In Chapter 2, the classical understanding of freezing process in soils is explained and there is reflection on the current situation in the field. The main research methods and approaches are also reviewed.

In Chapter 3 the research method and applied techniques for the current study are considered in detail. The initial classification test results and the setting of parameters prior to the main freeze-thaw cyclical tests are also specified in this chapter.

Chapter 4 presents the main results and outcomes from five long-term freeze-thaw cycling tests, including some after-test observations of engineering properties and chemical content measurement results.

In Chapter 5, the conceptual model of frost heave and moisture mass transfer is developed into the vapour flow model for unsaturated soils and supplemental hygroscopic water transfer in both saturated-unsaturated conditions. The driving force and chemical mass transfer mechanism are also explained.

In Chapter 6, the main outcomes of the study are summarised and areas for further research are identified, including some detailed advice regarding laboratory observation techniques.

Some classification and supplementary tests results for the particle size analysis, direct shear test, electrical conductivity measurements and the temperature distribution recordings are presented in appendices A - D. Finally, copies of the published paper and conference proceedings are attached in Appendix E.

## 2 LITERATURE REVIEW

### 2.1 Temperature distribution in the highway subsoils during the winter period

Changes in temperature throughout the day and during the year in road constructions cause volume change, which can lead to thermal stress and crack formation. Highway pavement layers have to withstand dynamic loads and are usually made from dense materials, which have increased thermal conductivity. Due to this, the freezing rate in the highway structure is more rapid and the temperature distribution is lower than that of adjacent roadside soils (Simonsen *et al.*, 1997; Chungpeng *et al.*, 2010; Vasilenko, 2011). A number of field studies have examined the temperature field distribution and the pore moisture change during freeze-thaw cycles (Figure 2.1). In recent years, there has been an increasing amount of literature based on mathematical modelling of the temperature field in highway subsoils (Arenson *et al.*, 2006; Abzhalimov, 2007; Junwei *et al.*, 2013).

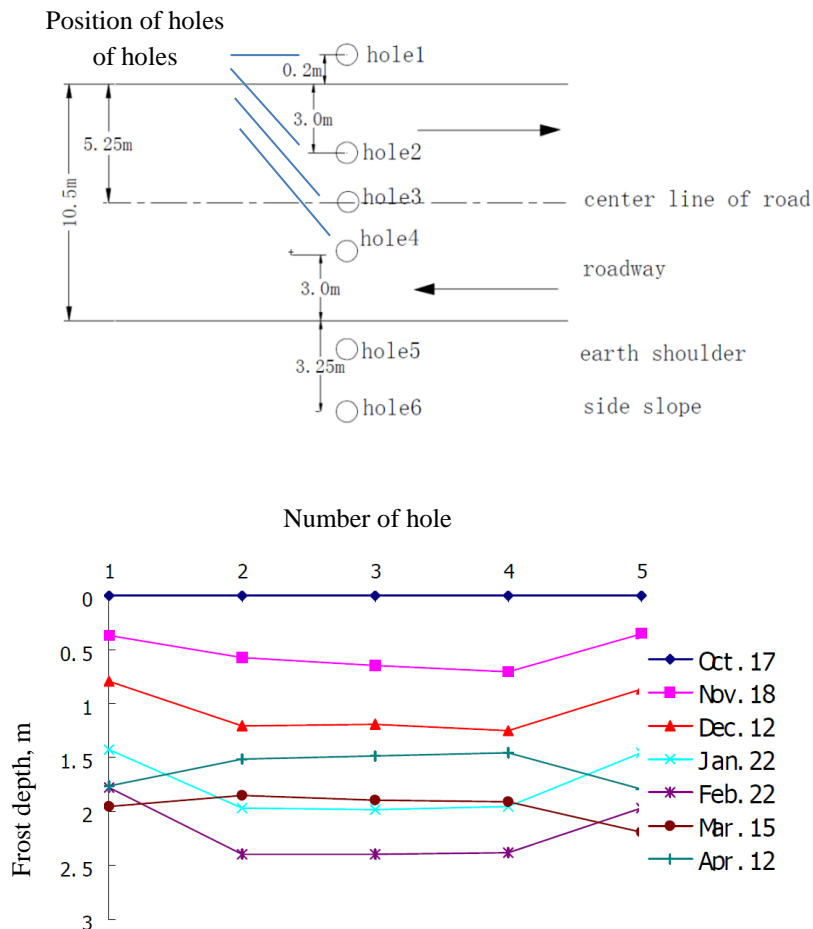


Figure 2.1 – Monthly frost depth across of road section after Chungpeng *et al.* (2010).

The application of a convective heat flow model on samples of highway subsoils and the effect of predicted warming were presented by Arenson *et al.* (2006). To simulate the air convection in highway subsoils the temperature in a 5m long tube was cyclically varied between -8 and +5 °C for 3.75 cycles, with each cycle lasting 15 days. According to Arenson *et al.* (2006), the convectational heat fluxes can lead to significant change of the temperature field in highway subsoils and must be accounted for in road design and in the prognosis of subsoils' temperature distribution. The numerical modelling of a 8m profile length of highway subsoils was considered to estimate and quantify the possible temperature field change within 5 years, such as from global warming.

Junwei *et al.* (2013) produced a mathematical model of ground temperature in the superficial layer of highways and the annual temperatures in embankments using a finite element method. Both concrete and asphalt pavements were considered in the model. The study was based on the field monitoring results of the G214 highway in a high permafrost area in China. They found that the maximum influencing depth for temperature fields under the embankments was over 8 m (Junwei *et al.*, 2013). Abzhalimov (2007) used a finite element method to define the negative temperature distribution over the soil depth in the Omsk region, Siberia, Russia, in winter time. The numerical data were based on the long-term observations and calculated for clayey loam soils covered with a snow layer or cleaned of snow surfaces, i.e. highways, airfields and urban areas. In his work, the author noted that temperature observations for over 50 years in Omsk Oblast exhibited enormous difference regarding the average depth of 0°C penetration in the soil: from 1.1m under snow-covered areas to 2.95m under a snow-free surface. This was explained by specific factor effects: moisture content, ground water table, thickness of snow cover, relief, among others.

Overall these studies highlighted the importance of an individual approach to the study of temperature distribution in each region, depending on the climatic zone and the thickness of the pavements. The fluctuation of freezing depth in Figure 2.1 shows the importance of considering a sufficiently long soil sample during laboratory and field temperature observation as shorter/shallower samples are likely to provide an incomplete picture of ground thermal change under natural conditions.

## **2.2 The site area**

For the current work, the context was the Astana region in Kazakhstan, which experiences a great complexity of climate conditions and highway use during the winter period (Figure 2.2). The territory of Kazakhstan covers 2.7 M square kilometres, which is equivalent to the size of Western Europe, with a variety of continental climatic conditions. Its geographical location is referred to as the Central part of Eurasia, bordering on Russia, China, Uzbekistan, Turkmenistan and the Caspian Sea. It is also the largest landlocked country in the world. A very high proportion of the terrain of Kazakhstan comprises the Kazakh Steppe, one of the largest dry regions in the world.

The climate of Kazakhstan is a moderate continental one, with dry hot summers and severe cold and windy winters. The temperature of the northern and central part of the country in winter time often reaches to  $-35\text{ }^{\circ}\text{C}$  and sometimes even  $-40\text{ }^{\circ}\text{C}$ . The snow cover period in the youngest and the second coldest capital of the world, Astana, lasts for 111 days, while the number of days with negative temperatures is up to 160-170 days. According to the local standard for building climatology (SNIP RK 2.04-01-2010, 2010), the Astana region is classified as a III Climate zone with a minimum day temperature of  $-41\text{ }^{\circ}\text{C}$  in winter and a record low temperature  $-52\text{ }^{\circ}\text{C}$ . The average annual humidity is 59% (SNIP RK 2.04-01-2010, 2010).

In 2014, a new map of seasonal freezing of the soils was announced (Teltayev and Suppes, 2014). According to this map, the seasonal freezing layer reaches 2.05 m depth in Astana, while the freezing point of the subsoils under the highways is 2.15 m from the pavement surface. Observation of the temperature distribution during the freeze-thaw period on the local highways in Kazakhstan was performed by Teltayev and the research group around him (Sakanov, 2007; Teltayev and Suppes, 2014).

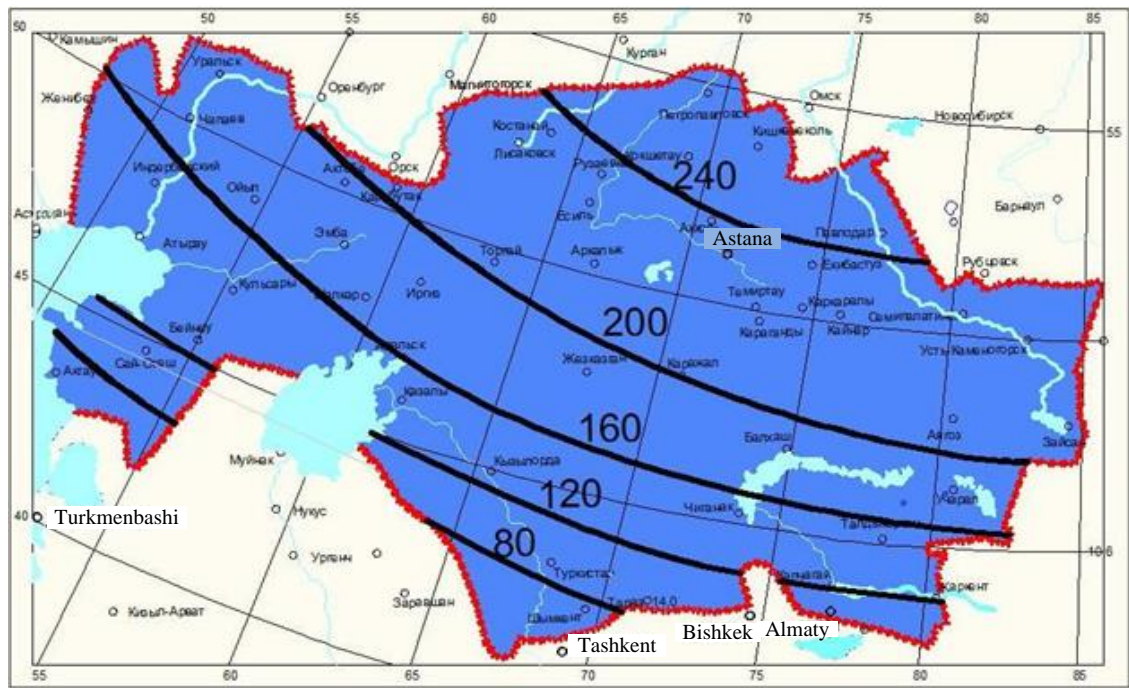


Figure 2.2 – Seasonal freezing depth of soils in Kazakhstan (Teltayev and Suppes, 2014)

In terms of the geological characteristics of the Astana soils pertaining to the Kazakh Steppe, these are underlain by ancient sedimentary rocks, including claystone, siltstone and sandstone. As a result of chemical and physical weathering, an irregular layer of residual soil mantle has been formed, which exhibits a progressive downwards transition to the weathered rock (Tulebekova *et al.*, 2012). The general vertical sequence of the soils consists of about 1m of alluvium over fine-grained residual soils on the left embankment of the Esil River, the newly built business centre of Astana city. The ground water level is typically relatively high, being between 0.5-0.8m of the existing ground surface (Tulebekova *et al.*, 2012; Zhussupbekov *et al.*, 2016).

### 2.3 Accepted knowledge in frost heave study

Thermal gradients induce changes in the moisture distribution with in the soil and as a result of this, it changes the dry unit weight, strength and deformation parameters (Oztas and Fayetorbay, 2003; Wang *et al.*, 2007; Qi *et al.*, 2008; Wang *et al.*, 2012; Wu *et al.*, 2015). Significant frost heaving deformations occur in Siberia, Canada, the USA, Norway, Mongolia and other cold weather countries (Kværnø and Øygarden, 2006; Matsumura *et al.*, 2012). Classical conditioning of ice formation in the freezing soils was first demonstrated experimentally in the early 1900s (Taber, 1930; Hoekstra, 1966;

Hoekstra, 1969a; Miller, 1972). Taber's 1930 freezing experiment on clay soil was in an 'open system', allowing the samples to be supplied from an external moisture source. Taber, in his tests, noted that an amount of water was left unfrozen, whilst in sands it was completely freezing and gave some early explanations for ice segregation and water transfer during frost heaving. In particular, he found that frost heave in clays exceeded the heaving in sands and that the ice lens formation starts from the top downwards, though during slow freezing the ice layers tends to be thicker (Taber, 1930). Since then, in almost all laboratory research into the freeze-thaw cycles of soils, the influence on the geotechnical properties, such as void ratio, hydraulic permeability and resilient modulus, has been noted.

### **2.3.1 Frost heave testing methods**

There are a number of established standard methods for assessing soil susceptibility to freeze-thaw: BS 812-124:2009, ASTM D 5918-06, GOST 28622-2012 and BS EN 64 1997-2:2007, section 5, 5.5.10 Frost susceptibility.

- Russia - GOST 28622-2012. According to the test procedure, the diameter of the soil samples is equal to 100mm and the length is 150mm. The number of the samples in a chamber is four. The top of the sample is to be cooled down to -4 °C, and the bottom plate with base water supply has to be held at +2 °C. The test is terminated when the freezing front level reaches 100mm of the length.
- British Standards - BS 812-124:2009. In this process, nine samples of unbound aggregates can be tested simultaneously for freeze-thaw cycles in an environmental chamber. The typical specimen diameter is 102mm, the length is 152mm and the temperature set for the freezing is -17 °C, while the lower end is maintained at +4 °C for the basal water supply. The duration of the test is 96 hours.
- Eurocode - 7BS EN 1997-2:2007, section 5, 5.5.10. It is recommended to test for frost heave by freeze-thaw cycles and thaw weakening by a CBR test. However no detailed recommendations regarding the test procedure are given here.
- USA - ASTM D 5918-06. This standard test method for frost heave and the thaw weakening susceptibility of soils is used to test four samples at the time. Each specimen of 146mm diameter and 150mm in height is to be compacted and extruded to the testing mold, which consists of a basement plate and six acrylic



rings, each 25mm in length. The temperature sets, after a conditioning period, achieve -12 °C in the top plate and 0 °C in the base. The total duration of the two freeze-thaw cycles, including the conditioning time, is 120 hours.

These above mentioned standard methods typically with the exception of British Standard have sample lengths only up to 15cm and limited temperature sets, which often include immediate cooling to the predetermined temperature and a short time of test duration. The capacity of the environmental chamber mostly does not exceed four soil samples. The temperature sets in the top and a bottom temperature controlled plates in most methods are +3 °C and -3 °C. In BS 812-124:2009, the top plate is cooled to -17 °C, although the rapid freezing of soil sample to such a low temperature does not allow a sufficient time for mass and phase transfer to occur and therefore, might not adequately indicate the true potential frost heave capacity with a basal water supply.

The standard methods are more suitable for typical industrial applications, such as to compare the obtained characteristics of the sample with that of predetermined soil types. These methods also ensure technological uniformity of the test proceeding and thus it suits classification purposes. However, for research problems, such as this project's study of the de-icing chemical solution effect on highway subsoils, the existing standard approaches do not meet the scientific requirements. The limitation of the samples' lengths leads to an increased temperature gradient between the top and bottom plates' settings. They also complicate the observation of the temperature distribution over the soil sample length. Consequently, many scientists have tried to upgrade or develop their own environmental chambers/cells and freeze-thaw cycle techniques to study the thermodynamic and mechanical properties of soils during or after the freezing (Table 2.1).

Table 2.1 – Examples of freeze-thaw cyclical testing in laboratory conditions

Name and published year	Test settings and freezing techniques	Contribution to the knowledge
Hermansson (2004)	Over 50cm length undisturbed silt samples with a naturally saturated condition were tested in ‘open’ system with free water access. The temperature was controlled by computer in order to provide a constant downward freezing rate. Eight freeze-thaw cycles with over 72h duration were interrupted when the lowest part of the sample reached freezing temperature.	The limited capacity of water redistribution was noted during the soil freezing. The laboratory tests indicated that the frost heave rate is independent to heat extraction during the slow freezing with a constant frost penetration, while the field observations distinguished a constant frost heave rate during the prolonged freezing.
Konrad (2005)	Saturated fine-grained soils with sample height varying between 12 and 16cm, with diameter 10cm, were the subject of step-freezing and free access to water supply. The top plate was maintained at a constant temperature, generally between -3 and -4 °C and the temperature of the warm end was constant at a value ranging from +1.0 to +1.5 °C.	An improved approach of segregation potential (SP) calculation was presented. The obtained SP revealed a strong relation to the overburden pressure and soil index properties, especially with non-clays fines content. It was observed that the moisture content in the top layer was reduced to 4-6% at the beginning of ice lens segregation, most likely caused by the evaporation from the freezing top surface.

Table 2.1 continued

<p>Qi <i>et al.</i> (2008)</p>	<p>Remoulded loess samples with 10.1cm diameter and 15cm height were the subject of one freeze–thaw cycle. The downward freezing with constant temperature sets was maintained until frost heave ceased. The top plate was kept at from –2 to –20 °C, and the bottom end was +1 °C. After, the top cap was set at +20 °C and all samples were let to thaw.</p>	<p>A critical dry unit weight was detected, whereby the cohesion and pre-consolidation pressure would remain the same after the freeze-thaw cycle, if the original dry weight would be equal to its' critical value. In case of exceeding the critical dry unit weight before the freeze-thaw test the mechanical properties would be weakening and vice versa.</p>
<p>Vidyapin and Cheverev (2008)</p>	<p>Saline remoulded samples of 12cm height and 5cm in diameter were downward frozen and supplied with sodium chloride solution identical to pore water concentration. The top plate was held at a constant -2.5... -4 °C, and the bottom plate at +0.2... -0.5 °C.</p>	<p>Hydraulic conductivity for the saline samples in frozen and unfrozen states was observed. The chemical mass transfer along with moisture stimulated by temperature gradient has been established.</p>
<p>Bronfenbrener (2008)</p>	<p>A sample of 0.6cm height and 5.4cm in diameter was placed in an environmental chamber at -15 °C and insulated with polyurethane at the sides. The one dimensional heat flux was measured.</p>	<p>Developed a non-instantaneous kinetic model to predict the temperature and moisture (ice) distribution over the loamy soil sample.</p>

Table 2.1 continued

<p>Grigoryev and Shabarov (2012)</p>	<p>The freezing rate for clayey soil samples was varied from -0.5 °C to -12.5 °C for between 3-3.5h. After this the amount of unfrozen sample was determined by the calorimeter method.</p>	<p>The relationship of frozen and unfrozen water was observed with the calorimetry method. It was determined that 70% of water was frozen during the interval of 0 - 0.5 °C, the rest being moisture, apart from the hygroscopic and mineralised part, froze between -0.5 and -3.0 °C.</p> <p>The freezing rate had a significant effect on the frozen and unfrozen water relation. According to the obtained results, the retardation of ice segregation during the rapid freezing indicated the need for time for crystal lattice formation.</p>
<p>Nagare <i>et al.</i> (2012)</p>	<p>Large sized samples of 110cm length and 56cm diameter along with remolded samples from undisturbed peat, were placed into a split environmental chamber. The lower part was simulating the permafrost layer and held at -1.9 °C. Each sample was subjected to two freeze-thaw cycles mainly in the upper 65-75cm part. The first freezing period lasted for 47 days, followed by 75 days of thawing and 93 days for the second. The freezing was for 31 days to -5°C and -10 °C for the remaining 16 days.</p>	<p>During the freezing experiment a fully saturated active layer was observed on the top 10cm of the peat sample. Significant moisture redistribution within the sample caused a thick desiccated zone formation.</p> <p>Freezing of the sample in the saturated condition was accompanied with simultaneous evaporation of moisture, which caused a notable weight reduction. It was expected that conducted observations facilitate the numerical modelling of moisture mass transfer.</p>

Table 2.1 continued

<p>Lai <i>et al.</i> (2014)</p>	<p>Silty clay samples of 10cm and 20cm height with equal sized diameters were the subject of a long-term freezing experiment. The test duration was either 90 or 288h. The freezing temperature gradient was set to 0.31-0.65 °C/cm, with the upper plate cooled to -1.6, -5 °C. Initial moisture content of the sample ranged from 20.50 to 20.89%.</p>	<p>A coupled thermo-hydro-mechanical model was considered to study ice lens formation, the effect of the overburden pressure, the cooling temperature rate and its distribution in relation to the frost heave and mass transfer. Based on the experimental results, a mathematical model was proposed for various temperatures, porosity and a displacement in the vertical axis. Numerical simulation was implemented with COMSOL software. The research outcomes emphasised the importance of decreased temperature to produce a negative pore pressure, adjusted for the overburden pressure and temperature gradient fluctuation. It was noted that soil porosity change was usually followed by water mass transfer and that an unsaturated condition was established in the unfrozen zone due to the suction effect in the freezing zone.</p>
<p>Wu <i>et al.</i> (2015) The testing results after by Mizoguchi, M. (1990)</p>	<p>Four identical loamy samples of 20cm height and 8cm in diameter were cooled from the top to - 6 °C for 12, 24 and 50h.</p>	<p>A mathematical model was presented with coupled heat-water mass transfer for fully saturated soils, courtesy of experimental results by Mizoguchi (1990). The developed kinetic model was used to quantify the processes of ice crystal nucleation and growth control. The driving force for moisture migration was explained as a chemical potential gradient, which in turn depends on the temperature.</p>

Table 2.1 continued

Ming and Li (2015)	Tested the silty clay samples of 10cm height and 10.1cm diameter for unidirectional downward freezing by setting the top plate temperature to -2, -4 and -6 °C and the base plate to 3 °C for a 72 hour period.	An inverse relationship between the water influx and freezing rate was investigated for different water content samples. Based on the experimental results the coupled water and heat mass transfer model was presented.
Zhou <i>et al.</i> (2014)	Performed an upward freezing experiment for silty soil samples with various temperature boundaries set. The diameter of the samples was 10cm and the height was 5.3-5.5cm. The top plate was 3.3 °C, while the bottom plate was cooled down to -1.3 °C, first and lowered to -4.1 °C after. The test was run for 10h, 22h, 30h for different samples, and there was selective moisture supply control.	It was found that a small amount of pore water was discharged at the beginning of the freezing experiment and thereafter, the frost heave was delayed until replenished from the unfrozen soils.  Based on the experimental results, empirical formula of frost heave was presented.  Modelled and simulated with numerical analysis: temperature field distribution, unfrozen water content with temperature, frost heave and freezing rates relations.

Laboratory approaches benefit from better technical control and the ability to set the initial parameters of the soil sample, such as the temperature control plates and freezing rate, as well as being able to adjust these parameters during monitoring. In the laboratory based studies a cylindrical soil sample (Ming and Li, 2015; Konrad, 2005) is placed into the environmental chamber/cell and cooled down from one side of the sample and supplied with water from the other. The length of the samples mostly ranged from 15cm to 20cm or less (Lai *et al.*, 2014) and rarely longer (Hermansson, 2004; Nagare *et al.*, 2012). The number of cycles is usually two, although in studies for mechanical properties there might be more (Bi Guiquan, 2012; Bing and He, 2011). Individual testing models have been developed for exclusively saturated soils and eliminating the vapour phase (Wu, Lai and Zhang, 2015).

Some of the experiments were conducted in an adapted triaxial cell, which allows measuring pore pressure, the major principal stress  $\sigma_1$  in vertical axis and radial minor principal stress  $\sigma_3$  (Zhang *et al.*, 2013; Hazirbaba, Zhang and Hulsey, 2011; Sinitsyn and

Løset, 2011; Ishikawa *et al.*, 2010; Qi, Vermeer and Cheng, 2006; Cui and Zhang, 2015. Sinitsyn and Loset (2011) tested frozen saline silt under triaxial compression and at close to freezing temperatures, -3.9 °C and -2.4 °C (Sinitsyn and Løset, 2011). Conducting the freeze-thaw cycles in the triaxial cell allowed them to observe a relationship between the strain rate and freezing temperature. However, triaxial cell tests enable a contemporaneous mechanical loading of only one soil sample at a time. The size of the tested sample is also restricted by the size of the test cell.

Experimental data collected from the field might be more realistic, as it is obtained under natural environmental conditions, rather than laboratory observations. However, field data observations are typically complicated with technological challenges and difficulties with testing complexity, along with high costs. Benson and Othman (1993) performed in situ freeze-thaw tests with large soil samples buried in the field for a 60 day period. The diameter of their compacted clay samples was 29.8cm and the length 91.4cm. The hydraulic conductivity, measured after the test period, indicated increased values in the freezing zone and decreased below the freezing plane in the desiccation zone. Another out of laboratory freeze-thaw experiment was performed by Starke (1989) and cited in Qi, Vermeer and Cheng's (2006) review. Starke (1989) kept soil samples outdoors, and afterwards compared their properties with unfrozen soil samples. Unfortunately, such testing techniques are very difficult to reproduce and it is even more difficult to compare their results. One key limitation of field-based experiments is the potential influence of unexpected parameters and events.

Consequently, in order to provide better control and precise results in the freeze-thaw cycles observations, many studies have been conducted in laboratory conditions (Iushkov and Sergeev, 2015; Bing and Ma, 2011; Kværnø and Øygarden, 2006; Brouchkov, 2002). The increased sample length and bigger number of samples that can be tested simultaneously in the same freezing condition has facilitated laboratory experimental study and provided more detailed observations. In several works it was emphasised that slow freezing is a necessary condition to obtain the realistic unfrozen water ratio during the ice lens segregation (Grigoryev and Shabarov, 2012).

### 2.3.2 Moisture redistribution during the soil freezing and existing approaches to frost heave study

Formation of frost heave within freezing soil is necessarily accompanied with moisture redistribution and heat transfer. After introducing freezing tests with an ‘open system’, Taber (1930) ascertained that frost heave does not occur just because of the water expansion effect during the crystallization of ice, but also owing to the migration from the unfrozen part (i.e. water) towards the freezing fringe. Beskow (1935) in Henry's review (2000), working independently, noted that the freezing process in soils can be correlated with drying. He also explained moisture mass transfer by the negative pressure that is produced when the film water layer becomes thinner and so, the system replenishes it (Henry, 2000).

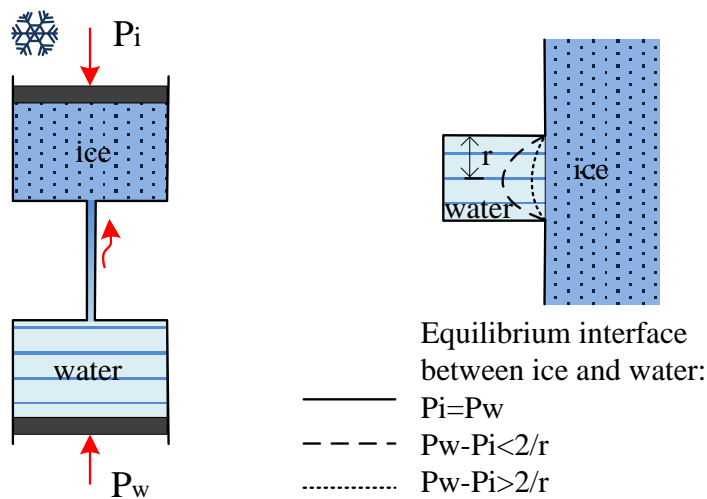


Figure 2.3 - Piston cylinder model of ice growth and “capillary theory”, after Everett (1961)

The first systematic study of moisture redistribution in frozen soils was presented as a ‘capillary theory’ by Everett (1961) and further developed by Penner (1967), Sutherland and Gaskin (1973) and Loch (1981). Everett demonstrated the freezing process using the example of two cylinders (Figure 2.3), positioned one above the other and connected with a tube. The freezing of the top cylinder led to ice formation in it and the drawing of water from the lower cylinder. Hence, it continues to equilibrate between the solid and liquid part  $P_i = P_w = P$ . He also explained that the maximum heaving pressure  $\frac{\partial A_r}{\partial V}$  is a function of pore size and interfacial energy between the ice and water. For the



hemispherical ice front in the pore channel the heaving pressure has an inverse relationship with the pore size radius  $\frac{\partial A_r}{\partial V} = \frac{2}{r}$ .

Hoekstra (1969) presented a relationship between water content and a distance from a cold plate and freezing time in unsaturated clay soils. He set a temperature gradient in the soil to be less than 0.2 °C/cm, so as to reduce the moisture transport in the unfrozen part caused by higher temperature gradients (Hoekstra, 1966) and obtained the relative water content during the “freeze drying” as a function of the dimensionless variable:  $\frac{x}{2\sqrt{D_0 t}}$

where,  $x$  - is the distance from the freezing front in cm.;  $D_0$  - soil water diffusivity at initial water content measured in cm/h;  $t$  - time in h.

According to Hoekstra's (1969) observations, the water content keeps relatively constant at the freezing front and with only 1% variation over 9h of experiment. The same results were obtained in Dirksen and Millers' (1966) experiment, where the moisture content changed by less than 2% over 41h at the freezing front. Hoekstra (1969b), cited in Loch's review (1981), demonstrated ice lens segregation behind the freezing fringe with successive experimental pictures, which showed progressive ice growth in a frozen part of a colloidal soil (Loch, 1981). Such a phenomenon could not be explained by capillary theory. Penner (1970) in his field observations, found that the excess force exerted by frost heave keeps increasing during a cold period, with the estimated frost suction being between 0.49 and 0.84 kg/cm<sup>2</sup> (Penner, 1970). Such a large measuring range was also obtained in Cheverev's experiments and with pressures of 0-0.09 MPa generated, which corresponds to 0-0.92 kg/cm<sup>2</sup> (Cheverev, 1999).

Significant knowledge in the field was contributed by the research group of R.D. Miller. Miller (1972) presented a concept of secondary heaving based on the phenomenon of ice growth in the frozen part. Miller (1978) simulated a starting position of ice lens segregation in a variable thermal field. Miller and Kozlov (1980) investigated the relationship between frost heaving and loading rate, subsequently developing a frozen fridge theory or so called ‘rigid ice model’. The phenomenon of ‘regelation’ was represented by the example of a wire (Figure 2.4), tightened over the ice block and loaded from both sides. Through the applied pressure the wire travelled smoothly through the ice block over time, with the ice refreezing above the wire (O'Neill and Miller, 1985).

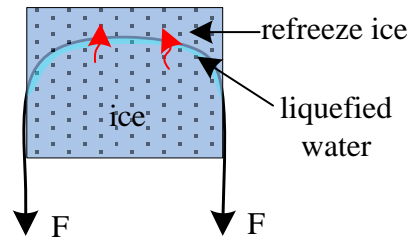


Figure 2.4 – The phenomenon of ‘regelation’ after O'Neill and Miller (1985)

Similar to this, the ice lens growth occurs in a vertical axis upward, while the soil particles due to gravitational pressure melt part of the ice below the soil particles, with the liquid then migrating up and refreezes in a new place (Figure 2.5).

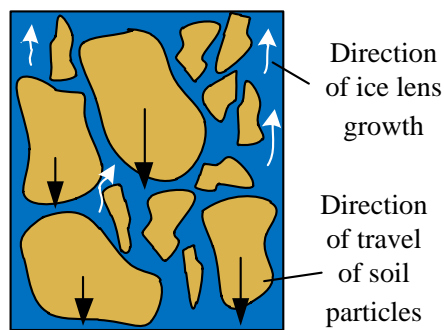


Figure 2.5 – Regelation of ice within the soils

The rigid ice model was considered using *semi-empirical*, *hydrodynamic* and *thermodynamic* approaches (Michalowski and Zhu, 2006).

#### ❖ Semi-empirical model

The empirical effort to explain freezing processes in a soil sample was the basis for the segregation potential (SP) model, first introduced by Konrad and Morgenstern (1981). According to the theory, during unidirectional freezing with a constant warm side and step-freezing cold side, the water influx  $v_0$  at the final ice lens formation is proportional to the temperature gradient  $T$  across the frozen fringe (Figure 2.6). This proportionality is called the segregation potential:

$$v_0 = SP_0 \text{ grad } T \quad (2.1)$$

where,  $v_0$  – velocity of pore water entering the unfrozen soil,  $SP_0$  – segregation potential at zero overburden pressure measured as  $\text{mm}/^\circ\text{C}\cdot\text{d}$ .

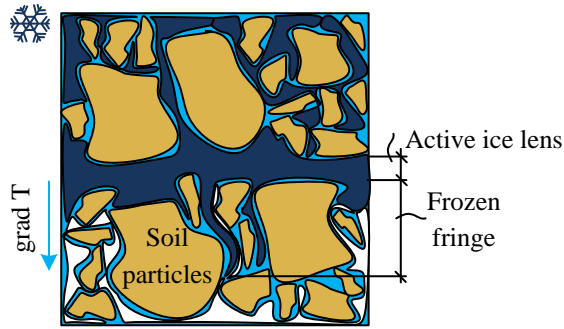


Figure 2.6 – A proportionality between ice lens formation and temperature gradient according to the ‘segregation potential’ theory

While zero overburden pressure is that near the thermal steady state, i.e. at the beginning of the final ice lens formation during the step freezing (Konrad, 2005).

### ❖ Thermodynamic model

The *thermodynamic model* does not consider a particular ice lens’ segregation, but rather, overall ice distribution in the soil and the porosity rate, as the main constitutive criteria (Michalowski and Zhu, 2006; Ji *et al.*, 2010). The porosity rate function represents the ability of the soil to expand during the freezing, caused by moisture mass transfer towards the freezing front (Figure 2.7). Thus, porosity growth replaces the hydraulic conductivity through the mass balance and, avoiding Darcy’s law, is expressed as:

$$n = n_{max} \left( \frac{T - T_f}{T_{max}} \right)^2 e^{1 - \left( \frac{T - T_f}{T_{max}} \right)^2}, \quad T < T_f, \quad \frac{\partial T}{\partial t} < 0 \quad (2.2)$$

where,  $n_{max}$  - the maximum porosity rate for the soil;  $T_{max}$  - the temperature corresponding to  $n_{max}$  in °C;  $T_f$  - temperature of the freezing water in °C; and  $T$  - given or measured temperature in °C.

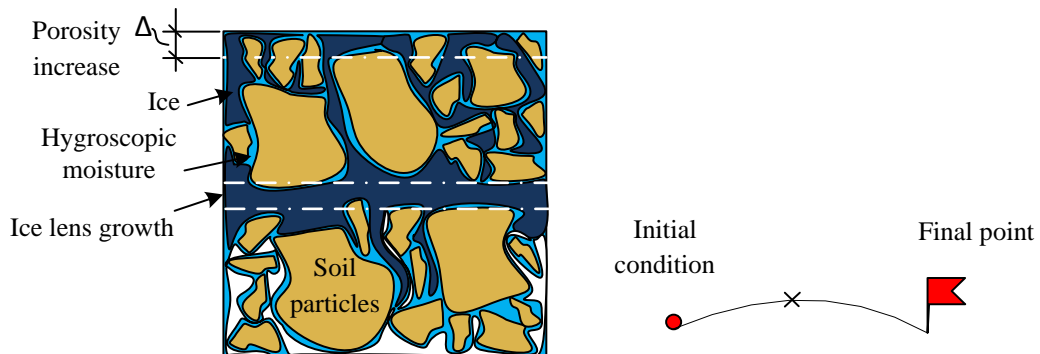


Figure 2.7 – ‘Porosity rate function’ according to thermodynamic model, after Michalowski and Zhu (2006)

Whilst this model does not consider individual ice lens formation, it does present the ice growth by an average porosity increase without replication of physical parameters, i.e. temperature distribution, strain and stresses. Therefore, Clausius-Clayperon equation was not used in the macroscopic modelling, as the porosity growth function replaces the need for calculation of the cryogenic suction. The model found wide replication with the finite element method in ice growth research during soil freezing, such as in ABAQUS (Michalowski and Zhu, 2006; Ji *et al.*, 2010; Zhang and Michalowski, 2015).

### ❖ Hydrodynamic model

The *Hydrodynamic* equilibrium between ice and water in porous media such as freezing soil is commonly expressed by the Clausius-Clapeyron relationship (Vidyapin and Cheverev, 2008; Benson and Othman, 1993):

$$\bar{V}_i P_i - \bar{V}_w (P_w - \pi) = -\frac{L}{T_0} \Delta T \quad (2.3)$$

where,  $(P_w - \pi)$  – total potential of liquid water;  $\pi$  – the osmotic pressure in the liquid water,  $\bar{V}_i$  and  $\bar{V}_w$  – specific volume of ice and water;  $L$  - the latent heat of fusion water;  $T_0$  – the absolute temperature (K);  $\Delta T$  – temperature change ( $^{\circ}\text{C}$ ).

According to this model frost heave starts when the ice content exceeds some critical amount and induces cryogenic suction. Kay and Groenevelt (1974) determined this critical proportion as soil porosity net of unfrozen water content, whilst a number of scientists accepted the ratio of 85% ice content of porosity as the criteria for frost heave initiation (Taylor and Luthin, 1978; Michalowski and Zhu, 2006).

Several attempts have been made to predict moisture transfer during the freeze-thaw cycles of unsaturated soils via modelling and large scale experiments (Chamberlain and Gow, 1979; Giakoumakis and Tsakiris, 1991; Othman and Benson, 1993; Giakoumakis, 1994; Shoop and Bigl, 1997). Chamberlain and Gow (1979) examined permeability and structure change during the freezing-thawing of fine-grained soils. A direct relationship between plasticity index and vertical permeability value was identified during freeze-thaw cycles. In addition, void ratio reduction due to effective stress increase after freeze-thaw cycles was observed (Chamberlain and Gow, 1979). Gilpin (1980) developed a model very similar to the rigid ice model, under the assumption that the chemical potential of the hygroscopic water was lowered, because of surface tension forces. He also idealised the frozen soil fringe model as a matrix of uniform spheres and developed a model where pore ice grows as a continuous 3-dimensional network. He

performed one of the first numerical solutions for the mathematical model for a 10cm length cylindrical sample. The heat and mass transfer equations were taken into account when estimating the frost heave (Gilpin, 1980).

Feldman (1967) identified a sinusoidal temperature variation at the boundary, which caused an irregularity in ice saturation in homogeneous soil. Owing to temperature oscillations at the boundaries, the freezing front also caused oscillations, which was as a consequence of the vacuum fluctuation followed by water migration fluctuation and irregularity in ice lens formation. Othman and Benson (1993) stated that an increased temperature gradient increases the value of hydraulic conductivity, leading to a greater amount of ice lens growth. They also noted that after three or more freezing-thawing cycles ice lenses growth and hence, the excess pores tend to be reduced (Othman and Benson, 1993).

In the 1970s the U.S. Army Cold Regions Research and Engineering Laboratory (CRREL) started developing a mathematical model to simulate a coupled heat-moisture transfer, which later was called FROSTB (Simonsen *et al.*, 1997). The main objectives of the model included frost heave simulation, calculation of the thaw settlement, temperature and moisture distribution and pore water pressure. Materials of a pavement structure were conducted as a mesh of discrete elements, while the heat balance was presented by the correlation of the amount of extracted heat compared to the heat loss required to turn all the remaining water into ice in each mesh (Figure 2.8). The hydraulic component of the model was calculated by Darcy's Law for the unsaturated flow, while volumetric water content  $\theta_l$  was presented using Gardener's (1958) equation:

$$\theta_l = \frac{n}{\alpha_w |h_p|^{\alpha_G} + 1} \quad (2.4)$$

where,  $\theta_l$  - volumetric unfrozen water content;  $n$  – soil porosity as a %;  $h_p$  – pore water pressure head in cm of water;  $\alpha_G$  - Gardener's exponent for the moisture characteristics;  $\alpha_w$  – Gardener's multiplier for the moisture characteristics.

Unsaturated hydraulic conductivity  $k_h$  is equal to:

$$k_h = \frac{k_l}{\alpha_k |h_p|^\beta + 1} \quad (2.5)$$

where,  $k_h$  – unsaturated hydraulic conductivity in cm/hour;  $k_l$  – hydraulic conductivity in cm/hour;  $\alpha_k$  - Gardner’s multiplier for hydraulic conductivity; and  $\beta$  – Gardner’s exponent for hydraulic conductivity.

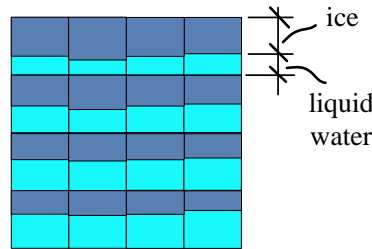


Figure 2.8 - A mathematical model FROSTB to simulate a coupled heat-moisture transfer

In the FROSTB model, hydraulic conductivity in the freezing zone  $k_f$  is assumed to decrease, because of ice crystals blocking the pore channels and is presented as a function of the pore water pressure head  $h_p$ , unsaturated hydraulic conductivity  $k_h$  and segregated ice content  $\theta_i$ . Drawing on laboratory test results the hydraulic conductivity decrease was presented exponentially across the freezing zone.

$$k_f = k_h |h_p| \cdot 10^{-\epsilon \theta_i} \quad (2.6)$$

where,  $k_f$  – hydraulic conductivity in freezing zone;  $\epsilon$  – empirical factor; and  $\theta_i$  – volumetric ice content.

FROSTB model-based studies have been conducted by Shoop and Bigl (1997), and Simonsen *et al.* (1997). Simulation of moisture migration by Shoop and Bigl (1997) in 1m thick frost susceptible silty sand located on 2m of gravelly sand gave predictions that overestimated the transfer of moisture, as compared with a large scale experiment of a 3.6m deep soil basin at the Frost Effect Research Facility (FERF), USA (Shoop and Bigl, 1997). The reason for the over prediction of ice content was caused by delay in thawing. The calculation results were downgraded with a deeper location of water table. The empirical method of calculating the hydraulic conductivity in the frozen soil might also have affected the estimated results of the moisture flow.

Simulation of the temperature and moisture change in a section of highway in Vermont, USA was performed by Simonsen *et al.* (1997). This showed good compatibility with field data. The site comprised 6.5cm asphalt concrete layer over 46cm silty sand with gravel and a subgrade layer of sandy silt (Simonsen *et al.*, 1997). Moisture

measurements on the site showed that the pavement layer is not completely impermeable in the frozen condition, however well predicted by the FROSTB model. According to Simonsen *et al.* (1997), to achieve better estimation results some data on field moisture and porosity should be obtained and used for the model calibration. Giakoumakis (1994) simulated a one-dimensional model to predict moisture and heat movement in a vertical porous soil column. This work showed that simulation of heat transfer in the freezing soil should be modelled together with water migration determination. He also explained that the cryogenic suction, caused by partial freezing of moisture in the cold side of the sample, induced the migration of liquid water from unfrozen side to the frozen, so as to reach the moisture equilibrium. Consequently, the moisture content of the unfrozen part drops dramatically, while the freezing side reaches the saturated condition (Giakoumakis, 1994).

The classical view of frost heave involved mainly considering water-ice interaction and their migration, while the vapour component in soils was widely ignored. Moreover, the widespread model of coupled heat and water transfer allowed for detailed calculation and estimation of moisture migration, by using the numerical methods. However it could not explain the driving forces and physical nature. Nevertheless, the developed methods and approaches formed the basis of the breakthrough of numerical methods and moreover, achieved tolerable results in frost heave calculations and prognosis.

### 2.3.3 Current understanding of frost heave

Recent studies have introduced more complex approaches in terms of frost heave modelling and simulation methods. Azmatch *et al.* (2012) investigated ice lens formation using the soil freezing characteristic curve (SFCC), which represents the unfrozen water content with temperature or suction corresponding to this temperature. In their model, Azmatch *et al.* (2012) hypothesised that ice lens initiation corresponds to the crack initiation point. Crack initiation was observed by digital camera and simultaneously the segregation temperature at the location was recorded by RTD sensors. The model was supported by unidirectional freezing tests with Devon Silt in Canada that had been consolidated at 100, 200 and 400 kPa. The unfrozen water content was obtained using the time domain reflectometer (TDR) technique. According to the results, the advice would be to use SFCC as an input to determine the segregation temperature in further frost heave modelling.

Moisture redistribution in peat conducted with repacked peat soil columns by Nagare *et al.* (2012) showed an insignificant effect of initial moisture content on the freezing characteristics of this soil, including the starting temperature of ice crystallisation and liquid moisture content. This means that a fixed relationship could be established between the temperature and liquid water content in a soil. Ji *et al.* (2010) worked out the segregated potential in a thermodynamic model initially presented by Konrad and Morgenstern (1981) and porosity rate function (2.7) originally described by Michalowski and Zhu (2006) in the following form of equation:

$$n = B \cdot e^{-\alpha P_e} \cdot (gradT) \cdot (1 - n_t), \quad T_s < T < T_{pw} \quad (2.7)$$

where,  $B = \frac{1.09 SP_0}{T_i - T_s}$  - is a constant;  $SP_0$  - segregation potential at zero overburden pressure;  $T_s$  - segregation freezing temperature,  $T_s = -0.1 - 0.3$  for silty soil;  $T_s = -0.3 - 0.8$  for clay;  $T_{pw}$  - pore water freezing temperature;  $\alpha$  - soil constant; and  $n_t$  - porosity at the time  $t$ .

Zhang and Michalowski (2015) developed a thermodynamic model of Michalowski and Zhu (2006) and calibrated a function of porosity to the further form:

$$n = n_{max} \left( \frac{T - T_f}{T_{max}} \right)^2 e^{1 - \left( \frac{T - T_f}{T_{max}} \right)^2} \cdot \frac{dT}{dT} \cdot e^{-\left( \frac{|\sigma'_{kk}|}{\zeta} \right)} \cdot e^{-\left( \frac{\theta_i}{\theta_w} \right)} \quad (2.8)$$



where,  $\frac{dT}{dl}$  – temperature gradient in the heat flow direction;  $g_T$  – thermal gradient in calibration;  $\sigma'_{kk}$  – first invariant of the effective stress tensor in the frozen soil;  $\varsigma$  – material parameter, defining the stress dependency; and  $e^{-\left(\frac{|\sigma'_{kk}|}{\varsigma}\right)}$  – a retardation function, representing that the frost heave can be significantly reduced by overburden stress.

The hydraulic conductivity component has been replaced with porosity growth for saturated soils in equation (2.7). Implementation of the model has been performed with the ABAQUS finite element code (Zhang and Michalowski, 2015).

The heat and mass transfer mechanisms in fully saturated soils were presented by Wu *et al.* (2015), where the ice nucleation and growth was considered by a kinetic model and correlated to a change in the Gibbs free energy for growing ice crystals: a volume free energy  $\Delta G_v$  and a surface free energy  $\Delta G_s$  (Wu *et al.*, 2015).

$$\Delta G_c = \Delta G_v + \Delta G_s = -\frac{4}{3} \cdot \frac{\pi r^3}{\Omega} \cdot \Delta g_v + 4\pi r^2 \gamma_{sf} \quad (2.9)$$

where,  $\Delta G_c$ ,  $\Delta G_v$ ,  $\Delta G_s$  - free energy variation in volume, surface and crystal;

$\Omega$  - volume of a single ice crystal molecule,  $\Omega = \frac{V_{M,w}}{N_A}$ ;

$V_{M,w}$  - molar volume of water;

$\gamma_{sf}$  - surface tension between ice embryo and water;

$\Delta g_v$  - decrease in the volume of a single molecule of the Gibbs free energy  $\Delta g_v = \frac{\Delta_M H_1}{N_A} \frac{\Delta T}{T_f}$ ;

$\Delta_M H_1$  - molar latent heat of crystallisation;

$N_A$  - Avogadro's number;

$T_f$  - freezing point;

$\Delta T = T_f - T$  - degree of supercooling.

The governing equation for effective specific heat capacity of the porous medium included the enthalpy and heat flux of the solid skeleton, liquid water and ice, however, any gaseous state inclusions were completely ignored. The finite element simulation for effective specific heat capacity was implemented on the COMSOL platform. The presented results indicated a strong influence of temperature in the formation of ice nuclei and the moisture redistribution.

Recent works based on water and heat transport are those of Ming and Li (2015) and Zhang *et al.* (2016). A mathematical model by Ming and Li (2015) replicated the experimental testing conditions mentioned in Table 2.1. According to the results, the frost heaving corresponds to some limit of the temperature gradient, below which the temperature change and the frost heaving are in direct relation. However, above this limit the frost heave amount is inversely related to the temperature gradient. They also noted that the frost heave amount can be controlled by the overburden pressure (Ming and Li, 2015). Zhang *et al.* (2016) implemented a coupled numerical model considering vapour and fluid flux transfer in freezing soils, heat transfer in terms of convection, a latent heat of vapour diffusion and its phase transfer effect (Zhang *et al.*, 2016). The authors found that water vapour contributes 15% of all water mass transfer in the soil. The equation for water flow in liquid and vapour phase is presented as:

$$\frac{\partial \theta_{tW}}{\partial t} = -\nabla(q_v + q_l) - S \quad (2.10)$$

where,  $\theta_{tW}$  – total volumetric water content ( $\text{m}^3\text{m}^{-3}$ );  $q_v, q_l$  – flux densities of the liquid and vapour parts ( $\text{m sec}^{-1}$ );  $t$  – time (sec); and  $S$  – transpiration for example for root water uptake ( $\text{sec}^{-1}$ ). Although the moisture for the root uptake is not applicable in geotechnical problems. Presenting the liquid flow by Richard's equation expressed with direct ratio of water potential gradient and temperature gradient (Harlan, 1973) along with vapour flow by Fick's flow driven by the vapour concentration gradient, as described by Philip and de Vries (1957), led Zhang *et al.* (2016) to combine the equation:

$$\begin{aligned} \frac{\partial \theta_{tW}}{\partial t} &= \frac{\partial \theta}{\partial t} + \frac{\rho_v}{\rho_w} \frac{\partial}{\partial t} (n - \theta_l - \theta_i) = \\ &= \nabla \cdot [k_{lh} \nabla(h + y) + k_{lT} \nabla T] + \nabla \cdot [k_{vh} \nabla h + k_{vT} \nabla T] \end{aligned} \quad (2.11)$$

where,  $\theta$  – the volumetric sum of unfrozen water and ice ( $\text{m}^3\text{m}^{-3}$ );  $\rho_v, \rho_w, \rho_i$  – density of vapour, liquid and ice;  $n$  – porosity;  $\theta_l, \theta_i$  – volumetric water and ice content ( $\text{m}^3\text{m}^{-3}$ );  $h$  – pressure head (m);  $y$  – vertical coordinate positive upward (m);  $k_{lh}, k_{lT}$  – isothermal and thermal hydraulic conductivities for liquid water, respectively;  $k_{vh}, k_{vT}$  – isothermal and thermal vapour conductivities; and  $T$  – soil temperature (K).

According to Zhang *et al.* (2016), the coupled heat transfer also has to include the phase changing heat during the evaporation, condensation, sublimation and deposition. The basic equation to determine the diffusion of vapour in soils was under Fick's law for the isothermal  $k_{vh}$  and thermal  $k_{vT}$  vapour hydraulic conductivities (Zhang *et al.*, 2016)

$$k_{vh} = \frac{D_a}{\rho_w} \rho_{vs} H_r \frac{Mg}{RT_k} \quad (2.12)$$

$$k_{vT} = \frac{D_a}{\rho_v} \eta H_r \frac{d\rho_{vs}}{dT} \quad (2.13)$$

where,  $D_a$  – is vapour diffusivity in soil,  $m^2/s$ ;

$\rho_v$  – vapour density,  $kg/m^3$ ;

$M$  – molecular weight of water,  $0.018kg/mol$ ;

$g$  – gravitational acceleration,  $9.81 m/s^2$ ;

$R$  – universal gas constant,  $8.314 J/mol \cdot K$ ;

$\eta$  – enhancement factor (Cass *et al.*, 1984);

$H_r$  – relative humidity.

The vapour-liquid flux simulation was implemented with COMSOL software and according to Zhang *et al.* (2016), the water vapour contributed more than 15 % of the water flux at all depths.

Notably, most of the studies that considered moisture mass transfer in freezing soils in a liquid state avoided or neglected the role of vapour mass transfer, which is the most likely transport implementation of moisture transfer at temperatures below zero degrees. Also, most of the prior research into soil freeze-thaw was performed under laboratory conditions with different freezing rates and sample sizes. One of the most promising areas in soil freezing research was presented by Zhang *et al.* (2016), who took into account both the liquid and vapour phases, the heat transfer in terms of convection, the latent heat of vapour diffusion and its phase transfer effect.

However, Zhang *et al.* (2016) still relied on the water in a liquid state as the main source of moisture transfer and consequently, attempted to determine the hydraulic conductivity via water flux, whereby numerous empirical relations were used to obtain the amount of unfrozen water content and the soil matrix potential. The vapour flux was derived by considering the relative humidity  $H_r$ , although it can be assumed that the gaseous state in the soil pores is close to the saturated condition, as it is in equilibrium with the water or ice content. The enhancement factor  $\eta$ , used to describe the increases in the thermal vapour flux, was also an empirical relation. And lastly, the simulation of the heat flux and soil water content had poor validation with the measured results on the active layer in the permafrost of Tibetan Plateau site, China, which might, nevertheless,

be acceptable as the first attempt to take into consideration the vapour flux in freezing soil.

#### **2.4 Study of the deformation-strength characteristics of soils during freeze-thaw cycles**

In recent times, considerable attempts have been made to study freeze-thaw impacts on deformation and strength properties of soils (Konrad, 1989; Simonsen and Isacsson, 1999; Konrad and Samson, 2000; Oztas and Fayetorbay, 2003; Wang *et al.*, 2007; Qi *et al.*, 2008; Ishikawa *et al.*, 2010; Nagare *et al.*, 2012). Nevertheless, the outcomes include significant discrepancies regarding the effect of freeze-thaw cycles on the hydraulic and thermal conductivity of soils, and their mechanical properties such as: cohesion, angle of internal friction, volumetric-density change and bearing capacity.

Laboratory testing of soil samples found in Erzurum Province, Turkey, was conducted in response to issues regarding aggregate stability by Oztas and Fayetorbay (2003). The results confirmed the significant influence of moisture content on soil stability and showed that soils with particles size bigger than 1mm are more stable after freeze-thaw cycles (Oztas and Fayetorbay, 2003). Kværnø and Øygarden (2006) studied the effect of freeze-thaw cycles on the aggregate stability of silt, clay loam and silty clay loam samples. The aggregate stability was conducted with the Norwegian standard procedure of a rainfall simulator and wet-sieving. According to their results, it was observed that freezing and thawing decreased the aggregate stability of all soil types, however, silty soil was the worst affected (Kværnø and Øygarden, 2006).

Qi *et al.* (2008) ran a freeze-thaw cycle on Lanzhou loess with a 15.3-17.3 kN/m<sup>3</sup> dry unit weight. An experimental box supplied freezing from the top until -20 °C, while the bottom was kept at a constant +1 °C. According to the results, lower dry density samples compressed after a freeze-thaw cycle and higher dry density increased in volume, also becoming looser. Strength parameters showed a decrease of cohesion and slight increase of friction angle, possibly caused by volumetric expansion of high density soil, as freezing proceeded. Moreover, the resilient modulus diminished after freezing-thawing in all cases. Notably, the study outcomes suggest that for some critical point of dry unit weight  $\gamma_d^{cr}$ , the engineering properties of the soil, including its dry density value, remain in the initial state after a freeze-thaw cycle (Qi *et al.*, 2008).

A freeze-thaw experiment on Qinghai-Tibet clay soil samples carried out by Wang *et al.* (2007) contributed to the understanding of the freezing and thawing impact on the mechanical properties of tested soils in terms of the number of testing cycles. After seven freeze-thaw cycles the heave-induced increase in height was stabilised. However, the freezing period covered just 18h in  $-7^{\circ}\text{C}$  in a closed system, without any supply of water. Neither a gradual increase temperature gradient, nor enough time was provided to allow water redistribution approximating to natural conditions. Cohesion was in inverse relationship with the number of cycles and dropped with the freeze-thaw cycle repetition. Notwithstanding this, the same seven cycles of freeze-thaw were critical to resilient modulus value, which decreased with increasing number of cycles; however after seven cycles the value of resilience modulus slightly increased till the further stabilisation (Wang *et al.*, 2007).

To understand better the strength properties of frozen soils, triaxial compression tests were performed with negative temperature values (Brouchkov, 2000; Brouchkov, 2002; Qi *et al.*, 2006; Ishikawa *et al.*, 2010; Sinitsyn and Løset, 2011; Hazirbaba, Zhang *et al.*, 2013). At increasing confining pressures the stress-strain behaviour curves of silty clay samples change from a strong strain softening, with a peak in deviator stress and then dropping, to weak strain tendencies (Zhang *et al.*, 2007). Zhang *et al.* (2013) made attempts to improve the triaxial testing technique. Recommendations for a volumetric calculation method were given to increase the accuracy of triaxial loading by means of the volumetric and compressibility characteristics of exploring oil in sub-zero temperatures (Zhang *et al.*, 2013).

Ishikawa *et al.* (2010) performed a monotonic triaxial compression test of volcanic granular soils in a modified compound freeze-thaw cell (Ishikawa *et al.*, 2010). A reduction of the angle of the internal friction and deformation modulus took place as the number of freeze-thaw cycles increased. However, no frost heave or thaw settlement occurred in the coarse-grained soils (Ishikawa and Miura, 2011). Hazirababa *et al.* (2011) conducted freeze-thaw cycles of fine-grained soils with respect to excess pore pressure genesis and its further influence on the liquefaction phenomenon in seismic response. Loading was implemented in a cooled triaxial cell, which permitted strain-control tests. Excess pore pressure developed in a range of 0.01% cyclical shear strain level. With an increase in the number of freezing-thawing cycles a reduction of excess pore pressure

generation occurred when compared to the soils that had not been subjected to freeze-thaw (Hazirbaba *et al.*, 2011).

According to Qi *et al.*'s (2006) review of the studies of freeze-thaw cycles and their influence on the geotechnical properties of soils, the phenomenon causes the degradation of structure in natural fine-grained soils, such as clays. However, it was noted that there was an improvement in the structure of reconstituted normally consolidated clays. In coarse soils, the freeze-thaw cycles cause dilation of dense soils and densification in the loose ones (Qi *et al.*, 2006). Regarding which, Kweon and Hwang (2013) elicited that the resilient modulus of subgrade soils under a 'closed' water supply system stays the same after freeze-thaw cycles. Similar results were obtained by Simonsen and Isacsson (2001), who tested both variable and constant confining pressure triaxial tests, could not observe consistent results on resilient moduli with regards to the freeze-thaw effect; noting that some samples showed a significant reduction after freeze-thaw, while the others remained unaffected (Simonsen and Isacsson, 2001). However, Wang *et al.* (2007) observed a decrease in resilient moduli in the range of 18-27% after freeze-thaw cycles.

Summarily, most of the extant studies have consistently concluded that freeze-thaw cycles in an 'open' system with free water access negatively affect bearing capacity and the resilient moduli (Wang *et al.*, 2007; Tang and Xu, 2016). However in a 'closed' system not much pore water is available to transport and therefore, no obvious change in mechanical properties is observed (Kweon and Hwang, 2013). Moreover, many of the studies have indicated that dynamic load under vibration may worsen the bearing capacity (Cui *et al.*, 2014; Tang and Xu, 2016). According to Cui and Zhang (2015), the freeze-thaw cycles under the subway vibration loading increased the strain by 26.7%, and the excess pore pressure by 53% in the clay samples when compared to undisturbed ones under the same testing conditions. Finally, the lower the frequency of vibration the more energy was transferred to soil, causing a greater accumulation in plastic strain (Cui *et al.*, 2014; Tang and Xu, 2016).

#### **2.4.1 Engineering properties of soils during thaw weakening**

Despite most of the studies reporting considerable weakening during the thaw period, the issue of the values, with a view to ensuring the bearing capacity, especially in highways and railway sub soils, still requires further investigation. As stated in Simonsen

and Isacsson's, (1999) review, mild winters with slow freezing cause greater rates of frost heave in frost susceptible soils compared to cold winters, when the ice segregation occurs at deeper sub soil levels.

Laboratory based studies aimed at obtaining the bearing capacity during thaw weakening involved conducting resilient modulus measurements, consolidation and observing hydraulic conductivity data (Lee *et al.*, 1995; Konrad and Samson, 2000; Shoop *et al.*, 2008). Mechanical behaviour modelling of thaw-weakening soils was performed by Shoop *et al.* (2008) in saturated and unsaturated triaxial tests of silty sand. Simulation of a moving vehicle as a rolling wheel on paved and unpaved road was modelled. A single load wheel impact was conducted in a finite element simulation model using ABAQUS code and correlated with laboratory triaxial loading results (Shoop *et al.*, 2008). The experimental testing of thawed soils showed them to be very weak with plastic deformations in both compression and shear. The simulation of the pavement structure, during the complete thawing and not yet drained (not recovered) condition, signified that tensile stress at the base of the asphalt layer was over four times higher than that experienced during the summer period, while the vertical stress in the subgrade, under the same conditions, was three times higher. Notably, lateral stresses, which are transverse to the highway direction, were 30 % higher than the longitudinal tension. However, the developed model over predicted the experimental results for residual shear forces by 4-15 % of the upper range of the data (Shoop *et al.*, 2008).

In field observations non-destructive methods are preferred, such as static deflection, vehicle generated deflection, vibrator generated deflection and impulse-load generated deflection methods (Chamberlain and Gow, 1979; Storme *et al.*, 2004). Based on field observations with a spectral analysis of surface waves, Storme *et al.* (2004) found the lowest level of stiffness modulus in pavement layers occurred between its complete thawing and 1 month later. Significant change was registered between -1 °C and 0 °C. The minimum value of the stiffness moduli was 80% of its pre-freezing value in the base and 60% in the sub base and subgrade (Storme *et al.*, 2004).

Collectively, the studies of thaw weakening outline the critical roles of soil permeability, drainage conditions and rate of thaw on the bearing capacity of soils during the thawing period. Both laboratory based studies and field observations highlighted the prime relation of the amount of moisture content accumulated during the frost heave to thaw weakening in spring time. A 50-60% decrease in the resilient modulus was

registered after freeze-thaw cycles in fine-grained soils (Lee *et al.*, 1995; Simonsen *et al.*, 1997; Simonsen and Isacsson, 1999). Several models have been presented in recent years regarding thermal analysis, settlement and consolidation during the thaw weakening. However, the implementation of these models is complicated with the complexity of the problem, including the freezing conditions and mass transfer characteristics in freezing soil, which should be studied foremost.

## 2.5 Deposition and distribution of de-icing chemicals in the road soil area

Frost heave in highway subsoils in cold countries is often accompanied by precipitation causing black ice and frazil on pavements. De-icing chemicals are eventually deposited in road side areas due to precipitation runoff, ploughing or runoff with melted mass from the road. The most common types of de-icing chemicals used in highways in the winter exploitation are presented in Table 2.2.

De-icing of highway surfaces from ice formation and providing a ‘safe’ level of skid resistance on the pavements is achieved by applying large amounts of de-icing chemicals, with an even coverage on the road surface. According to Lundmark and Olofsson (2007), each km of highway in Sweden is applied with 5-15 tonnes of sodium chloride per cold season and nationally, more than 200,000 tonnes of de-icing chemicals are used for road maintenance in a year. A mathematical model of de-icing transport, which comprises splash and spray, estimates that about 45% of the applied de-icing agents accumulate in 0-100m distance from the road (Lundmark and Olofsson, 2007).

Table 2.2 – De-icing chemicals commonly used on highways

De-icing chem.group	De-icing chemical	Chemical formula	Notes
Inorganic salts	Sodium Chloride (or table salt)	NaCl	The most common de-icing chemical; the cheapest one.
	Magnesium Chloride	MgCl <sub>2</sub>	Often added to lower the working temperature of another de-icing chemical.
	Calcium Chloride	CaCl <sub>2</sub>	Often added to lower the working temperature of another de-icing chemical.
	Potassium Chloride	KCl	A common fertiliser, effective down to -11°C



Organic compounds	Calcium magnesium acetate	CaMg <sub>2</sub> (CH <sub>3</sub> COO) <sub>6</sub>	Environmental friendly and effective down to -27 °C
	Ammonium acetate	CH <sub>3</sub> COONH <sub>4</sub>	“Antisneg” de-icer
	Potassium acetate	CH <sub>3</sub> COOK	“Nordix” de-icer
	Potassium formate	CHO <sub>2</sub> K	Environmental friendly
	Sodium formate	HCOONa	“Safeway” de-icer, environmental friendly
	Calcium formate	Ca(HCOO) <sub>2</sub>	Environmental friendly, used as an additive to urea or other de-icing chemicals
	Urea	CO(NH <sub>2</sub> ) <sub>2</sub>	A common fertiliser, generally used as an additive to sodium chloride.
Alcohols, diols and polyols	Methanol	CH <sub>4</sub> O	These are antifreeze agents and rarely used for ice removal on roads.
	Ethylene Glycol	C <sub>2</sub> H <sub>6</sub> O <sub>2</sub>	
	Propylene Glycol	C <sub>3</sub> H <sub>8</sub> O <sub>2</sub>	
	Glycerol	C <sub>3</sub> H <sub>8</sub> O <sub>3</sub>	

Surveys conducted by Blomqvist and Johansson (1999) show that 20-63% of the mass of applied de-icing agents' was found at 2-40m distance from the road. Deposition of de-icing chemicals along the roadside area was investigated by Lundmark and Olofsson (2007), who conducted field observations by airborne deposition sampling in buckets with funnels, soil sampling, soil resistivity and analysis. According to their observations, 340 g/m<sup>2</sup> chloride deposition occurred in a 2m distance from the road (Figure 2.9). Notably, the results showed that the chloride content in clayey soils was higher than in sandy soil, obviously due to the drainage and the resultant abilities of the chemicals to accumulate. A modelling approach to de-icing deposition and distribution was considered in Lundmark and Jansson (2008). According to Peterson (2008), simulation of de-icing flow shows that predominantly vertical transfer of de-icing chemicals is imposed by molecular diffusion. The dilution of a chloride reservoir in unsaturated layers takes a long period of up to 20 years. A high chloride concentration of 1000 mg/L was recorded by Hart *et al.* (1991) in topsoil in Little Kickapoo Creek, Central Illinois as a result of seasonal dicing maintenance of highways. During field observation by Pedersen *et al.* (2000), 441g/m<sup>2</sup> NaCl deposition was recorded in roadside soil within 0.6m of the road edge in Copengagen, Denmark. The average concentration of NaCl at soil water at the same 0.6m distance was equal to 1.595 g/L, while the maximum values exceeded 2.500 g/L.

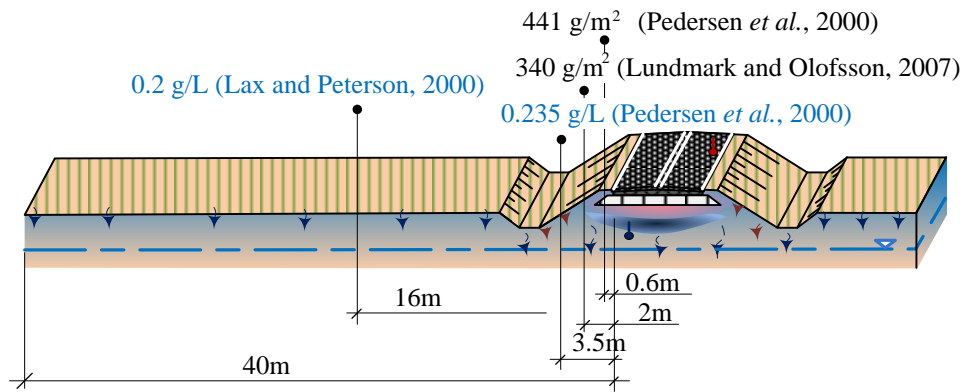


Figure 2.9 - Accumulation of de-icing chemicals in the road soil area

Norrström and Jacks (1998) analysed the pollution of roadside soils by assessing the concentration of heavy metals present in de-icing chemicals. The study showed that exchangeable cations of sodium chloride lead to the leaching of large amounts of Pb, Cu, Zn in roadside zones. Furthermore, a high concentration of Na predominantly displaced Ca, which negatively affected the soil quality (Norrström and Jacks, 1998). The effect of de-icing chemicals on ecosystems and soil mineralogy was widely studied by Vengosh, (2003), Godwin *et al.* (2003), Farifteh *et al.* (2006), Findlay and Kelly (2011), and Kelting *et al.* (2012). Concerns about the increased chlorination level were raised in terms of its impact on the acidification of surface waters and consequently, on aquatic plants and invertebrates (Godwin *et al.*, 2003). Regarding which, Findlay and Kelly (2011) noted that concentration of NaCl can be elevated to more than 100 Cl<sup>-</sup>/L during the winter highway exploitation, which may consequently affect sensitive organisms (Findlay and Kelly, 2011).

There are various ways to derive the chemical concentration used by different scientists, including the amount of de-icing chemical per dried sample mass in g or per ml of ground water. To simulate the saline ground water in current research the data received by Pedersen *et al.* (2000) was used as a basis. To achieve the de-icing chemical content in ground water corresponding to 1.595 g/L or 441 g/m<sup>2</sup> the soil samples need to be supplied with 11 g/L of NaCl solution.

### 2.5.1 Impact of salinity on the freezing point

Early studies into how salt affects soils during the freeze-thaw cycles were presented by Hoekstra (1969a), Chamberlain and Gow (1979), Kay and Groenevelt (1983), and Cary (1987). It is clear that chemical content in soils influences the freezing

temperature depending on the concentration and the chemical type (Figure 2.10). Furthermore, according to Frolov and Komarov (1983) the freezing temperature for sodium chloride and obviously for other de-icing chemical solutions can be lower than the eutectic temperature, presumably due to surface tension forces. The common soluble salts contained in the soils include the cations  $\text{Na}^+$ ,  $\text{K}^+$ ,  $\text{Ca}^{2+}$ ,  $\text{Mg}^{2+}$ , and anions  $\text{Cl}^-$ ,  $\text{CO}_3^{2-}$ ,  $\text{SO}_4^{2-}$ ,  $\text{NO}_3^-$ . The freezing process of saline soils can be explained as a sufficient temperature drop to cause the interstitial water to start to segregate into ice crystals. The remaining unfrozen water becomes progressively enriched with dissolved salts and depresses the freezing point towards the eutectic temperature (Panday and Corapcioglu, 1991; Marion, 1995; Torrance and Schellekens, 2006; Bing and Ma, 2011). Koopsman and Miller (1966) in Torrance and Schellekens' (2006) review explained 'below-normal' freezing temperatures in fine-grained soils as the increased freezing-point depression in small spaces of soil pores (Torrance and Schellekens, 2006). Another reason for unfrozen water in soil is osmotic depression, which is caused by the exchangeable salt ions network (Yariv and Cross, 1979).

The relationship of freezing point depression and solute molarity is presented in Van't Hoff's equation (Marion, 1995):

$$dT/dm_B = -RT^2/55\Delta H \quad (2.14)$$

where,  $m_B$  – molarity of solute B ( $\text{mol kg}^{-1}$ )

T – temperature (K)

R – gas constant ( $\text{J K}^{-1} \text{mol}^{-1}$ )

$\Delta H$  – enthalpy of fusion of ice ( $\text{J mol}^{-1}$ )

This equation simplifies to:

$$\Delta T \approx -1.86(\nu m_B) \quad (2.15)$$

where,  $\Delta T$  – temperature depression in  $^{\circ}\text{C}$ ;  $\nu$  – is a number of aqueous species resulting from the dissolution of the salt molecule, for example, for NaCl  $\nu=2$ , for  $\text{CaCl}_2$   $\nu=3$ . So, for  $m_B=0.1 \text{ mol kg}^{-1}$  NaCl the depression will be  $\Delta T \approx -1.86(2 \cdot 0.1) = -0.37 \text{ }^{\circ}\text{C}$ . The temperature depression for different types of de-icing chemicals is presented in Figure 2.3, the specifications of which were presented in Table 2.2.

Bing and Ma (2011), using laboratory investigations, tested silty clay, silty sand, sand and clay soils, remolded with predetermined chemical content to 30mm diameter and 50mm height samples, for the freezing point temperature. According to their

experimental results, the influence of cations on the freezing point was distributed in the following order:  $\text{Na}^+ > \text{K}^+ > \text{Ca}^{2+}$ ; and  $\text{Cl}^- > \text{CO}_3^{2-} > \text{SO}_4^{2-}$  for the anions. (Bing and Ma, 2011) have also confirmed that smaller soil particles have a stronger effect on the temperature depression during freezing, which was explained by greater specific area and larger thickness of film water around the soil particles (Bing and Ma, 2011). Aksenov (2008) presented a comprehensive field and laboratory study of saline soils from Arctic shore, oil and gas fields of the Yamal and Yugor peninsulas, Russia. According to the Russian Federation standard for construction, the saline soils are subdivided by degree of salinity  $D_{\text{sal}}$  (%), the ratio of the mass of dry soluble salt to the mass of dry soil, to light, moderate and severe saline soils and solonchak (Table 2.3.).

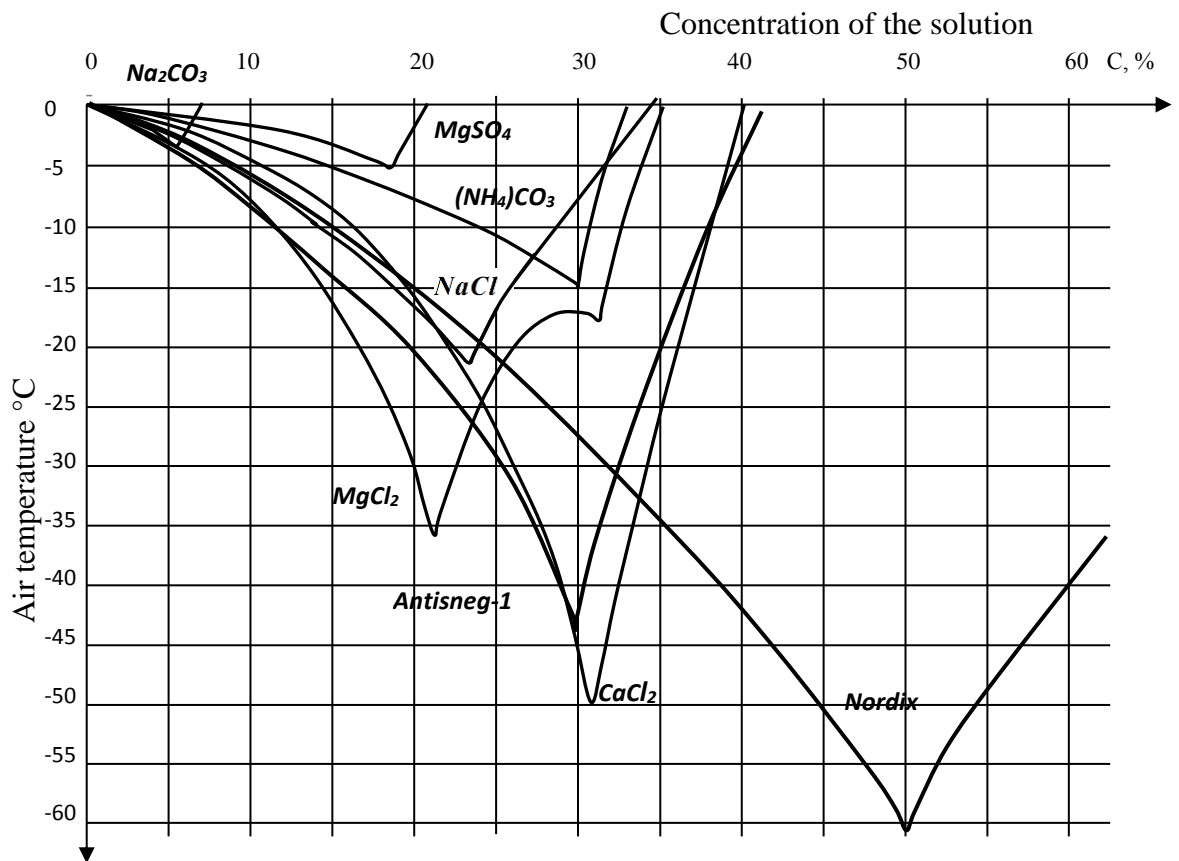


Figure 2.10 – Stability diagram for the most common de-icing chemicals in Kazakhstan highway exploitation (Sarsembayeva, 2005)

Table 2.3 – Soil types by the degree of salinity  $D_{sal}$ , according to the Russian Federation and Kazakhstan standards for construction

No	$D_{sal}$ , %	Soil salinity degree
1	0.3-0.5	Light saline
2	0.51-1	Moderate saline
3	1-2	Severe saline
4	2-4	Solonchak

For poly-disperse and poly-mineral soils the salinity degree  $D_{sal,cr}$  has been obtained by Panchenko's formula:

$$D_{sal,cr} = 0.9V \cdot \frac{\sum E_{Wi} \cdot N_i}{\sum N_i} \quad (2.16)$$

where,  $D_{sal,cr}$  – critical value of salinity, %;

0.9 – safety factor;

$V$  – exchange volume of the soil;

$E_{Wi}$  – equivalent weight;

$N_i$  – normality of the  $i$ -th component of the pore solution.

Poly-disperse soils here mean those soils with non-uniform particle size distribution. According to the equation, in soils such as clay, with high organic inclusions and also in the soils with carbonates and calcium sulphate salts, the critical salinity increases as particle size decreases (Aksenov, 2008).

Aksenov also cited Sheikin's formula to define the phase equilibrium in saline soils (Sheikin, 1990):

$$\theta_i = (\theta_{tW} - W_p/4)(1 - T_f/T) \quad (2.17)$$

$$\theta_l = \left(W_p/4\right) + (\theta_{tW} - W_p/4) T_f/T \quad (2.18)$$

where,  $\theta_l$  – unfrozen water content;  $\theta_i$  – ice content,  $\theta_{tW}$  – total water content;

$W_p$  - plasticity limit;  $T_f$  – freezing point temperature in °C;  $T$  – actual temperature in °C.

It should be noted that these equations were designed only for the solutions below the eutectic concentration and the corresponding temperature.

Comprehensive research regarding the freezing point temperature for sandy and clay soils at the Amderma permafrost station, Russia, was conducted by Yarkin (1990) in 1986, which included sodium chloride, calcium chloride, magnesium sulphate, sea salt and Yakutian salt with the following chemical content:  $\text{Ca}^{2+}$  -17%,  $\text{Mg}^{2+}$  -11%,  $\text{SO}_4^{2-}$  -29%,  $\text{Cl}^-$  -17% (Yarkin, 1990). The results of the field research for saline soils at the Amderma permafrost station are presented in Table 2.4.

Table 2.4 – Freezing temperature for the saline soils by Yarkin (1990)

Soil type	Degree of salinity $D_{\text{sal}}$ , %	Concentration	Freezing point depression for saline soils, °C				
			NaCl	Sea salt	CaCl <sub>2</sub>	Yakutian salt	MgSO <sub>4</sub>
Clayey loam W=28%	0.2	0.0071	-0.50	-0.30	-0.25	-0.20	-0.15
	0.5	0.0178	-1.10	-1.0	-0.60	-0.40	-0.25
	1.0	0.0357	-2.30	-1.80	-0.95	-0.75	-0.35
Sandy loam W=28%	0.2	0.0087	-0.65	-0.55	-0.45	-0.35	-0.25
	0.5	0.0217	-1.60	-1.40	-0.80	-0.65	-0.40
	1.0	0.0435	-3.50	-2.65	-1.45	-1.25	-0.50
Fine sand from the sea shore W=19.5%	0.2	0.0108	-0.55	-0.50	-0.40	-0.30	-0.20
	0.5	0.0256	-1.35	-1.15	-0.75	-0.55	-0.30
	1.0	0.0513	-	-2.35	-1.40	-1.20	-0.45

Torrance and Schellekens (2006) in their theoretical model considered the temperature induced osmotic potential at the ice-water interface in the frozen fringe. According to the authors, the salinity enhances moisture mass transfer as the osmotic potential increases dramatically. Wan *et al.* (2015) examined the freezing temperature in sulphate saline silty samples selected near the abandoned Quinghai-Tibet Highway on the Quinghai-Tibet Plateau, China (Wan *et al.*, 2015). After ion analysis, the samples were first desalinated and then remolded back with an updated chemical and moisture content. The measured freezing temperature indicated an inverse relationship of the chemical concentrations impact to the freezing temperature depression. Under the assumption that latent heat, released during the phase transfer, is used to counteract the

energy on the curved ice-liquid interface, the freezing temperature of saline soils  $T_{f-sal.soil}$  was found by the following equation:

$$T_{f-sal.soil} = \Delta T_{f-solution} + \Delta T_{\gamma} \quad (2.19)$$

where,  $\Delta T_{f-solution}$  – freezing temperature depression caused by the solution;

$\Delta T_{\gamma}$  – temperature depression, when free energy of the ice-liquid interface is counteracted.

Assuming that ice grow refers to a spherical interface, equation (2.19) was developed to a new empirical form (2.20), which represents the impact of the solution concentration and ice crystal size (Wan *et al.*, 2015):

$$T_{f-soil} = \frac{T_f^*}{1 + \frac{T_f^* R}{L_{wi}} \ln a_w} - T_f^* + \frac{2\Delta G_{i-l} V_{M,i} T_{f-solution}}{L_{wi} r_0} \quad (2.20)$$

$T_f^*$ - freezing point of pure water at the absolute temperature;

$T_{f-solution}$ - freezing temperature of the solution;

$R$ - gas constant;

$L_{wi}$ - latent heat of freezing;

$a_w$ - water activity;

$r_0$ - initial radius of spherical crystal;

$\Delta G_{i-l}$ -free energy of the ice-liquid interface;

$V_{M,i}$ - molar volume of ice crystal.

Equation (2.20) was mainly designed to calculate the initial freezing temperature of free water content, as the radius of the curved ice-liquid interface has a great impact on the freezing temperature of saline soils. The effect of supersaturation and salt crystal segregation was not considered in this work. Together, the studies outlined the relation between salt concentration and the freezing temperature depression, which might be enhanced by the growth of osmotic potential energy.

### 2.5.2 Chemical and moisture mass transfer in the soil induced by temperature gradient

Following Torrance and Schellkens (2006), the osmotic potential, induced by the temperature gradient in unfrozen water films, appears to be a major driving force causing water to move towards the freezing front. A numerical method of coupled flow of water, salt and heat during freezing in unsaturated soil was simulated by Cary (1987). From the

results of the tests, he hypothesised that salt solute might minimise frost heave by reducing the moisture transport toward the freezing front (Cary, 1987).

Previous studies have reported conflicting results for the chemical mass transfer within a soil sample induced by the temperature gradient over the sample length. Bing and He (2008) conducted an experimental study of water and salt redistribution in a clay soil sample, induced by a constant temperature gradient and simultaneously supplying the soil with water from a source at the bottom. The results of the tests confirmed steadily increasing water content in the ice segregation area and a decrease in the unfrozen part. However, ion distribution was dominated by diffusion, which indicates, that ion transfer is also a chemical process. Brouchkov (2002), who observed salt and water migration at the Amderma permafrost station for 12 years, reported that he could not register any direct flow of water or salt in a 0.05 °C temperature gradient over this long-term period. However, some minor localised signs of moisture transfer were noted (Brouchkov, 2000; Brouchkov, 2002).

Vidyapin and Cheverev (2008) conducted experimental research of hydraulic conductivity in freezing saline soils, where the chemical content migration along with water was observed towards the freezing front. Concentration on the cold side of the sample was significantly higher than the initial value of the supplied solution, which suggests, that salt movement was ahead of water migration. At the same time, it was established that hydraulic conductivity in freezing zones was decreased by the presence of salt. The coefficient of hydraulic conductivity depended on an excess pore water pressure gradient, and at small pore pressure gradients a deviation from the linear filtration pertaining to Darcy's Law was identified (Vidyapin and Cheverev, 2008). Cheverev *et al.* (1998) explained this deviation as being due to the existence of the boundary pressure gradient, below which moisture transfer retardation occurs. According to the authors, this phenomenon is caused by a rheological problem when the freezing time is shortened (Cheverev *et al.*, 1998).

Overall, these studies outline the reduction in hydraulic conductivity during the freezing of saline soil samples when compared to non-saline ones. However, there is no consensus regarding the chemical mass transfer in the unidirectional freezing of soils.



### 2.5.3 Variations of engineering properties in subsoils affected by de-icing chemicals and freeze-thaw cycles

A large and growing body of literature has investigated the effect of salinity on the engineering or mechanical properties of soils. According to Marion (1995), a number of studies have found that chemical content presence in the soil pore water generally decreases the mechanical strength (Chamberlain and Gow, 1979). Arenson and Sego (2006) emphasised the importance of the presence of chemicals in unfrozen water to the freezing process in coarse-grained soils. The water in a liquid phase in the frozen soils was determined with a fluorescent tracer. The photographs registered a change in the freezing process at concentrations of sodium chloride as low as 1 g/L (Arenson and Sego, 2006).

A power-law relationship of uniaxial unconfined compressive strength and a strain rate, salinity and temperature, was reported by Nguyen *et al.* (2010) as the result of a radially freezing sand experiment. 1m high and 2m diameter samples of uniform sand were saturated in 5.13 and 20 g/L sodium chloride and frozen by 0.3 °C per day. The results also showed a power-law relationship between the secant stiffness modulus and salinity, strain rate and temperature, which can be expressed with an empirical relation and used to determine this modulus (Nguyen *et al.*, 2010).

Many experiments have been performed in the adapted triaxial cell, which allows applying precise stresses and direct measurement of the pore water pressure during the freeze-thaw cycles. Sinitsyn and Løset (2011) carried out freezing tests with saline silt soil and applied high rate compression in a triaxial cell. The results revealed that a growth in strain rate in the range  $10^{-2}$  -  $10^{-3}$  sec<sup>-1</sup> and depression of the freezing temperature increases the shear stress  $\tau_{max}$ . While the increase in radial stress  $\sigma_3$  up to 0.1-0.3 MPa leads to decrease of  $\tau_{max}$ . The achieved strain rates once again confirmed the inversely proportional relationship between the strain rate and freezing temperature decrease. Reduction of pore volume is followed by a  $\sigma_3$  rise and amplification of volumetric deformation, which in turn leads to a reduction in  $\tau$  (shear strength) accompanied by ice melting (Sinitsyn and Løset, 2011).

Experimental investigation by uniaxial compressive strength with freeze-thaw cycles was performed on saline loess by Bing and He (2011). It was reported that salinisation by application of a chemical solution of the soil sample caused strain

weakening. According to the results, around six cycles were needed to reach a dynamical equilibrium after the addition of sodium sulphate. An increased number of freeze-thaw cycles caused a reduction in failure strain and failure stress (Bing and He, 2011). A huge number of tests to identify the mechanical properties were conducted at the Amderma permafrost station and other north-polar regions by groups of Russian scientists (Tsytovich *et al.*, 1973; Yarkin, 1990; Brouchkov, 2002; Aksenov, 2008). According to Tsytovich *et al.* (1973) the soils in a state firmly cemented by ice and with bearing capacity greater than 100 MPa are classified as a ‘firmly frozen’. The freezing temperatures for the ‘firmly frozen’ non-saline soils range from  $-0.1\text{ }^{\circ}\text{C}$  for sands down to  $-1.5\text{ }^{\circ}\text{C}$  for clays. Frozen soils with a bearing capacity less than 100 MPa and exhibiting viscosity properties over time, are termed ‘plastic frozen’. The freezing temperature for these soils’ state is higher than for the ‘firmly frozen’. Yarkin (1990) and Aksenov (2008) noted a great impact of soil salinity on the rheological properties of clayey soils as creeping and modulus of deformation change with time and temperature. Depending on the unfrozen water content, the experimental results were considered in relation to soil salinity and temperature and classified according to further soil states: firmly frozen, plastic frozen and thawed soils (Figure 2.11).

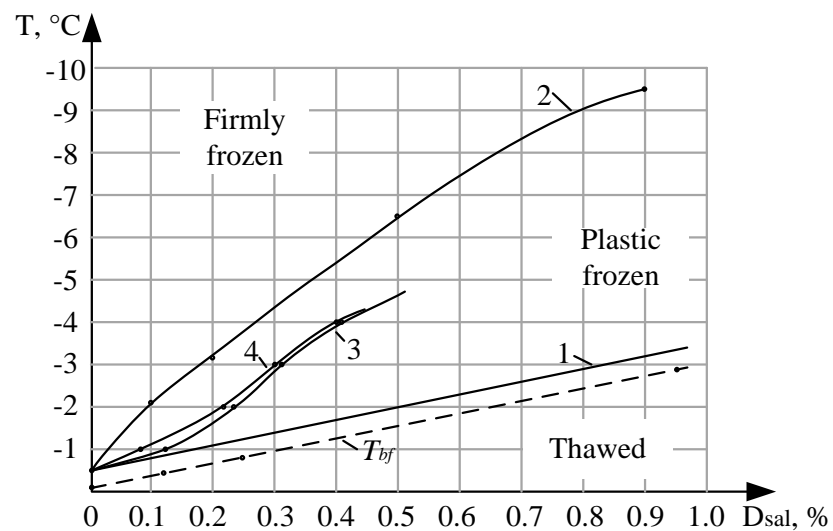


Figure 2.11 – Temperature boundary between firmly frozen and plastic frozen soils, according to: 1- initial freezing temperature; 2 – unfrozen water content; and 3 – modulus of deformation; cohesion (by Aksenov, 2008)

Overall, these studies outline a critical role of soluble salts on the freezing temperature and unfrozen water content of soils, which invariably leads to an effect on the engineering properties of the soils.

## 2.6 Phase equilibrium and the Gibbs' phase rule

The Gibbs' phase rule, formulated in 1876, is one of the most widely used rules in Thermodynamics. With little modification, to date, the rule has played a key role in this field of science, as it can provide the means of calculating the number of independent thermodynamic properties (Feinberg, 1979). Specifically, the Gibbs' phase rule defines the degrees of freedom, number of components and the relationship of the phases in equilibrium with each other. According to Gibbs' theory, any substance has solid, liquid and gas phases, with equilibrium boundaries between them. Such phases for moisture in freezing soil media are: ice-water-vapour and the phase stability graph for these states are presented in Figure 2.12.

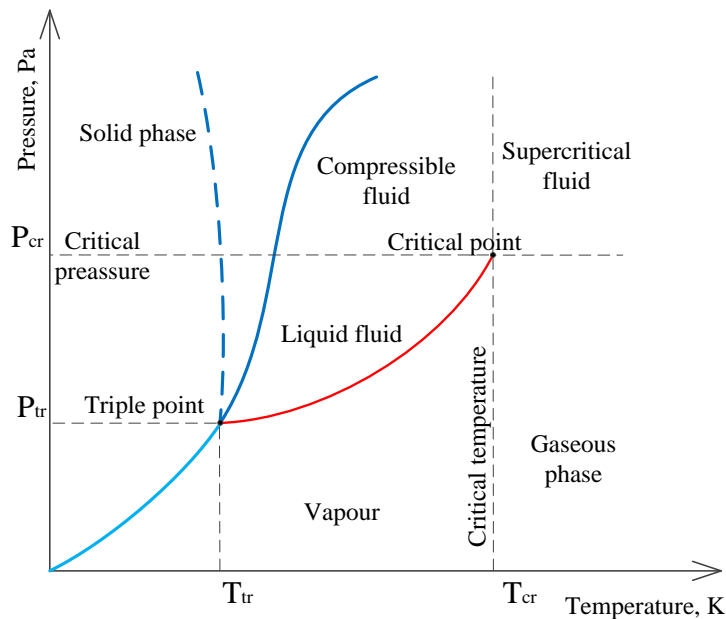


Figure 2.12– Phase diagram for a single substance system, according to Gibbs' phase equilibrium

According to Gibbs' phase rule, the number of degrees of freedom, number of phases, number of components and number of intensive variables are related to each other by the following equation:

$$f = c - p + n \quad (2.21)$$

$f$  - intensive degrees of freedom;  $p$  - number of phases, like gas, homogeneous liquid phases, homogeneous solid phases;  $c$  – number of components, which is equal to the minimum number of independent constituents; and  $n$  – number of intensive variables that can be changed independently without disturbing the number of phases in equilibrium.

### 2.6.1 Phase equilibrium for a single substance system: Clausius-Clayperon equation

The main parameters defining the freezing of soils are: pressure, temperature and volumetric deformation of the moisture during the phase transformation (Dreving, 1954). According to Gibbs' phase rule, the stability equation for a single substance (water) for two variables (temperature and pressure) is:

$$f = 1 - p + 2 \quad (2.22)$$

This means that in equilibrium state, when the number of degrees of freedom is  $f=0$ , there are three phases  $p=3$ . For general cases the number of phases might be  $p \leq 3$  (Dreving, 1954).

In the case when two phases are considered, i.e. water and gas  $f=1-2+2=1$ . This means the coexistence of water and gas is possible at any temperature, however, each temperature corresponds to a particular value of pressure.

For the material sciences, when the pressure is equal to that of the atmosphere, the equation (2.22) will have a further form:

$$f = 1 - p + 1 \quad (2.23)$$

So, the amount of substance in each phase depends on the temperature, which is possible to derive from a 2-dimensional temperature–concentration chart (Dreving, 1954).

The thermodynamic equilibrium between ice and water, based on the method of hydraulic conductivity, has been examined by scientists of the former Soviet Union countries, Europe, the U.S. and Canada (Loch and Kay, 1978). The coupled flow of heat and a liquid phase of moisture migration towards the freezing front were presented using the original form of the Clausius-Clayperon equation:

$$\frac{\Delta P}{\Delta T} = \frac{L}{T \cdot \Delta V} = \frac{\Delta s}{\Delta V} \quad (2.24)$$

$L$  - is a specific latent heat;

$T$  - the temperature;

$\overline{\Delta V}$  - is the specific volume change of the phase transition;

$\Delta s$  - is the specific entropy change of the phase transition.

For general phase transfer calculations, equation (2.24) is integrated within a temperature interval:

$$\ln \frac{P_1}{P_2} = L \left( \frac{1}{T_1} - \frac{1}{T_2} \right) \quad (2.25)$$

## 2.7 Summary

Summing up the evolution of geocryology the following stages of development have been highlighted:

- ❖ The freezing process in soils accompanied by hydraulic conductivity was a subject under consideration from the early 1930s onwards. One of the adherents of the hydraulic conductivity theory was Hoekstra (1996), who also demonstrated the advantages of the laboratory testing of freezing soils.
- ❖ The capillary theory was popular in the 1960s and 1970s, being followed by successful scientists as Miller, Penner, Everett and others ( Everett, 1961; Penner, 1967; Williams, 1968; Miller, 1972; Penner, 1977).
- ❖ Around the same time the ‘rigid ice’ model was introduced, presenting the ability of high pressure to cause ice to melt and refreeze (O'Neill, 1983).
- ❖ More recently, Michalowski and Zhu (2006) have introduced a ‘porosity function’ into their micromechanical model simulation of ice growth during frost heave.
- ❖ A number of studies were performed with the FROSTB model, developed by the U.S. Army Cold Regions Research and Engineering Laboratory in order to predict temperature and moisture changes in soil masses during freezing (Simonsen *et al.*, 1997; Shoop and Bigl, 1997). The model facilitated numerical application and represented a coupling of water and heat transfer, thus avoiding the physical explanation of the driving force.
- ❖ Further research, based on the hydraulic conductivity theory, was continued by Othman and Benson (1993), and Vidyapin and Cheverev (2008). The teamwork of scientists from China, Japan and Russia has led to them presenting their model

of the calculation of unfrozen, i.e. moveable water content, in freezing soils (Xu *et al.*, 1997).

- ❖ A kinetic approach to ice crystal nucleation and growth was considered by Bronfenbrener and Bronfenbrener (2010) and Wu *et al.* (2015).

A Further research, based on the coupled water and heat transfer model, was performed by Ming and Li (2015) and Zhang *et al.*, (2016), where Zhang *et al.*, (2016) presented a coupled water-heat transport model considering the moisture mass transfer by both liquid water and vapour fluxes.

In fact, there has been an impressive amount of studies, approaches and models developed to represent the process of mass transfer induced by low temperatures. However, the physical explanation of driving force for mass transport, the amount, speed and the state of fluxes with time is still unclear. The hydraulic conductivity based models, founded on Darcy's Law, consider the moisture mass transfer mainly in a liquid state. Consequently the issues regarding the surface tension, pore pressure and phase equilibrium remain unresolved. Based on laboratory testing and field observations, it is clear that frost heave occurs in soils with particle size less than 0.05 mm, that is silty and clayey soils. Whilst the pore size in these soil types is also small, the surface tension is great (Arenson *et al.*, 2008).

The thermodynamic based models do not consider a driving force at all, substituting it with the ability of soils to expand at low temperatures, and a similar approach has been pursued in coupled heat-water based models. Intensification of technical support and numerical modelling has facilitated the empirical approaches to the study of mass transfer during freezing and their prognosis. However, no uniform approach or estimation model for mass transfer prediction has yet been developed. In fact, moisture mass transfer in a vapour state has been widely neglected in freezing soils and the rare attempts at considering the gaseous component using the water and heat coupled model (Zhang *et al.*, 2016), have not taken into account the driving force of the moisture transport.

The temperature field distribution in highway subsoils significantly differs from that in the roadside area, because the loading on the former has an extra dynamic component and increased overburden pressure. Consequently, the increased thermal conductivity of pavement materials leads to enlarged temperature gradient and significant

frost heave. According to Simonsen *et al.* (1997), pavement materials are not impermeable during cold periods and their condition depends on the level of precipitation. In order to improve the adhesive properties on roads during the winter, pavement surfaces often have de-icing chemicals applied, being the most effective and cheapest way of ice removal.

The chemical mass transfer induced by temperature gradient is still disputed. Previous studies have reported contradictory evidence for the chemical mass transfer within soils during unidirectional freezing: Vidyapin and Cheverev (2008), in their experiments, confirmed the migration of de-icing chemicals towards the freezing front, while Brouchkov (2000) in his long term experiments, detected no obvious salt migration during the freezing period. It is also unclear how the application of de-icing chemicals' impacts on initially non-saline soils. However, the temperature field distribution and the chemical-moisture mass transport in the freezing soils are beyond the scope of this research.

Overall, these studies highlight the need for:

- ❖ Detailed temperature-moisture observations of freeze-thaw cycles in sample of increased length and with a slow freezing technique;
- ❖ Research with a focus on the vapour mass transfer within the isolated soil pore space;
- ❖ Study of de-icing chemical mass transport induced by unidirectional freezing;
- ❖ Consideration of the conceptual model of frost heave, taking into account the vapour mass transfer and the phase transformations.

### 3 METHODS AND MATERIALS

#### 3.1 Introduction

Based on the literature, it is evident that de-icing chemicals when applied to pavement surfaces also settle on the ground beyond the road pavement, thus leading to their accumulation in roadside soils and producing secondary salinisation of the ground water (Hart *et al.*, 1991; Norrström and Jacks, 1998; Lundmark and Olofsson, 2007). To simulate highway conditions with de-icing chemicals in winter, remolded non-saline samples have been supplied from the base with a chemical solution and compared with the samples supplied with de-ionised water. The method, using freeze-thaw cycles, was developed from the ASTM D 5918-06 Standard and included some principal changes. To improve the temperature gradient observations during the freeze-thaw cycles it was decided to increase the soil samples length to 1 m (Figure 3.1).

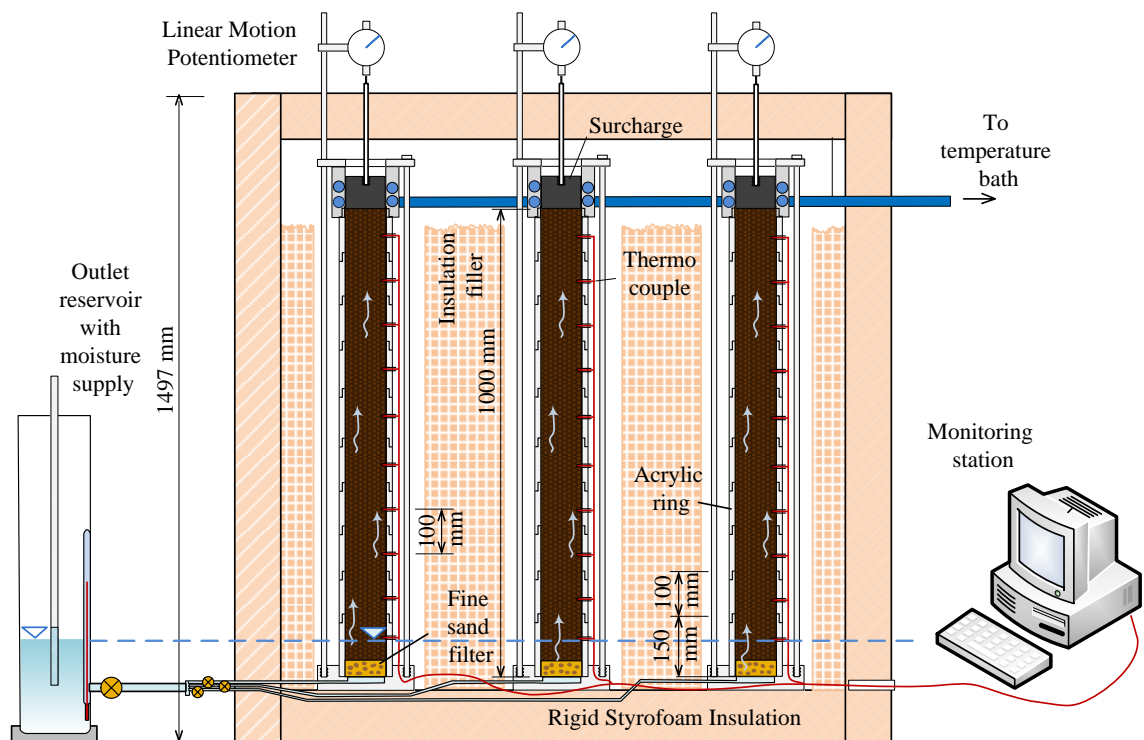


Figure 3.1 - Environmental chamber for freeze-thaw cycles with nine soil sample capacity

Several studies have indicated that using a slow freezing rate results in frost heave in the soils similar to natural conditions (Simonsen and Isacsson, 1999; Grigoryev and Shabarov, 2012). Consequently, it was decided to run the freezing cycles with 2 °C temperature reductions per day. To implement these requirements, it was necessary to



design an environmental chamber equipped with soil samples of increased length and slow freezing techniques in order to approximate the testing conditions to be close to those encountered in natural highway subsoils. An ‘open system’ was used in the freeze-thaw experiments that allowed for de-ionised water or chemical solution to be fed from the base of the column.

### 3.2 Environmental chamber design

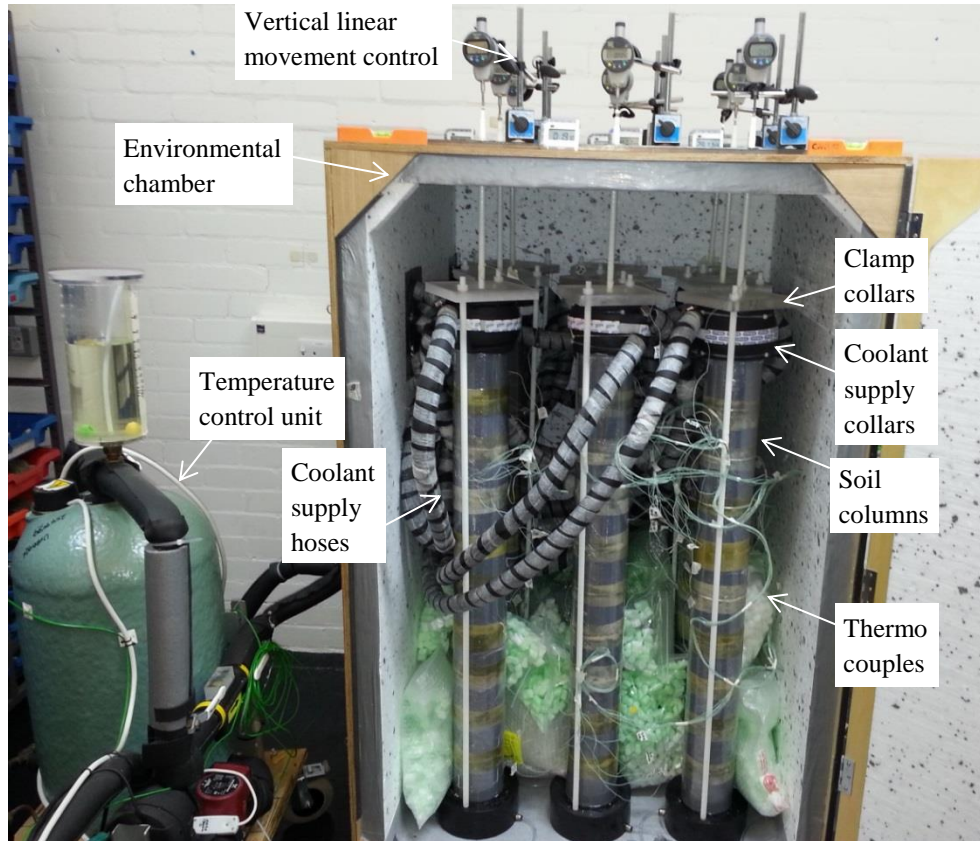


Figure 3.2 – Environmental chamber for freeze-thaw cycles with a capacity of nine 1m length soil columns

The increased capacity environmental chamber was designed and built to enable the testing of nine soil columns at a time each of 10cm diameter and of lengths 1m and 0.5m (Figures 3.2 and 3.3). Each soil column was equipped with a basement water supply from the reservoir and an air tap fitted at 10cm above from the base, allowing the excess air pressure to be released as the column filled with water. The bottom 5cm of the test soil sample was kept saturated during the test, while the other 95cm remained in an unsaturated condition. To provide the uniform distribution of water supply over the

sample cross section, the feed was provided via a 5cm thick fine sand filter layer at the base of the column (Figure 3.1).

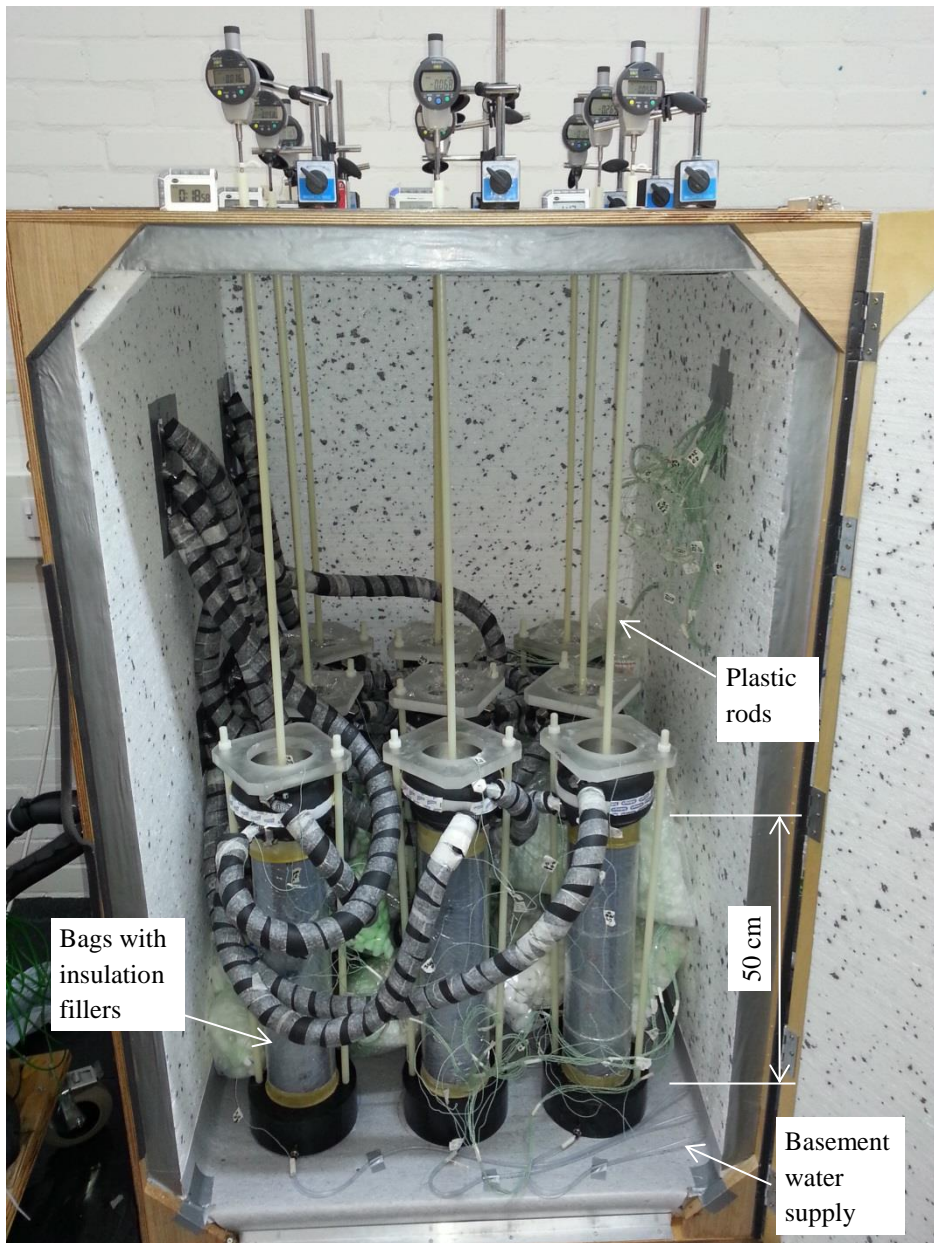


Figure 3.3- Experimental settings for 50 cm length samples with variable density

Volume change of the sample during frost heave was permitted only in the vertical direction. The observation of the vertical linear movement was via plastic rods screwed into metal surcharge caps resting on the top of the soil surface and monitored from the top of the rods with digital dial gauges located outside the chamber lid (Figure 3.3). When frost heave or settlement occurred the plastic rods were sliding through the perforated hole in the chamber roof. The digital dial gauges were set outside the environmental chamber to ensure thermal insulation during the freeze-thaw cycles. The metal caps

provided surcharge pressures of 3.5 kPa and were inserted inside the cooling ring, which was lubricated to reduce friction during sliding and to provide better thermal conductivity between the cooling elements. They also contributed to ensuring that the temperature was even over the top layer of the soil. To prevent condensation on the cooling elements and possible freezing into ice the metal surcharges were covered with cling film on the top surface.

Cold temperature distribution was implemented by forced glycol circulation using elastic silicon pipes between the temperature control unit and chilling collars on the top of the soil samples (Table 3.1, n.3). The cooling unit had an automatic temperature regulator, which was manually set once a day and a temperature control unit to keep the temperature within the fixed range (Figure 3.2). The distribution valves and manifolds, enabling the control of glycol flow circulation, were mounted on the side of the environmental chamber (Figure 3.4 c). Each cooling element was thoroughly wrapped with pipe insulation (Table 3.1, n.2). The temperature data logs were mounted on the other side of the environmental chamber and connected to 96 thermocouples through the perforated inlets (Table 3.1, n.4). The temperature was recorded hourly using a data logger for the full period of the tests.



Figure 3.4 – Preparation of the experiment: a – perforation of a plastic mold for thermocouple insertion; b – surcharge sliding inside the chilling collar; c – cooling system control manifolds

The base water supply reservoir was located in a fridge at a stable temperature of +4 °C and connected with 7mm diameter clear elastic pipes to the water distribution manifolds also mounted on the side wall of the chamber (Table 3.1, n.5). The water connection took place in stages of three samples at a time.



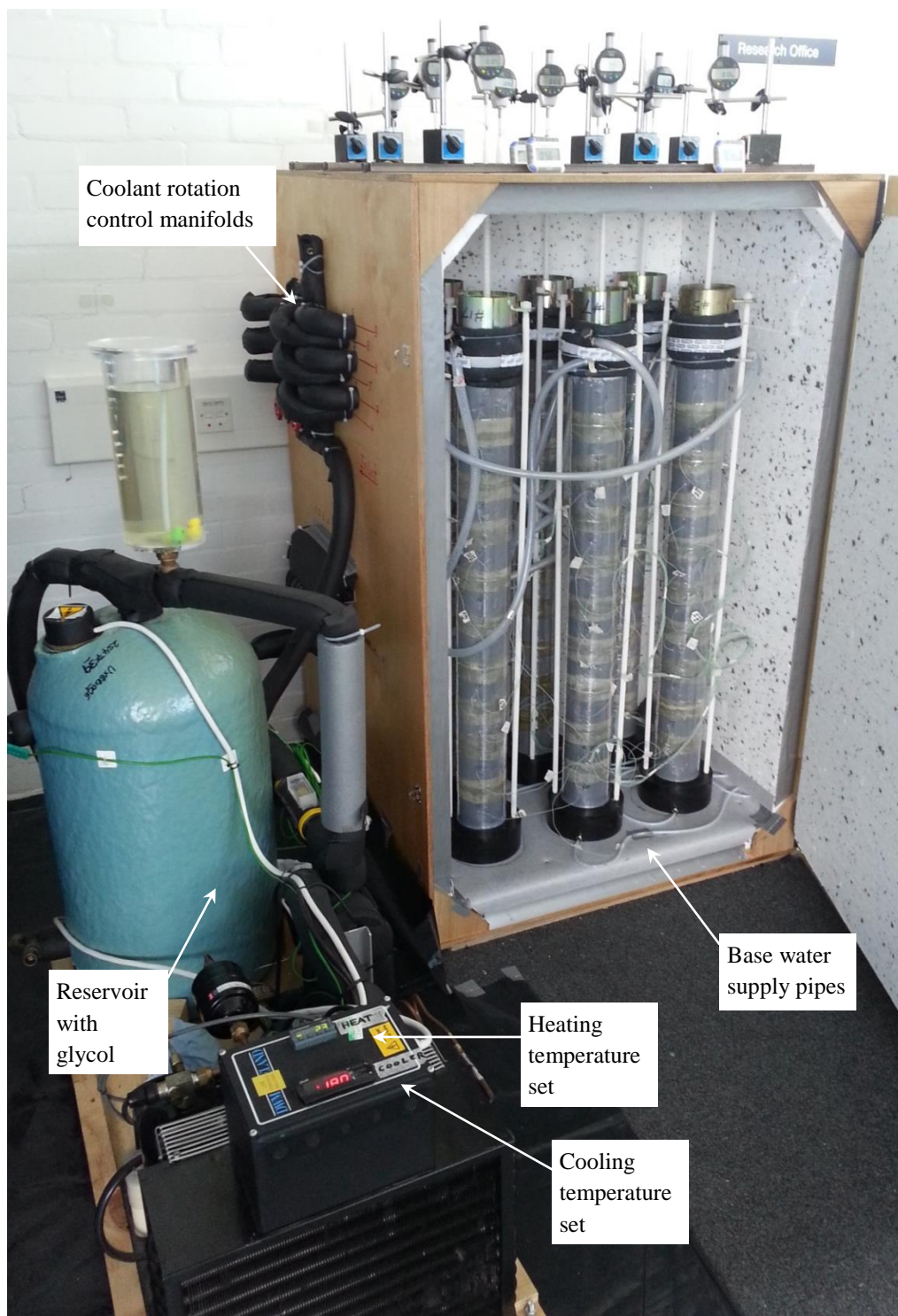


Figure 3.5 – Temperature control unit with a glycol reservoir

Glycol circulation between the temperature control unit and the chilling collars and its mutual position is presented in the Figure 3.5.

Table 3.1 – Environmental chamber equipped elements


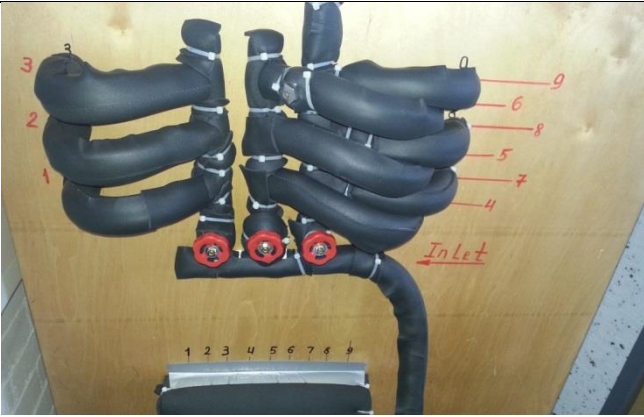


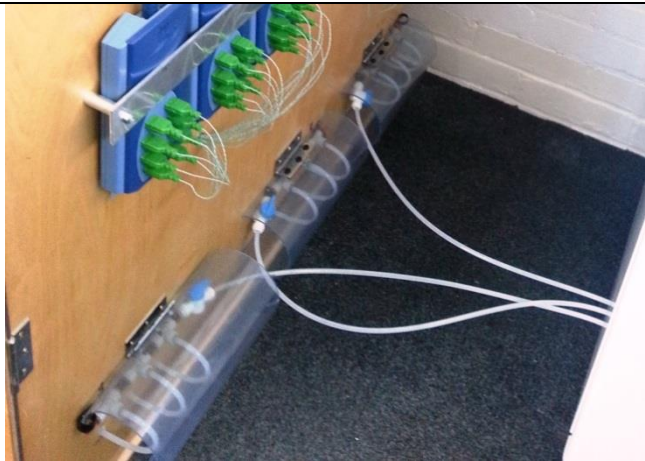
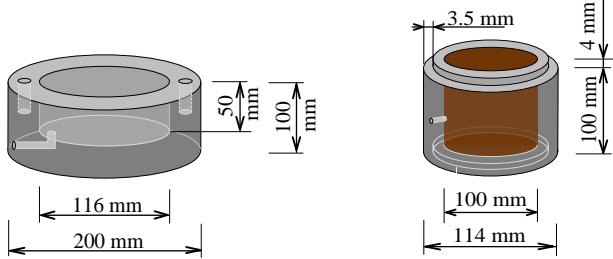
<p>1</p>	<p>Vertical linear movement observation during the setting period.</p>	
<p>2</p>	<p>Coolant supply rotation control.</p>	
<p>3</p>	<p>Temperature control unit with a glycol reservoir.</p>	
<p>4</p>	<p>Temperature monitoring with Pico loggers.</p>	

Table 3.1 continued

5	Basement water distribution pipes	
6	Soil mould elements sketch	

### 3.3 Soil modelling and classification tests

The soil samples were prepared to simulate the engineering properties of soil from Astana, Kazakhstan. Local soils of the area presented the ancient sedimentary rocks, which comprise irregular thicknesses of residual layers and alluvium depositions, according to borehole data from Karaganda GIIZ (Tulebekova *et al.*, 2012; Zhussupbekov *et al.*, 2016). The recorded properties of the Astana soils were replicated in the remoulded soil samples, which were mixed using equal proportions of sharp sand of less than 2mm and kaolinite clay by dry mass. The particle size analysis of the sand part of the soil was performed by dry sieving in accordance with BS 1377-2:1990. Three samples were taken of the sand for sieve analysis and the results are presented in Appendix A, Figure A.1. The accepted grading curve in Figure 3.6 shows the sand to be uniformly-graded with a uniformity coefficient  $C_u=2.4$  and a coefficient of curvature  $C_c=3.65$  (Appendix A). Also, neither of the criteria for sand  $C_u \geq 6$  and  $1 < C_c < 3$  were met and therefore, the sand part of the soil was classified as SP or poorly graded sand.



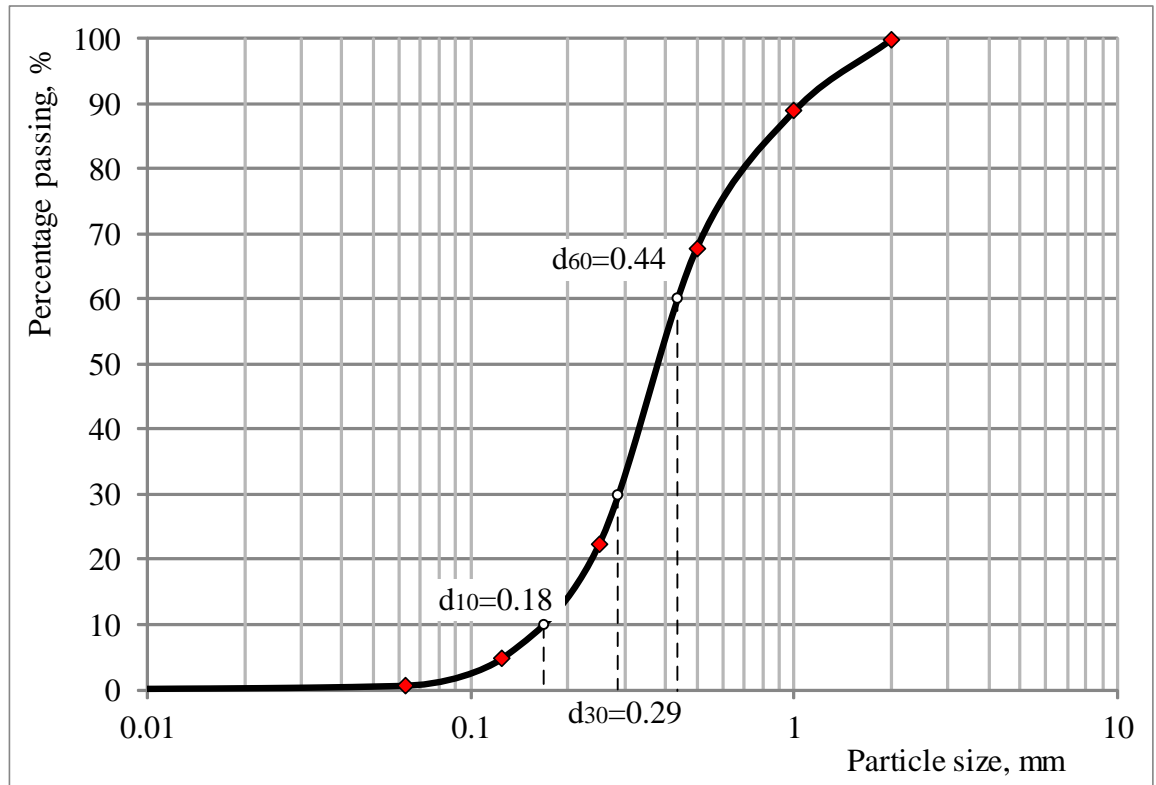


Figure 3.6 – Particle size analysis of the sand part in the modelled soils, determined by dry sieving

To ensure the accuracy of the dry density – moisture relation eight standard proctor tests were conducted according to the BS1377-4:1990 standard proctor test with a 2.5kg rammer with a moisture range  $W=11.7-23.23\%$  (Figure 3.7). The graph also shows 0%, 5% and 10% air void lines (BS 1377-4:1990, 1990). The moisture content for the sample preparation was taken as the value corresponding to 95% of the maximum dry density in Figure 3.7. According to the proctor test, the maximum dry density was equal to  $1.89 \text{ Mg/m}^3$ , while 95% of this value was found as  $1.80 \text{ Mg/m}^3$ . Hence, the corresponding moisture content for the preparation of soil samples was taken as 17.2% and the bulk density value corresponding to this percentage was  $2.11 \text{ Mg/m}^3$ .

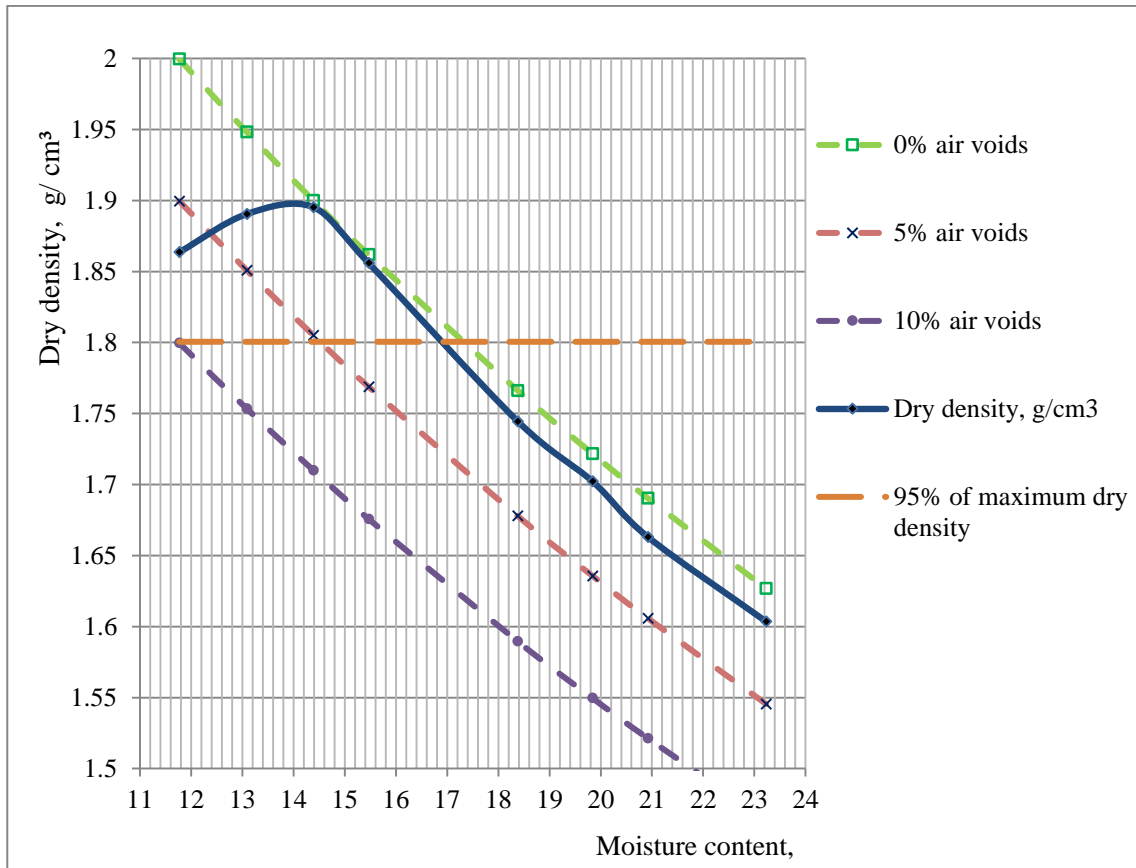


Figure 3.7 - Dry density – moisture content curves for sandy clay with 2.5 kg rammer compaction test

A direct shear test was conducted, according to BS 1377-7:1990, with 60x60mm sample preliminary consolidated with 5, 10 and 15kg load, which corresponds to 136.25, 272.5 and 408.75 kN/m<sup>2</sup> pressure on the sample. The beam ratio was 1:10. A machine displacement speed of 0.5mm/min was applied, which is less than the recommended maximum displacement rate by BS 1377-7:1990. The minimum time to failure  $t_f$  was found by the equation:

$$t_f = 12.7 \cdot t_{100} = 12.7 \cdot 1.0 = 12.7 \text{ min} \quad (3.1)$$

where,  $t_{100}$  – is the final point on primary consolidation by square-root time plot in mm.  $t_{100} = 1.0 \text{ mm}$  (Appendix A, Figure A.2).

The likely horizontal shear formation was taken as 15min. The maximum displacement rate was found by the formula:  $\frac{t_f}{t_{horiz}} = \frac{12.7 \text{ mm}}{15 \text{ min}} = 0.8 \text{ mm/min}$ .

The maximum obtained shear stress  $\tau$  was found for all loading sets by the equation:



$$\tau = \frac{C_R \cdot R}{L^2} \cdot 1000 \text{ kPa} \quad (3.2)$$

where,  $L$  – length of the side of the shear box, 60mm here and the continual change in the area of contact is not formally taken into account (BS 1377-7:1990);

$C_R$  – the load ring calibration  $C_R = 2162.5 \text{ N}$  per 1mm of division on the loading ring dial gauge;

$R$  – reading of the loading ring in mm.

The normal stress  $\sigma_n$  corresponding to the maximum value of shear stress was found by the formula:

$$\sigma_n = \frac{9.81 \cdot W}{L^2} \cdot 1000 \text{ kN/m}^2 \quad (3.3)$$

where,  $W$  – total load applied to the specimen in kg.

According to consolidated drained direct shear test for the sample with moisture content  $W=17.2\%$  and dry density  $\rho_{dry} = 1.80 \text{ Mg/m}^3$ , the angle of internal friction obtained was  $\varphi = 24^\circ$  and the cohesion  $C = 10 \text{ kN/m}^2$  (Figure 3.8). Initial bulk density of the specimen  $\rho = 2.11 \text{ Mg/m}^3$ , void ratio  $e_0 = 0.45$  and the degree of saturation  $S_0 = 99.4\%$ .

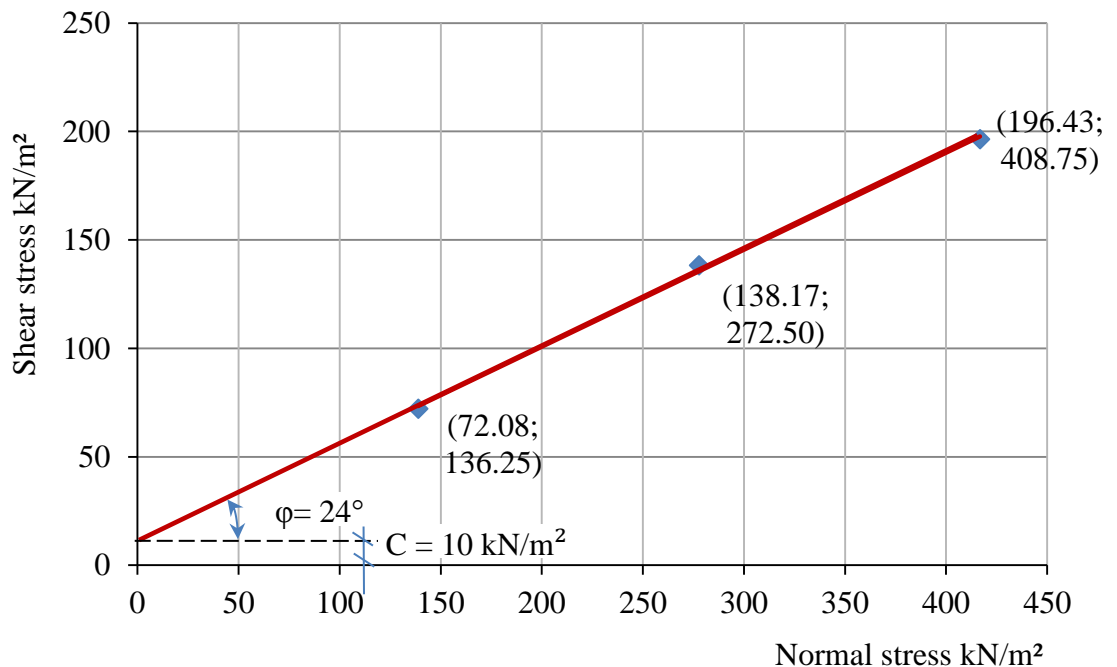


Figure 3.8 – Direct shear results for 17.2% moisture content sandy clay soils with particle size less than 2mm

A sequence of tests for the California Bearing Ratio (CBR) was performed for a moisture content range from 14 % up to 22 % (Figure 3.11). The soil samples were compacted using a 2.5kg proctor rammer into a 152±0.5mm diameter and 127mm high cylindrical CBR mould, in three layers with 62 blows to each (Head and Epps, 2011; BS 1377-4:1990, 1990). A surcharge of 2.5kg weight was applied the soil surface to simulate the overburden pressure from the pavement materials during the CBR test and pushed by a metal plug using a triaxial machine rig (Figure 3.9). A constant rate of penetration plunger of 50mm diameter was pushed with a 1.2mm/min displacement rate. The measured penetration force at 2.5mm, 5mm and 7.5mm was compared with the appointed 'standard' force. The percentage ratio of the load-penetration relationship forces is presented in Figure 3.10. Each test was performed from both ends of the mould.

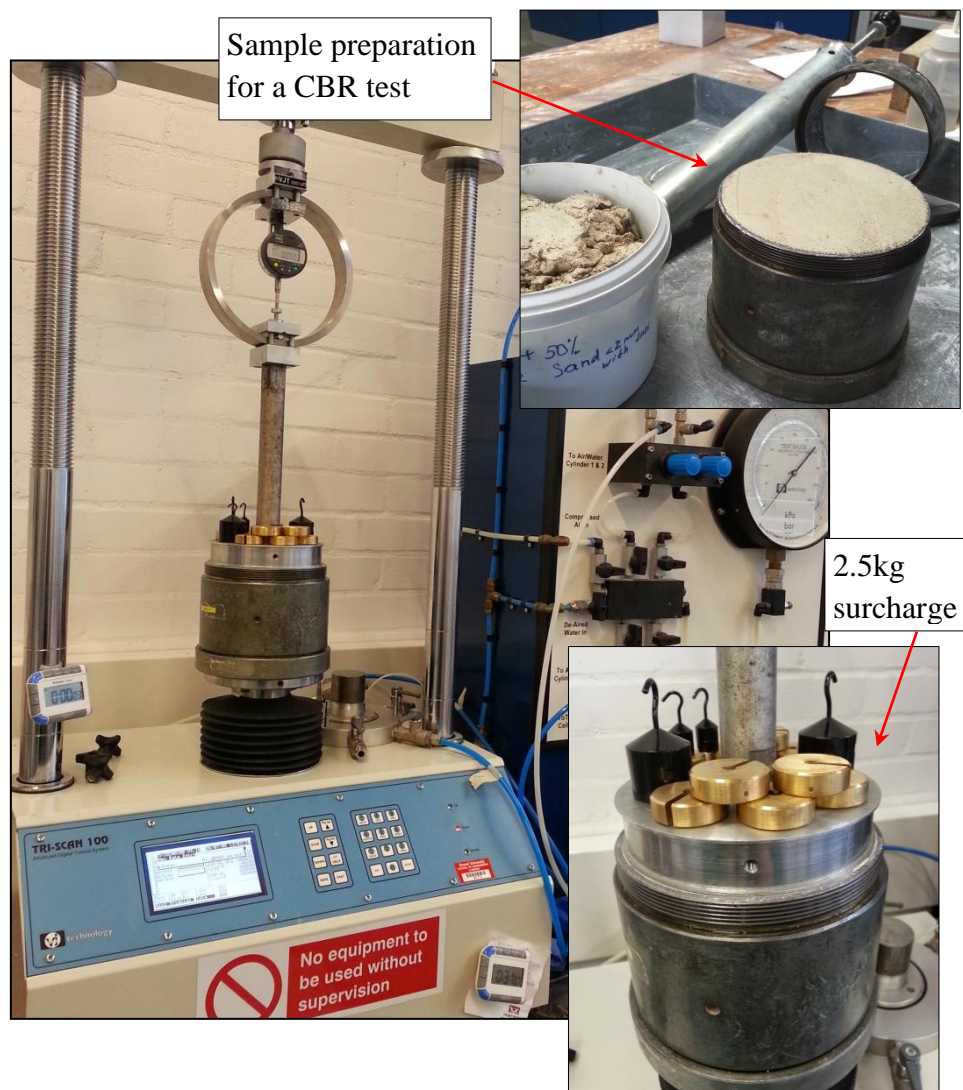


Figure 3.9 - California bearing ratio test on the triaxial machine rig

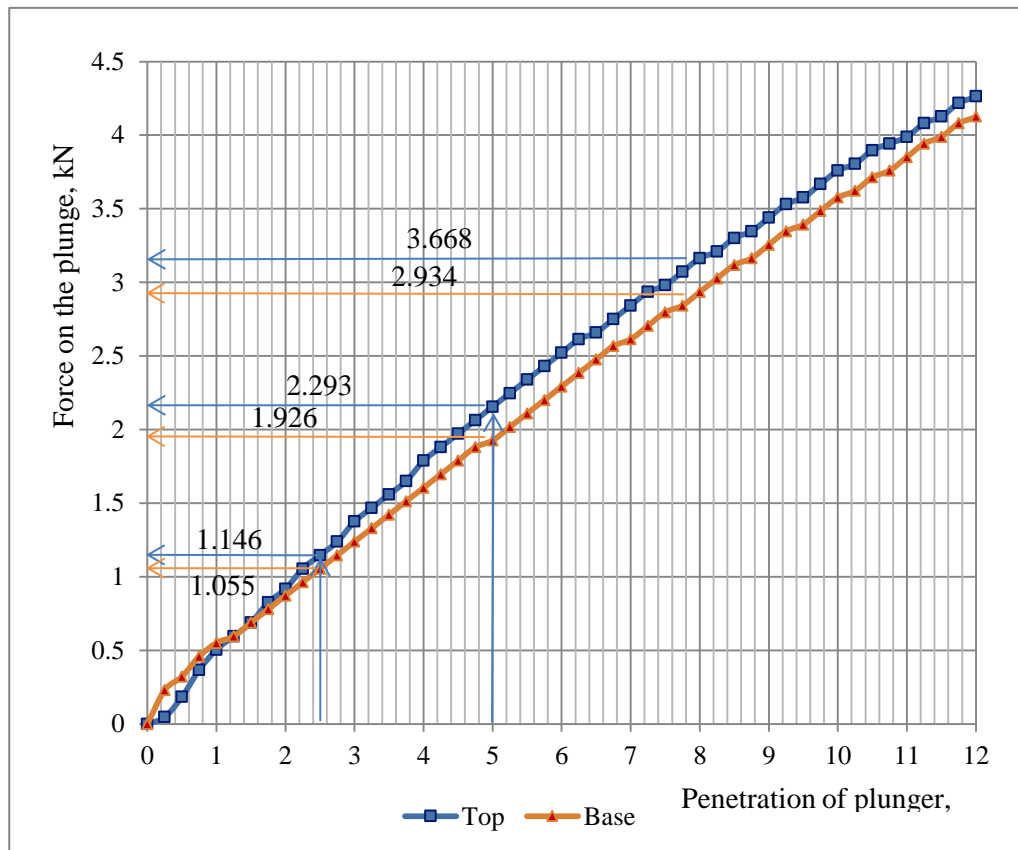


Figure 3.10 – Load-penetration curve for CBR for a moisture content of  $W=17.6\%$

Table 3.2 – California Bearing Ratio test results when moisture content is  $W=17.6\%$

Loading side	Penetration, mm	Load, kN	Standard load, kN	CBR, %
Top	5	2.3	20	10.8
Base	5	2.0	20	9.6

The range of CBR values for the test soil directly depended on the moisture content. The load-penetration curve in Figure 3.10 reports the CBR test results for the 17.6 % moisture content soil samples presented in Table 3.2. A general relationship between CBR and moisture content for the BS ‘light compaction’ sandy clay is presented in Figure 3.11, where CBR is plotted on a logarithmic scale. The CBR value corresponding to moisture content  $W=17.2\%$  was obtained from Figure 3.11 by interpolation, and presented 14 % of the ‘standard’ force of 20 kN for 5 mm penetration (BS 1377:4:1990, 1990).

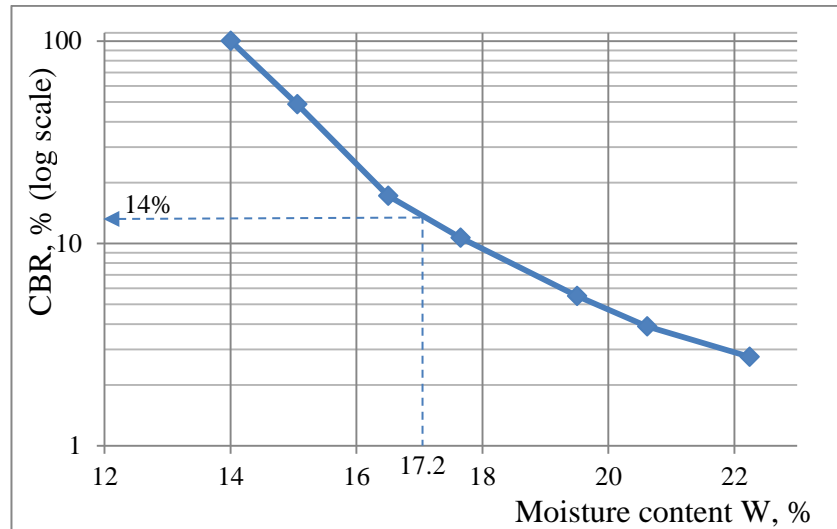


Figure 3.11 – CBR – moisture content relationship curve

The particle density test or specific gravity of the sample was obtained according to BC 1377:1990:2 section 8.3 by the small pycnometer method for each soil component separately:  $G_s = 2.501 \text{ Mg/m}^3$  for kaolinite clay and  $G_s = 2.646 \text{ Mg/m}^3$  for the sand (Figure 3.12a). For the soil mixture containing 50% kaolinite and 50% sand by dry mass equivalent the specific gravity is  $G_s = 2.615 \text{ Mg/m}^3$ .



Figure 3.12 – Specific gravity test by the small pycnometer method:

a – filled with a sample and de-ionised water, b – in a desiccation camera

The mass of the soil samples and the density bottles were weighted with high resolution balances. After placing a portion of each soil sample into the density bottles, they were filled with de-aired water. The existing air was removed from the bottles by placing them into the vacuum desiccator with a protective cage for  $-25 \text{ kPa}$ , where they were kept for 1h without lids (Figure 3.12 b). The particle density was found as the ratio

of the displaced water mass and the bottle weight difference filled just with water and the soil added (BS 1377-1: 1990:, 1990; BS 1377-2:1990, 1990).

$$\rho_s = \frac{\rho_L(m_2 - m_1)}{(m_4 - m_1) - (m_3 - m_2)} \quad (3.4)$$

where,  $\rho_L$  - density of the liquid used, at the constant temperature;

$m_1$  – mass of density bottle in g;

$m_2$  – mass of bottle and dry soil in g;

$m_3$  – mass of bottle, soil and liquid in g;

$m_4$  – mass of bottle and liquid, in g.

A linear shrinkage test, according to BS 1377: Part 2: 1990: 6.5, was conducted on that part of the soil sample, which passed through a 425  $\mu\text{m}$  sieve (Head, 2011). The linear shrinkage for each specimen was found by the following equation:

$$L_S = 100\left(1 - \frac{L_D}{L_0}\right) \quad (3.5)$$

where,  $L_S$  – linear shrinkage as a percentage of the original length of the specimen;  $L_D$  – length of oven-dry specimen in mm; and  $L_0$  – initial length of the specimen in mm.

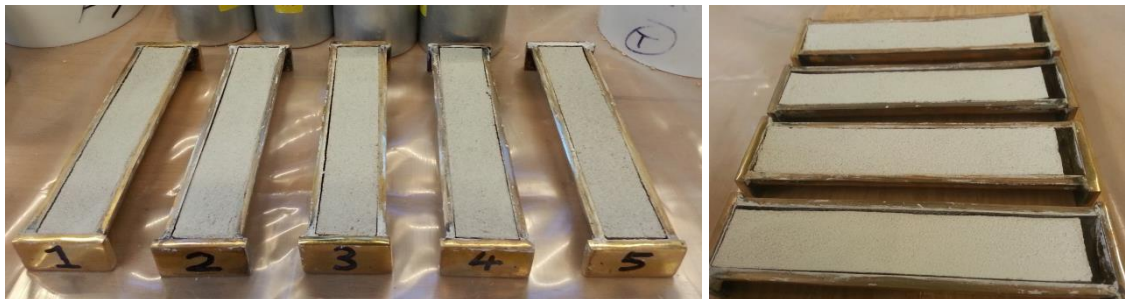


Figure 3.13 – Linear shrinkage

The average linear shrinkage for the five specimens compiled is 4.95 % (Figure 3.13). The classification test results, obtained before freeze-thaw cycle testing, are presented in Table 3.3

Table 3.3 – Initial soil characteristics and soil tests following the procedures in BS1377-1:1990

Characteristic	Symbol	Unit	Value	Annotation
Initial moisture content	$W$	%	17.2	See Figure 3.1 – according to 95% max. dry density – moisture content relationship
Angle of internal friction	$\phi$	°	24.1°	CD direct shear test, moisture content $W=17.2\%$
Cohesion	$C$	kN/m <sup>2</sup>	10	
Particle density of sandy clay	$\rho_s$	Mg/m <sup>3</sup>	2.615	Soil mixture by mass: 50% sand and 50% kaolinite
Average dry density before freezing cycle	$\rho_d$	Mg/m <sup>3</sup>	1.814 ± 0.012	BS Light compaction test operating with 2.5 kg rammer. The mechanical energy applied to the soil is 596 kJ/m <sup>3</sup>
Initially bulk density at the beginning of the test	$\rho$	Mg/m <sup>3</sup>	2.128 ± 0.015	
Uniformity coefficient	$C_u$	-	2.4	Uniformly-graded sand
Coefficient of curvature	$C_c$	-	3.65	
Activity of Clays	$A$	-	0.25	Inactive clays
Liquid limit	$w_L$	%	37.18	CI – Medium plasticity cone penetrometer test used
Plastic Limit	$w_P$	%	23.77	Fraction of soil sample passed through 0.425 mm sieve
Average linear shrinkage	$L_S$	%	5	
Plasticity Index	$PI$	%	13	

### 3.4 Sample preparation

A proportional amount of water corresponding to 17.2 % was added to the dry mixture of equal parts of kaolinite clay and sand, and then blended manually to a uniformly mixed state. The prepared soil samples were kept sealed for at least 48 hours to allow the moisture to be distributed evenly throughout the volume before filling the mould. The assembled plastic mould contained 10 acrylic rings, 10cm in diameter each. The length of the base ring was 15cm, the extra 5 cm of which was used for a sand filter material. The remaining nine rings were each 10cm in lengths and 7,854cm<sup>3</sup> in volume. The initial mould height was built from three acrylic rings, while the rest were added during compaction, as the length of the soil sample increased (Figure 3.14). The lowest ring was inserted into a solid acrylic base with a thick layer of silicone rubber gel and left to dry for 24 hours. A latex sleeve was also used as an extra layer of isolation. Before filling the base with filter material, the lowest acrylic ring was filled with water and tested for leaks (Figure 3.15).



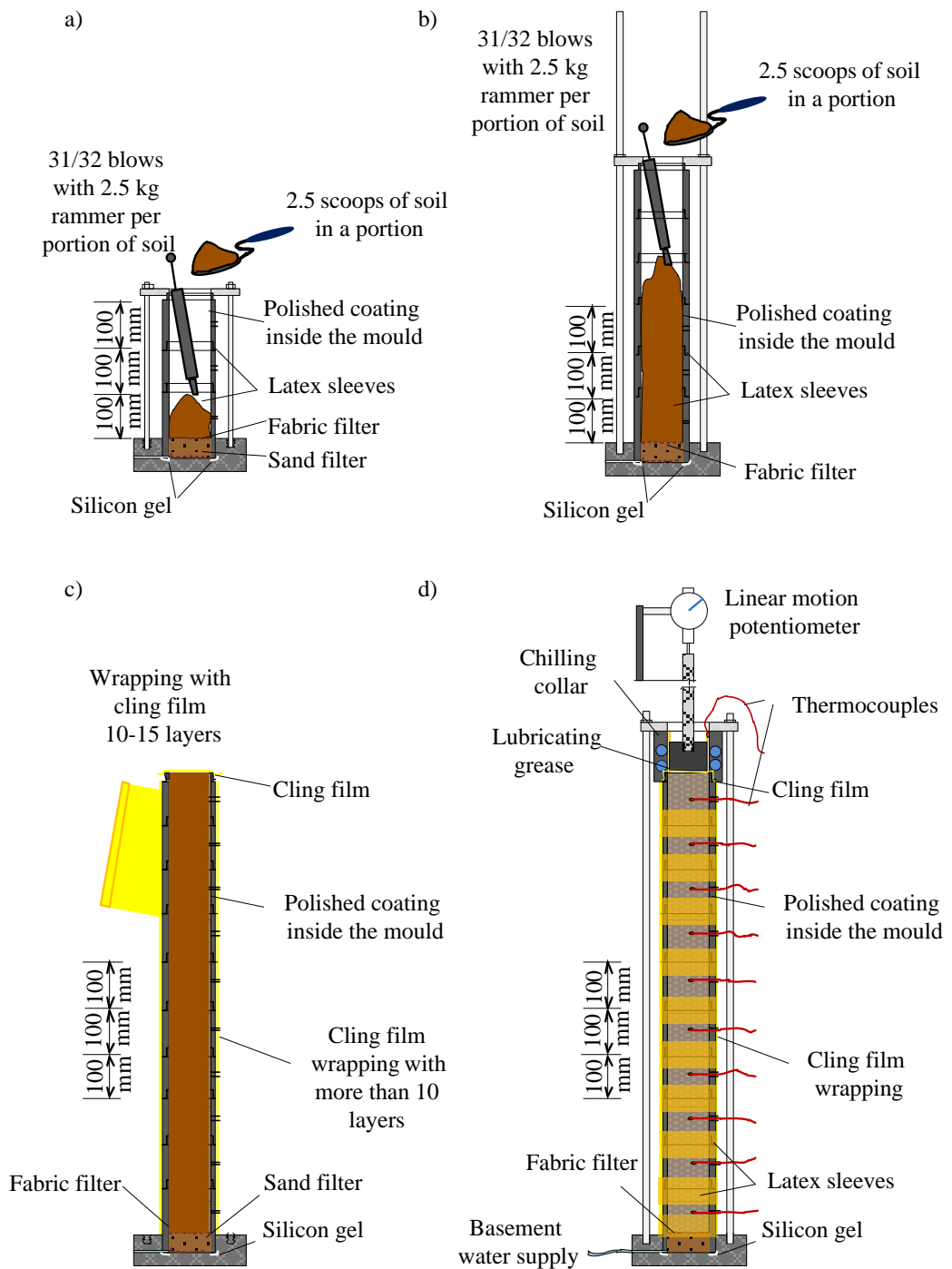


Figure 3.14 – Sample preparation

After testing for leaks a fabric filter was placed inside the base and fixed with silicone rubber gel from the edges, so that the sand could not block the drainage and water supply inlet tubes. After filling the base ring with 5cm of sand another fabric filter was placed on it, thus separating the sample material from the sand filter. To reduce the friction between the soil sample and the assembled acrylic rings the inner surface of the mould had a polished coating. Whilst such arrangement could not exclude friction

between the soil and the mould completely, it did prevent excessive mechanical disruption from having to transfer from the compaction mould to the testing form in series. It also provided a consistent compaction of the soil sample over the 1m length. The connections between the rings were sealed with a rubber silicone gel and latex sleeves. Next, the compacted soil columns were wrapped thoroughly over the entire length with 10-15 layers of cling film, along with measures to provide moisture insulation, i.e. covering the connections with rubber silicone gel and latex sleeves (Figure 3.16).



Fig 3.15 – Testing for leaks before assembling the mould





Figure 3.16 – Sample weighing

After the soil column was compacted, labelled and weighed, it was put into the environmental chamber and connected from the base to the water supply reservoir. The thermocouples were inserted into the sample through a 1.5 mm hole drilled in the middle of each plastic ring and connected to the data logger (Figure 3.4 a, Table 3.1). The cooling elements were fixed at the top of the sample and simultaneously, the surcharges of 3.5 kPa were applied to simulate the overburden pressure from the pavement material (Figure 3.4 b). The soil samples were kept for 24-36 hours for temperature stabilisation at +3 °C and consolidation settlement with the applied overburden pressure. The perforated tubes of 2.0mm diameter and 7mm length were inserted into the base ring in order to let the excess air pressure be released during the stabilisation of the water table level at 10cm from the base (5cm of which was the sand filter and 5 cm was the saturated level of the sample).

### **3.5 Initial density parameters of the soil samples before testing**

The compaction of the soil was in accordance to BS1377-1:1990. The number of blows applied per 10cm diameter and 10cm length section was corresponding to the compactive effort. A standard proctor test was conducted with a 2.5kg rammer in the assembled mould for the freeze-thaw cycles. In tests 1 and 2 all columns were compacted

with maximum dry density corresponding to a 17.2% moisture content. 63 blows per a section volume, each being subdivided into two layers of 5cm and compacted with 31/32 blows by rotation. The air void content under the applied compaction procedure was close to “zero” and the soil sample was very close to the fully saturated state. The internal volume of variation in the assembled plastic mould might have slightly differed due to the sand filter volume. The initial mass, volume and density parameters in tests 1 and 2 are presented in Tables 3.5 and 3.6.

Table 3.4 –Soil characteristics before the freeze-thaw cycles in test 1

Column number	Average volume in a mould, cm <sup>3</sup>	Weight of assembled column with metal base and plastic collars, g	Weight of the compacted sample in the mould before test, g	Weight of soil before test, g	Bulk density before the test, Mg/m <sup>3</sup>	Dry density before the test, Mg/m <sup>3</sup>
#1	7,933	5,495	22,281	16,786	2.108	1.797
#2	7,933	5,495	22,236	16,741	2.110	1.799
#3	7,933	5,495	22,216	16,721	2.108	1.797
#4	7,933	5,495	22,200	16,705	2.106	1.795
#5	7,933	5,495	22,226	16,731	2.109	1.798
#6	7,933	5,495	22,240	16,745	2.111	1.800
#7	7,933	5,495	22,252	16,757	2.112	1.801
#8	7,933	5,495	22,209	16,714	2.107	1.796
#9	7,933	5,495	22,254	16,759	2.113	1.801

Table 3.5 –Soil characteristics before the freeze-thaw cycles in test 2

Column number	Average volume in a mould, cm <sup>3</sup>	Weight of assembled mould with sand filter layer, g*	Weight of the compacted sample in the mould before test, g	Weight of soil before test, g	Bulk density before the test, Mg/m <sup>3</sup>	Dry density before the test, Mg/m <sup>3</sup>
#1	7,948	5,440	22,181	16,741	2.106	1.796
#2	7,909	5,494	22,128	16,634	2.103	1.793
#3	7,893	5,494	22,091	16,597	2.103	1.793
#4	7,956	5,450	22,089	16,639	2.091	1.783
#5	7,885	5,494	22,093	16,599	2.105	1.795
#6	7,940	5,494	22,201	16,707	2.104	1.794
#7	7,893	5,494	22,152	16,658	2.110	1.799
#8	7,956	5,450	22,107	16,657	2.094	1.785
#9	7,940	5,494	22,133	16,639	2.095	1.786

\* Weight and volume of the mould might vary slightly depending on the sand filter weight, although they were balanced in most columns before filling with soil

As can be seen in Table 3.7, the samples were compacted with increasing order of dry density between the columns. To obtain the uniform distribution of the material within the volume, an equal amount of soil (by scoops) was compacted with the same energy effort over the sample length. For example, in Test 3 each portion of 2.5 scoops of soil was pushed with a purpose-made 15 kg compacter throughout the column. The applied effort was consistent over the sample length and the cross section of the compacter was equivalent to the inner diameter of the acrylic mould. The achieved dry density in column #1 was equal to 1.178 Mg/m<sup>3</sup>. The compacting procedure for each soil column in Test 3 is presented in Table A.5. In column #2 every portion including 2 scoops of soil was pushed twice with the 15 kg compacter throughout the sample. As a result, the initial density in sample #2 increased to 1.302 Mg/m<sup>3</sup>. The density of each further sample was higher than in the previous column. In column #5 and further a standard proctor test 2.5kg rammer was used. The number of blows was reduced by 3 for every 2.5 scoops of soil, which is equal to 5cm of compacted material in terms of length. In column #6 it was 5 blows of a 2.5 kg rammer, whilst in column #7 it was 8 blows and in column #8 it was 15 blows per each 2.5 scoops portion of soils used. In the last column #9, the full energy effort standard proctor test of 31/32 blows with the 2.5 kg rammer per 2.5 scoops of soil material was applied.

Table 3.6 – Variable density distribution within the soil samples in test 3

Column number	Average volume in a mould, cm <sup>3</sup>	Weight of assembled mould with sand filter layer, g	Weight of the compacted sample in the mould before test, g	Weight of soil before test, g	Dry density before the test, Mg/m <sup>3</sup>
#1	3,966	4,121	9,602	1,382	1.178
#2	3,966	4,105	10,160	1,527	1.302
#3	3,966	4,117	10,372	1,577	1.345
#4	3,966	4,120	10,961	1,725	1.471
#5	3,966	4,095	11,201	1,792	1.527
#6	3,966	4,115	11,591	1,885	1.607
#7	3,966	4,110	11,792	1,937	1.651
#8	3,966	4,114	12,466	2,106	1.795
#9	3,966	4,122	12,485	2,109	1.798

The same compacting procedure was used in Test 4 and 5. The dry density was increasing from being loose in column #1 to the densest in column #9. The compaction procedure used in Tests 4 and 5 are presented in Tables A.6 and A.7. The aim of the varied dry density design between the soil columns was to cover all the possible range for dry density variation in the testing soils and to study the frost heaving, heat and mass transfer during the freezing cycles.

Table 3.7 – Variable density distribution within the soil samples in test 4

Column number	Average volume in a mould, cm <sup>3</sup>	Weight of assembled mould with sand filter layer, g	Weight of the compacted sample in the mould before test, g	Weight of soil before test, g	Bulk density before the test, Mg/m <sup>3</sup>	Dry density before the test, Mg/m <sup>3</sup>
#1	3,958	4,105	10,072	5,967	1.507	1.285
#2	3,958	4,121	10,202	6,081	1.536	1.310
#3	3,958	4,115	10,498	6,383	1.613	1.375
#4	3,958	4,095	10,837	6,742	1.703	1.452
#5	3,958	4,117	11,096	6,979	1.763	1.503
#6	3,958	4,120	11,231	7,111	1.796	1.531
#7	3,958	4,110	11,747	7,637	1.929	1.645
#8	3,958	4,114	11,931	7,817	1.975	1.684
#9	3,958	4,122	12,382	8,260	2.087	1.779

Table 3.8 – Variable density distribution within the soil samples in test 5

Column number	Average volume in a mould, cm <sup>3</sup>	Weight of assembled mould with sand filter layer, g*	Weight of the compacted sample in the mould before test, g	Weight of soil before test, g	Bulk density before the test, Mg/m <sup>3</sup>	Dry density before the test, Mg/m <sup>3</sup>
#1	7,933	5,402	17,859	12,457	1.570	1.339
#2	7,933	5,408	18,126	12,718	1.603	1.367
#3	7,933	5,381	18,690	13,309	1.678	1.430
#4	7,933	5,397	19,430	14,033	1.769	1.508
#5	7,933	5,389	19,622	14,233	1.794	1.530
#6	7,933	5,384	19,725	14,341	1.808	1.541
#7	7,933	5,394	20,973	15,579	1.964	1.674
#8	7,933	5,394	21,958	16,564	2.088	1.780
#9	7,933	5,388	22,147	16,759	2.113	1.801

### 3.6 Freeze-thaw cycles procedure

A total of five tests were at the same time, with two freeze-thaw cycles in each test (Table 3.4). Tests 1, 2 and 5 were run with 1m sample length, while tests 3 and 4 were run with 50cm length. The water table level was at 95cm from the top surface of the soil, i.e. the lowest 5cm was saturated, while the upper 95cm of soil was unsaturated. However, the soil samples in tests 1 and 2 were compacted with maximum density correlated to  $W=17.2\%$  of moisture content, which is very close to the ‘zero air voids’ line in Figure 3.2, i.e. the soil due to the dense compaction was close to the saturated condition. In tests 3, 4 and 5 the dry density changed from very loose to very dense soils with a range of 1.18 to 1.80  $Mg/m^3$ . The compaction of the soils with loose density was achieved in the same way as that of dense soils, but with the application of a fewer number of blows or lower energy effort per soil layer of 5cm.

Table 3.9 – Freeze-thaw test characteristics

Test no.	Sample length	Base water supply	Dry density of the sample	Sample testing technique
1	100cm	De-ionised water	max dry density 1.80 $Mg/m^3$	Three columns removed after the first freeze cycle, three columns after the first thaw and the remained three after the second freeze cycle
2	100cm	11 g/L sodium chloride solution	max dry density 1.80 $Mg/m^3$	Nine columns kept until the end of the second freeze cycle
3	50cm	De-ionised water	varied dry density: 1.18-1.80 $Mg/m^3$	Nine columns kept until the end of the second freeze cycle
4	50cm	11 g/L sodium chloride solution	varied dry density 1.31-1.78 $Mg/m^3$	Nine columns kept until the end of the second freeze cycle
5	100cm	22 g/L sodium chloride solution	varied dry density 1.34-1.80 $Mg/m^3$	Nines columns kept until the end of the second freeze cycle

The testing process consisted of two freezing-thawing cycles. After 24-36 hours of the conditioning period, the chilling collars at the top of the soil sample were cooled down to 3 °C. The moisture supply temperature at the base of the soil columns was kept stable at +4 °C. After the conditioning period, the circulated coolant temperature at the

temperature control machine was reduced to  $-3\text{ }^{\circ}\text{C}$ , and subsequently, was dropped daily by a further  $2\text{ }^{\circ}\text{C}$ . It should be noted that the heat loss between the temperature control unit and the cooling ring on the top of soil sample was approximately  $2\text{--}3\text{ }^{\circ}\text{C}$ . The red stepped line in Figure 3.17 represents the temperature at the temperature control unit, while the temperature reaction of the soil surface is shown as a flowing line. The freezing rate of the soil sample was dropped by  $2\text{ }^{\circ}\text{C}$  every 24 hours for 12 days and reduced down to  $-23\text{ }^{\circ}\text{C}$  at the temperature control unit. When the coolant supply temperature had decreased to  $-23\text{ }^{\circ}\text{C}$  it was held there for the next 24 hours. Afterwards, all the cooling system was switched off and the environmental chamber was slowly returned to room temperature through natural thawing.

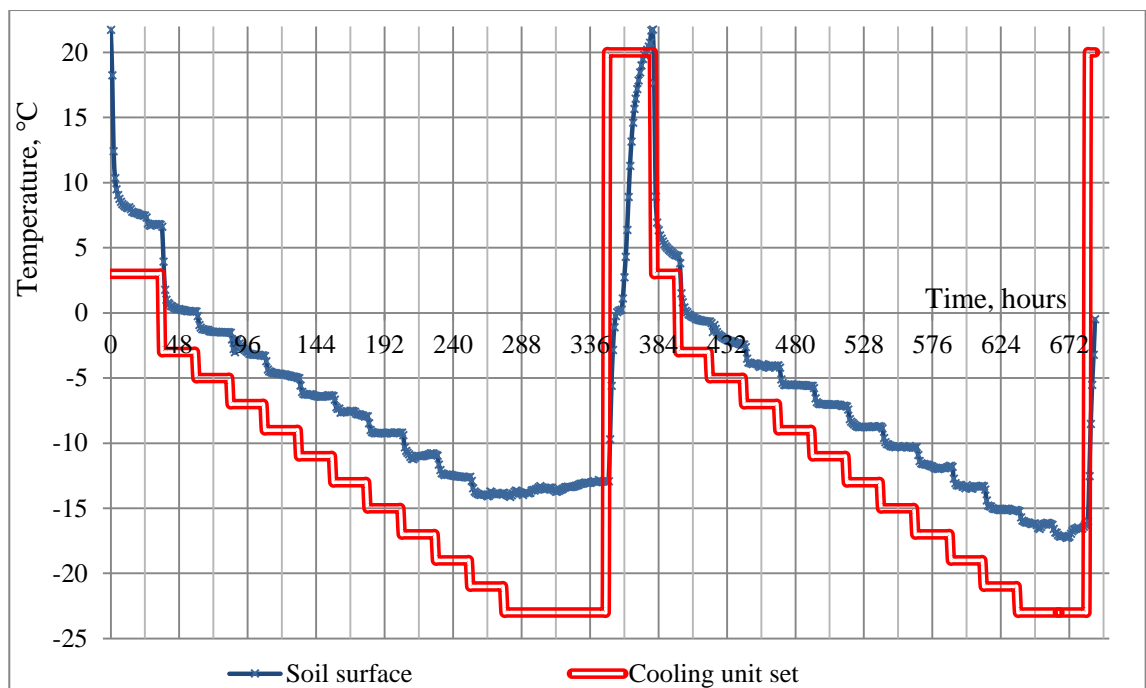


Figure 3.17 – Example of the cooling unit set temperature and the corresponding temperature on the soil surface in Test 2

The second freezing cycle temperature started 24 hours after the completion of the thawing period and was identical that of the first period. At the end of the second freezing cycle after keeping the temperature of control unit at  $-23\text{ }^{\circ}\text{C}$  for the 24 hour period, the cooling unit was again switched off. Although the temperature of soil samples was down only to about  $-15\text{--}16\text{ }^{\circ}\text{C}$ . At the end of freeze-thaw cycles the supply basin was unplugged and the samples were removed for further moisture and chemical content testing, being frozen and hence, the moisture not being allowed to drain.

### **3.6.1 Temperature monitoring of the freeze-thaw cycles**

The temperature control of the soil samples was implemented via K type thermocouples, inserted into the middle of soil column cross section every 10cm length over the soil sample. In order to determine accurately the position of thermocouples in the soil a pilot hole was made with a needle, by piercing the cling film insulation. The thermocouples were carefully inserted to 4.5-5 cm depth and after that the inlet hole was thoroughly sealed with silicone gel, providing moisture insulation of the sample during the test (Figures 3.2, 3.3 and 3.5). In total, 96 thermocouples were connected to 12 Pico loggers and recorded the temperature every hour throughout testing period. The duration of the two freeze-thaw cycle tests was between 600 – 690 hours. At the end of the tests the recorded data from Pico loggers were saved to disc and the thermocouples were carefully removed from the sample before its extrusion from the plastic mould.

### **3.6.2 Vertical linear movement observation during the test**

The vertical linear movement gauges with magnetic bases were installed on the rails with a square cross section, mounted on the lid of environmental chamber, in order to provide a firm footing to the dial gauges (Table 3.1). The rails were based on the chamber frame, but not on the roof surface, the avoiding possible deflection. Dial gauges with 0-5cm travel range were used to monitor the vertical linear movement during the freeze-thaw cycles. The readings from the digital dial gauges were started since the consolidation period, straight after the surcharges were applied. For the entire period of the freeze-thaw cycles the readings were taken twice a day, at 9am in the morning and at 9pm in the evening, being recorded manually to the observation register.

### **3.6.3 Post freeze-thaw sampling and testing**

After the end of the second freezing cycle, the soil columns were unplugged from all monitoring and fixing elements, removed from the environmental chamber and weighed immediately in the frozen state. After that, each column was positioned horizontally to avoid the possible draining of melting moisture in a longitudinal direction (Figure 3.18). The soil columns were disassembled in ring sections and sampled for moisture content determination every 1cm in the top and the bottom ring sections and every 10cm in the middle lengths of the soils (Figure 3.19).



Figure 3.18 – Soil columns positioned horizontally for sampling immediately after the removed from the environmental chamber

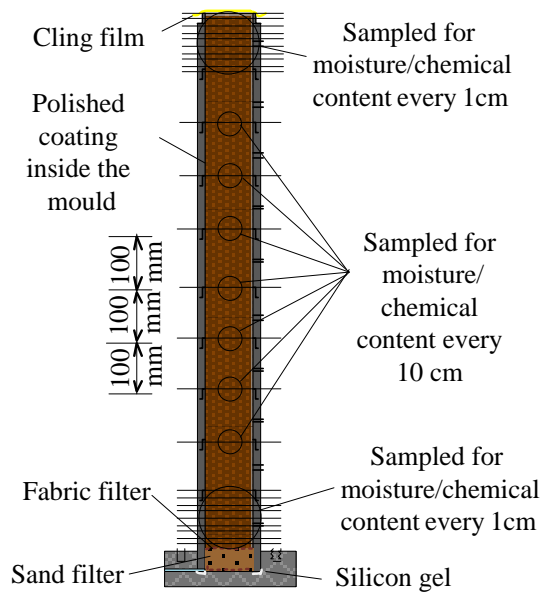


Figure 3.19 – Sampling after freeze-thaw cycles

The oven dried soil samples, after the moisture content determination, were used for evaluation of the chemical content after tests 2, 3 and 5, where the base feeding was applied with a de-icing chemical solution. The rest of the sample material was used to measure the elastic modulus, heat conductivity and occasional direct shear and consolidation tests (Figure 3.20).





Figure 3.20 – Preparation of the remaining sample material for ultrasound testing

The sampling procedure was generally carried out the same day, preferably before the soil started to thaw, in order to prevent moisture redistribution or structure change during melting. Supplementary observational photographs and ice lenses measurements were made during the dismantling and sampling of the soil columns after the freeze-thaw cycles (Figures 3.21 and 3.22).

#### **3.6.4 Determination of the moisture content**

The moisture content was found according to standard BS 1377-4:1990 by weight difference of the wet and oven dried sample at 105 °C for a 24 hour period. The total moisture content included that attributed to the mass of ice lenses and the mass of water in a liquid condition. The top 10cm section was sampled every 1cm due to the increased ice lens formation and the anisotropic structure, while the lower part of the soil column was only sampled every 10cm, mainly at the junctions of the mould sections. In the tests with a de-icing chemical solution supply the lowest 10cm section was tested for moisture content every 1cm to track the corresponding changes of moisture and chemical mass transfer.



Fig 3.21 – Sampling for moisture content determination



Fig 3.22 – Oven dried samples were used for chemical content determination

### 3.6.5 Obtaining the sodium chloride content

The de-icing chemical content of the soil samples, supplied with sodium chloride solution, was obtained, after drying them in the oven. The sampling for the de-icing chemical was undertaken together with moisture content determination, so that the obtained sodium chloride content might be compared with the pore water amount. A multi-range conductivity meter HI 9033 (Figure 3.23) was used to measure the electrical conductivity and derive the corresponding sodium chloride concentration by the calibration chart (Figure 3.24).



Figure 3.23 – Electrical conductivity meter for sodium chloride measurements

The calibration chart was determined with an HI 9033 probe by measuring the electrical conductivity of 50g of the oven dried initial soil sample dissolved in 500ml of deionised water. The solution formed was mixed with electromagnetic mixer for four hours and left with a closed lid for 24 hours to ensure that all the soil particles had settled down and the liquid was clear of non-soluble particles. The obtained electrical conductivity was assigned to relative “zero”, which pertained to the ion content of soil sample at the beginning of the test. Further electrical conductivity values were measured by adding an equal amount of NaCl powder to the initial soil sample solution and dissolving it with the electromagnet mixer. The mass of the added salt was weighed on high resolution balances. A linear relation of the salt concentration and the obtained electrical conductivity value, directly proportional to the sodium chloride content, was found (Figure 3.24).

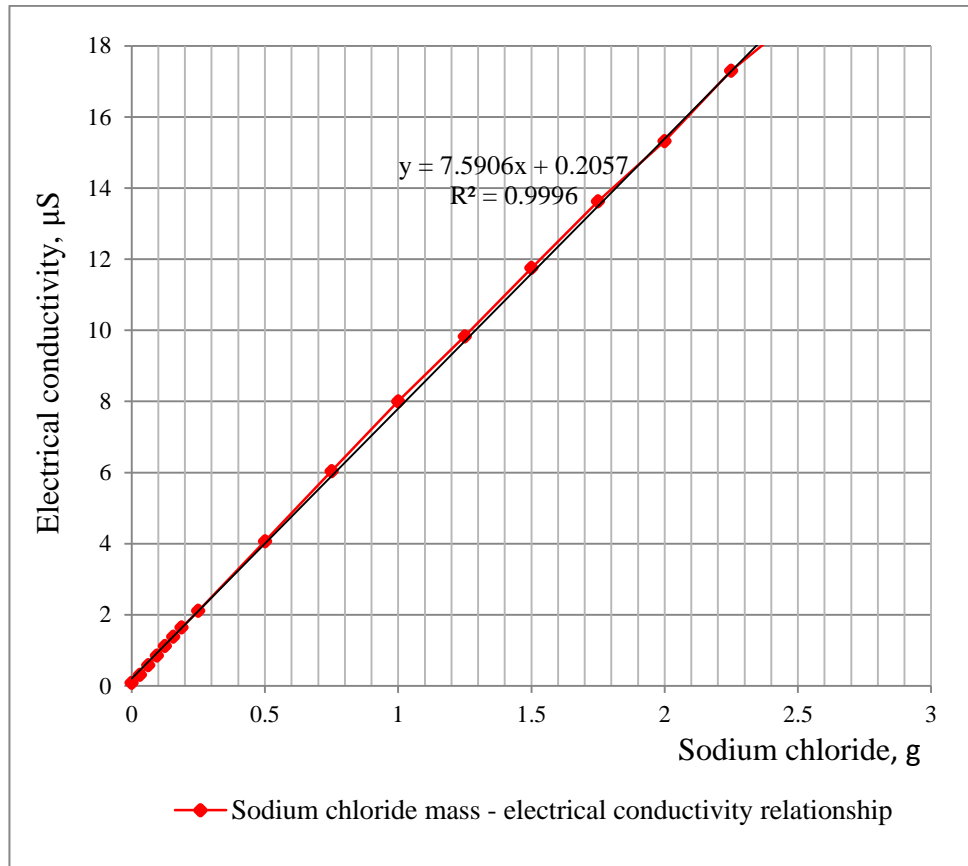


Figure 3.24 - Calibration chart for the sodium chloride - electrical conductivity relation

At the end of freeze-thaw cycle tests with sodium chloride solution supply, the oven dried soil samples, after weighing for the moisture content determination, were used for the chemical content measurements. A 50g portion of the oven dried soil sample was dissolved in the deionised water in the same ratio as for the calibration test and measured with an electrical conductivity probe (BS 1377-3:1990). The corresponding salt concentrations were obtained and registered. The moisture content of the soil samples after the freeze-thaw cycles was taken into account for determining the sodium chloride content corresponding to the pore water solution.

### 3.6.6 Tests for mechanical and thermo- hydro- dynamical properties

Some auxiliary tests were performed to determine the mechanical properties in addition to those described in Section 3.3, to ascertain the soil condition characteristics before and after testing. The results of an oedometer consolidation test, conducted with  $W=17.2\%$  moisture content and  $\rho_d = 1.80 \text{ Mg}/\text{m}^3$  soil sample before the freeze-thaw cycles, are presented in Table 3.10.

Table 3.10– Oedometer consolidation test results for the sample with a moisture content of 17.2% and a dry density  $\rho_d = 1.80 \text{ Mg/m}^3$

N	Void ratio			Coefficient of volume compressibility		Coefficient of consolidation			Coefficient of permeability
	Pressure P, kN/m <sup>2</sup>	Settlement $\Delta H$ , mm	$e_l = e_o - \Delta e$ $e_o = 0.453$	$\delta_e$ , mm	$m_v$ , $\frac{m^2}{MN}$	$t_{50}$ , mm	$\overline{H^2}$ , mm <sup>2</sup>	$c_v = \frac{0.026H^2}{t_{50}}$ m <sup>2</sup> /year	$k = c_v m_v \rho_v g$ , m/s
0	0	0	0.453	0.000	0	0	0	0	0
1	25	-0.499	0.417	0.036	1.0236	3.7	390.08	2.741	$8.722 \cdot 10^{-10}$
2	50	-0.662	0.405	0.012	0.3372	3.6	377.12	2.724	$2.855 \cdot 10^{-10}$
3	100	-0.901	0.387	0.017	0.2503	1.5	369.35	6.402	$4.981 \cdot 10^{-10}$
4	300	-1.426	0.349	0.038	0.1413	0.88	354.81	10.483	$4.606 \cdot 10^{-10}$
5	700	-1.955	0.311	0.038	0.0733	0.45	335.24	19.369	$4.413 \cdot 10^{-10}$
6	1500	-2.49	0.272	0.039	0.0382	0.22	316.04	37.350	$4.435 \cdot 10^{-10}$

Coefficient of consolidation  $c_v$  for the load increment was found as a relation of specimen height with double drainage to the time factor corresponding to 50% of primary consolidation, in  $m^2/year$ :

$$c_v = \frac{0.026\overline{H}^2}{t_{50}} \quad (3.6)$$

where,  $\overline{H}$  - is the specimen height during the load increment in mm;  $t_{50}$  - is a theoretical time factor, corresponding to 50% primary consolidation in minutes.

The coefficient of compressibility  $m_v$  was found by the equation,  $m^2/MN$ :

$$m_v = \frac{\delta_e}{\delta_p} \frac{1000}{(1 + e_1)} \quad (3.7)$$

The compression index  $C_c$  is equal to the slope of the field consolidation curve in Figure 3.25 plotted to a logarithmic scale of pressure  $P$ . According to Head and Epps (2011), the corresponding compression index  $C_c'$  for remoulded clay might be found by the approximation formula:

$$C_c' = 0.007(w_L - 10\%) \quad (3.8)$$

$$C_c' = 0.007(37.05 - 10) = 0.189$$

However, according to the plot in Figure 3.25, compression index was  $C_c = 0.15$ .



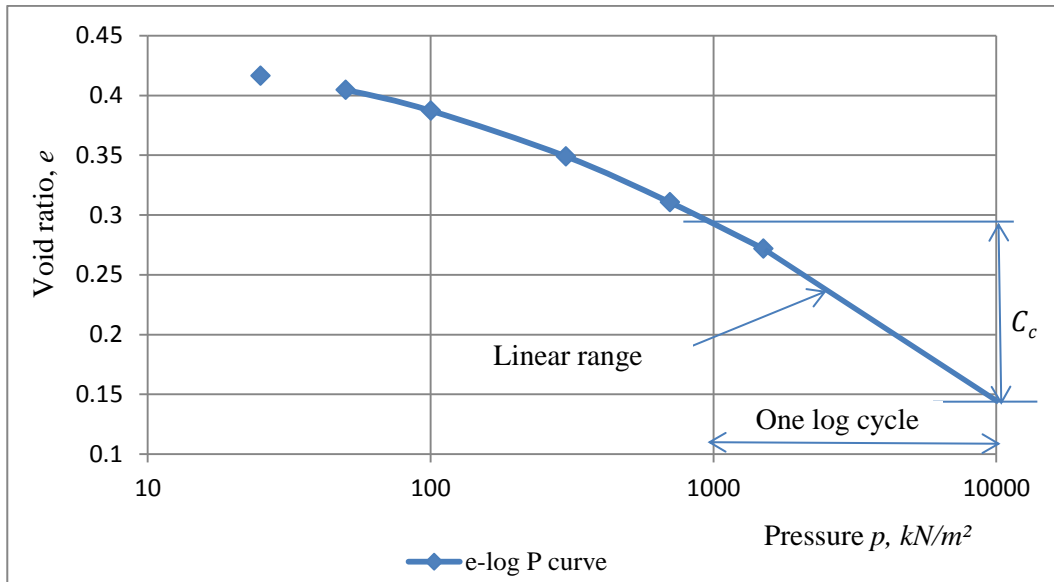


Figure 3.25 - Log-pressure – voids ratio curve for the soil sample with freeze-thaw cycle parameters

The coefficient of permeability  $k$  corresponding to each pressure value was found by the equation,  $m/s$ :

$$k = c_v m_v \rho_w g \quad (3.9)$$

The coefficient of permeability during loading varied within the range  $2.85 - 8.72 \cdot 10^{-10} m/s$ .

A triaxial compression test sequence was performed with constant speed axial load and confining pressures of 200, 400 and 600 kPa. The sample characteristics corresponded to the pre-freezing conditions with moisture content  $W=17.2\%$  and dry density  $\rho_d = 1.80 Mg/m^3$ . The displacement speed was set to 1mm/min. The failure was deemed to have occurred at 20 % axial strain, and had a plastic mode of deformation (Figure 3.26).

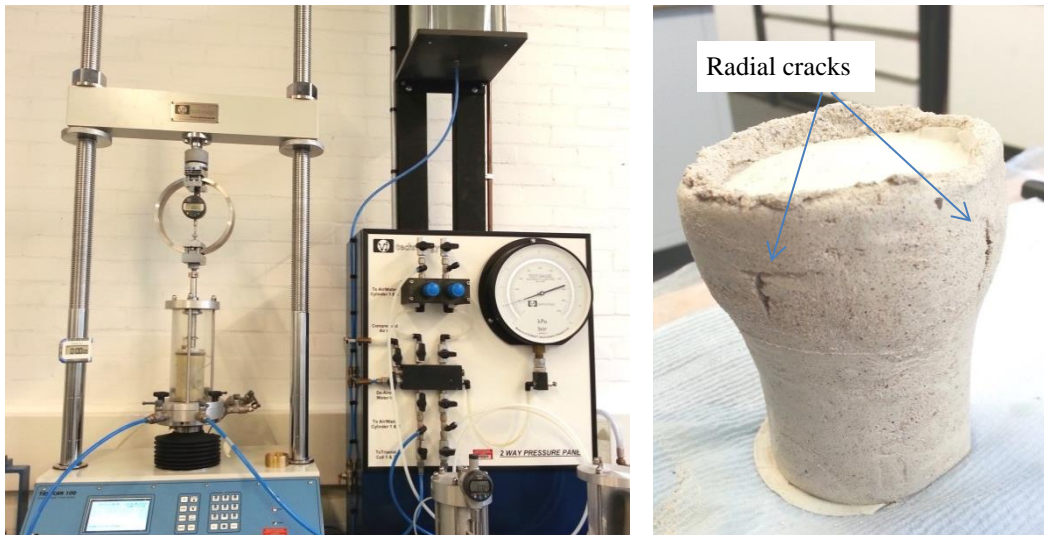


Figure 3.26 – Triaxial test

According to the Mohr envelop result in Figure 3.25, which is almost horizontal, the tested clay soil is very close to the saturated condition (Head and Epps, 2011) and the shear strength is 40 kPa. The obtained results are presented in Table 3.11.

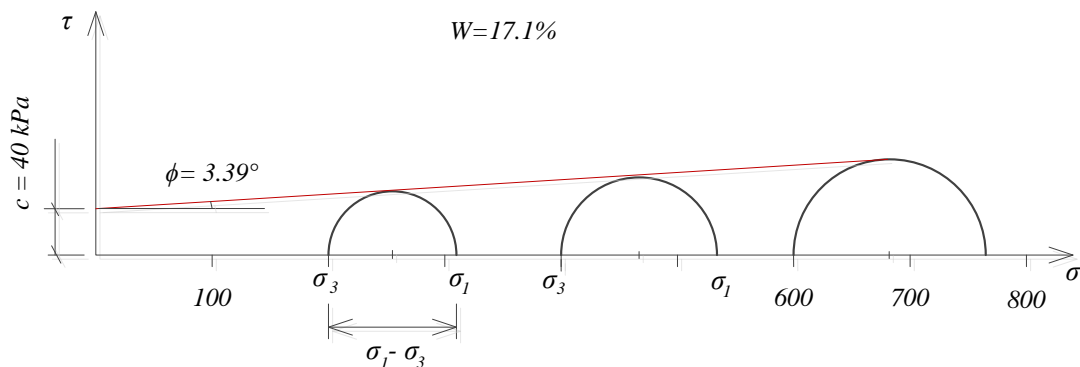


Figure 3.27 – Mohr circles for a sandy clay soil sample

Table 3.11 – Triaxial test results

$\sigma_3$	Proving ring division	Ring factor, kN/div	Deviator stress kN/m <sup>2</sup>	$\sigma_1$ , kN/m <sup>2</sup>
200 kPa	59	0.004585	110.27	310.27
400 kPa	70	0.004585	130.83	530.83
600 kPa	79	0.004585	147.65	747.65

Ultrasound testing was performed with a Pundit ultrasound machine for all soil columns over the entire length of the soil column to obtain the change in the elastic modulus change after the freeze-thaw cycles (Figure 3.26). Each soil section was

measured by placing the locators on the top and bottom ends of the cylindrical sections. A transmitting gel was applied at the points of contact. The samples were tested in wet and dry conditions, after extruding them from the acrylic rings with minimal disturbance. To obtain the initial thermal conductivity the soil samples were cut into the 10cm in diameter and 1-1.5cm length acrylic rings density of  $1.80 \text{ Mg/m}^3$ , after which they were gently extruded from the rings. Before every testing session the machine was calibrated for the thickness. The upper plate was set at  $10 \text{ }^\circ\text{C}$  and the lower plate at  $30 \text{ }^\circ\text{C}$ . The obtained thermal conductivity  $\lambda$  for the sample packed with maximum dry density  $\rho_d = 1.80 \text{ Mg/m}^3$  and moisture content  $W = 17.2 \%$  was found as the average value of five measurements:  $\lambda = 0.4813 \text{ W/m} \cdot \text{K}$ .



Figure 3.28 – Thermal conductivity measurements

### 3.7 Summary

The proposed experimental method has several advantages for studying the heat and moisture mass transfer and monitoring frost heave development depending on the degree of salinity in the basement water supply.

1. The increased height of the column and the slow freezing technique make the soil conditions close to the natural environment and facilitate temperature field monitoring during the freeze-thaw cycles.
2. More accurate chemical mass transfer observation when feeding the initially non-saline soil sample with a de-icing chemical solution from the base and



unidirectional freezing from the top. Such a testing scheme clearly benefits chemical mass transfer monitoring compared with the method where the initially saline soils are the subject of freeze-thaw cycles.

3. The proposed method involves the use of samples with different densities and various ground water supply concentrations: from de-ionised water to saline brine. The environmental chamber is also provided with separate switches of basement water supply and coolant supply for the chilling collars.
4. The loading of the soil top surface with metal surcharges has several objectives: firstly, the metal surface of the surcharges contributes to even cold distribution from the chilling collars; secondly, it allows the vertical linear movement of the soil by sliding along the chilling collar inside; and lastly, it facilitates linear movement control by the attached incompressible plastic rods passing through the lid of the chamber.
5. The plastic mould of the soil column is assembled with 10cm section rings. Such construction facilitates the build-up height of the soil compaction operation and eases the sampling after the freeze-thaw test when the soil is still in the frozen condition.
6. The environmental chamber, owing to its careful thermal insulation, accurately conveys the daily temperature fluctuations in the soil, which benefits the long-term observations of the soil samples during the freezing and thawing.

## 4 RESULTS

### 4.1 Introduction

This chapter describes the results of freeze-thaw cycle tests on samples of 50 and 100 cm height, compacted with maximum dry density in Tests 1 and 2 and varied density between the columns increasing on each further soil column in Tests 3, 4 and 5. The columns were either supplied with deionised water or a chemical solution of 11 g/L and 22 g/L of sodium chloride. Details of the sample preparation and initial conditions for each of the five freeze-thaw cycle tests are presented in Table 3.4, Chapter 3.

The samples were studied to observe the following parameters: the temperature field change during the freeze-thaw cycles, the moisture redistribution and the chemical mass transfer. Additionally, density and structure change were compared before testing and after the freeze-thaw cycles were applied. The strength-deformation characteristics of the soil samples after freeze-thaw cycles was also examined. However, the testing was complicated in terms of the volumetric and structure changes in the sample due to the complex melting processes and the testing equipment not being intended to work at sub-zero temperatures.

### 4.2 Temperature field change

The temperature field in Test 1, carried out using deionised water, exhibited a similar pattern of temperature distribution within all nine soil columns (Appendix B, Figure B.1a-i) and it differed greatly from the temperature distribution of the soil samples in Test 2, where the feeding of the soil columns was provided with 11,000 mg/litre sodium chloride solution (Appendix B, Figure B.2a-i). This was particularly evident in the second freeze cycle (Figures 4.1 and 4.2). All the soil columns in the Tests 1 and 2 were compacted to maximum dry density using a 2.5 kg rammer with 17.2% moisture content and conducted at the same freezing rate of 2 °C per day. A similar pattern of temperature distribution was recorded in both tests during the first freezing cycle within 250 hours. In the second freezing cycle the temperature curves exhibited reductions that were more pronounced in Test 2, where the supply was 11 g/L sodium chloride solution. By the end of the second freezing cycle, the temperature reduction progressed to -5 °C at the base of the column and dropped to below -10 °C in the top 30 cm of the sample.

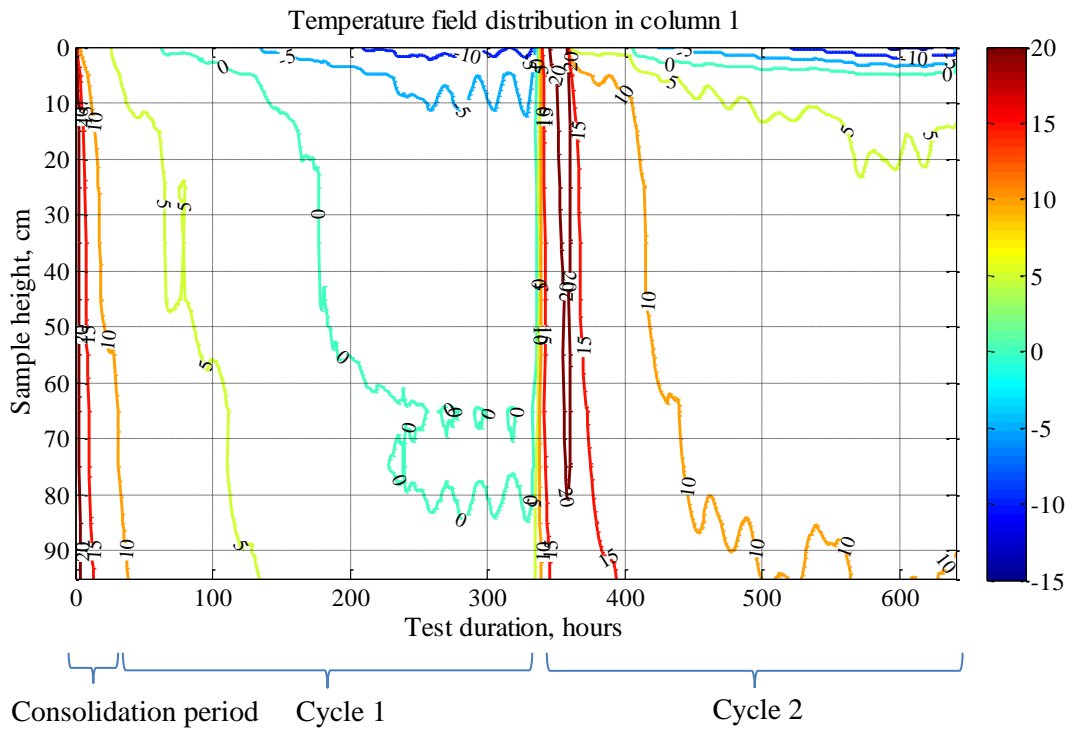


Figure 4.1 – Temperature field contours in Test 1 for the example of column #1

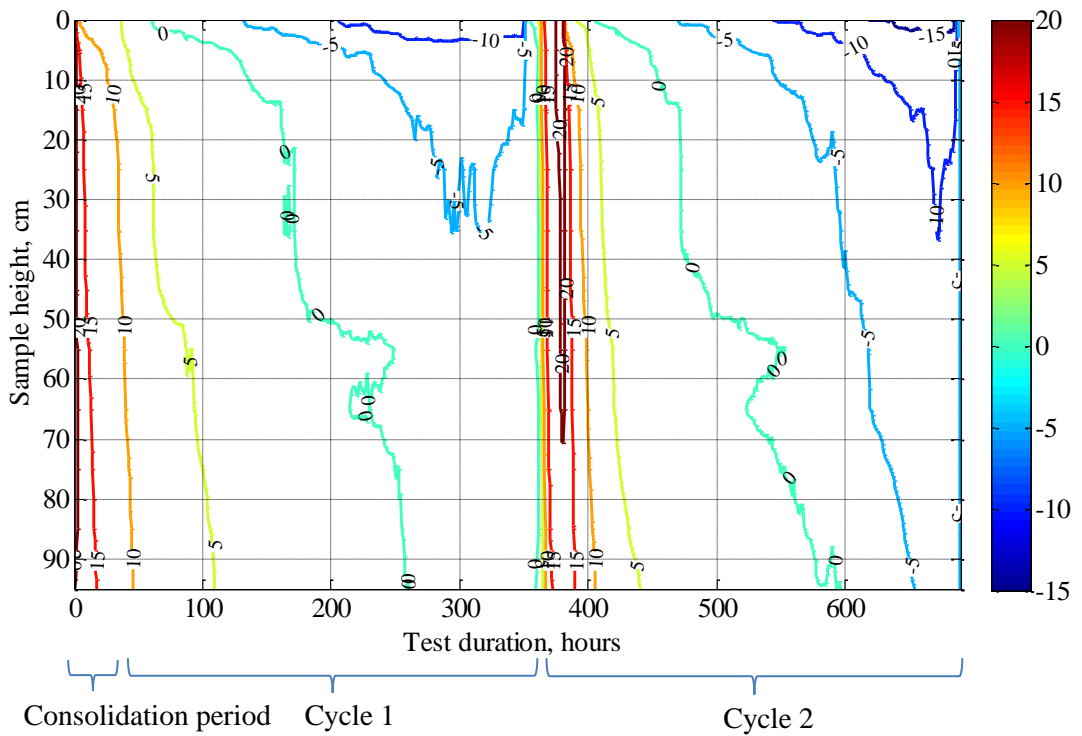


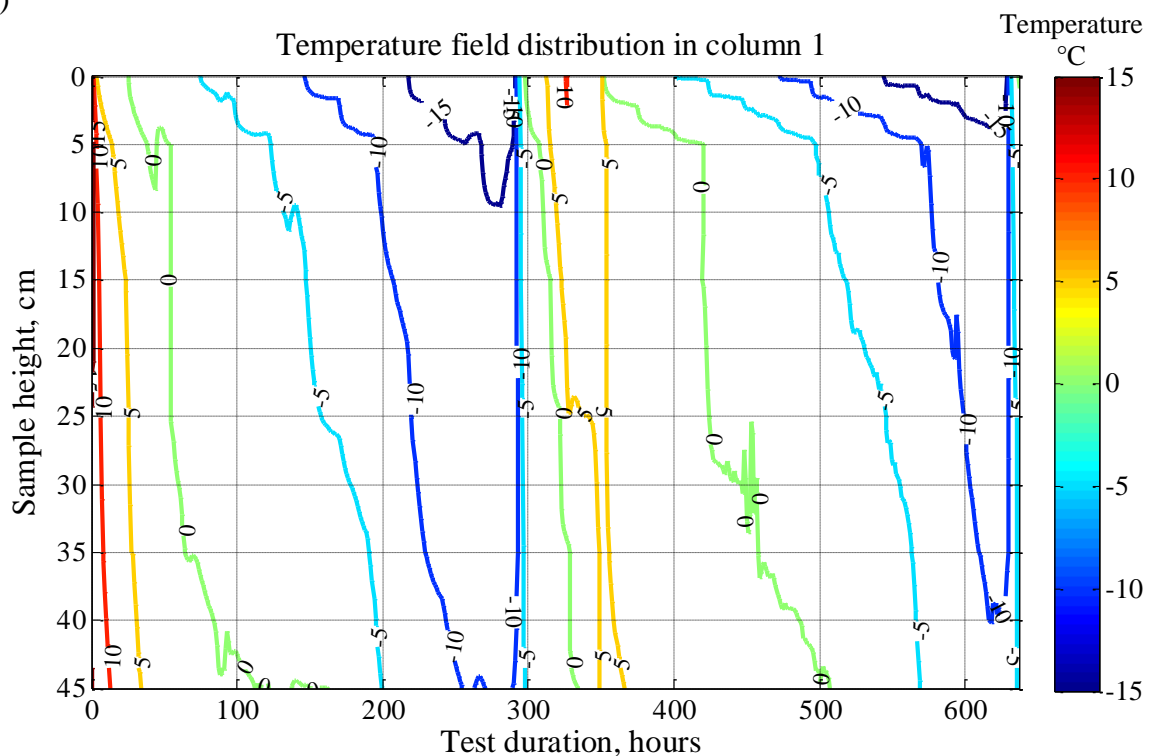
Figure 4.2 - Temperature field contours in Test 2 for the example of column #1

In Test 1, the temperature drop was less pronounced due to the formation of ice lenses at the top of the soil columns and the resulting latent heat released for the increased amount of water. It can be seen in Figure 4.1 that the top 5 cm of soil laid down sub-zero

temperatures, while the temperature dispersion over the length of the soil samples was in a range of +5 - +10 °C. It also should be noted that wide spread ice lens formation was observed at the top of the sample, which appears to act as a heat insulator and prevented the further freezing of the soil.

The temperature distribution in Test 3, with a range of soil density, did not obtain a steady pattern of freezing rate in terms of initial density (Figure 4.3 and Appendix B, Figure B.3 a-i). This is possibly because the freezing rate of 2 °C per day provided sufficient time for uniform temperature distribution and stabilisation of the temperature field across the range of soil densities. However, a deceleration of the freezing rate was noted in the second freezing cycle. The temperature field distribution with time in Test 3 was similar to Test 1, where the temperature contours in the second freezing cycle were warmer compared to the first. Notably, both Test 1 and Test 3 samples were supplied with deionised water and revealed an increased moisture content at the top of the soil by the end of the tests.

a)



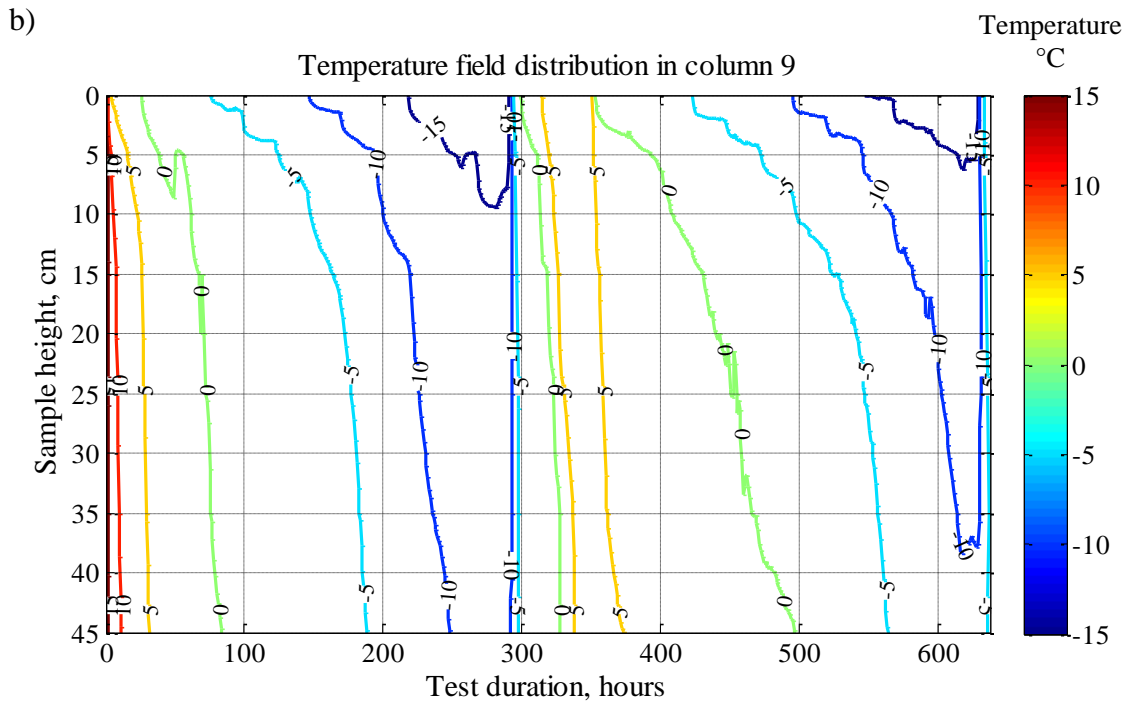


Figure 4.3 – Temperature contours in columns #1 and #9 in Test 3, with deionised water introduced to the column bases of samples with variable soil densities

Table 4.1 shows the time intervals when the temperature reached 0, -5 and -10 °C for the part 15 cm from the top of each soil sample, during both the first and second freezing cycles. In column #1, -5 °C was registered at 15 cm depth from the soil surface after 147 hours for the first freezing cycle and this took 518 hours in the second freezing cycle.

Table 4.1 - Temperature distribution within the soil samples in Test 3

Column number	Sample density before the test, Mg/m <sup>3</sup>	Dry density before the test, Mg/m <sup>3</sup>	Time to achieve the temperature limit at 15 cm depth during 1 <sup>st</sup> cycle/2 <sup>nd</sup> cycle, h		
			0 °C	-5 °C	-10 °C
#1	1.380	1.177	54/419	147/518	207/581
#2	1.519	1.295	54/425	148/529	208/596
#3	1.575	1.343	86/466	175/546	230/603
#4	1.721	1.467	73/438	171/533	221/590
#5	1.783	1.520	55/414	148/499	203/567
#6	1.883	1.605	52/405	145/495	199/553
#7	1.936	1.650	55/415	148/499	204/568
#8	2.105	1.794	59/418	149/500	203/568
#9	2.111	1.799	67/430	164/523	219/581

Test 4, with variable density of soil samples, was supplied with 11,000 mg/L sodium chloride solution at the base. The temperature field distribution did not exhibit significant fluctuations in terms of variable density (Figure 4.4 and Appendix B, Figure B.4 a-i). The temperature distribution over the soil sample length in Test 4 was equivalent that for Test 2, which was supplied with de-icing chemical solution from the base and also demonstrated a low temperature zone in the second freezing cycle.

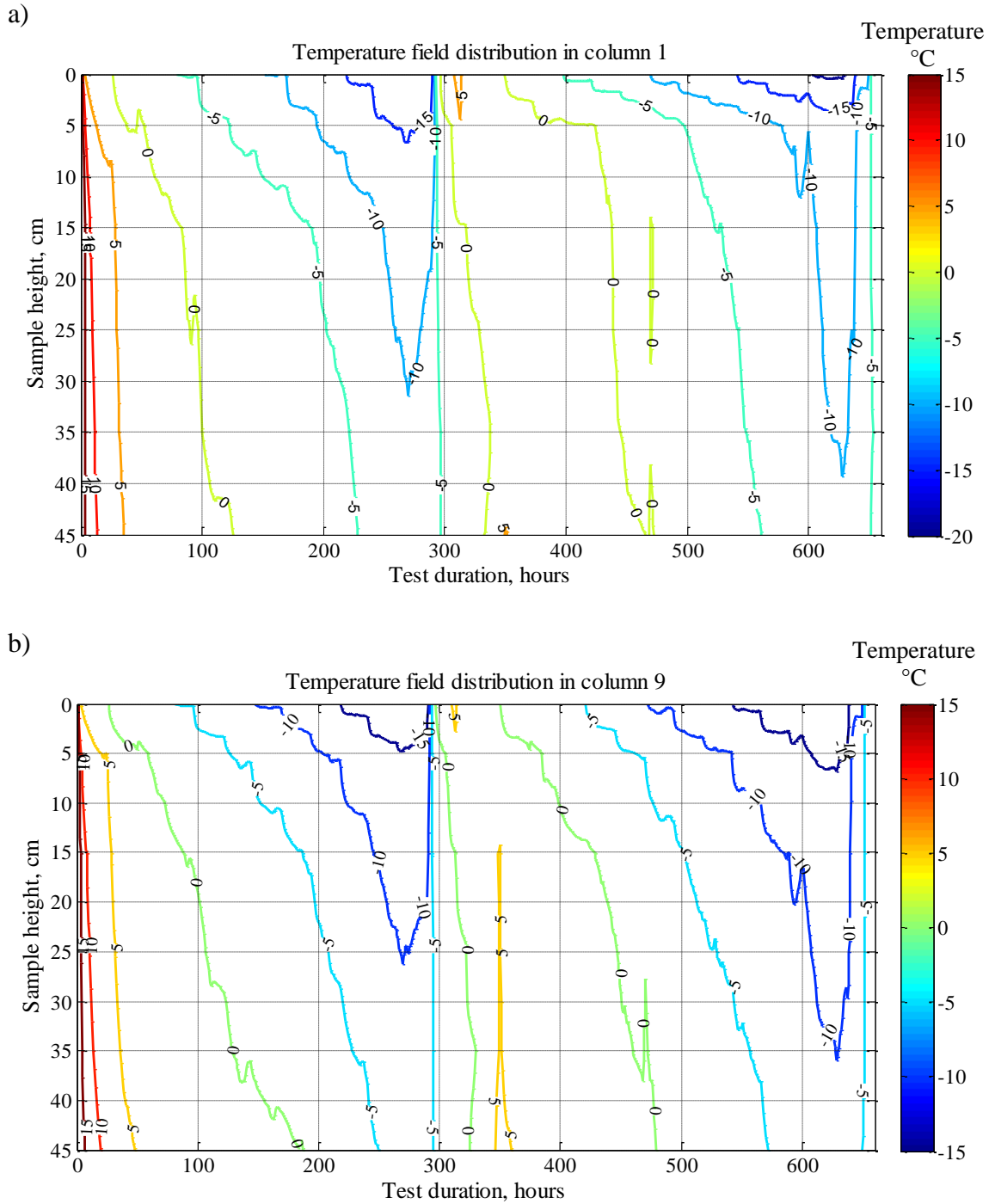
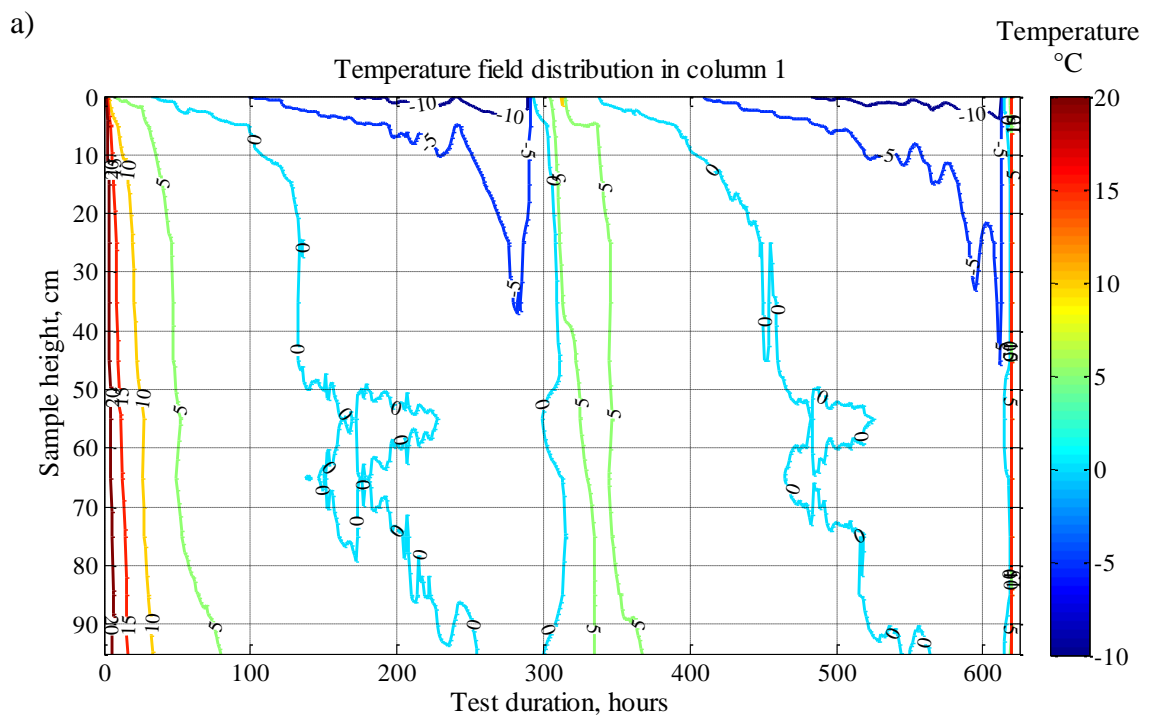


Figure 4.4 - Temperature distribution in columns #1 and #9 in Test 4, with 11,000 mg/litre sodium chloride solution supply and various soil densities

In Test 5, 1m length soil samples were packed with varied density and the base was supplied with an increased concentration of sodium chloride solution of 22,000 mg/L. The samples were packed with varying dry density soils: from the loosest in sample #1 to the densest in sample #9. However, the columns were compacted uniformly over the entire length. The freeze-thaw cycles did not record a clear pattern in the temperature field distribution in terms of density. Moreover, the observed temperature distribution over the whole length indicated an identical temperature depression and a similar freezing rate in the first and second freezing cycles (Figure 4.5 and Appendix B, Figure B.5 a-i).



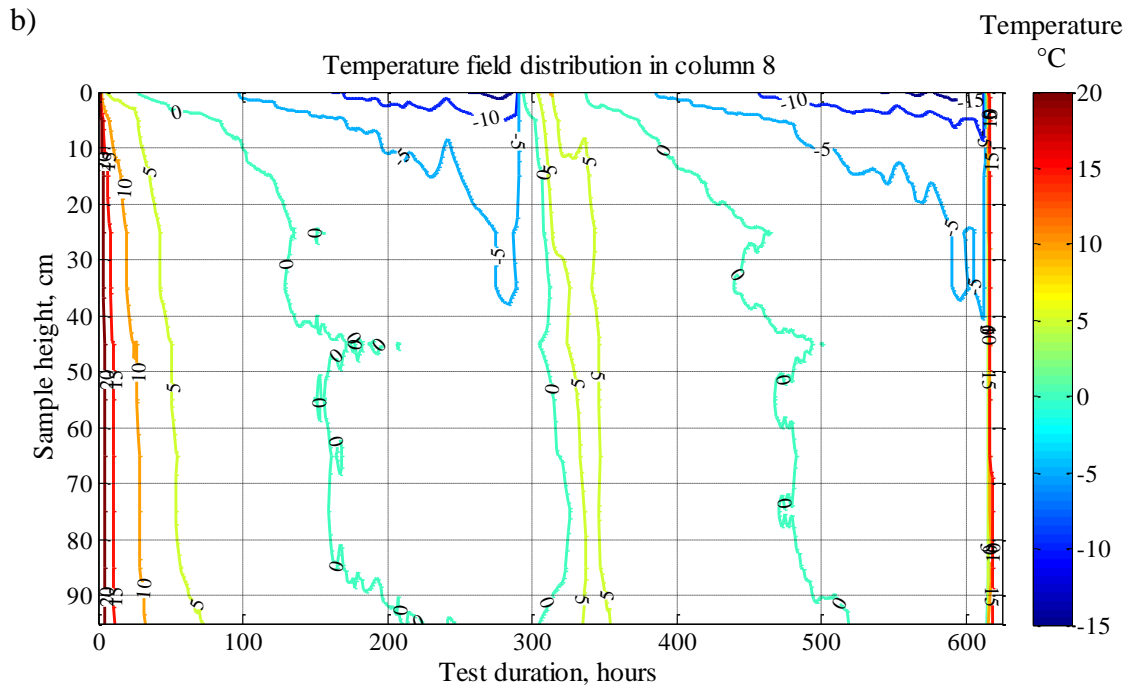


Figure 4.5 – Temperature field distribution in Test 5 with a 22,000 mg/litre sodium chloride supply and various soil densities

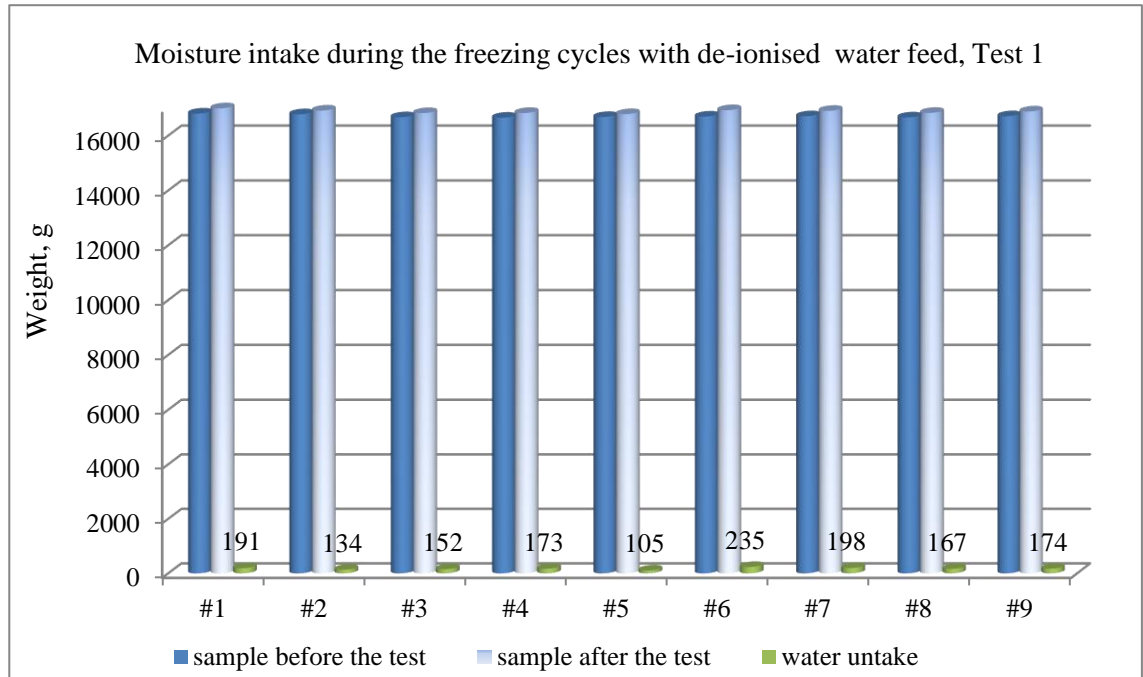
According to the obtained results, the temperature distribution within the soil samples largely depends on the salinity of the ground water supplied from the base and is less dependent on the density of the soil samples. This is explained by the relatively slow freezing rate of 2 °C per day, which ensured an even distribution of heat and achieving a thermal equilibrium by the end of the step freezing.

### 4.3 Moisture content change

Moisture content was found as total moisture mass, including the ice lenses and the water in a liquid condition. The total moisture input was measured as the difference of the weights of the whole soil columns before and after the test. Figures 4.6. *a* and *b* show the examples regarding this for Tests 1 and 2.



a)



b)

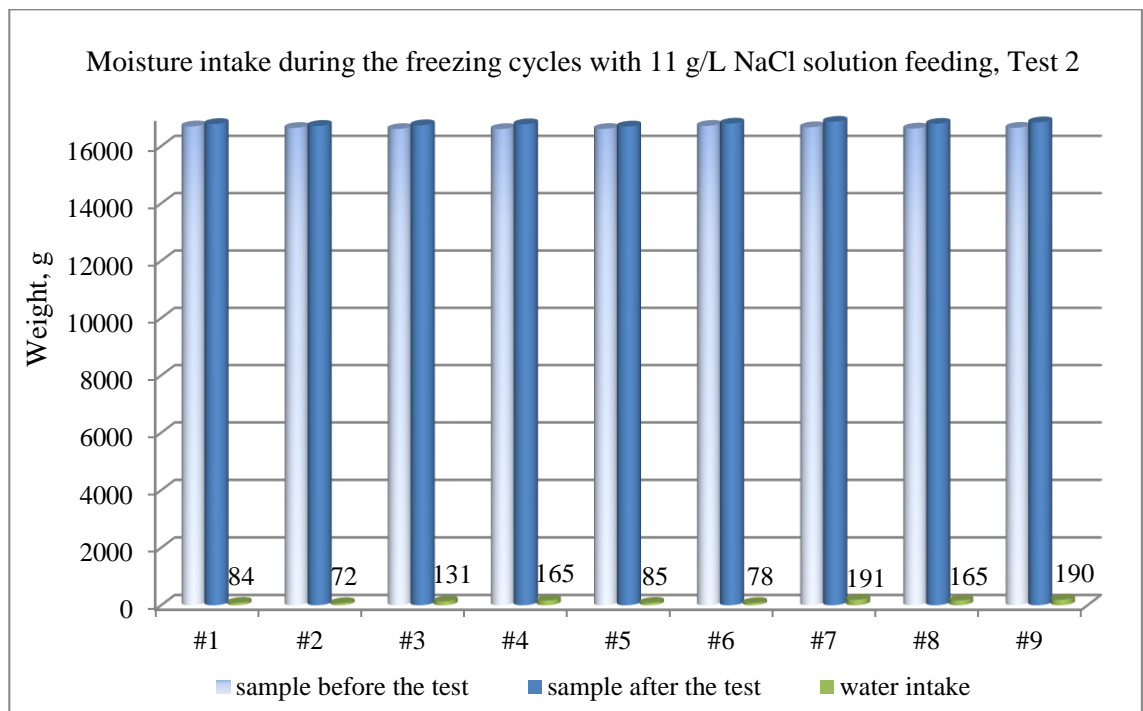
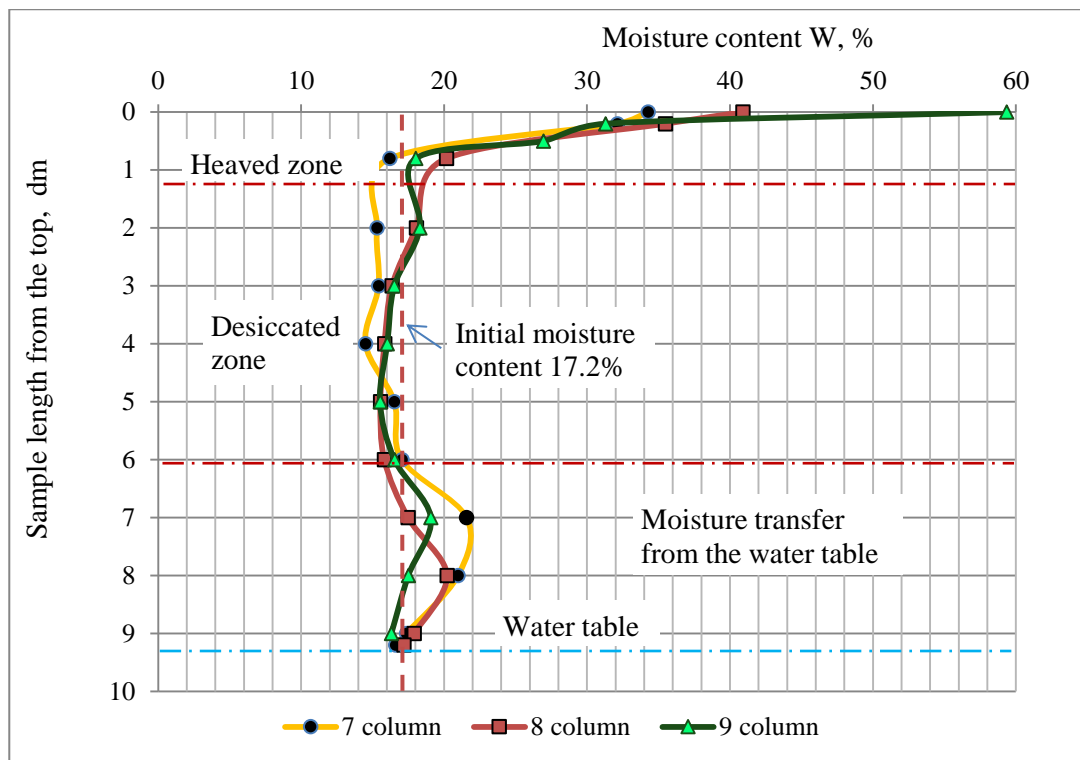


Figure 4.6 – Moisture intake during Test 1 (a) and Test 2 (b) with maximum dry density and 1 m soil sample height

Average water intake in the soil samples with a deionised water supply was 30% more than for those with 11,000 mg/litre sodium chloride solution supply. Moreover, general water intake in both tests did not exceed 200 g by weight at the end of freeze-

thaw cycles, which corresponded to 21.37% of the moisture content, if this were uniformly spread over the sample length. The distribution of the moisture according to the sample length can be divided into the heaved zone, i.e. the top 10 cm and the zone from which moisture was drawn, namely, the desiccated zone which is between 10 and 60 cm depth. The moisture content in the desiccated zone was reduced to 15%. However, in the bottom zone the moisture content was comprised 20-21 %, which can most likely be attributed to water being drawn in from the base water supply. In Test 1, only three soil columns were kept until the end of the second freezing cycle (Figure 4.7 a), with three having been removed after the first freezing cycle and the remaining three after the first thawing cycle.

a)



b)

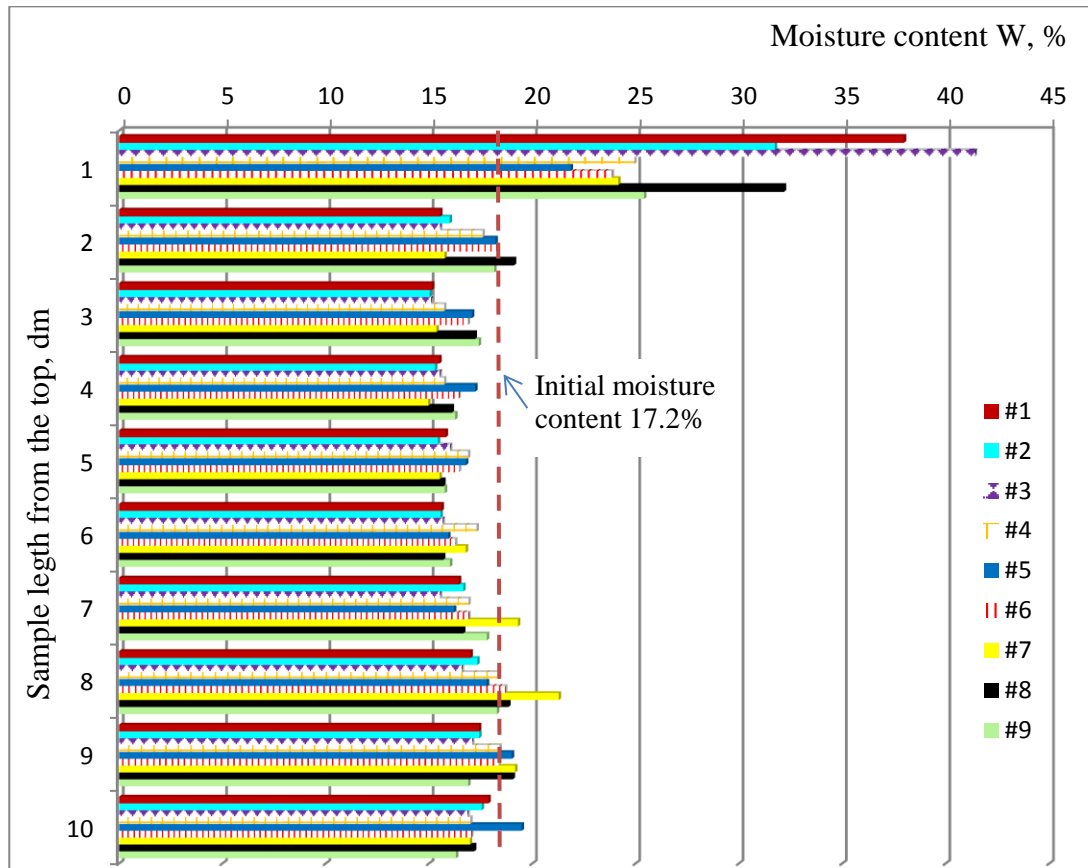


Figure 4.7 – Moisture redistribution by the sample length in Test 1 with a deionised water supply: a – in columns #1-3 after two freeze-thaw cycles, b – in all nine columns terminated after: first freezing cycle (columns #7-9), first thawed cycle (columns #4-6) and second freezing cycle (columns #1-3)

There was a significant increase in moisture, reaching 40% in the top 10 cm layer of the soil samples, which were draining and moistening the 20 cm under this layer during the thawing period, although when the second freezing cycle started, the water was drawn upwards again. The same trend of moisture redistribution was observed in the test with sodium chloride supply. When comparing moisture redistribution within the column length, the samples with deionised water supply had a greater difference of moisture content between the top heaved layer and the desiccated zone, while in the soils supplied with de-icing chemical solution the moisture redistribution was less uneven. Notably, both Tests 1 and 2 were carried out with maximum dry density soil compaction. The initial degree of saturation in the compacted samples was  $S_r = 0.95$  and the air content was close to 0%.

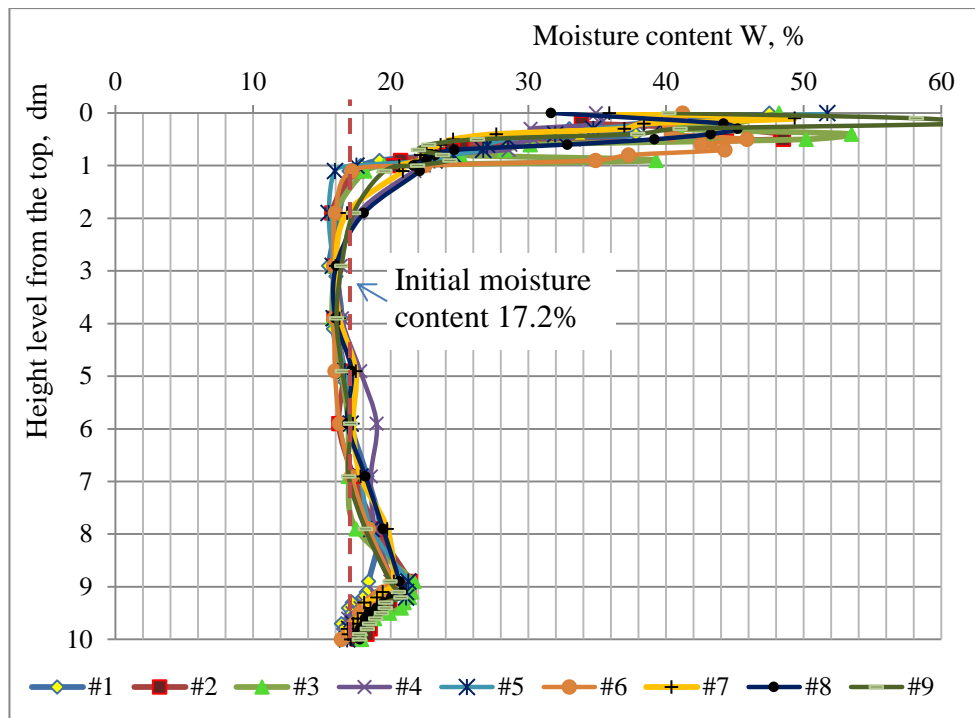


Figure 4.8 – Moisture distribution in Test 2 after two freeze-thaw cycles with 11,000mg/litre de-icing chemical solution supply

In Tests 3 and 4 the soil samples were made up with various densities. The sample length in these cases was reduced by half to 50 cm and filled into five assembled acrylic collars each 10 cm in length. The moisture intake in the soil samples supplied with deionised water during the freeze-thaw cycles varied from 190 g to 720 g per soil column (Figure 4.9).

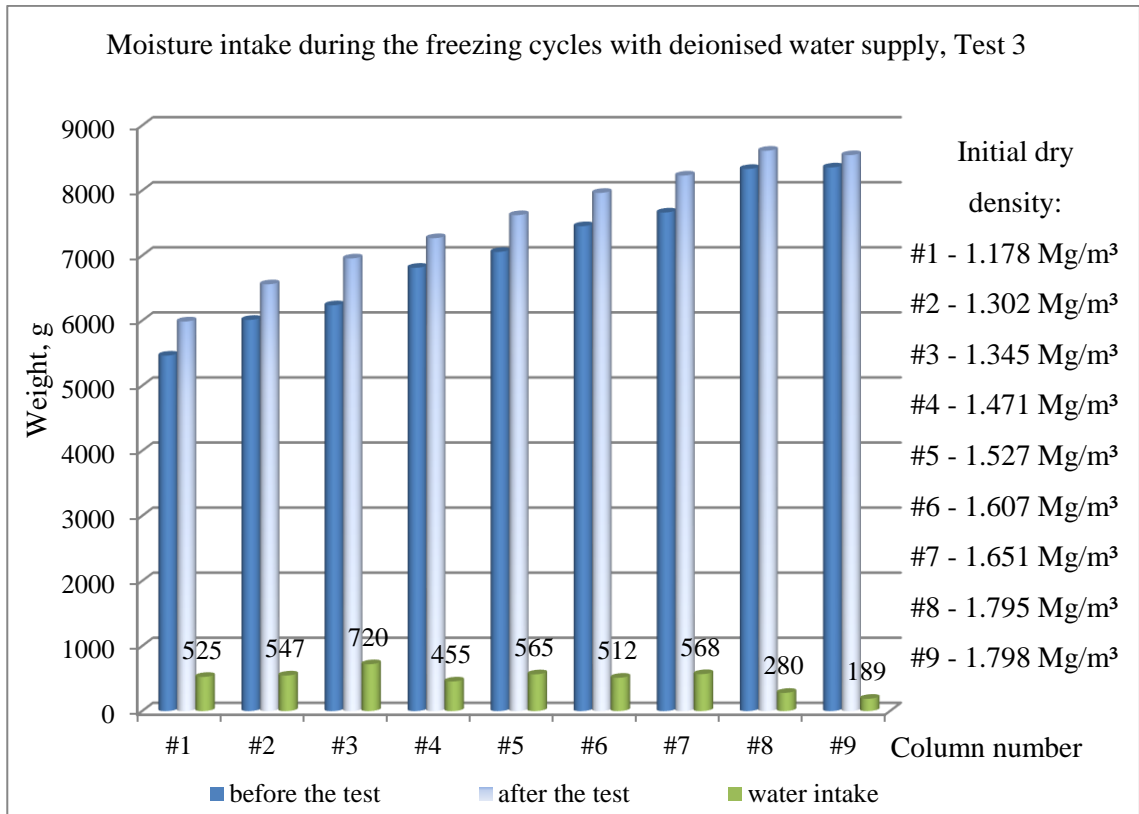


Figure 4.9 - Moisture intake during the freeze-thaw cycles of the soils in Test 3 with deionised water supply and various densities, as presented in Table 4.2

According to the results in Test 3, the moisture content represents advanced water intake in the loose soil, with a dry density range between 1.18-1.65 Mg/m<sup>3</sup>, comparing to dense soils with dry density 1.8 Mg/m<sup>3</sup>. With the exception of sample #4, in all the columns the moisture content reached 24.5% or above by the end of the test. The reason for low moisture intakes in sample #4 could have been due to occasional violation of the water supply during the freeze-thaw test.

In Test 4, where the soil samples were supplied with 11,000 mg/litre sodium chloride solution, the moisture intakes considerably exceeded the increases for Test 3, supplied by deionised water. In the loose density samples #1-#7, ranging between 1.50 and 1.93 g/cm<sup>3</sup> and unsaturated state of soils with consequently greater void ratio, an increasing water intake trend was observed.

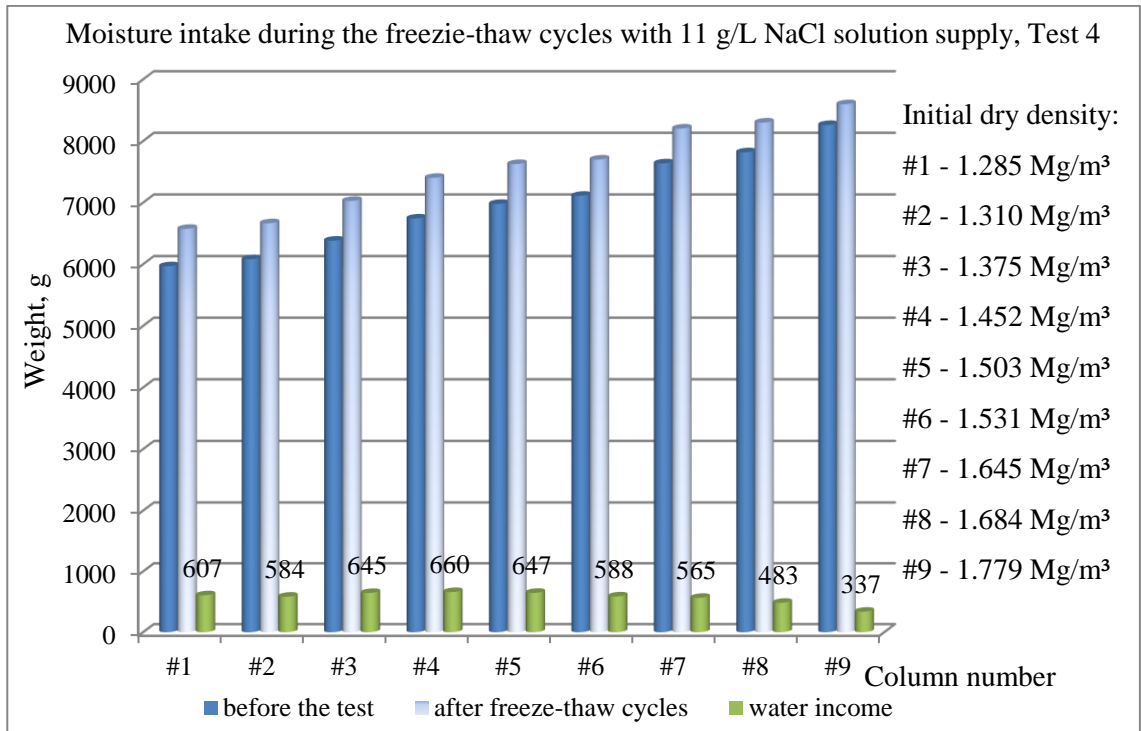


Figure 4.10 - Moisture intake during the freeze-thaw cycles of the soils for Test 4 with 11,000 mg/litre sodium chloride solution supply and various densities

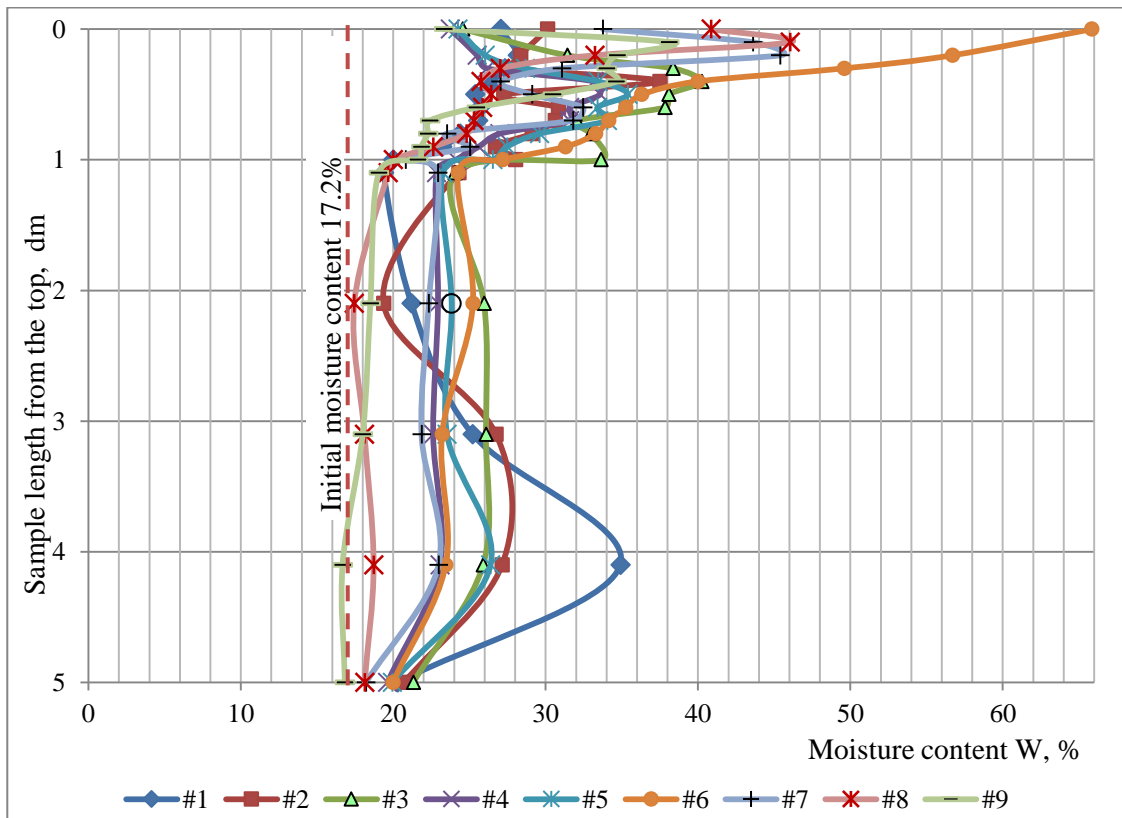


Figure 4.11 - Moisture distribution for Test 3 after two freeze-thaw cycles using samples with deionised water supply

In the top 10 cm layer, ice lens formation caused a highly irregular distribution of moisture, which was confirmed by the centimetre sampling in Figure 4.11 and also in the soil structure image in Figure 4.20. Since the ground water supply table was quite shallow, at 45 cm depth, the moisture intake was higher than for Tests 1 and 2, where the water supply was located at 95 cm depth and the soil samples were made with maximum dry density. For this reason, the moisture content between 15 and 45 cm from the soil surface was relatively stable and depended just on the density of the soil samples (Figures 4.11 and 4.12). In Test 4, the bottom 10 cm layer was sampled every 1 cm to monitor closely the chemical mass transfer in the next to water table location.

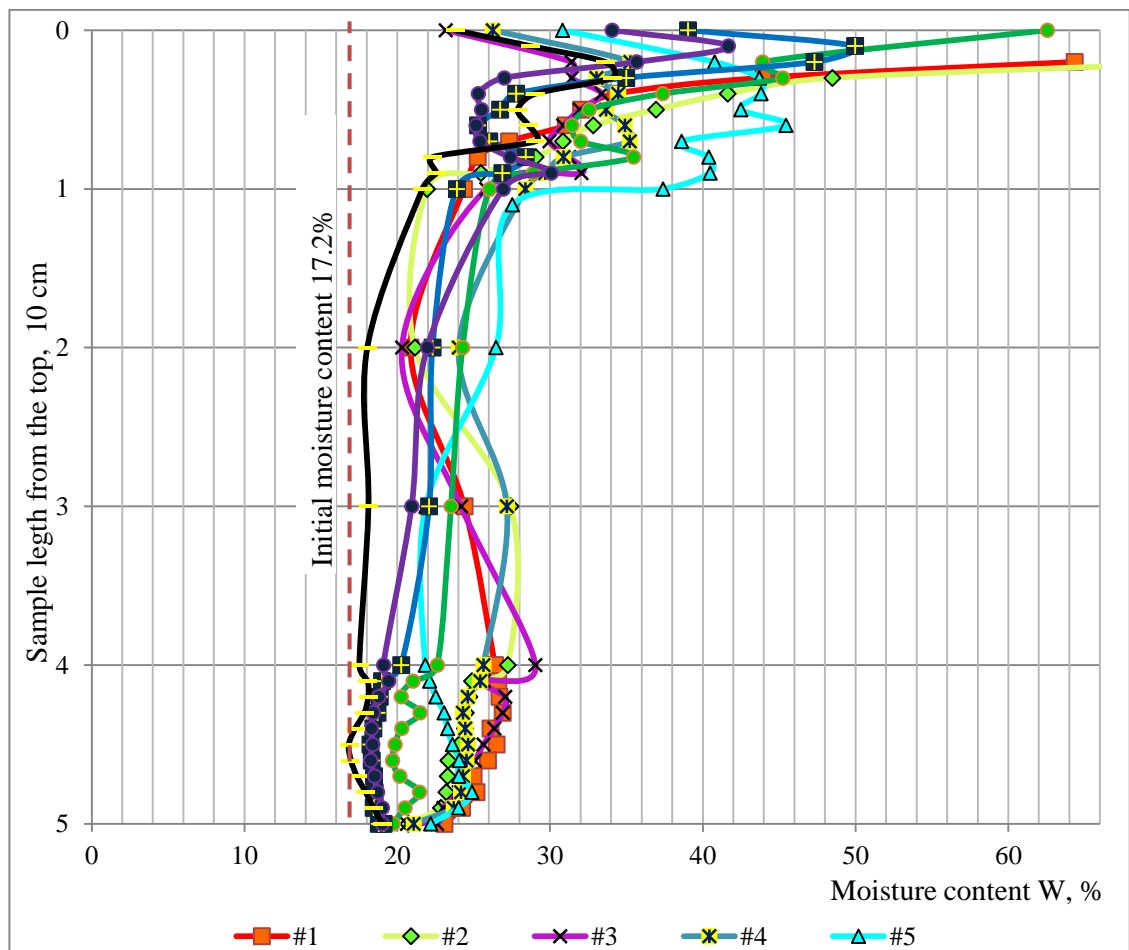


Figure 4.12 – Moisture distribution for Test 4 after two freeze-thaw cycles using samples with various dry densities and 11,000 mg/litre sodium chloride solution supply

The maximum water intake during Test 5 was around 700-800 g and was observed in the loose soil samples with bulk density between 1.60 and 1.70 g/cm<sup>3</sup> for columns #1, #2 and #3. Dense soils had a very low coefficient of permeability, which was in the range of  $2.9-8.8 \times 10^{-9}$  m/s according to Table 3.10, and the moisture content was close to the

correspondent maximum dry density value. So the soils were close to the saturated condition. Consequently, the total water intake in column #9 (the densest) was approximately four times less than in columns #1-#5, three times less than columns #6-#7 and half that of the soil with  $\rho=2.09 \text{ g/cm}^3$  density in column #8. The initial density sets and water intake after the freeze-thaw cycles with variable densities and 22,000 mg/litre sodium chloride content basement feeding in Test 5 are presented in Table 4.2 and Figure 4.13.

Table 4.2 – Moisture-density change in Test 5

Column number	Weight of the soil sample, g		Water income, g	Bulk density, Mg/m <sup>3</sup>		Dry density, Mg/m <sup>3</sup>		Average W per column after test, %
	before test	after test		before test	after test	before test	after test	
#1	12,457	13,230	773	1.570	1.673	1.339	1.359	23.093
#2	12,718	13,552	834	1.603	1.712	1.367	1.399	22.362
#3	13,309	14,107	798	1.678	1.772	1.430	1.445	22.612
#4	14,033	14,736	703	1.769	1.851	1.508	1.511	22.485
#5	14,233	14,945	712	1.794	1.875	1.530	1.531	22.501
#6	14,341	14,883	542	1.808	1.870	1.541	1.550	20.632
#7	15,579	16,163	584	1.964	2.012	1.674	1.646	22.240
#8	16,564	16,940	376	2.088	2.116	1.780	1.764	19.921
#9	16,759	16,952	193	2.113	2.127	1.801	1.784	19.205



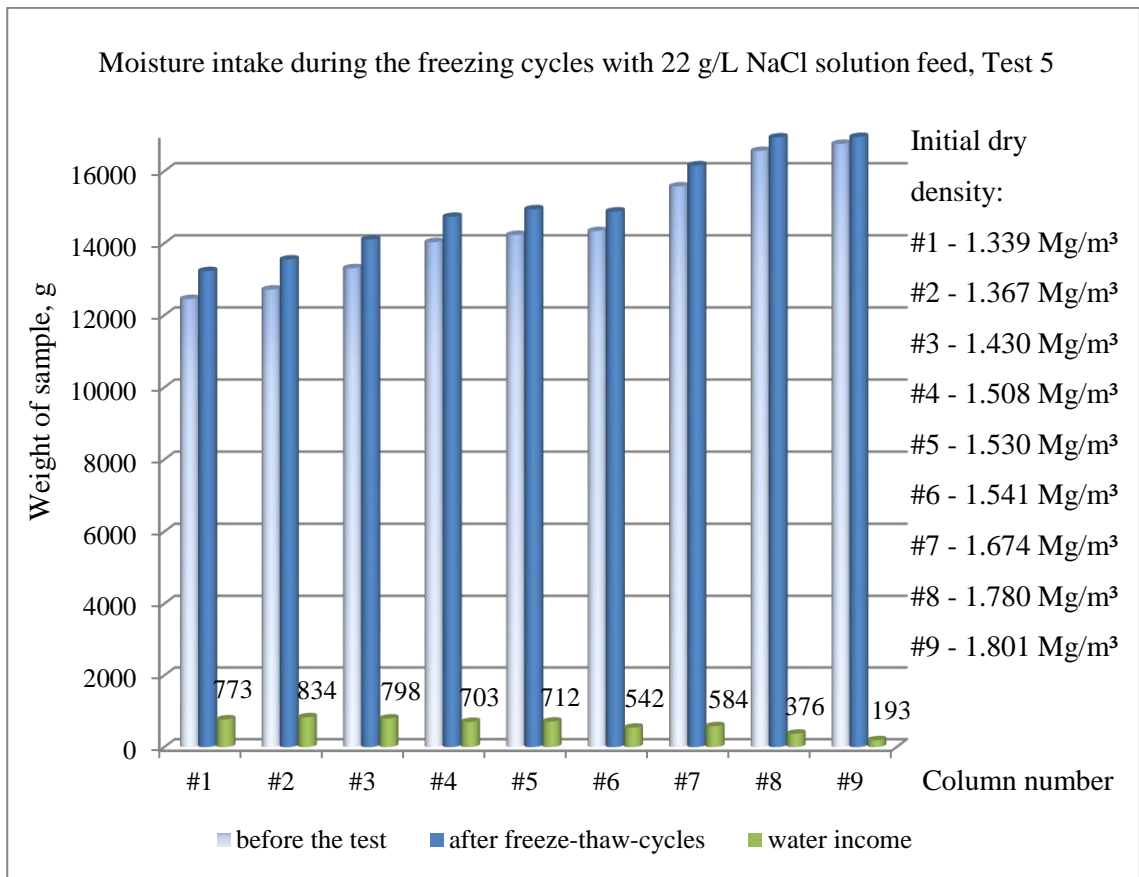


Figure 4.13 – Moisture intake during the freeze-thaw cycles in Test 5

Whilst the initial moisture content was 17.2 % in all the tests and columns before the freeze-thaw cycles, after the testing, an inversely proportional relationship emerged, as presented in Figure 4.14.

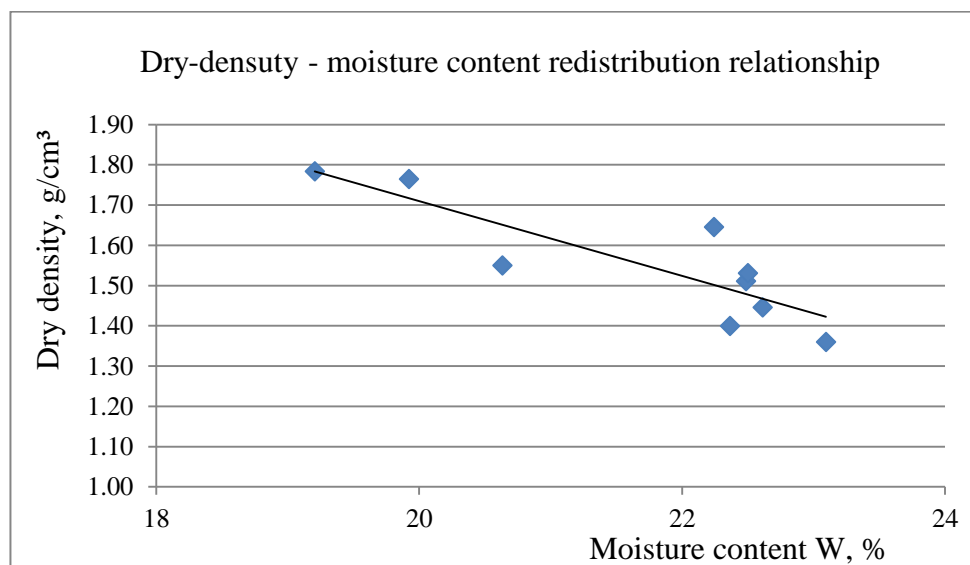


Figure 4.14 – Dry density - moisture content redistribution relationships after the freeze-thaw cycles in Test 5

The moisture redistribution over the column lengths is presented in Figure 4.15. Conditional division into moisture transit zones distinguishes the ice lens segregation zone – top 20 cm, desiccated zone – 20 to 50 cm depth and the moisturised zone, supplied from the ground water table - below 50 cm to 95 cm. The ice lenses formation in the ‘heaved’ zone prevailed in the dense soils rather than the loose one. In the desiccated zone, the moisture content remained stable regardless of the density and was relatively similar to the initial moisture content of 17.2 %. However, below 50 cm the absorption from the water table and the moisture transfer produced increased mass transfer in the loose soil samples compared to the dense ones (Figure 4.15).

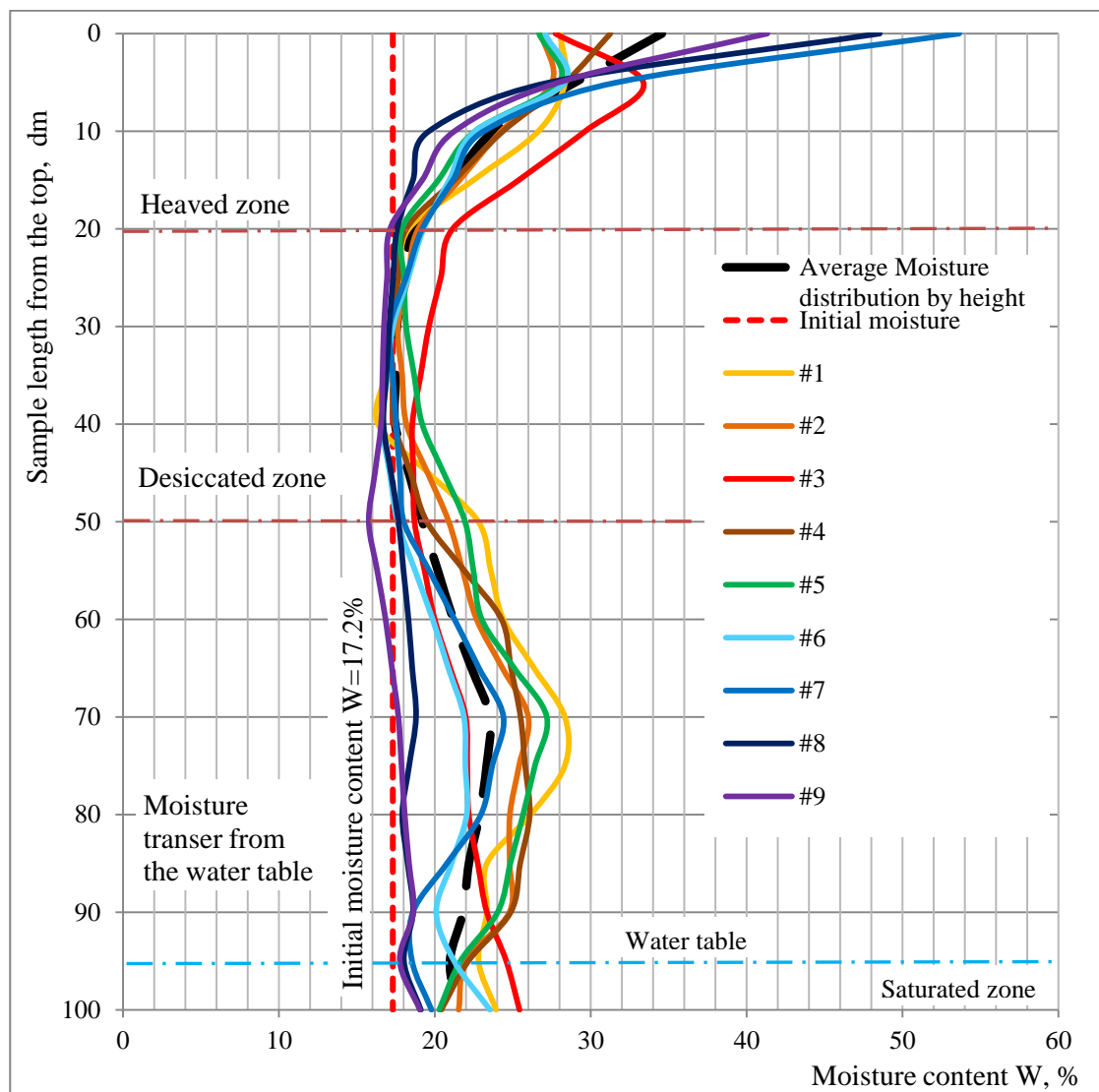


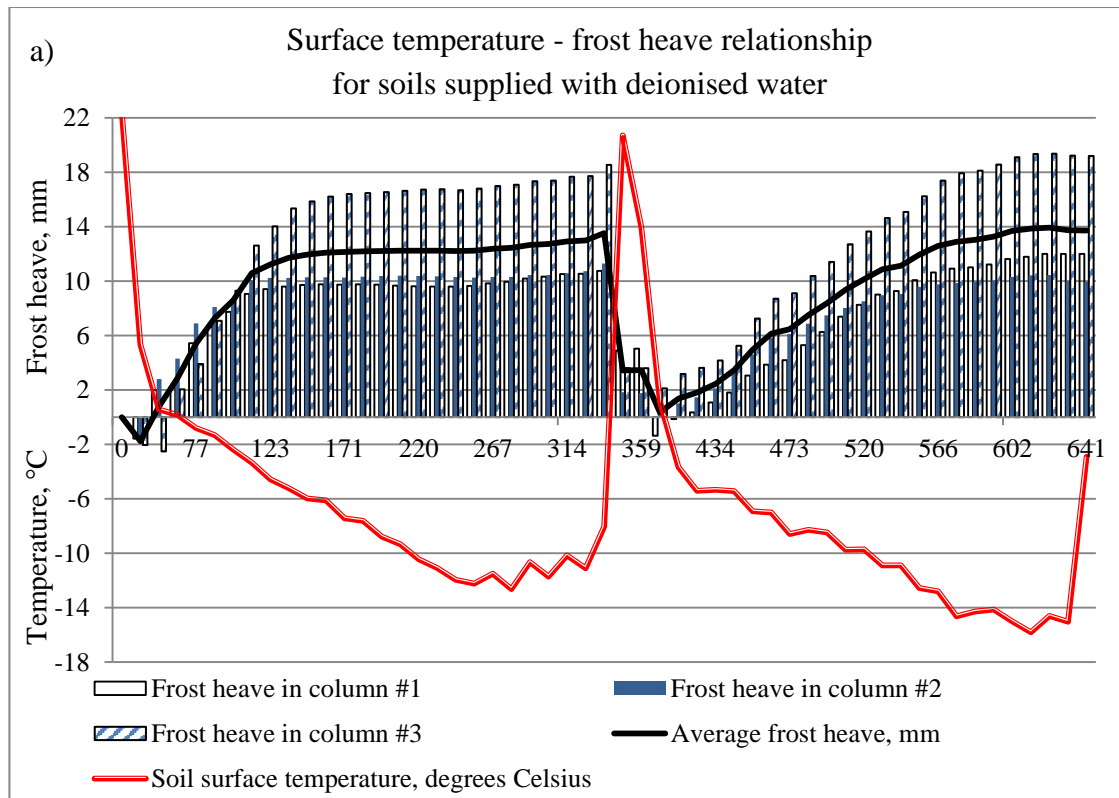
Figure 4.15 – Moisture redistribution in soil samples after freeze-thaw cycles in Test 5, with 22 g/L NaCl solution supply

Thus, according to the obtained results, ice lens formation in the freezing front is prevalent in dense soils free of chemical content, while moisture absorption from the

water table dominates in loose soils. Moisture redistribution within the soil sample during the freeze-thaw cycles verified a direct relation of moisture intake with the dry density, and respectively, with the void ratio.

#### 4.4 Frost heave observations

The frost heave curves in Figures 4.15-4.19 include the consolidation period, first freezing cycle, first thawing cycle, second freezing cycle and the beginning period of post-test thawing, when the thermocouples were still plugged in. The average duration of testing comprised over 600 h. The relationship between the surface temperature and frost heave value over time for the soil samples compacted with maximum dry density in Tests 1 and 2 are presented in Figure 4.15. A comparison of the volumetric deformation in the vertical axis signifies a steady progression of frost heave in samples supplied with deionised water, which is more pronounced in the second freezing cycle. (Figures 4.16 a and b). At the same time, the frost heave is less progressed in the second cycle of Test 2. The reduction of frost heave by time in Figure 4.15b verifies the significant impact of de-icing chemical application to the soils compacted with maximum dry density during their secondary salinisation.



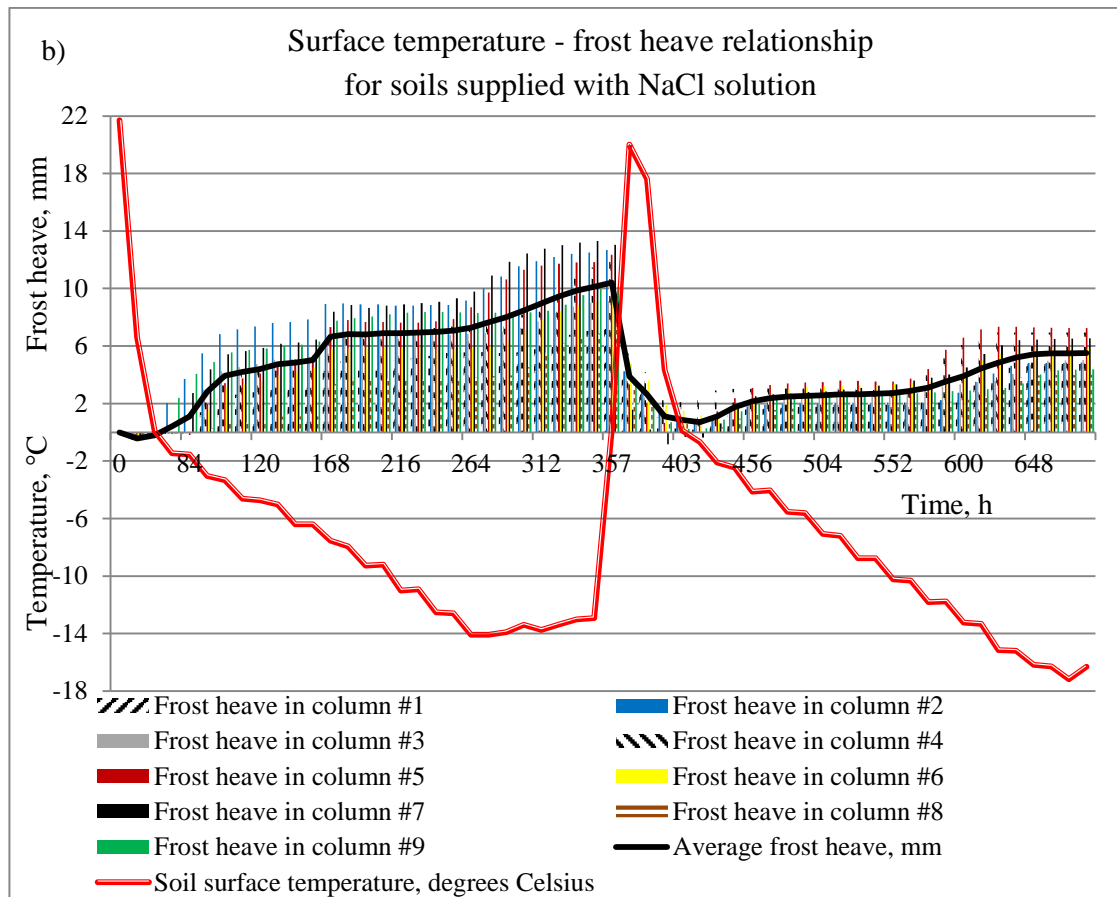


Figure 4.16 - Relationship between the surface temperature and frost heave by time, h: a – for samples supplied with deionised water in Test 1; and b - for samples supplied at the base with 11,000 mg/litre NaCl solution in Test 2 (Sarsembayeva and Collins, 2017)

The relation between the frost heave and temperature is presented in Figure 4.16, while time is variable here. An intensive heaving at the start of the test in the temperature range 0 to -6 °C at 5 cm depth from the soil surface and its further damping in the lower degrees were observed (Figure 4.17). Notably, the temperature difference between the top surface and the next thermocouple located 5 cm distance from the top was 5-6 °C during the freezing. A sudden small heave occurred in all the dense samples at the beginning of thaw period, possibly due to the cryosuction potential, which has not been carried out while the soil structure was frozen. Some oscillation in the frost heave results means there is uniqueness of the pore channels formation during the freezing, the structure of which further mass transfer depends upon.

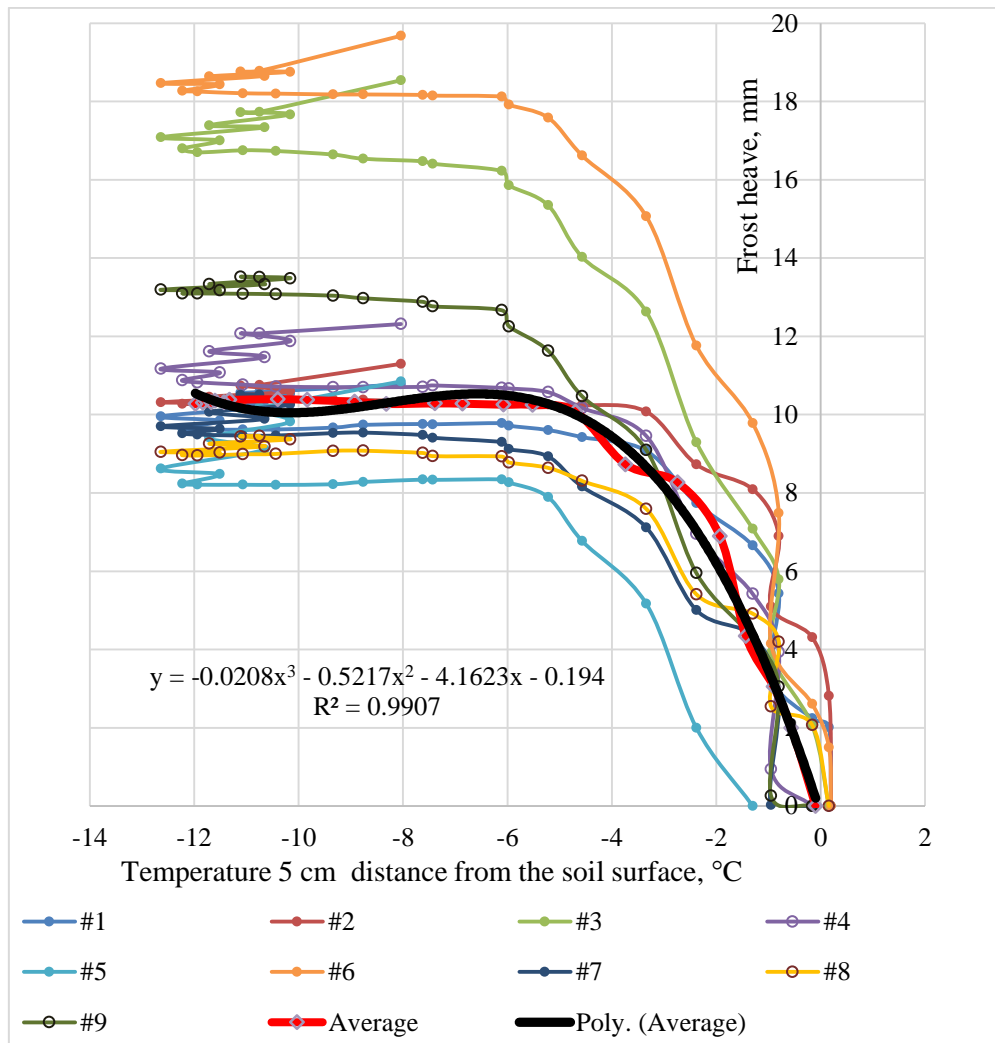


Figure 4.17 – Relation between the frost heave and temperature 5 cm distance from the soil surface with variable time parameter in Test 1. The black line represents the average polynomial relationship

In the soils in Tests 3 and 4, packed with various densities and with closer access to the water table, the effect of salinity on the frost heave was less pronounced compared to the impact of density (Figures 4.18 and 4.19). In Test 3 with a deionised water supply, the maximum rates of frost heave were achieved in columns #7 and #8, where the dry density was close to the maximum value 1.65-1.79 Mg/m<sup>3</sup>, while the loose soil samples, with dry density 1.18-1.47 Mg/m<sup>3</sup>, registered very weak heaving in the first cycle and consolidation or compression in the second cycle compared to the initial volume. In Test 4, the curves almost ideally positioned the frost heave scale according to their initial density values. In both Tests 3 and 4 the greatest variation of volumetric deformation in the vertical axis was registered by the end of the second freezing cycle (Figures 4.18 and 4.19).

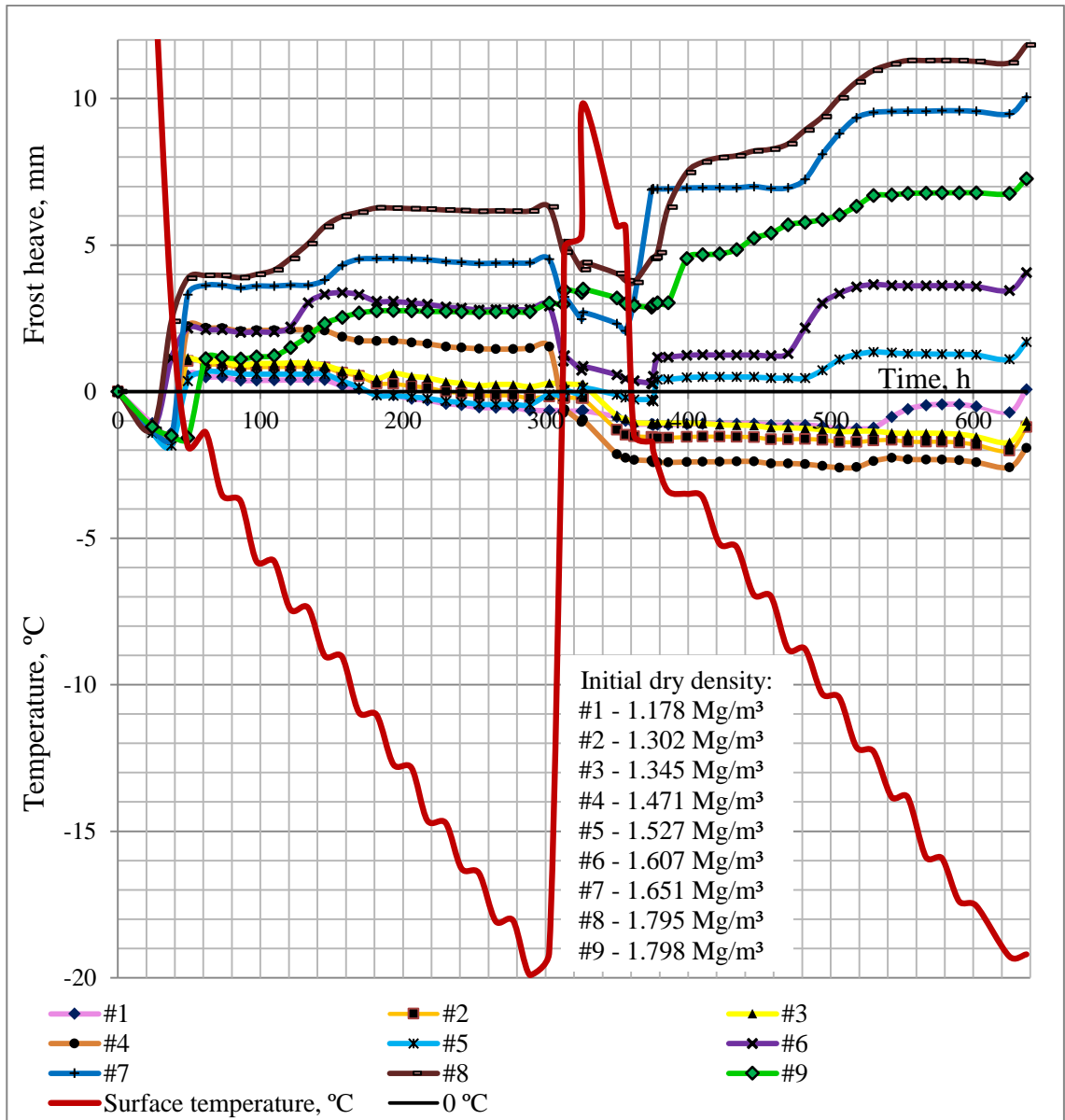


Figure 4.18 – Frost heave in the samples with varied density in Test 3.

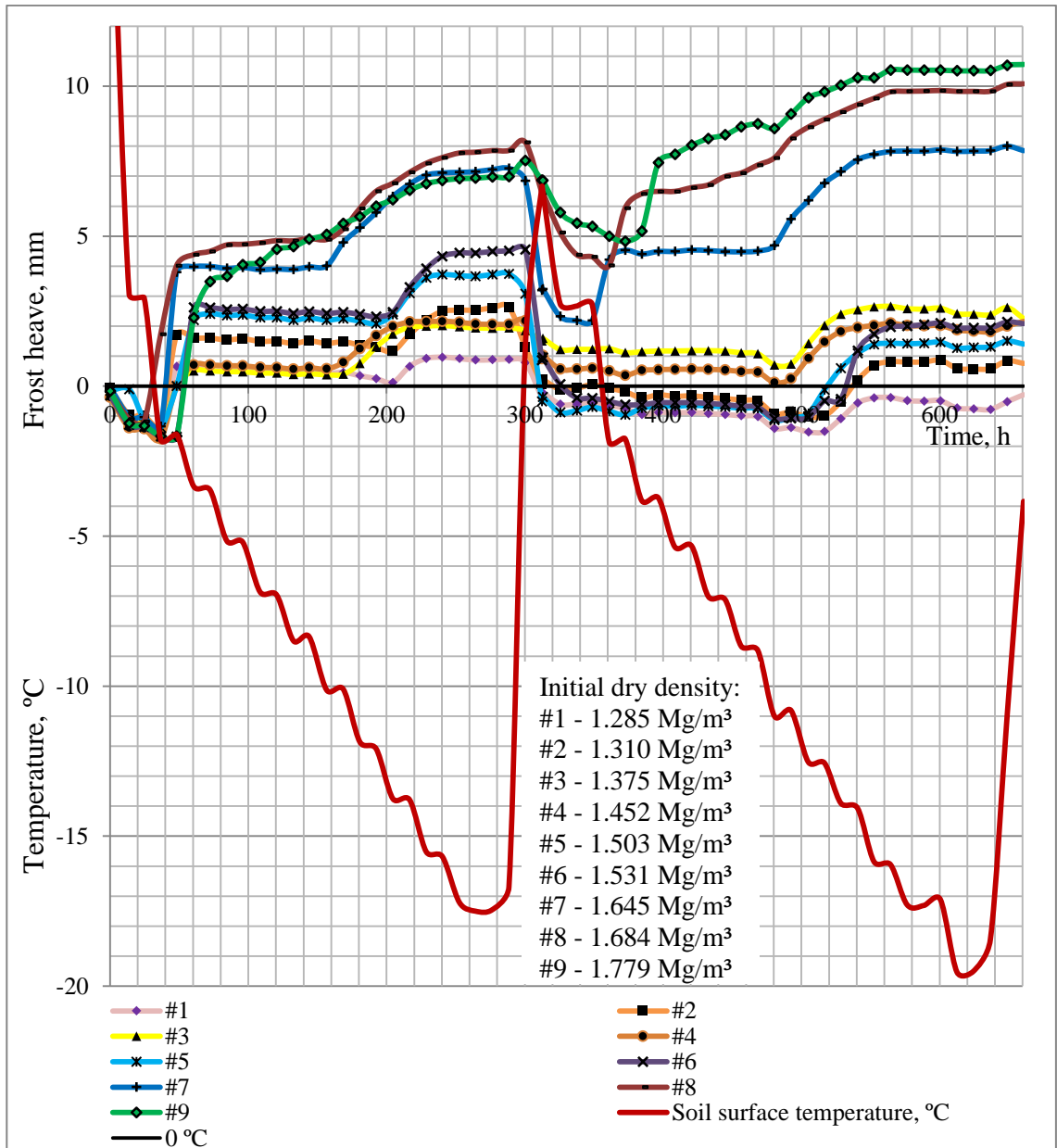


Figure 4.19 – Frost heave in the samples with varied density in Test 4

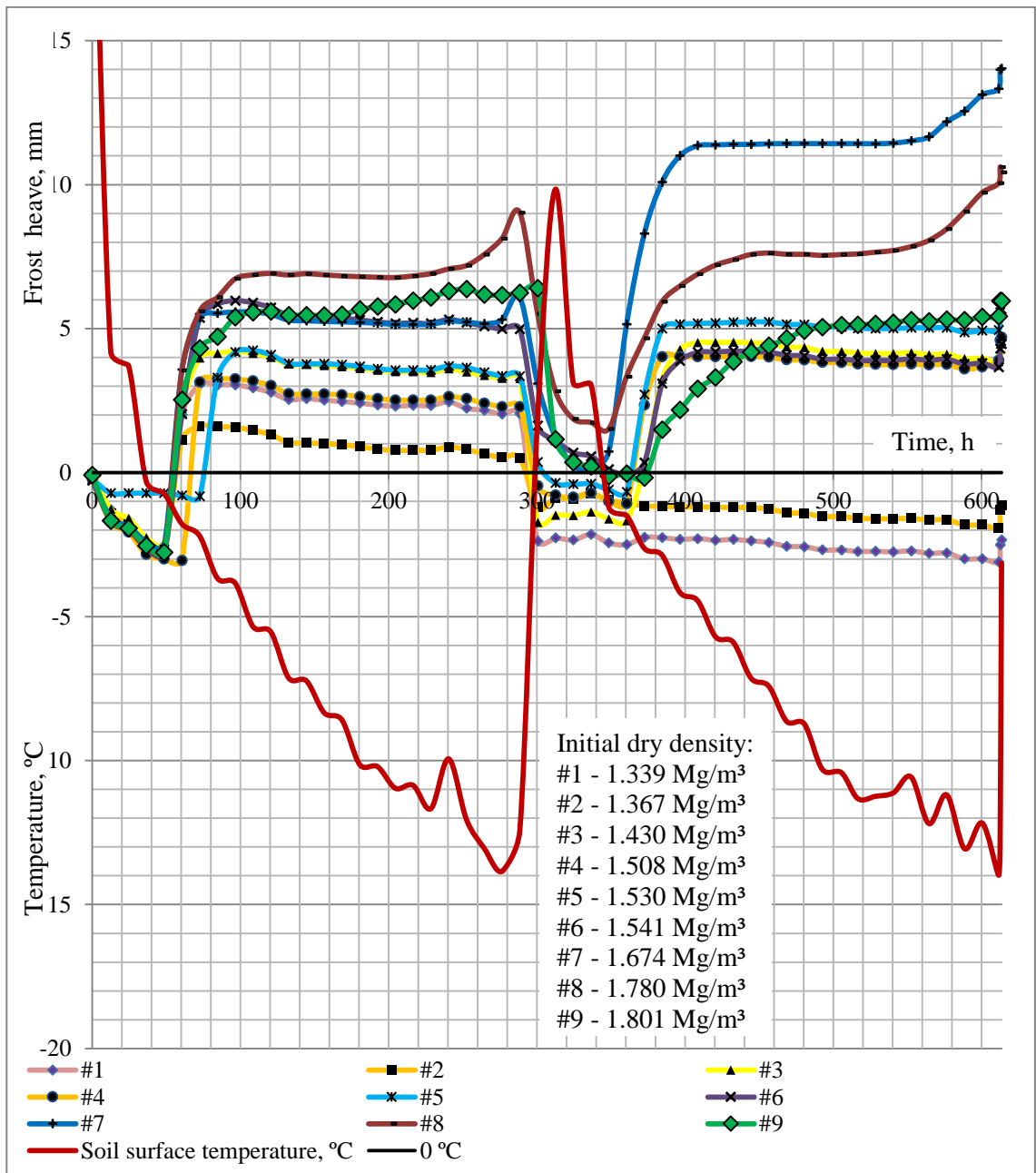


Figure 4.20 – Frost heave in the samples with varied density, supplied with 22 g/L NaCl solution, in Test 5

In Test 5, the soil samples were presented in a full length, comprising 1 m and supplied from the base with a twofold concentration of sodium chloride of 22 g/L, reaffirming the previous results on a greater scale (Figure 4.20). The maximum values of frost heave were recorded in columns #7 and 8 with initial dry density 1.67-1.78 Mg/m<sup>3</sup>, which is correspondent to 92-99% of the maximum dry density of 1.80 Mg/m<sup>3</sup>, and it is the desired level of compaction of the subsoils under the soils. It is clear that the



secondary salinisation in this density range is still very high and in case of the near access to the water table may be even greater.

Summarily, both the density and chemical content are important for frost heave formation, but dense soils tend to loosen and the less compacted soils are compressed during the freeze-thaw cycles. Finally, non-saline soil samples supplied with de-ionised water have a more pronounced tendency to frost heave and the greatest effect is observed in the second freezing cycle.

#### **4.5 Chemical content change**

Freeze-thaw cycles with the soil samples supplied with de-icing chemical solution were conducted in Tests 2, 4, and 5 (presented in the Table 3.4, Chapter 3). In Test 2, the non-saline soil samples were packed to 1 m lengths with a maximum dry density  $1.8 \text{ Mg/m}^3$  corresponding to initial moisture content  $W=17.2\%$  in all nine columns. In Tests 4 and 5 the samples were packed with various densities and the sample length was either 50 cm or 100 cm. The sodium chloride solution in Tests 2 and 3 was 11 g/L, while in Test 5 it was 22 g/L. According to electrical conductivity measurements by the method described in subsection 3.5.6, the average value of chemical content for the nine columns in Test 2 was obtained through oven dried soil samples after two freeze-thaw cycles, as presented in Figure 4.21. The chemical content here was plotted regarding the ‘relative zero’ – conventionally taken initial chemical content of the soils before supplying them with sodium chloride solution.

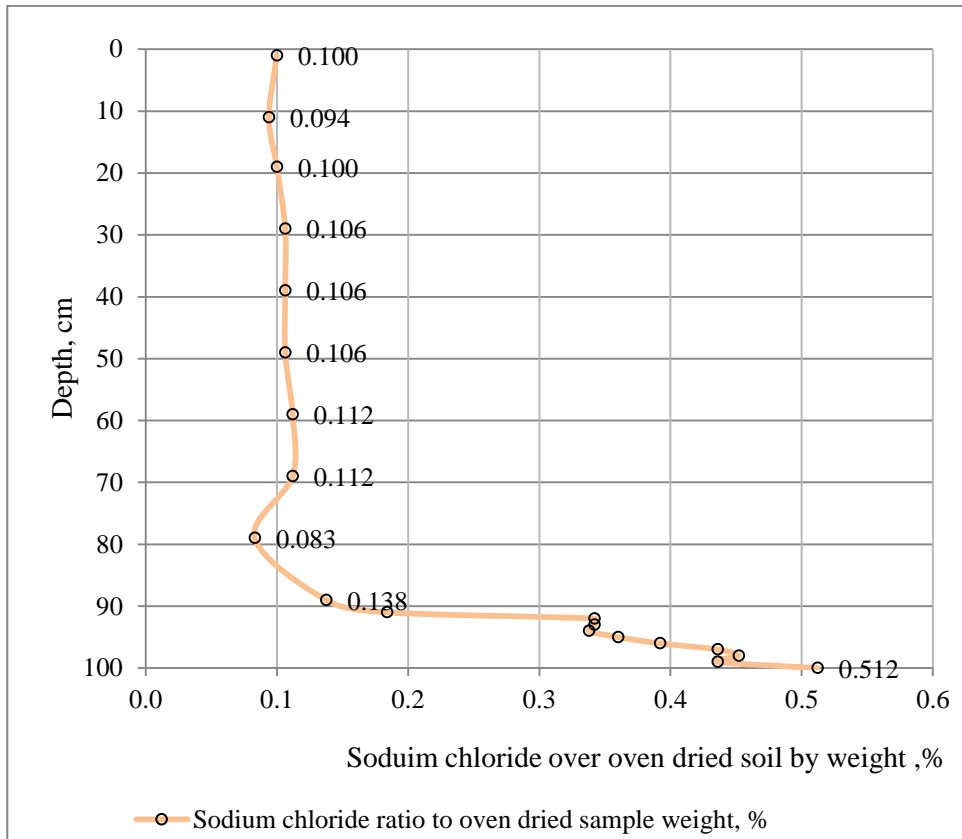


Figure 4.21 – The percentage of sodium chloride to oven dried soil by weight, on average, after freeze-thaw cycles for Test 2

The electrical conductivity readings for each column over the sample length are presented in Appendix C, Tables C.1 and C.2. The calculation of sodium chloride content after Test 2 and its expression in different units is presented in Table 4.3.

Table 4.3 – Calculation of sodium chloride content: the average for nine columns after freeze-thaw cycles for Test 2

Sample depth, cm	Electrical conductivity $\mu\text{S}$ , average by 9 columns	NaCl concentration, obtained by calibration chart g/250ml	Moisture content, average for 9 columns W, %	Mass of water dried out from 25 g of soil sample, g	Mass of NaCl per 1 Litre of pore water, g /litre	NaCl content expressed in		
						Percentage to oven dried soil weight, %	Molarity, number of mols NaCl to volume of solution, Moll (NaCl)	Parts per million, ppm
1	0.27	0.0250	46.25	11.563	<b>8.649</b>	0.100	0.037	2.162
11	0.26	0.0235	18.9	4.728	<b>19.884</b>	0.094	0.085	4.971
19	0.27	0.0250	16.9	4.225	<b>23.669</b>	0.100	0.101	5.917
29	0.29	0.0266	16.3	4.075	<b>26.110</b>	0.106	0.112	6.528
39	0.29	0.0266	16.3	4.075	<b>26.110</b>	0.106	0.112	6.528
49	0.29	0.0266	16.7	4.175	<b>25.485</b>	0.106	0.109	6.371
59	0.30	0.0280	17.2	4.300	<b>26.047</b>	0.112	0.111	6.512
69	0.30	0.0280	17.8	4.450	<b>25.169</b>	0.112	0.108	6.292
79	0.24	0.0208	18.9	4.725	<b>17.608</b>	0.083	0.075	4.402
89	0.35	0.0344	19.6	4.900	<b>28.082</b>	0.138	0.120	7.020
91	0.45	0.0460	19.6	4.900	<b>37.551</b>	0.184	0.160	9.388
92	0.78	0.0855	19.6	4.900	<b>69.796</b>	0.342	0.298	17.449
93	0.78	0.0855	19.6	4.900	<b>69.796</b>	0.342	0.298	17.449
94	0.77	0.0845	19.6	4.900	<b>68.980</b>	0.338	0.295	17.245
95	0.81	0.0900	19.6	4.900	<b>73.469</b>	0.360	0.314	18.367
96	0.89	0.0980	19.6	4.900	<b>80.000</b>	0.392	0.342	20.000
97	0.98	0.1090	19.6	4.900	<b>88.980</b>	0.436	0.380	22.245
98	1.01	0.1130	19.4	4.850	<b>93.196</b>	0.452	0.398	23.299
99	0.98	0.1090	19.1	4.775	<b>91.309</b>	0.436	0.390	22.827
100	1.14	0.1280	18.9	4.725	<b>108.360</b>	0.512	0.463	27.090

The results of the electrical conductivity measurements confirmed the chemical mass transfer phenomenon across 1 m soil sample length. The chemical mass transfer in Test 2 was conditioned by the temperature gradient during unidirectional freezing from the top and also through feeding non-saline dense soil samples with sodium chloride solution. The observed chemical mass transfer results demonstrate that the de-icing chemical ratio in the pore water exceeds the concentration of the supplied solution from the water table. Notably, the chemical concentration of sodium chloride corresponding to the pore water volume was 2-2.5 times higher than the initial supplied concentration of the solution from the base at the interval between 10 and 90 cm from the top surface.

Table 4.4 – Sodium chloride content for column #1 with density  $\rho=1.51 \text{ g/cm}^3$  (Test 4 with 11 g/L NaCl supply from the base)

Sample depth, cm	Electrical conductivity $\mu\text{S}$ , for column #1 in Test 2	NaCl concentration, obtained by calibration chart g/250ml	Moisture content at the end of the test, average for 9 columns W, %	Mass of water dried out from 25 g of soil sample, g	Mass of NaCl per 1 Litre of pore water, g/litre	NaCl content expressed in		
						Percentage to oven dried soil weight, %	Molarity, mols of NaCl to volume of solution, Mol(NaCl)	Parts per million, ppm
1	0.21	0.0161	64.33	16.08	4.009	0.064	0.017	1.002
5	0.12	0.0052	35.31	8.83	2.350	0.021	0.010	0.588
9	0.17	0.0113	24.35	6.09	7.399	0.045	0.032	1.850
19	0.23	0.0185	20.87	5.22	14.221	0.074	0.061	3.555
29	1.43	0.1643	24.4	6.10	107.748	0.657	0.460	26.937
39	1.28	0.1461	26.39	6.60	88.576	0.584	0.379	22.144
45	1.79	0.2080	25.61	6.40	129.978	0.832	0.555	32.495
50	1.24	0.1412	23.08	5.77	97.911	0.565	0.418	24.478

In Test, 4 the length of the sample was 50 cm and the water table, with an 11 g/L sodium chloride solution supply, was at 45 cm depth from the top. After two freeze-thaw cycles a secondary chemical salinisation over the entire length of the soil samples of all densities was detected (Figure 4.22). From a depth of 20 cm and below, the concentration of the sodium chloride in the pore water exceeded the initial concentration of the supply solution. From a depth of 30 cm and below, the concentration of the sodium chloride in the pore water was 8-10 times higher than the initial values. This confirms that upward chemical mass transfer and its significant deposition in 15-20 cm distance above the water table was caused by capillary suction during freeze-thaw cycles.

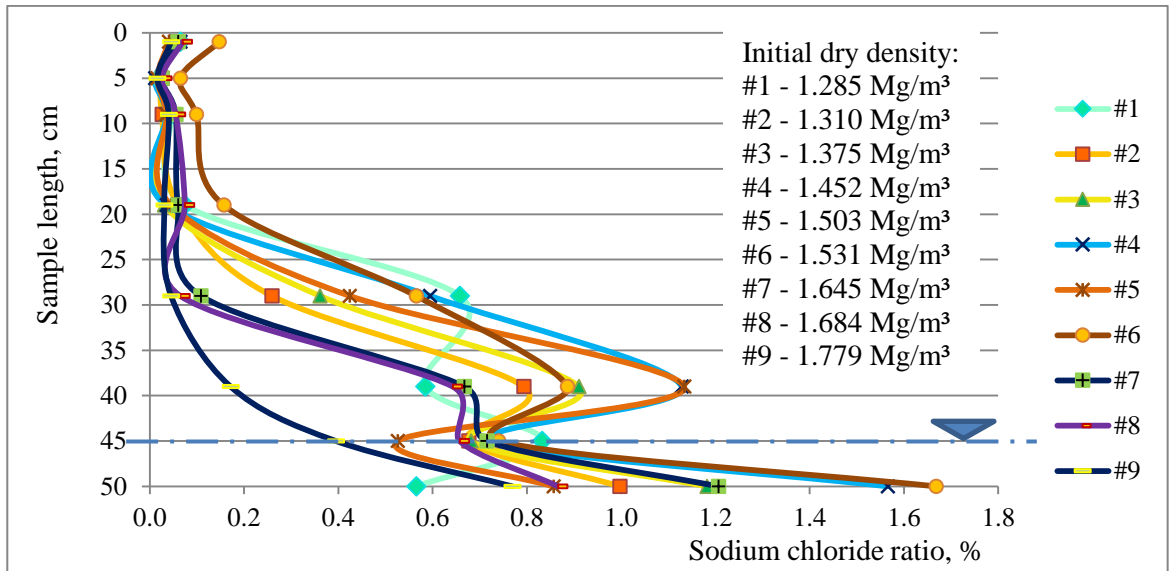


Figure 4.22 – Sodium chloride ratio in variable density samples after Test 4, in % to oven dried soil mass

In Test 5, samples of 1 m height were supplied with 22 g/L sodium chloride solution from the base, where the lowest 5 cm was saturated. The results indicated that secondary chemical salinisation took place during the freeze-thaw cycles over the entire soil sample length (Figure 4.23). In fact, 0.05 – 0.15 % sodium chloride rate over the dried soil sample weight was discovered from the top surface to 70 cm depth, which was hypothesised, according to the processes of chemical osmosis and thermal gradient during unidirectional freezing from the top. Below 25 cm, considerable de-icing chemicals deposition was registered, which might be associated with capillary raise.

In sum, the results of conducted the experiments verified that chemical mass transfer occurred at between 0.05 and 0.15 % for the oven dried sample weight. According to the electrical conductivity probe tests, the chemical mass transfer happened regardless of the sample length and density, being supplied with sodium chloride solution of concentration of either 11 or 22 g/L. A significant amount of the chemical content was deposited in the 15-25 cm soil layer overlying water table and obviously, was caused by the capillary raise. Finally, the amount of deposited chemicals depended on the concentration of the supply solution and soil density.

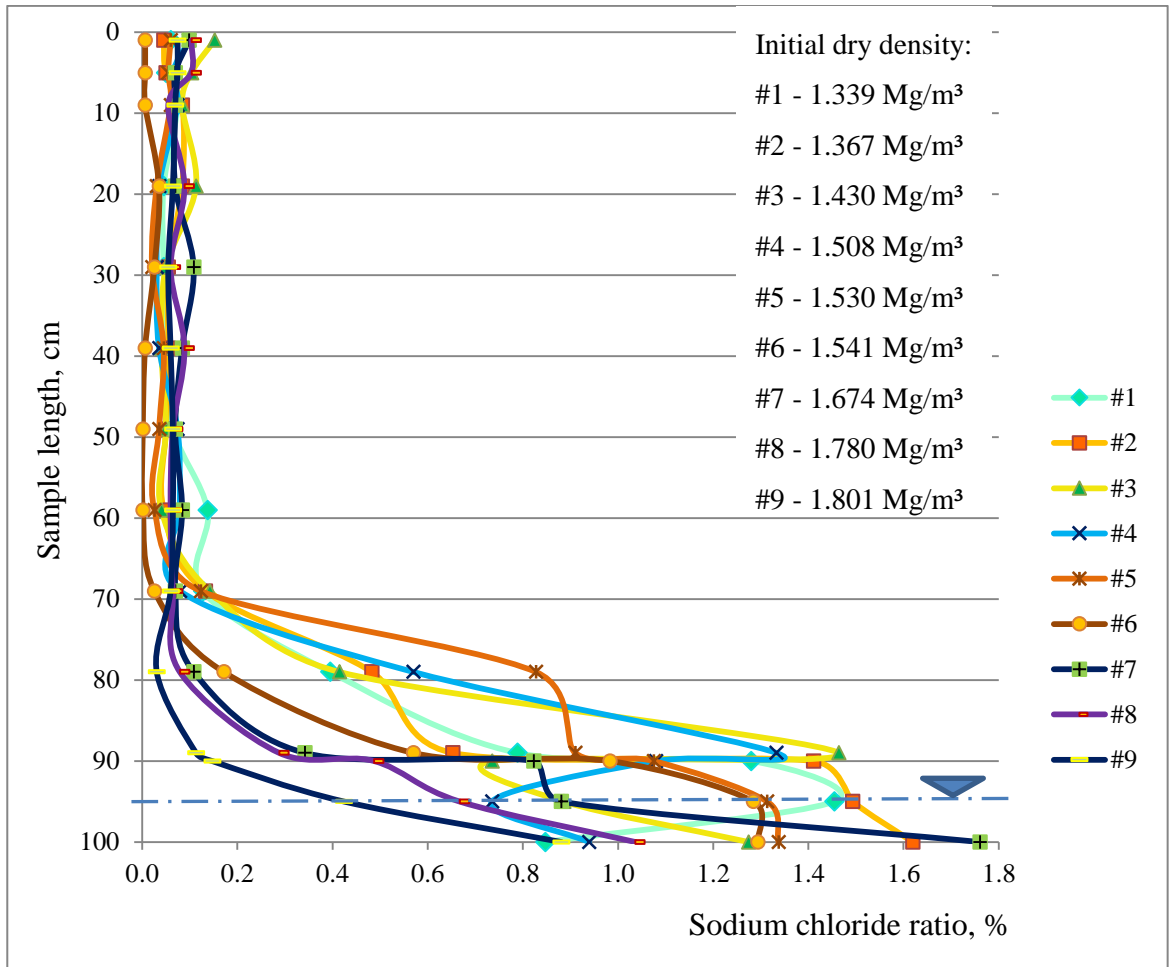


Figure 4.23 – Sodium chloride ratio in variable density samples after Test 5, in % to oven dried soil mass

#### 4.6 Density and structure change

The dense soil led to dilation after two freeze-thaw cycle tests due to the moisture absorption in the freezing zone and its expansion during ice segregation. The loose soils, in contrast, started to consolidate during the thawing, which is in accordance with results of Qi *et al.* (2008). It is notable that density changes in the frozen soils depended on their moisture content, which in turn, depended on the chemical content and freezing regime, i.e. temperature drops and number of freeze-thaw cycles. Tables 4.5 and 4.6 shows the density change after Test 1, in which the soils were supplied with deionised water and Test 2, when the soils were supplied with 11,000 mg/litre sodium chloride solution. All the remoulded samples in both tests were compacted with maximum dry density 1.8 Mg/m<sup>3</sup> corresponding to 17.2% moisture content.

Table 4.5 – Moisture – density change before and after the freeze-thaw cycles with a deionised water supply in Test 1

Column	Moisture content, %		Bulk density, g/cm <sup>3</sup>		Dry density, g/cm <sup>3</sup>		Change in dry density, %
	before the test	after the test	before the test	after the test	before the test	after the test	
#1	17.2	25.48	2.108	2.129	1.797	1.697	5.58
#2	17.2	20.97	2.110	2.123	1.799	1.755	2.47
#3	17.2	25.83	2.108	2.093	1.797	1.664	7.42
#4	17.2	19.43	2.106	2.108	1.795	1.765	1.68
#5	17.2	19.45	2.109	2.106	1.798	1.763	1.94
#6	17.2	19.40	2.111	2.106	1.800	1.764	2.00
#7	17.2	19.41	2.112	2.120	1.801	1.775	1.44
#8	17.2	20.78	2.107	2.115	1.796	1.751	2.53
#9	17.2	21.61	2.113	2.113	1.801	1.737	3.55

Table 4.6 - Moisture –density change before and after the freeze-thaw cycles with 11,000 mg/litre sodium chloride feeding in Test 2

Column	Moisture content, %		Bulk density, g/cm <sup>3</sup>		Dry density, g/cm <sup>3</sup>		Change in dry density, %
	before the test	after the test	before the test	after the test	before the test	after the test	
#1	17.2	20.847	2.106	2.108	1.796	1.744	2.85
#2	17.2	21.127	2.103	2.103	1.793	1.737	3.15
#3	17.2	21.837	2.103	2.110	1.793	1.732	3.39
#4	17.2	20.455	2.091	2.099	1.783	1.742	2.28
#5	17.2	21.418	2.105	2.102	1.795	1.731	3.51
#6	17.2	20.946	2.104	2.103	1.794	1.739	3.07
#7	17.2	21.440	2.110	2.121	1.799	1.747	2.92
#8	17.2	21.583	2.094	2.106	1.785	1.733	2.93
#9	17.2	22.457	2.095	2.111	1.786	1.724	3.51

It should be noted that columns #7 - #9 in Test 1 were removed after the first freezing cycle. Columns #4 - #6 were sampled after completion of the first thawing cycle and their soil structure had considerably compressed due to the drainage. Whilst #1 - #3 columns were kept in the environmental chamber until the end of the second freeze-thaw cycle and those columns' results could be compared with the soil samples in Test 2, for which all columns were also tested for two freeze-thaw cycles.

In Table 4.5, it can be seen that the average moisture content of the samples was around 23-24 % after Test 1, while after Test 2 it was around 21% (Table 4.6) and thus, the chemical component contributed to a reduction in the ground water intake of the

samples during the freeze-thaw cycles. Moreover, change in moisture content had an inversely proportional effect on the values of dry density. Further, the post-test dry density of samples supplied with deionised water from the base was significantly lower than for those, fed with saline solution (Table 4.5 и 4.6).

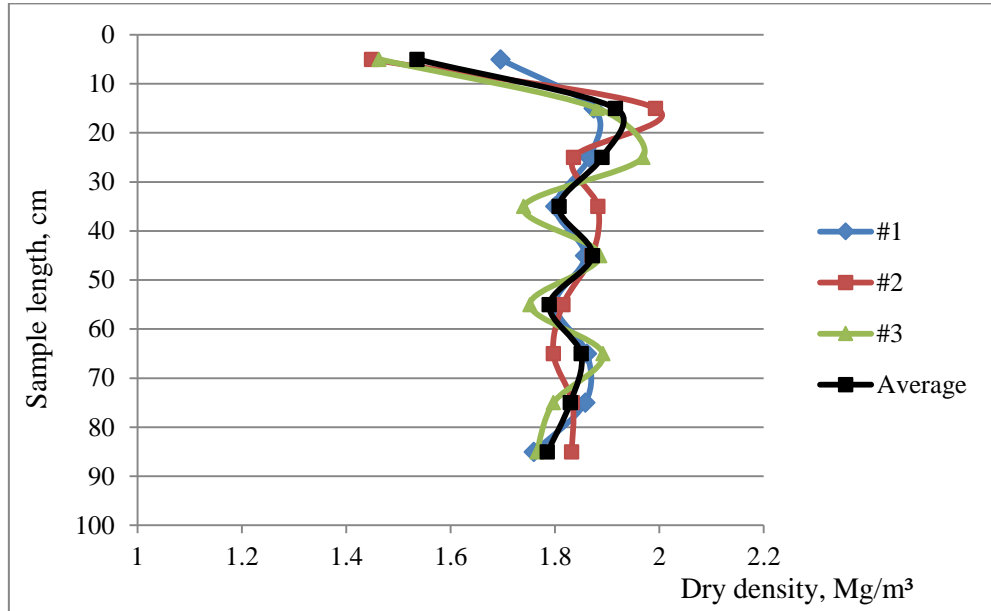


Figure 4.24 - Dry density distribution through the length of the sample after Test 1

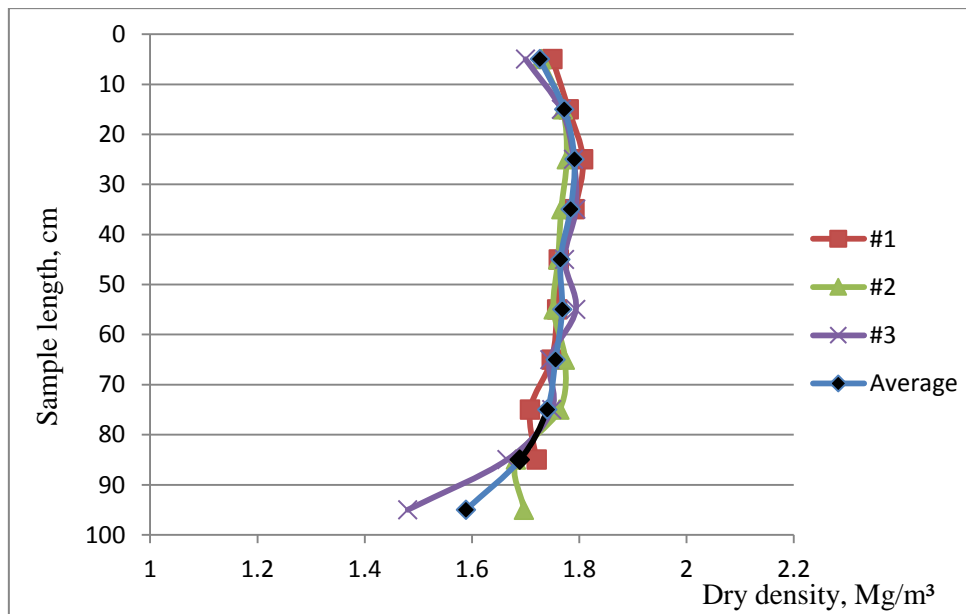


Figure 4.25 - Dry density distribution through the length of the sample after Test 2

Density also fluctuated through the length of the samples depending on the moisture content and ice lens formation during the freeze-thaw cycles. The dry density of the 20 cm upper layers which was in a frozen condition, was 1.45-1.70 g/cm³ in Test



1 and 1.70-1.77 g/cm<sup>3</sup> in Test 2 (Figures 4.24 and 4.25). In the middle length zone, at 20-70 cm from the soil surface, the average dry density in Test 1 varied between 1.80-1.85 g/cm<sup>3</sup> and 1.74-1.79 g/cm<sup>3</sup> in Test 2. This is explained by the high desiccation rate of moisture from the middle zone to the freezing top in the deionised water supplied soils. While in the soil samples supplied with saline water the moisture redistribution was less variable along the column length. The moisture content in the lower zone, below 80 cm, was increased and the dry density was reduced to 1.75-1.83 in Test 1 and 1.48-1.69 in Test 2.

In Tests 3, 4 and 5, with variable initial density packing, the samples with loose soils condensed during the freeze-thaw cycles, whilst the dense samples were loosened (Figures 4.26 and 4.27). Regarding sample length, the top layers were always loosened due to the high content of ice lenses formed at the cold front. The bulk density distribution by the column length is presented in the example of Test 3 in Appendix E, Figure E.1. The columns with loose density were consolidated throughout the column length, with the most value in the lower parts of the samples. Whilst in the dense soil samples, only the 10 cm layer on top was loosened and had attracted a large amount of water to form ice lenses (Figure 4.28).

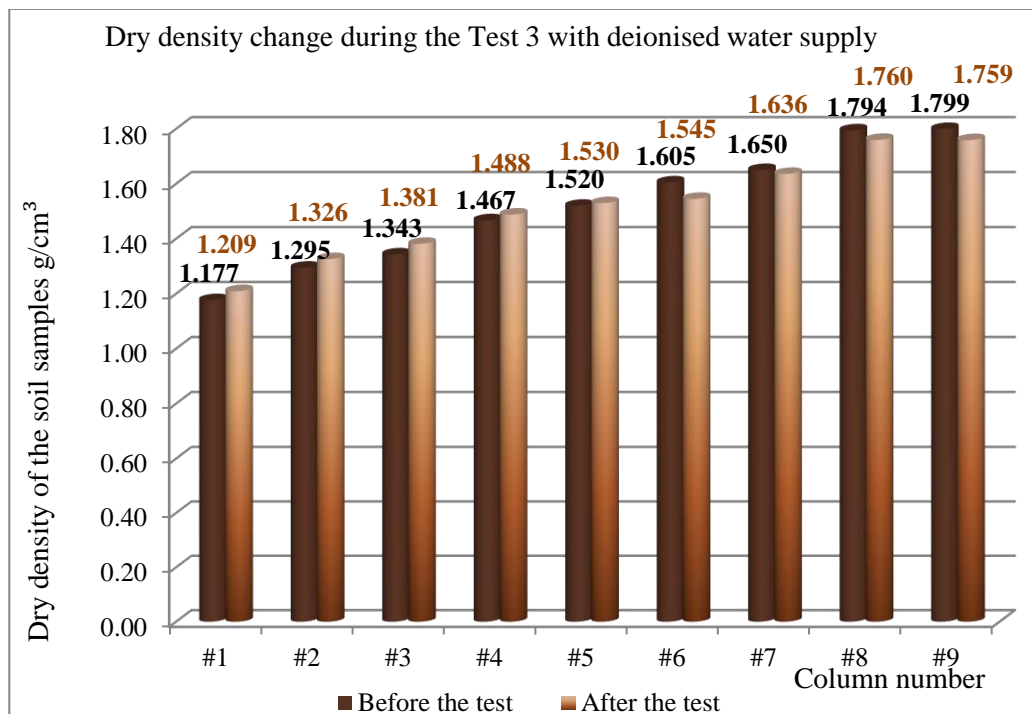


Figure 4.26 – General density change in the samples with variable dry density for Test 3

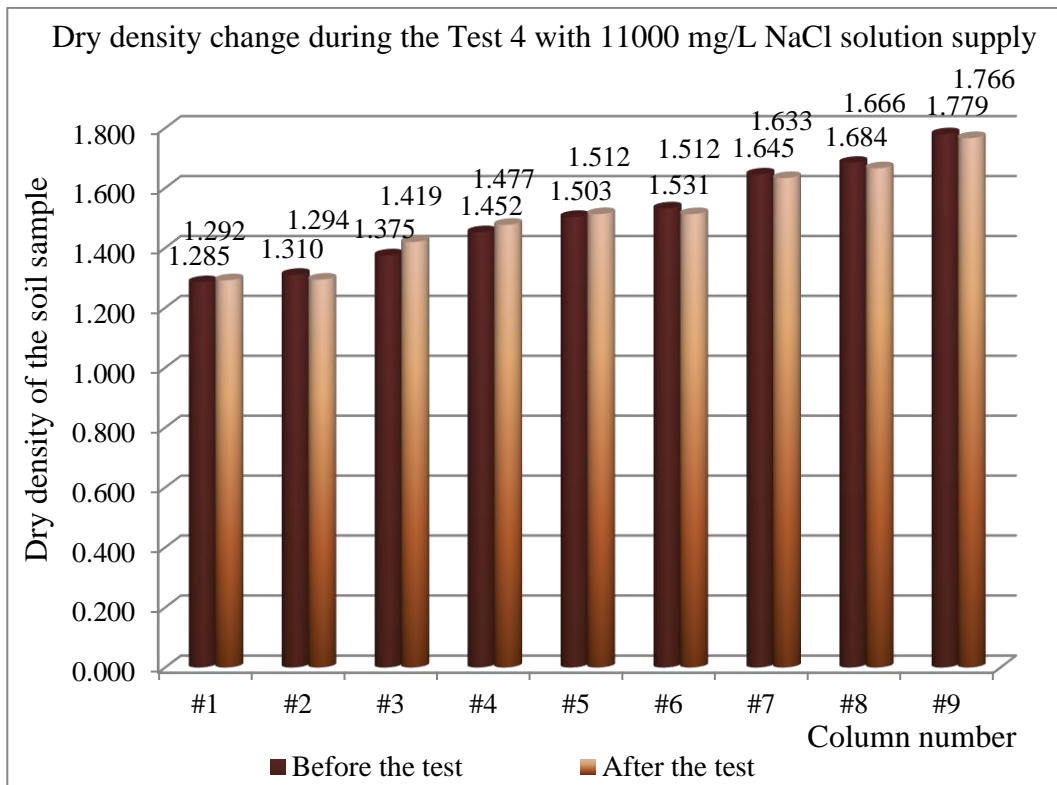


Figure 4.27 – Dry density change during the freeze-thaw cycles in Test 4



Figure 4.28 – Horizontal stratified structure of ice lenses at the top 10 cm layer of the sample supplied by deionised water for Test 1 (the sample is lying on its side)



Figure 4.29 – Structure of the soil sample after freeze-thaw cycles supplied with 11,000 mg/l sodium chloride solution in Test 4 (the sample is lying on its side)

The ice lenses that formed in the frozen samples were horizontally stratified with a greater presence at the freezing top, corresponding to unidirectional expansion in the vertical direction. The thickness of the ice lenses in Test 1 varied from several microns to 3 mm (Figure 4.28). In the samples of low chemical content with a deionised water supply from the base (in Tests 1 and 3) the thickness of the formed ice lenses 10-50 times exceeded the thickness of those formed in the samples supplied with de-icing chemicals, as in Tests 2, 4 and 5 (e.g. Figure 4.29). In fact, the chemical content in the freezing soils directly affected not just the freezing point of the pore water, but also the moisture mass transfer, density change and accordingly, the bearing capacity of the soils.

#### **4.7 Strength-deformation properties change**

The mechanical characteristics of the soils after the freeze-thaw cycles were obtained by directly sampling the testing material after removal from the environmental chamber, where possible, or by remoulding the soil samples later. The remoulding technique was required to reconstruct several samples with identical moisture-density characteristics for a set of the tests, including direct shear and triaxial tests. An ultrasound test was performed at the end of the freeze-thaw cycles to obtain the elastic modulus of

all the soil samples every 10 cm along the length (Appendix E). In tests such as California bearing ratio, the quantity of the sampled material was insufficient to perform a test. Also, because of dynamic change of the soil properties over the column lengths, the remoulded material was required with a range of different moisture content. Some interventions for the soil structure might have been affected during the sampling and cutting to moulds in the elasticity modulus or the heat conductivity tests. However, the following tests were performed to produce a general indication of changes in the mechanical properties following the freeze-thaw cycles.

#### 4.7.1 Cohesion and angle of internal friction change

Cohesion and the angle of internal friction pertain to the stability of the soil particles and the stresses causing their sliding relative to one another. The crucial condition for stability analysis after freeze-thaw cycles is moisture change of the sample. However, because of uneven redistribution of the moisture content with sample length during the freeze-thaw cycles, it was difficult to produce a unique measurement for the shear resistance. The test was also complicated by the fact that three identical samples were needed to define the cohesion and angle of internal friction characteristics via direct shear or a triaxial rig. As the moisture change was dynamic over the sample length, it turned out to be impossible to carve out identical samples directly from the soil columns. Moreover, the testing machine was not designed to work at sub-zero temperatures. Consequently, the samples were remoulded with the moisture content corresponding to the post-freezing state in order to obtain the strength and stress characteristics after freeze-thaw cycles.

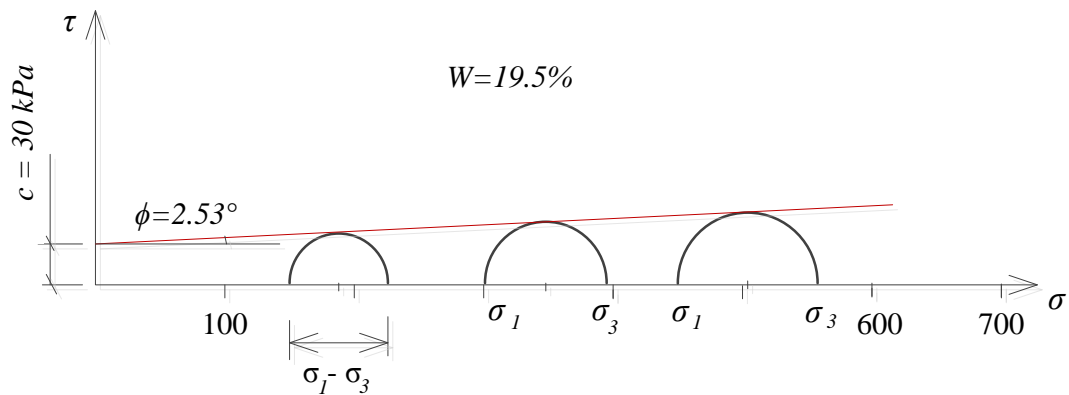


Figure 4.30 – Triaxial test for the soil sample with  $W=19.5\%$

Undrained triaxial tests were performed for remoulded samples with moisture content  $W=19.5\%$  (Figure 4.30) and the displacement speed was 2 mm/min. The test results are presented in Table 4.7. Compared to the initial soil characteristics with initial moisture content 17.2%, the angle of internal friction for the sample with 19.5% was reduced from  $3.39^\circ$  to  $2.53^\circ$  and the cohesion changed from 40 kPa to 30 kPa.

Table 4.7 – Triaxial test results after freeze-thaw cycles

$\sigma_3$	PR division	Ring factor, kN/div	Deviator stress kN/m <sup>2</sup>	$\sigma_1$ kN/m <sup>2</sup>
150 kPa	41	0.004585	76.63	226.63
300 kPa	51	0.004585	95.32	395.32
450 kPa	64	0.004585	119.62	569.62

#### 4.7.2 California bearing ratio

The sequence for the California bearing ratio tests were carried out for the moisture range 14.0-22.2% and presented in Chapter 3, Figure 4.30 and Table 4.8. The remoulded samples were compacted by the standard procedure and specified in Chapter 3, section 3.3. According to the obtained results, at 14 % moisture content the CBR value was equal to 100%, while at 22.2 % the bearing capacity of the sample dropped to 2.75 % when compared to the standard value.

Table 4.8 – California bearing ratio

Moisture content W, %	CBR, %	Dry density, Mg/m <sup>3</sup>
14.00	100.41	1.59
15.06	48.83	1.54
16.50	17.29	1.50
17.65	10.69	1.47
19.50	5.5	1.44
20.61	3.9	1.41
22.24	2.75	1.37



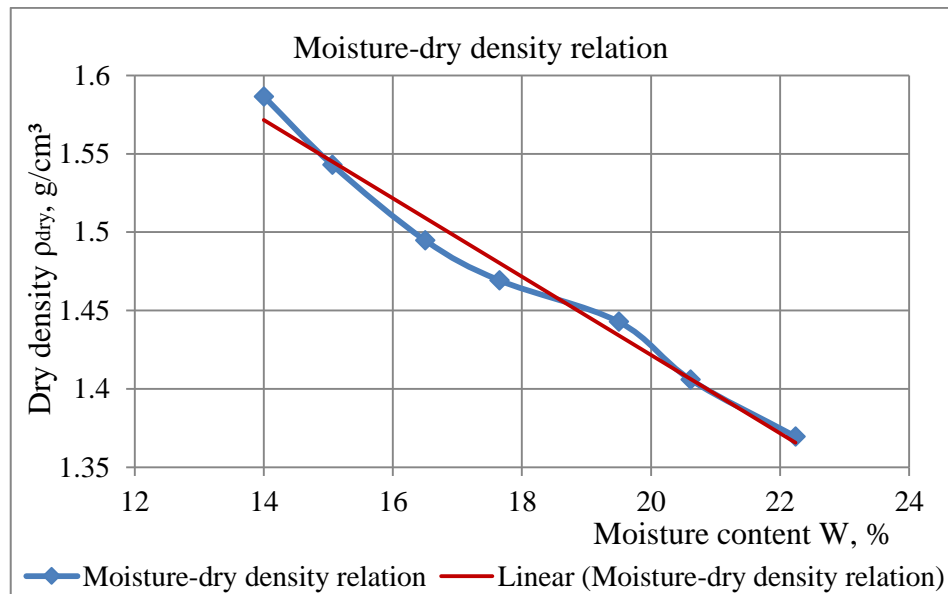


Figure 4.31 – Dry density-moisture relation according to the CBR test

In Figure 4.31 the dry density and moisture relation with almost a linear trend was determined by the CBR compaction test. According to the graph, every one percent of the moisture drop corresponded to 0.027 g/cm<sup>3</sup> dry density increase and 12 % bearing capacity rise.

#### 4.7.3 Permeability and compressibility characteristics

A range of consolidation tests was performed for the increased moisture content after the freeze-thaw cycles. The coefficient of consolidation, coefficient of permeability and volume of compressibility for the corresponded loadings for the sample with 20.82% moisture content are presented in Table 4.9. The specimen observed in Table 4.9 was remoulded with the moisture content corresponding to the post freeze-thaw cycles. Notably, the pressure application was slightly different for each consolidation test. So, the loading of the sample with 20.82% moisture content was carried out in seven stages, whilst the sample with initial moisture content 17.2 %, corresponding to the pre-freezing condition, was loaded in six stages.

Table 4.9 – Oedometer consolidation test results of the sample with W=20.82%

N	Void ratio			Coefficient of volume compressibility		Coefficient of consolidation			Coefficient of permeability
	Pressure P, kN/m <sup>2</sup>	Settlement ΔH, mm	$e_l=e_o-\Delta e$ $e_o=0.485$	$\delta_e$ , mm	$\frac{m_v}{MN}$	$t_{50}$ , mm	$\frac{H^2}{mm^2}$	$\frac{c_v = 0.026H^2}{t_{50}}$ m <sup>2</sup> /year	$k = c_v m_v \rho_w g$ , m/s
0	0	0	0.485	0	0	0	0	0	0
1	25	-0.477	0.450	0.035	0.977	4.6	390.52	2.207	$6.706 \cdot 10^{-10}$
2	50	-0.716	0.432	0.018	0.496	2.7	376.50	3.626	$5.587 \cdot 10^{-10}$
3	100	-1.018	0.409	0.022	0.318	1.37	366.07	6.947	$6.872 \cdot 10^{-10}$
4	200	-1.457	0.377	0.033	0.237	0.96	352.03	9.534	$7.017 \cdot 10^{-10}$
5	400	-1.982	0.338	0.039	0.146	0.67	334.18	12.968	$5.873 \cdot 10^{-10}$
6	750	-2.511	0.299	0.039	0.086	0.56	315.19	14.634	$3.931 \cdot 10^{-10}$
7	1600	-3.219	0.246	0.053	0.049	0.33	293.61	23.133	$3.569 \cdot 10^{-10}$

Calculation of the coefficient of consolidation,  $c_v$ , for 25 kN/m<sup>2</sup> pressure and 20.82% moisture content, according to table 4.10, expressed in square metres per year:

$$c_v = \frac{T_{50}}{t_{50}} \cdot \frac{H}{2} = \frac{0.197 \left( \frac{H}{2} \right)^2}{t_{50}} \cdot 60 \cdot 24 \cdot 365.25 = \frac{0.026H^2}{t_{50}} = \frac{0.026 \cdot 390.52}{2.7} = 2.207 \text{ m}^2/\text{year}$$

where,  $\frac{H}{2}$  - the height of the specimen with double drainage;  $T_v$  - time factor 0.197, according to 50 % for one-dimensional consolidation;  $t_{50}$  - specimen settlement, corresponding to 50% of the primary consolidation, analysed by the log time – settlement curve.

The coefficient of permeability was found as:

$$k = c_v m_v \rho_w g, \text{ m/s}$$

Corresponding to the measuring units  $\frac{m^2}{s} \cdot \frac{m^2}{N} \cdot \frac{kg}{m^3} \cdot \frac{m}{s} = \frac{m}{s}$ , since  $N = \frac{kg \cdot m}{s^2}$ :

$$k = \left( \frac{2.207}{365.25 \cdot 24 \cdot 3600} \right) \cdot \left( \frac{0.977}{10^6} \right) \cdot 1 \cdot 10^3 \cdot 9.81 = 6.706 \cdot 10^{-10} \text{ m/s}$$

A slight improvement of the coefficient of permeability was observed for moisture content 20.82 % when compared to the initial condition before the freeze-thaw cycles with moisture content 17.20 %.

The calculation of coefficient of consolidation for the undisturbed sample from the top layer of column #9 after the first thawing cycle in Test 1 with 23.25% moisture content is presented in Table 4.10. The coefficient of permeability changed from 2.8-

8.8·10<sup>-10</sup> before the freeze thaw cycles to 5.345·10<sup>-9</sup>- 4.018·10<sup>-10</sup>, when the moisture increased from 17 to 23% after first thawing cycle. At the beginning of the oedometer consolidation test the coefficient of compressibility was 1.556 and as the pressure increased this value dropped to 0.048. By the end of the consolidation test the sample was loaded with 1600 kPa pressure and had been drained to 16.5% of moisture content.

Table 4.10 – Oedometer consolidation test results of the sample with W=23.25%

N	Void ratio			Coefficient of volume compressibility		Coefficient of consolidation			Coefficient of permeability
	Pressure P, kN/m <sup>2</sup>	Settlement ΔH, mm	$e_l = e_o - \Delta e$ $e_o = 0.546$	$\delta_e$ , mm	$\frac{m_v, m^2}{MN}$	$t_{50}$ , mm	$\overline{H^2}$ , mm <sup>2</sup>	$\frac{c_v = 0.026H^2}{t_{50}}$ m <sup>2</sup> /year	$k = \frac{c_v m_v \rho_v g}{\gamma}$ , m/s
0	0	0	0.546	0.000	0.000	0	0	0	0
1	25	-0.749	0.488	0.058	1.556	2.34	385.16	4.280	2.070·10 <sup>-9</sup>
2	50	-1.676	0.416	0.072	2.024	1.08	352.97	8.497	5.345·10 <sup>-9</sup>
3	100	-2.027	0.389	0.027	0.391	1.11	329.37	7.715	9.367·10 <sup>-10</sup>
4	200	-2.542	0.350	0.040	0.295	0.52	313.84	15.844	1.453·10 <sup>-9</sup>
5	400	-3.087	0.307	0.042	0.161	0.43	295.34	18.068	9.049·10 <sup>-10</sup>
6	800	-3.675	0.262	0.045	0.090	0.27	276.19	27.098	7.585·10 <sup>-10</sup>
7	1600	-4.279	0.215	0.047	0.048	0.25	256.74	26.916	4.018·10 <sup>-10</sup>

The void ratio and log pressure relation registered has a steeper slope for post freeze-thaw samples (Figure 4.32). Moreover, the specimens with increased moisture content had a higher voids ratio at the beginning of loading, but were compressed more intensively when compared to the soil samples with less moisture content.



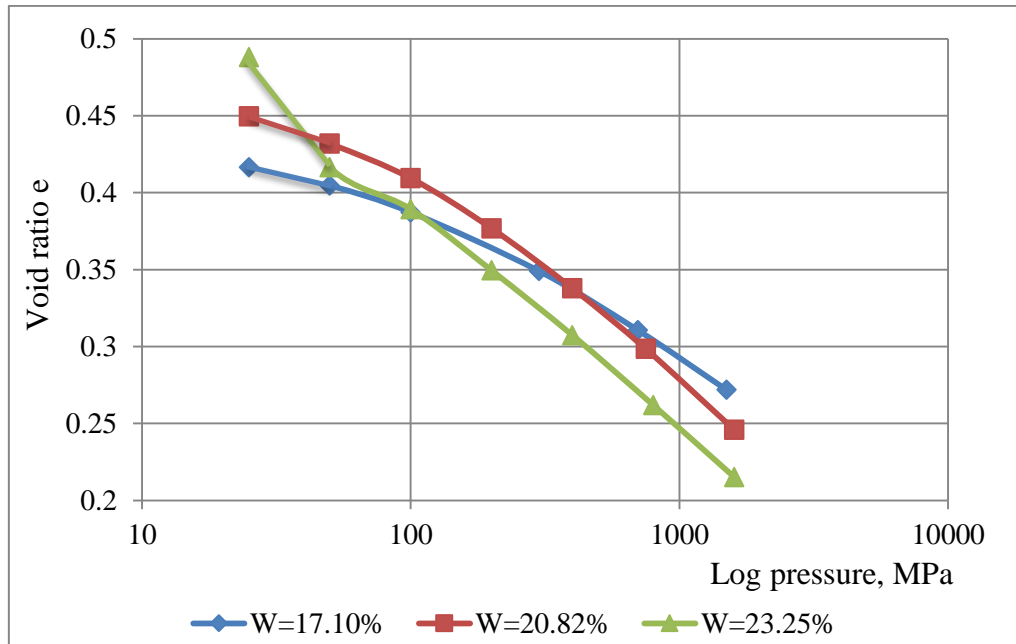


Figure 4.32 – Effect of disturbance of the soil samples with different moisture content

#### 4.8 Heat conductivity

Heat conductivity results were carried out with both oven dried and wet soil samples consisting of 50% kaolinite clay and 50% sand by dry mass and are represented in Figures 4.33 and 4.34. For the dry samples with 0% moisture content, the heat conductivity obtained was around 0.33 W/m·K, while for the wet soil samples, with moisture content between 14-25%, these values were in the range 0.38-0.54 W/m·K.

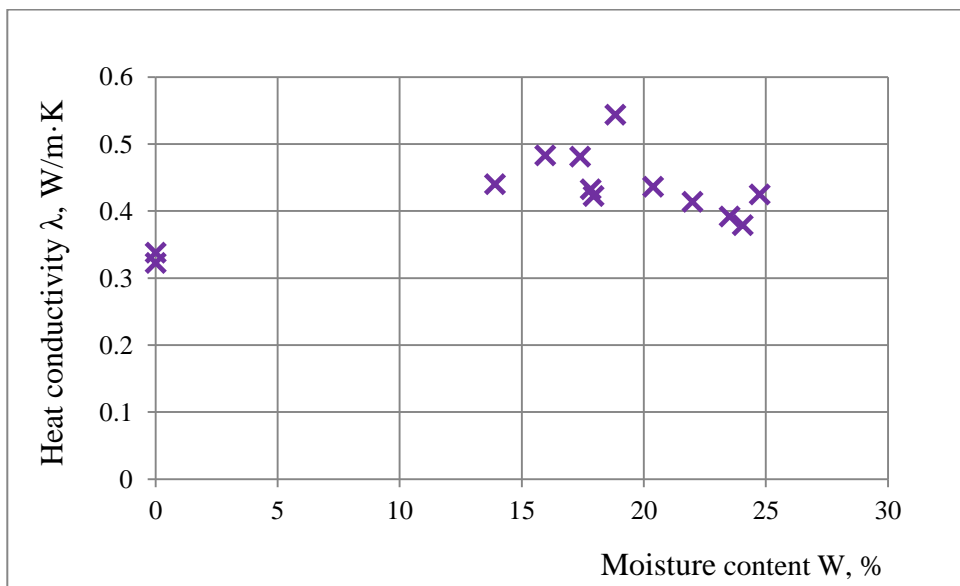


Figure 4.33 – Heat conductivity results within the moisture content range

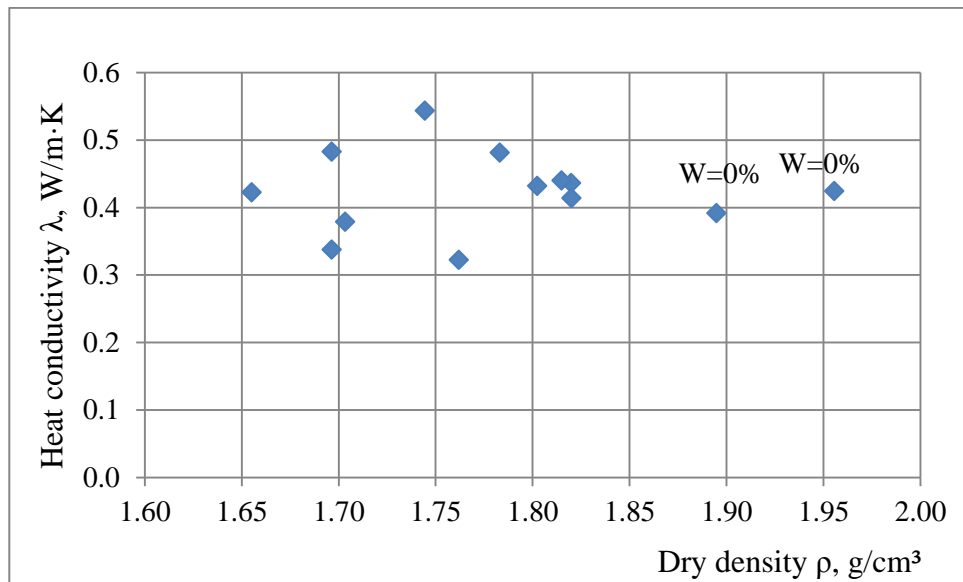


Figure 4.34 – Dry density-heat conductivity relation

According to the obtained results, it was not possible to establish any kind of definite relation between of the thermal conductivity properties and the moisture context or dry density impact (Figure 4.34). Whilst a combination of both characteristics moisture-density is important, any mechanical or thermodynamic disturbance that preceded testing might affect the ‘memory’ of the soil structure and influence the formation of pores and channels.

#### 4.9 Summary

The proposed testing scheme permitted comparison of the moisture-temperature distribution in the soil samples with unidirectional freezing when supplied with deionised water or sodium chloride solution. The increased sample length also benefitted the observation of de-icing chemical and moisture mass transfer during the freeze-thaw cycles with relation to the various densities of the soils. According to the obtained results, the following outcomes have been highlighted.

1. A difference in temperature distribution between the deionised water supply and de-icing chemical solution samples was evident in the second freezing cycle. The de-icing chemical solution enhanced the thermal conductivity of the freezing soils. By the end of the second freezing cycle, the temperature had not dropped much in Test 1 with a deionised water supply, apparently because of megascopic ice lens formation at the top of the soil columns and an increased heat capacity required to cool down the large volume

of moisture. While in Test 2, the temperature reduction progressed to  $-5\text{ }^{\circ}\text{C}$  and below throughout the column height, and reached  $-10\text{ }^{\circ}\text{C}$  in the top 40 cm layer of the sample.

2. Temperature redistribution during the freeze-thaw tests of the samples with variable density between the columns did not have obvious pattern regarding the temperature field. Such a feature can be explained by the slow freezing technique, which provided sufficient time for uniform freezing regardless of the soil density.

3. Observation of the temperature distribution revealed a reduction of temperature change in the transition zone next to the  $0\text{ }^{\circ}\text{C}$  isotherm. While the cooling rate was set to be stable, at  $2\text{ }^{\circ}\text{C}$  per day, the temperature drop over the soil length and the resulting frost heave were varied. The maximum frost heave was observed when the freezing rate over the sample length was 2 cm/day. A slow freezing rate was observed in the top 10-15 cm layer, and the boosted freezing was registered in the lower part of the soil samples

4. The moisture redistribution in the soil samples with a deionised water supply exhibited a greater gap between the moisture content of the ‘heaved’ and ‘desiccated’ zones than for the samples with sodium chloride solution supply. Moreover, the total water intake was greater in chemical solution supplied samples when compared to the clean water supplied ones and also distributed more uniformly.

5. Low density soil samples contributed moisture mass transfer, while increased bulk density, in contrast, decelerated the passage of water. In addition, ice lens formation in the freezing front was prevalent in dense soils free of chemical content, while moisture absorption from the water table predominated in loose soils.

6. Chemical mass transfer induced by the temperature gradient was registered over the entire length of soil samples and occurred in all the tests supplied with the chemical solution, regardless of the sample density and voids content. The amount of chemical increment during the freeze-thaw cycles was 0.05-0.15 % of the oven dried sample weight. The chemical content in the pore water after the test was 2.0-2.5 times higher than the amount of salt in the supplied solution. Significant concentration of the de-icing chemical was located 15-25 cm above the water table and registered around 30,000-70,000 mg/l, when the supply solution was 11,000/mg/l. The enrichment of soils with salt was clearly induced by capillary raise from the water table.

7. The columns with low density were consolidated throughout the column length, with the densest part in the bottom of the samples. Whilst in the dense soil samples only

the 10 cm layer on top was loosened, which also attracted a large amount of water to form ice lenses.

8. Most of the tests for engineering properties registered a slight reduction in relation in strength, cohesion and angle of internal friction. However, there was significant increase in the coefficient of permeability after the freeze-thaw cycles with initially dense compacted soil samples, which was due to loosening and moistening of the soil samples during the heave at sub-zero temperatures.

## 5 DISCUSSION

### 5.1 Discussion of the obtained results

The modified freeze-thaw cycles with slow freezing rate and longer sample length allowed for approximating the freezing process of soils close to the natural conditions. According to Iushkov and Sergeev (2015), the greatest values of frost heave are achieved when the freezing rate in the unidirectional freezing test of the soil is between 2 and 3 cm/day. While Arenson (2005) admitted that steady state thermal conditions were achieved for the final ice lens growth at a cooling rate of 3 °C/day. In the current study, the temperature dropping of the cold plate was set to 2 °C/day and run independently from the freezing rate in the samples. The most favourable conditions for frost heave formation were at a freezing rate of 2 cm/day, which coincides with the results obtained by Iushkov and Sergeev (2015).

Most of the studies on freeze-thaw cycles have conducted unidirectional freezing with a constant temperature (Bing and He, 2011), which certainly has an effect on the temperature field distribution along the sample length. In the current work, a significant distinction of the temperature redistribution along the sample length between tests 1 and 2, supplied with deionised water content and 11000 mg/l sodium chloride solution respectively, revealed the importance of chemical content in highway subsoils. The non-uniform freezing rate along the sample length observed the reduction of temperature drop between 10 cm sections in zones close to the frozen fringe (Figures 4.1-4.5). So, the temperature changes in frozen and unfrozen zones registered several degrees between 10 cm sections by the sample length. While in the middle layers, where the temperature was close to 0 °C, the temperature changes reduced to 0.1-0.5 °C between sections. Such retardation was necessary for the energy balance and further phase transition.

Previously conducted experiments on chemical mass transfer observation during freeze-thaw cycles, include using remoulded or natural samples with a preliminary saline content before the freezing. Baker and Osterkamp (1989) conducted downward and upward unidirectional freezing tests in a 'closed system' with remolded saline samples and observed no significant chemical mass transfer in upward freezing. However, they noted that salt was rejected from the frozen zone and produced an enriched brine in the unfrozen part during downward freezing (Baker and Osterkamp, 1989). Brouchkov (2000) also could not observe any evidence of chemical mass transfer in a horizontally laid saline sample kept for a long period under a longitudinal temperature difference.

Vidyapin and Cheverev (2008) have established that chemical mass transfer exceeds several times the concentration of the supplied solution, when initially the chemical content of the supply solution is equal to the salinity in the pore water. Bing and He (2008) have reported chemical migration in specified content saline samples to the freezing front during freeze-thaw cycles supplied with 5% sodium sulphate solution. These scholars also explained the chemical mass transport as being associated with water transfer and dominated the diffusion process. The migration of salt from the frozen zone to unfrozen prevailed in the coarse soils, while in cohesive soils this happened in a reverse direction.

In the current study the remoulded non-saline samples were supplied with sodium chloride solution and it emerged that the secondary salinisation increased twofold the pore water chemical concentration compared to the supplied solution, which corresponds to the results obtained by Vidyapin and Cheverev (2008). Moreover, the chemical distribution profiles of the soil content were similar to Bing and He's (2008) outcomes. The moisture redistribution curves during the unidirectional freezing of both saline and non-saline soil samples were similar to those of previous studies (Aksenov, 2008; Bing and He, 2008; Arenson *et al.*, 2008). Depending on the moisture distribution characteristics, the samples are conventionally divided according to the following sites: a frost heaved zone, a desiccated zone and a water table adjoining zone, where the moisture was replenished from the base. The thickness of these zones and the moistening-drying parameters differ depending on the soil content, sample size, freezing rate and initial moisture content of the testing material. Comparison of the results with the other studies is not always appropriate owing to the increased sample length, slow freezing techniques and specified secondary salinisation technique for non-saline soil samples. However, reduced moisture uptake to the frozen zone in samples fed with de-icing chemicals solution was observed by Arenson *et al.* (2005) in his experiments with saline silty samples.

The saline samples with a lower freezing point remained unfrozen at negative temperatures. Consequently, all the samples experienced a reduction in bearing capacity after the freeze-thaw cycles regardless of the degree of salinisation, as was mentioned in section 4.6. The moisture content distribution was a crucial factor affecting the soil strength, whilst the chemical content did not reveal an obvious difference; however, it had a greater effect on the moisture redistribution during the freeze-thaw cycles. Most similar studies have also indicated a decrease of the strength in saline soils, which is exacerbated with salinity growth (Hivon and Segó, 1995; Brouchkov, 2002). Bing and

He (2011) reported that soil strength was increased in low chemical content (1%) samples and reduced in high concentrated (>2%) saline soils during freeze-thaw cycles. Nguyen *et al.* (2010) have reported a power-law relationship between unconfined compressive strength and strain rate, temperature and salinity.

Summing up the obtained results, chemical and moisture mass transfer occurred in the initially non-saline samples that were supplied with de-icing chemicals during the freeze-thaw cycles, regardless of the initial soil density and moisture content distribution. Evidence emerged that the density and moisture content had affected the mass transfer capacity. In the current study, the transport mechanism occurred in the previously non-saline samples and with the chemical solution feeding from the base, whilst in tests performed by Bing and He (2008), Vidyapin and Cheverev (2008) it happened during the freezing of initially saline samples. Since the ions of salt were transported in a dissolved state with the liquid water, the moisture transport was considered first and foremost in this chapter.

## **5.2 Evaluation of moisture mass transfer theory**

Henry (2000) in her review has summarised that frost heave is conversion from the liquid part to solid, which is dependent on: a removal of heat, a means of transporting the ice away from the pores and a water supply. She also proposed that there is a relationship between frost heave and the drying or evaporating from liquid water, but went no further in defining this. She emphasised the initiation mechanism of ice lenses is associated with the phase transformation from a liquid to a solid state, accompanied by replenishment of desiccated areas with water flowing from the unfrozen soils. However, this understanding has been implied only regarding the liquid and solid states of the soil structure.

Developing the idea of water evaporation and moisture transport to the freezing front, the further stages of frost heave have been considered for unsaturated soils without a chemical component (Figure 5.1).

i. In Figure 5.1a, the soil sample with relatively low moisture content is represented in the unfrozen part at above the zero temperature condition. The degree of saturation is  $S_0 < 1$ , so the sample is unsaturated. The soil was considered as a closed system with a phase equilibrium condition. The moisture here was in two phases: the liquid part with gravitational, hygroscopic and capillary water and in the gas phase in the form of saturated vapour.

The equilibrium between the water and vapour phases in a porous soil media establishes when the temperature  $T$  and pressure  $P$  are stabilised. According to the Gibbs diagram for the single substance system (subsection 2.6.1), the equilibrium between the water and vapour can be described as:

$$q_{\text{water}}(p, T) = q_{\text{vapour}}(p, T) \quad (5.1)$$

The volume of vapour has been found to be the difference between the volume of the voids and water volume.  $V_{\text{vapour}} = V_v - V_w$ , accepting that  $\rho_w = 1 \text{ g/cm}^3$ , the volume of water was derived by water mass or the moisture content. The mass of vapour has been found by the volume of saturated vapour, according to the thermodynamic equilibrium, which has two variables temperature  $T$  and corresponding to it pressure over water surface  $P_{sw}$ :

$$m_{\text{vapour}} = \frac{\mu \cdot P_{sw} \cdot V_a}{R \cdot T} \quad (5.2)$$

where,  $\mu$  – molar mass of vapour and equal to 18.01528 g/mol;

$P_{sw}$  – saturated vapour pressure corresponding to temperature, at 20 °C  $P_{sw}=2.34$  kPa;

$V_a$  – volume of air in the soil section,  $\text{cm}^3$ ;

$R$  – Universal gas constant, 8.314 4598 J/(mol·K)

$T$  – temperature in Kelvin.

Equation (5.2) is valid, only if a part of the gravity water in soils remains in an unfrozen state, otherwise, the corresponding pressure over ice,  $P_{sw}$ , is needs to be used (equation 5.2').



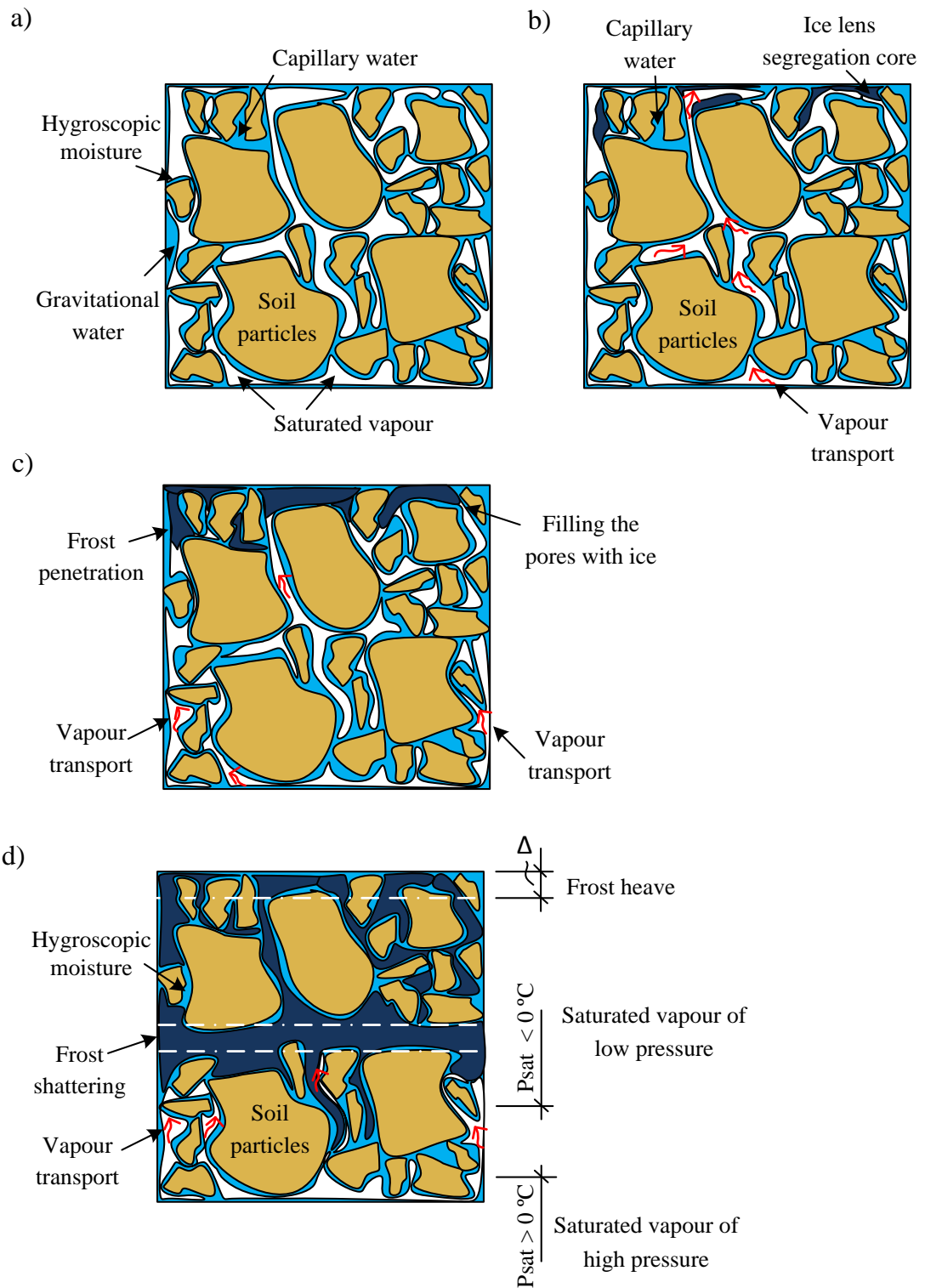


Figure 5.1 – Soil sample structure at the different stages of freezing: a - unfrozen equilibrium; b - beginning of the freezing of ice lenses segregation; c - further freezing or frost penetration; and d - frost shattering and frost heave stage

**ii.** In Figures 5.1b the sample is considered at the beginning of the freezing period, when the ice lenses' cores have just started to segregate. The soil structure in the freezing fringe includes the moisture in three phases: the solid part - ice lenses; the liquid phase – hygroscopic and capillary water; and the gas phase – saturated and unsaturated vapour. It should be noted that ground soils are subject to unidirectional freezing, which is usually derived from the top downwards. Ice lenses nucleation starts in the pores and channels with gravimetric water, where the pore water pressure is close to atmospheric level. The surface tension in the ground water is around  $63 - 64 \cdot 10^{-7} J cm^2$  (Tschapek, 1978). Withdrawal of the thermal energy during soil freezing induces the following phase transformations: the segregation of water in the liquid phase to ice, accompanied by thermal energy release and condensation of the gas phase to liquid, according to the phase equilibrium. A sharp reduction of the water and gas phases in the freezing pores was ascribed the analogy of drying by Henry (2000).

As noted in Chapter 2, there are two widely recognised concepts of frost heave: the segregation potential perspective was introduced by Konrad and Morgenstern (1981), which implies water migration; and the discrete ice lens theory modified by Gilpin (1980). Both of these imply that moisture mass transfer is in a liquid state, i.e. a water-ice phase transfer. The water-ice energy balance was also considered in the coupled heat-moisture transfer, the application of which was later used in the FROSTB model, as mentioned in Chapter 2. Unlike them, in this work the moisture transfer in a gas state was considered. The pressure reduction in the cold temperatures on the top of the sample and higher pressure in the warm layers, induced saturated vapour transport from the high pressure towards the freezing fringe zone (Figure 5.1b). It is notable that phase transfer from a gas to a liquid state happens with high compression of molecules and energy release. The latent heat for condensation to 1 kg of water  $C_{cond} = 2.3 \cdot 10^6 J$  is more than six times higher than that for segregation to ice  $C = 335 \cdot 10^3 J$ . Moreover, the vapour does not have a capillary surface tension and hence, its transportation is more reliable in terms of hydrodynamics and tension. The vapour mass transfer from the nearest pores results in their drying and subsequent, evaporation from the liquid state, which in turn, stimulates a chain reaction in the farthest pores and so on. Such mass transport continues while the temperature and pore pressure in all sides stabilise and equilibrate.

**iii.** In Figure 5.1c, the moisture mass transfer in terms of vapour migration continues, progressively filling all the pore volume with ice, which starts with the pores nearest to the vertical channel or so-called ice veins. This hypothesis is supported by

Arenson *et al.*, (2008) snapshots, who discovered that vertical ice vein growth precedes the horizontal ice lens formation. Arenson *et al.*, (2008) has also noted that vertical veins do not grow in thickness as the horizontal lenses do over time. However, Arenson did not identify in what phase the moisture was transported, but did note concerns about the suction required to drive the hydraulic conductivity at atmospheric pressure, by determining that the negative pressure should be not less than 900 kPa to draw up the water.

**iv.** When all the nearest pores of the layer are filled with ice and the suction in the vertical vein is still inducing the vapour mass transfer, the uneven filling of the soil layer induces a horizontal crack. The crack formed continues to fill with ice and lifts the soil layer in the only possible direction – upwards (Figures 5.1d and 5.2). The thickness of the horizontal crack increases until the overburden pressure equilibrates with cryosuction. After which, the vapour mass continues to fill the lower layer pores.

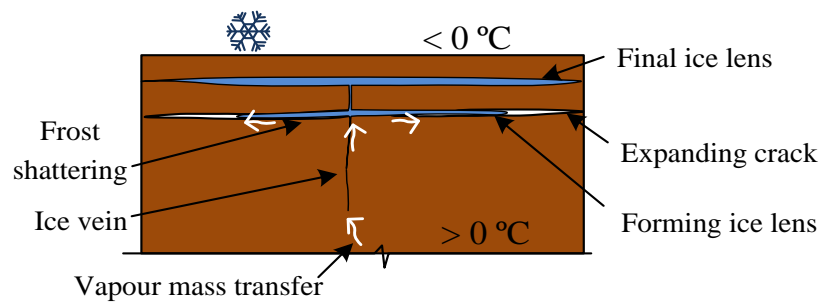


Figure 5.2 – Ice lenses formation in the freezing soil

Concerning the crack formation concept, Azmatch *et al.* (2012) noted that it is still unclear whether the horizontal cracking of the soil during ice lenses formation occurs because of desiccation shrinkage or from thermal strain.

Developing the above mentioned theory, it should be noted that after stage **iv** the upper layers of freezing soils achieve the fully saturated condition, regardless of the initial conditions: either with high value voids ratio or close to the saturated condition. Further mass transfer continues mainly through the film water; though capillary water migration is possible if it remains unfrozen at sub-zero temperatures. The saturated freezing system behaves similar to Everetts' piston-cylinder model of ice growth (Figure 2.1). Constantly freezing water below the freezing fringe increases the ice volume around the ice vein and lifts the overlaid surcharge, thereby expanding the crack, which in turn, is immediately filled with ice, again transported in a vapour state (Figure 5.2). Here, unlike the

hypothesis of Azmatch (2012), it is believed that the formation of horizontal crack is caused by the mechanical strains of the increased ice body supplied from the ice vein. The volumetric expansion continues when the cryosuction forces equilibrate with the surcharge pressure.

In the freeze-thaw cycles in Tests 1 and 2, the moisture content was correlated to the maximum dry density and the voids ratio in the samples was close to zero. As a result, the freezing stages i-iii very soon turned to stage iv with fully saturated soils. While in Tests 3, 4 and 5 the samples were compacted with variable density, which made it possible to establish the voids ratio-mass transfer relation and also to evaluate the moisture mass transfer calculation method in unsaturated soils. For the current study, the main emphasis was on the heat and mass transfer in a gaseous state, including the gas-solid phase transition.

Gorelik and Kolunin (2001) demonstrated that the ice body has low hydraulic permeability and all solutes and inclusions concentrate in air bubbles, which slowly move towards the warm side where the surface tension has a reduced value. This approach explains the formation of a uniform ice body blanket with soil particle inclusions. Arenson and Sego (2006) in their conceptual model for the ice growth in the coarse soils observed that ice segregation in the coarse soils starts from the grain skeleton, as the thermal conductivity of the sand particles surpasses that of the water. Moreover, growth of ice needles starts from the sand particles' surface in a perpendicular direction and the concentrated brine was steadily moved to the pore centres (Arenson and Sego, 2006). The conceptual model of Arenson and Sego (2006) is correct for coarse grain soils with lower surfactant forces and a greater proportion of gravitational water; however, it is not applicable to frost susceptible soils, where the surface tension and particle surface charge comes to the fore.

Water-ice transformation modelling in fully saturated soils and moisture mass transfer in a liquid state have been widely studied and explained by Ming and Li (2015), Bronfenbrener and Bronfenbrener (2010), among others. Consequently, further elaboration of moisture mass transfer in a liquid state, as well as calculation algorithm and prediction were not a primary purpose of the current study.

In this study, the main focus was on moisture mass transfer in unsaturated soils, as this is the most likely state of soils under highways in the winter period. Specifically, the determination of moisture mass transfer implemented with vapour flow was considered.

### 5.2.1 Energy balance during vapour mass transfer

The amount of transported moisture is related to the cooling rate and thus to the amount of energy lost, which is distributed to the phase transfer energy and cooling of each soil component, according to its heat conductivity. The supplementary requirement for the mass transfer is sufficient time. This is, by the way, related to the travel distance of the vapour along the pore channels and thus to the tortuosity of those channels.

So, the freezing energy is equal to:

$$Q = Q_s + Q_w + Q_i + Q_v + Q_{w-i} \quad (5.3)$$

where, -  $Q_s$ ,  $Q_w$ ,  $Q_i$ ,  $Q_v$  – heat loss for cooling down the solids, water, ice and vapour components, respectively and  $Q_{w-i}$  – latent heat for the phase transfer from water to the ice state.

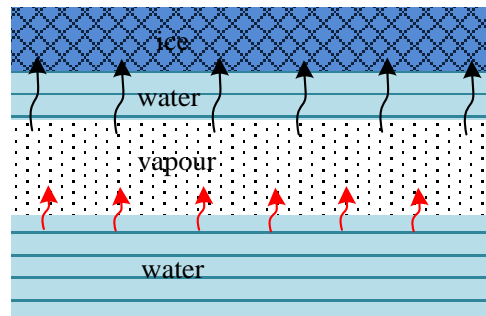


Figure 5.3 - Energy balance of moisture mass transfer during freezing in soils

Here, the heat loss for phase transfer from vapour to ice includes the heat required to transfer the vapour from a gas to liquid state, first and subsequently, into the solid state. The energy loss for the vapour to water phase transfer in the frozen fringe equilibrates with the water to vapour transition in the lower soil layers so as to stabilise the negative pressure. Eventually, the mass moisture transfer energy corresponds with the crystallisation heat release from the liquid to solid state and the cooling rate.

### 5.2.2 Moisture mass transfer in the highway subsoils application

Due to the high density and increased thermal conductivity of the pavement and sub-base materials the temperature field in highway subsoils differs with only slightly when compared to soils in a natural state (Chunpeng *et al.*, 2010). Dynamic traffic load increases the pressure and melts some parts of the ice for a short period of time in highway subsoils. The mechanism of short-term load application to the frozen subsoils can be explained by regelation theory, when that part of the ice located closest to the soil particles starts to melt under the pressure. The liquefied water migrates upwards to the cold side as soon as the dynamic load is removed and refreezes in the new place. The dynamic loading here acts as a piston pump.

In Figure 5.4a-c, a short-term load application is presented as an example of the frost heaved soils, where the developed ice lenses have already filled the pores' volume. The short-term loading, in this case, enhances the frost shattering and progresses the ice lens growth further. While in unsaturated soils the dynamic load application would cause short-term ice melting in the places of soil particles contact. It would also increase the overburden pressure of water and vapour states and endeavour the phase transitions. The subsoil behaviour primarily depends on the overburden pressure and the applied frequency.

According to the above described approaches, it is reasonable to proceed with the moisture mass transfer calculations in the highway subsoils based on the voids ratio and the degree of saturation. The vapour mass transfer approach is applicable for unsaturated soils with a degree of saturation  $0 < S_r < 1$ . Once the pores are filled with ice and hygroscopic water and the degree of saturation reaches  $S_r = 1$ , further mass transfer is carried only with hygroscopic water, the calculation of which is based on the water-ice interaction, effective stress and soil particles' surface tension.

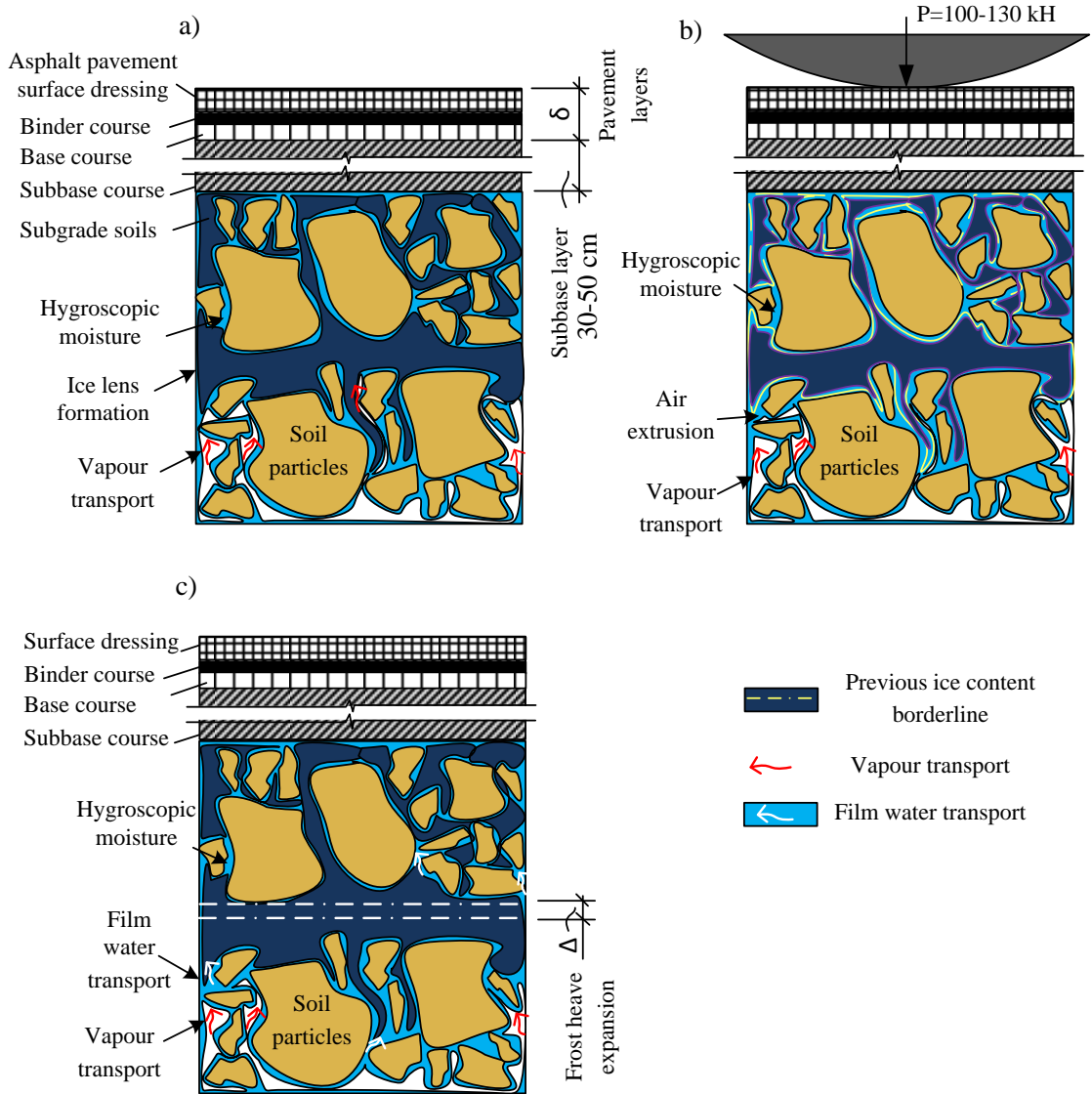


Figure 5.4 – Dynamic load effect on moisture mass transport under the highways: a - static condition; b – application of the short-term dynamic load and c – frost heave thickness expansion

### 5.3 Calculation of the vapour mass transfer in unsaturated freezing soils

#### 5.3.1 Algorithm for vapour mass transfer calculations in unsaturated soils

The algorithm for calculation of vapour mass transfer includes determination of volumetric and mass constituents of soils such as water, soil particles, vapour. Porosity and the volume of air are the crucial characteristics for the vapour mass transfer in freezing soils.

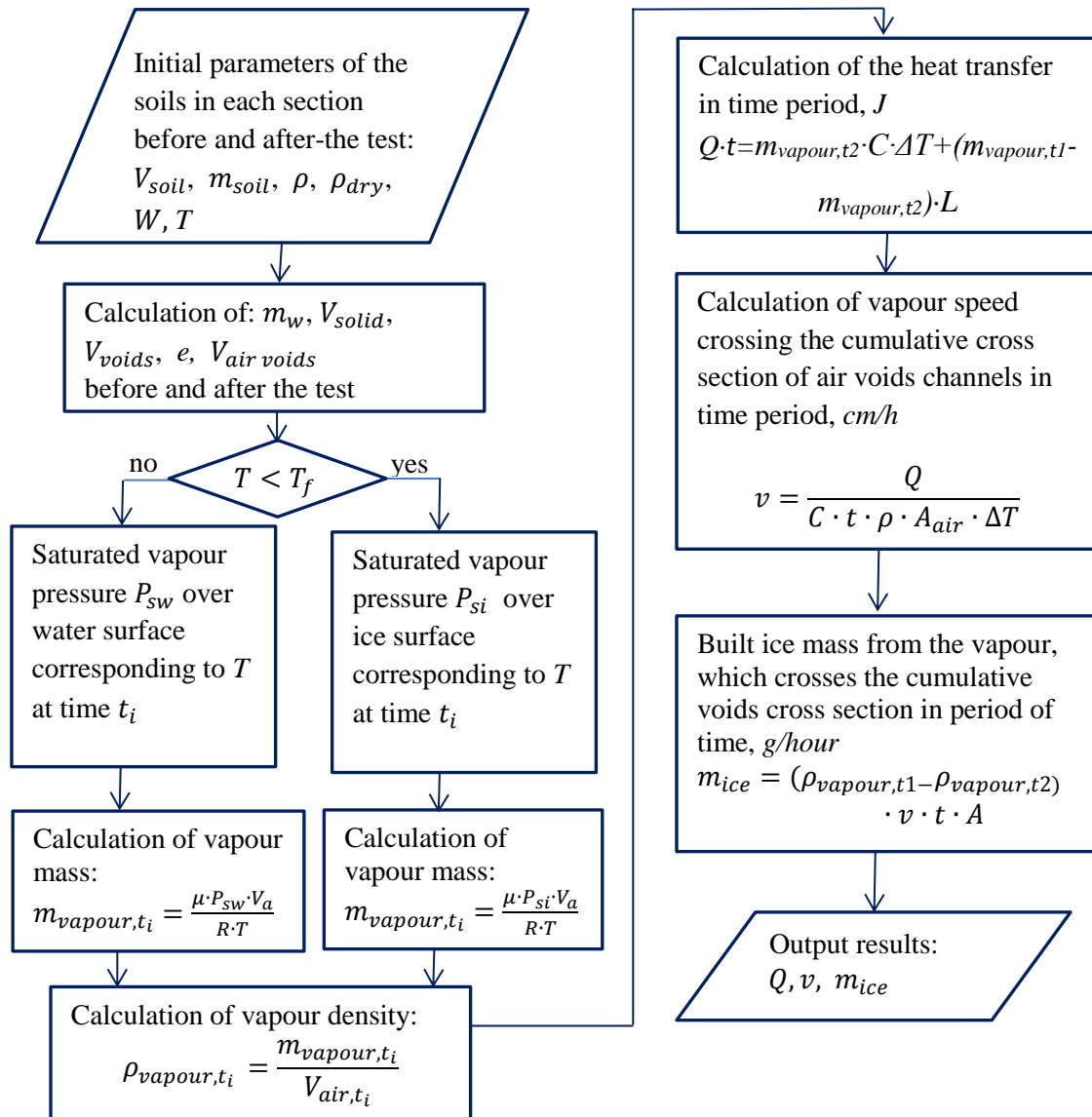


Figure 5.5 – Algorithm for the vapour mass transfer calculation

The heat change  $Q$  in a mould section over the time  $t$  is found as the sum of the cooling heat and the latent heat during the phase transfer:



$$Q \cdot t = Q_1 + Q_2 \quad (5.4)$$

where,  $Q_1$  – heat energy used for cooling the vapour mass to the temperature  $\Delta T$  (equation 5.5); and  $Q_2$  – heat energy used for the phase transfer (eq. 5.7).

$$Q_1 = m_{vapour, t_i} \cdot C \cdot \Delta T \quad (5.5)$$

where,  $m_{vapour, t_i}$  – mass of vapour at the starting time  $t_i$ , g;  $C$  – specific heat of vapour passing through the cumulative air voids cross section,  $J/kg \cdot ^\circ C$ ;  $\Delta T$  – temperature change,  $^\circ C$ ; and  $t$  – time interval, h.

If part gravitational water remains in the unfrozen condition the mass of vapour is found by equation (5.2). Density of the vapour is calculated for each period of time, corresponding to the temperature and saturated vapour pressure:

$$\rho_{vapour, t_i} = \frac{m_{vapour, t_i}}{V_{air, t_i}} \quad (5.6)$$

where,  $\rho_{vapour, t_i}$  - vapour density for period of time,  $g/cm^3$ .

Heat energy for the phase transfer includes the latent heat for the condensation and solidification of the vapour mass difference at the beginning  $\tau_1$  and end time  $\tau_2$  of the calculation period.

$$Q_2 = (m_{vapour, 1} - m_{vapour, 2}) \cdot L \quad (5.7)$$

where,  $m_{vapour, 2}$  – mass of the vapour at the end period  $t_2$ ;  $L$  – is a total latent heat  $L = L_1 + L_2$ , where  $L_1$  - specific latent heat for condensation  $L_1 = 2.3 \cdot 10^6 J/kg$  and  $L_2$  - specific latent heat for solidification  $L_2 = 0.335 \cdot 10^6 J/kg$  of 1 kg of water.

The volume of vapour  $V_{vapour}$  is equal to the speed of vapour passing through the air voids' cross section  $A$  over the time  $t$ :

$$V_{vapour} = v \cdot t \cdot A_{air\ voids} \quad (5.8)$$

where,  $v$  – average speed of vapour, cm/h; and  $A_{air\ voids}$  – cumulative section cross of the air voids'  $A_{air\ voids} = \frac{\pi \cdot d_a^2}{4}$ ,  $cm^2$ , corresponding to the porosity coefficient and moisture content (Figure 5.6).

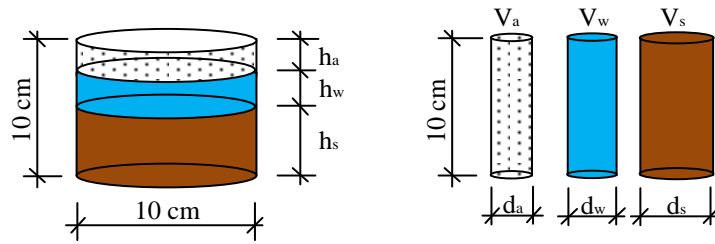


Figure 5.6 – Cumulative air voids channel cross section

Substituting the  $V_{vapour}$  in equation (5.2) the vapour speed is found at the starting time and at the end:

$$v_{vapour} = \frac{4Q}{C \cdot \rho \cdot \pi \cdot d_a^2 \cdot \Delta T \cdot t} = \frac{Q}{C \cdot \rho \cdot A_{air} \cdot \Delta T \cdot t} \quad (5.9)$$

The mass of ice built from the vapour passing through the air voids channels in a 10 cm length mould section with correspondent cumulative cross section  $A_{air}$  and speed  $v$  over time  $t$  is calculated:

$$m_{ice} = \rho_{vapour} \cdot V_{air\ voids} = \rho_{vapour} \cdot v \cdot t \cdot A_{air} \quad (5.10)$$

where,  $m_{ice}$  - mass of built ice in grams;  $\rho_{vapour}$  – is taken as an average density value of the vapour densities at the start and end time point,  $g/cm^3$ .

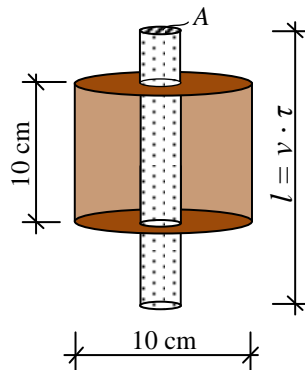


Figure 5.7 – Calculation of the vapour rate passing through the cumulative air voids channel in the mould section over time  $t$

Here, it is assumed that the porosity coefficient of the sample remains constant during the calculation period. Consequently, the volume of the air voids and the cumulative cross section of the air voids also remain constant. It should be noted that only heat consumed for the gas phase energy exchange was considered in this problem. The solid and liquid parts have also been cooled down with the heat withdrawn by the cooling

machine. However, they are not counted, because all the necessary energy exchange has been done by an automatic set of temperature controls.

The model is suitable for numerical solutions, like finite element analysis or a model similar to a coupled heat-water transfer, in terms of considering the vapour flow and taking into account the cryosuction forces. The latent heat for the phase transitions and the dynamic change of the coefficient of porosity and air void volume need also to be taken into account.

### 5.3.2 Calculation of vapour flow on example of Test 3

The results of the density-moisture parameters before and after Test 3 are presented in Table 5.1. Here, under the “before test” title the initial setting parameters at  $t=0$  h are presented. Whilst under the “after test” title, the data collected after two freeze-thaw cycle at  $t=636$  h are shown.

Table 5.1 – Soil sample parameters before and after the freeze-thaw cycles with deionised water supply: Test 3

Co- lumn	Weight of soil, g		Bulk density, average by sample length $\rho$ , Mg/m <sup>3</sup>		Moisture content, average by sample length $W$ , %		Dry density, average by sample length $\rho_{dry}$ , Mg/m <sup>33</sup>		Void ratio, average by sample length $e$	
	Before test	After test	Before test	After test	Before test	After test	Before test	After test	Before test	After test
#1	<b>5,463</b>	<b>5,988</b>	<b>1.380</b>	<b>1.512</b>	<b>17.20</b>	<b>25.01</b>	<b>1.177</b>	<b>1.209</b>	<b>1.223</b>	<b>1.162</b>
#2	6,012	6,559	1.519	1.660	17.20	25.23	1.295	1.326	1.020	0.972
#3	6,236	6,956	1.575	1.760	17.20	27.39	1.343	1.381	0.947	0.893
#4	7,452	7,964	1.883	1.842	17.20	23.78	1.605	1.488	0.629	0.604
#5	7,057	7,622	1.783	1.918	17.20	25.35	1.520	1.530	0.721	0.709
#6	6,813	7,068	1.721	1.994	17.20	29.07	1.467	1.545	0.782	0.907
#7	7,662	8,230	1.936	2.037	17.20	24.50	1.650	1.636	0.585	0.598
#8	8,332	8,612	2.105	2.124	17.20	20.70	1.794	1.760	0.457	0.486
#9	8,355	8,544	2.111	2.126	17.20	20.85	1.799	1.759	0.453	0.487

The period of time between 590h and 614h, which corresponded to the end of the second freezing cycle period, was considered for analysing the mass transfer within the frozen soils. Sub-zero temperature distribution is presented in Tables 5.3a and 5.3b. The length of the soils sample in Test 3 was 50 cm, which was composed of five assembled

mould sections, each 10 cm in length. Moreover, each of the sections had an overlay joint of 5 mm. Because the density varied from the loosest one in column #1 to the densest #8 and #9 it was decided to consider the moisture mass transfer in the unsaturated samples #1 and #7.

The mass of soil in a section was found by dividing the weight of the entire length of the sample of 50.5 cm, including 5 mm of overlap at the top. So, the extra 5 mm overlap in the top section was accounted for with a coefficient of 1.05. To obtain the mass of the solid particles in the section, the mass of soil before the freeze-thaw cycles was divided by the final moisture content  $(1 + w_0)$ .

$$m_{\#11} = m_{\#1} \frac{1.05}{5.05} = 5463 \frac{1.05}{5.05} = 1135.87 \text{ g}$$

$$m_{s,\#11} = \frac{m_{\#11}}{(1 + \frac{w_0}{100\%})} = \frac{1135.87}{1.172} = 969.17 \text{ g}$$

The mass of the solid particles in sections #12-15 was found accordingly:

$$m_{\#12-15} = \frac{m_{\#1}}{5.05} = \frac{5463}{5.05} = 1081.78 \text{ g}$$

$$m_{s,\#12-15} = \frac{m_{\#12-15}}{(1 + \frac{w_0}{100\%})} = \frac{1081.78}{1.172} = 923.02 \text{ g}$$

The mass and volume of the solid particles was believed to stay unchanged during the freeze-thaw cycles, while the moisture content and the volume of voids had been modified. The ice lenses formed mostly in the top section layer, which caused some linear deformation in the vertical direction and was taken into account only for the top section.

Table 5.2 – Calculation of soil parameters for the 590-614 h time interval of the Test 3 for the example of sample #1

Sample section	Distance from the top surface, cm	Volume in a section, cm <sup>3</sup>	Mass of solids, g	Mass of water, g	Mass of the soil in a section, g	Bulk density, Mg/m <sup>3</sup>	Average moisture content W, %	Dry density, Mg/m <sup>3</sup>
#11	0-10	819.08	969.17	245.59	1214.76	1.483	25.34	1.183
#12	10-20	785.40	923.02	187.28	1110.30	1.414	20.29	1.175
#13	20-30	785.40	923.02	214.14	1137.16	1.448	23.20	1.175
#14	30-40	785.40	923.02	277.37	1200.39	1.528	30.05	1.175
#15	40-50	785.40	923.02	254.75	1177.78	1.500	27.60	1.175

Further calculations were performed on top section #11 in soil column #1 for the time interval between 590 and 614 h (Table 5.2). The moisture content intake and its distribution over the sample length were set at the beginning and measured at the end of the two freeze-thaw cycles. Because the time slot was considered during the final freezing stage of the test, the moisture content distribution and correlated volumetric-density calculations have been performed according to the data presented in Table 5.1.

In the time interval 590-614h the moisture distribution over the sample length changed, although the amount of solid particles remained the same. The average moisture content during the considered time slot was 25.34%, which included the total mass of the ice and water content:

$$m_{w,\#11} = m_{i,\#11} = m_s \frac{W\%}{100\%} = 969.17 \cdot \frac{25.34}{100} = 245.59 \text{ g}$$

Total sample mass in a section was found from the moisture mass: both water and ice; and a mass of the soil particles:

$$m_{\#11,\tau} = m_{s,\#11} + m_{w,\#11} = 969.17 + 245.59 = 1214.76 \text{ g}$$

Volume of soil in section #11 with 10 cm length and extra 5 mm overlap:

$$V_{\#11} = \frac{\pi \cdot d_{\#11}^2}{4} l_{\#11} = \frac{3.14 \cdot 10^2}{4} (10 + 0.5) = 819.076 \text{ cm}^3$$

Bulk density and dry density were found accordingly:

$$\rho_{\#11} = \frac{m_{\#11,\tau}}{V_{\#11}} = \frac{1214.76}{819.076} = 1.483 \text{ g/cm}^3$$

$$\rho_{d,\#11} = \frac{1}{1 + w} \rho_{\#11} = 1.483 \frac{1}{1.2534} = 1.183 \text{ g/cm}^3$$

Table 5.3a - Calculation of the moisture mass transfer in the soils for the example of Test 3, sample #1

Sample section	Volume of solids, $cm^3$	Volume of voids, $cm^3$	Voids ratio $e = \rho_s / \rho_{dry} - 1$	Volume of air, $cm^3$	Temperature at 590 h	Saturated vapour pressure over ice, $P_{si}$ , Pa	Mass of vapour at 590, g	Density of the saturated vapour at 590h, $Mg/m^3$
#11	<b>370.62</b>	<b>448.46</b>	<b>1.21</b>	<b>180.55</b>	<b>-10.99</b>	<b>237.93</b>	<b><math>3.55 \cdot 10^{-4}</math></b>	<b><math>1.97 \cdot 10^{-6}</math></b>
#12	352.97	432.43	1.23	228.13	-10.30	253.24	$4.76 \cdot 10^{-4}$	$2.09 \cdot 10^{-6}$
#13	352.97	432.43	1.23	198.83	-9.49	272.16	$4.45 \cdot 10^{-4}$	$2.24 \cdot 10^{-6}$
#14	352.97	432.43	1.23	129.85	-8.36	300.63	$3.19 \cdot 10^{-4}$	$2.46 \cdot 10^{-6}$
#15	352.97	432.43	1.23	154.52	-6.46	354.77	$4.45 \cdot 10^{-4}$	$2.88 \cdot 10^{-6}$

Table 5.3b - Calculation of the moisture mass transfer in the soils for the example of Test 3, sample #1 (continuation of Table 5.3a)

Sample section	Temperature at 614 h, $^{\circ}C$	Saturated vapour pressure over ice, $P_{si}$ , Pa	Mass of vapour at 614 h, g	The heat realised in 24 hours $Q \cdot t = m \cdot C \cdot \Delta T$ , J	Vapour rate $v = 4 \cdot N / (C \cdot \rho \cdot \pi \cdot d^2 \cdot \Delta T)$ , cm per 24 h	Vapour rate, cm/h	Build-up of ice mass between the period 590/614 h, g/hour
#11	<b>-13.30</b>	<b>193.26</b>	<b><math>2.91 \cdot 10^{-4}</math></b>	<b>0.1702</b>	<b>9.008</b>	<b>0.375</b>	<b><math>2.67 \cdot 10^{-6}</math></b>
#12	-12.60	205.98	$3.91 \cdot 10^{-4}$	0.2269	9.014	0.376	$3.56 \cdot 10^{-6}$
#13	-11.68	223.81	$3.69 \cdot 10^{-4}$	0.2016	9.067	0.378	$3.16 \cdot 10^{-6}$
#14	-10.43	250.35	$2.68 \cdot 10^{-4}$	0.1363	9.126	0.380	$2.14 \cdot 10^{-6}$
#15	-8.96	284.98	$3.61 \cdot 10^{-4}$	0.2237	8.956	0.373	$3.51 \cdot 10^{-6}$

The volume of solids in a section was found as the mass of solids over the density of the solid soil particles  $\rho_s = 2.615 \text{ g/cm}^3$ :

$$V_{s,\#11} = \frac{m_s}{\rho_s} = \frac{969.17}{2.615} = 370.62 \text{ cm}^3$$

The volume of voids here would be:

$$V_{v,\#11} = V_{\#11} - V_{s,\#11} = 819.08 - 370.62 = 448.46 \text{ cm}^3$$

It was assumed that all the gravitational water was frozen at negative temperature. If the density of ice  $\rho_i = 0.9167 \text{ g/cm}^3$ , then the volume of ice would be found as:

$$V_{i,\#11} = \frac{m_{\#1}}{\rho_i} = \frac{245.59}{0.9167} = 267.91 \text{ cm}^3$$

The volume of air is the difference of voids and ice volume in the pores:

$$V_{air} = V_{v,\#11} - V_{i,\#11} = 448.46 - 267.91 = 180.55 \text{ cm}^3$$

Voids ratio:

$$\text{either } e = \frac{\rho_s}{\rho_d} - 1 = \frac{2.615}{1.183} - 1 = 1.21$$

$$\text{or } e = \frac{V_v}{V_s} = \frac{448.46}{370.62} = 1.21$$

The values of the saturated vapour and its sublimation pressure over ice were calculated from the equation recommended by the International Association for the Properties of Steam (IAPS) in 1993 (Wagner *et al.*, 1994). The corresponding pressure of saturated vapour over the ice surface at 590 and 614 h in sample #1 of Test 3 was found by interpolation in terms of the recorded temperature distribution. The mass of the water in the gaseous condition was determined by the Clausius–Clapeyron equation (5.2). The vapour mass for time slot  $\tau_1 = 590$  h at  $-10.99$  °C in sample section #11 was calculated:

$$\begin{aligned} m_{vapour,\#11}^{t_1} &= \frac{\mu \cdot P_{si} \cdot V_a}{R \cdot T_1} = \frac{0.018 \cdot 237.93 \cdot 180.55 \cdot 10^{-6}}{8.3144598 \cdot (273 - 10.99)} \\ &= 0.355 \cdot 10^{-6} \text{ kg or } 3.55 \cdot 10^{-4} \text{ g} \end{aligned}$$

$$\text{the units ratio } m_{vapour,\#11} = \frac{\text{kg} \cdot \text{Pa} \cdot \text{m}^3}{\frac{\text{m}^3 \cdot \text{Pa}}{\text{K} \cdot \text{mol}} \cdot \text{K} \cdot 100\%} = \text{kg}$$

where,  $\mu$  – molar mass of vapour and equal to 18.01528(33) g/mol;

$P_{si}$  – saturated vapour pressure over ice surface corresponding to  $-4.4$  °C temperature is  $P_{si}=237.93$  Pa;

$R$  – Universal gas constant,  $8.3144598\text{J}/(\text{mol} \cdot \text{K})$ , which corresponds to  $8.3144598 \frac{\text{m}^3 \cdot \text{Pa}}{\text{K} \cdot \text{mol}}$ ;  $T$  – temperature in Kelvin;

$V_a$  – volume of air,  $\text{m}^3$ ,  $V_a = 180.55 \cdot 10^{-6} \text{m}^3$ . The volume of air was assumed to be constant at  $t_1$  and  $t_2$ , as there were no data of the total moisture content distribution change over the sample length within the considered 24 h period.

At  $t_2 = 614$  h and  $-13.30$  °C the mass of vapour was found:

$$\begin{aligned} m_{vapour,\#11}^{t_2} &= \frac{\mu \cdot P_{si} \cdot V_a}{R \cdot T_2} = \frac{0.018 \cdot 193.26 \cdot 180.55 \cdot 10^{-6}}{8.3144598 \cdot (273 - 13.30)} \\ &= 0.291 \cdot 10^{-6} \text{ kg or } 2.91 \cdot 10^{-4} \text{ g} \end{aligned}$$

The vapour density at  $t_1$  and  $t_2$  was found:

$$\rho_{\tau_1} = \frac{m_{vapour,\#11}^{t_1}}{V_a} = \frac{3.55 \cdot 10^{-4}}{180.55} = 1.97 \cdot 10^{-6} \frac{\text{g}}{\text{cm}^3}$$

$$\rho_{\tau_2} = \frac{m_{vapour, \#11}^{t_2}}{V_a} = \frac{2.91 \cdot 10^{-4}}{180.55} = 1.61 \cdot 10^{-6} \frac{g}{cm^3}$$

The heat transfer between 590h and 614h period of the test in section #11 was found as total energy spent on the temperature drop of the gaseous phase and the latent heat of the vapour part transitioning from the gas phase to the solid ice phase, called the deposition.

$$\begin{aligned} Q \cdot \tau &= Q_1 + Q_2 = m_{vapour, \#11}^{t_2} \cdot C \cdot \Delta T + (m_{vapour, \#11}^{t_1} - m_{vapour, \#11}^{t_2})L = \\ &= 2.91 \cdot 10^{-4} \cdot 2 \cdot ((273 - 13.30) - (273 - 10.99)) \\ &\quad + \frac{(3.55 \cdot 10^{-4} - 2.91 \cdot 10^{-4})(2.3 \cdot 10^6 + 335 \cdot 10^3)}{1000} = 0.17 J \end{aligned}$$

where,  $t$  – period of time between 590 and 614 h,  $t = 24$  hours;

$m_{vapour}$  – mass of vapour according to the temperature at time  $t_2$ , g;

$C$  – specific heat for vapour  $C = 2 \text{kJ}/(\text{kg} \cdot \text{K})$ ;

$\Delta T$  – temperature change, K;

$L$  - latent heat for condensation and freezing (or sublimation) of 1kg of moisture (water)  $L_c = 2.3 \cdot 10^6 \text{ J}$  and  $L_f = 335 \cdot 10^3 \text{ J}$ , accordingly.

The mass of vapour was also calculated using the formula:

$$m_{vapour} = \rho_{vapour} \cdot V = \rho_{vapour} \cdot v \cdot t \cdot A_{air}$$

where,  $A_{air}$  - is the cross section of the cumulative air voids channel in the soil sample section. If the volume of the air voids in a 10 cm length sample is equal to  $185.51 \text{ cm}^3$ , then the cross section area will be  $18.55 \text{ cm}^2$ .

Substituting the value of vapour mass to the produced heat formula, the average vapour rate was found by the following expression:

$$\begin{aligned} v &= \frac{Q_1}{m_{vapour} \cdot C \cdot \Delta T \cdot t} = \frac{Q_1}{\rho_{vapour} \cdot A_{air} \cdot C \cdot \Delta T \cdot t} = \\ &= \frac{-1.344 \cdot 10^{-3}}{(1.97 \cdot 10^{-6} + 1.61 \cdot 10^{-6})/2 \cdot 18,055 \cdot 2 \cdot (13.30 - 10.99) \cdot 24} = \\ &= 9.008 \cdot 10^{-3} \frac{cm}{24h} = 0.4 \text{ cm/h} \end{aligned}$$

$$\text{The units' relation here } v = \frac{J}{\frac{g}{cm^3} \cdot cm^2 \cdot \frac{J}{gK} \cdot h} = \frac{cm}{h}$$

As the vapour density depends on the temperature, which changes over time, the average density value for the considered period  $\tau$  was applied here.

The mass of ice built between 590 and 614 h in section #11 was formed from the vapour passed across the soil sample and was calculated as a vapour rate passing through



the cumulative air voids cross section in the 24 hour period. The average value of vapour density was applied to calculate the ice mass that built during the vapour mass transfer:

$$m_i = (\rho_{t1} - \rho_{t2}) \cdot v \cdot t \cdot A_{air} = (1.97 \cdot 10^{-6} - 1.61 \cdot 10^{-6}) \cdot 0.4 \cdot 1 \cdot 18.055$$

$$= 2.41 \cdot 10^{-6} g$$

$m_i$  – mass of built ice formed in 24 h period in sample section #11;  $v$  - vapour speed passing through the air voids cross section per unit time, cm/h;  $A_{air}$  - is a cross section of the cumulative air voids channel, cm<sup>2</sup>;  $\rho_{t1}$  and  $\rho_{t2}$  - vapour density at  $t_1$  and  $t_2$  accordingly, g/cm<sup>3</sup>.

The results of moisture mass transfer calculations in column #5 are presented in Tables 5.4, 5.5a and 5.5b. The average bulk density of the soil at the end of freeze-thaw cycles was 1.89 g/cm<sup>3</sup>. The moisture content comprised 30% at the top section and 23-24% in the rest of the sample. The obtained ice mass formation rate was in the range of  $6.18 \cdot 10^{-8} - 3.82 \cdot 10^{-7}$  g/h (Table 5.5b). In the top 10 cm layer by initial time of the testing period 590 h the soil had reached the fully saturated condition and further mass transfer was implemented via hygroscopic water in a liquid state. Consequently, the vapour mass transfer calculation in the top section was not applicable from that moment onwards.

Table 5.4 – Calculation of soil parameters for the 590-614 h time interval for Test 3 for the example of sample #5

Sample section	Distance from the top surface, cm	Volume in a section, cm <sup>3</sup>	Mass of solids, g	Mass of water, g	Mass of the soil in a section, g	Bulk density, Mg/m <sup>3</sup>	Average moisture content W per section, %	Dry density, Mg/m <sup>3</sup>
#11	0-10	854.73	1251.96	374.086	1626.05	1.902	29.88	1.465
#12	10-20	785.40	1192.34	280.797	1473.14	1.876	23.55	1.518
#13	20-30	785.40	1192.34	282.347	1474.69	1.878	23.68	1.518
#14	30-40	785.40	1192.34	297.609	1489.95	1.897	24.96	1.518
#15	40-50	785.40	1192.34	276.147	1468.49	1.870	23.16	1.518

Table 5.5a - Calculation of the moisture mass transfer in the soils for the example of Test 3, sample #5

Sample section	Volume of solids, cm <sup>3</sup>	Volume of voids, cm <sup>3</sup>	Void ratio $e = \frac{\rho_s}{\rho_{dry}} - 1$	Volume of air, cm <sup>3</sup>	Temperature at 590 h, °C	Saturated vapour pressure over ice, P <sub>si</sub> , Pa	Mass of vapour at 590, g	Density of saturated vapour at 590h, Mg/m <sup>3</sup>
#11	478.76	375.97	0.79	0	-13.48	190.14	-	-
#12	455.96	329.44	0.72	23.12	-11.45	228.51	$4.37 \cdot 10^{-5}$	$1.89 \cdot 10^{-6}$
#13	455.96	329.44	0.72	21.43	-10.69	244.59	$4.33 \cdot 10^{-5}$	$2.02 \cdot 10^{-6}$
#14	455.96	329.44	0.72	4.78	-10.29	253.46	$9.99 \cdot 10^{-6}$	$2.09 \cdot 10^{-6}$
#15	455.96	329.44	0.72	28.20	-8.98	284.46	$6.58 \cdot 10^{-5}$	$2.33 \cdot 10^{-6}$

Table 5.5b - Calculation of the moisture mass transfer in the soils for the example of Test 3, sample #5 (continuation of Table 5.5a)

Sample section	Temperature at 614 h, °C	Saturated vapour pressure over ice, P <sub>si</sub> , Pa	Mass of vapour at 614 h, g	The heat realised in 24 h $Q \cdot t = m \cdot C \cdot \Delta T$ , J	Vapour rate $v = 4 \cdot N / (C \cdot \rho \cdot \pi \cdot d^2 \cdot \Delta T)$ , cm per 24 h	Vapour rate, cm/h	Build of ice mass between 590/614 h period, g/h
#11	-15.46	158.49	-	-	-	-	-
#12	-13.61	187.89	$3.63 \cdot 10^{-5}$	0.0199	9.066	0.378	$2.82 \cdot 10^{-7}$
#13	-12.83	201.65	$3.60 \cdot 10^{-5}$	0.0194	9.078	0.378	$2.76 \cdot 10^{-7}$
#14	-12.36	210.49	$8.36 \cdot 10^{-6}$	0.0043	9.113	0.380	$6.18 \cdot 10^{-8}$
#15	-10.92	239.48	$5.58 \cdot 10^{-5}$	0.0265	9.178	0.382	$3.82 \cdot 10^{-7}$

### 5.3.3 Limitations of the mass transfer calculation in the above example

In hypothesising that moisture mass transfer is achieved by vapour, then the amount of migrated moisture is directly dependent on the air voids volume. In turn, the change of air volume is related to the pore pressure corresponding to the absolute temperature. The observation of the air voids change in by each section was not possible with the technical equipment available during the experiment, however it was possible to calculate the average void ratio for the soil sample from the vertical linear movement observations. The parameters were applied for the entire soil sample and hence, could not represent the density-volumetric fluctuations over the sample length. Although the measured vertical linear movements registered by gauges, they included 9% expansion in the frozen water

content. It was not possible to derive the air voids volume from the obtained volume of voids due to the high compressibility characteristics of the gases. Therefore, in the example of the moisture mass transfer, used to demonstrate calculations, the last freezing day of the second cycle was considered. Consequently, the final moisture content and correlated volumetric-density characteristics were accepted to replace the actual voids and moisture parameters. This assumption might have caused some deviation from the moisture redistribution data. However, this does not detract from the calculation method.

#### **5.3.4 Interaction and comparison with other approaches to vapour mass transport calculation**

There are not many works that have considered the gaseous component of mass transfer. The vapour flux has widely been omitted or underestimated by scientists in the calculation of mass transfer. One of the few works that have considered it was presented by Zhang et al. (2006). The main distinctions and similarities of the current proposal with what they put forward are considered here:

1. In the current work it is accepted that moisture mass transport is implemented primarily in the gas phase, i.e. vapour in the freezing fringe transport zone. Otherwise, it is supplied in the capillary zone from the water table source in a liquid state. Zhang *et al.* (2016) accept the intake moisture flow as combined from liquid and water fluxes, conforming to thermal and isothermal hydraulic conductivities. The liquid water flow was presented by Richard's equation and explained as driven by water potential or temperature gradient, which is proportional to hydraulic conductivity.
2. In this work, it is assumed the vapour is fully saturated and filling all the volume of air voids in the soil. While Zhang et al. (2016) calculated the relative humidity  $H_r$  and vapour diffusivity  $D_a$  in equation (2.13) derived, including the empirical parameter of an enhancement factor  $\eta$ . The vapour density was also found by the empirical formula of saturated vapour density multiplied by its relative humidity.
3. Zhang et al. (2016) determined the unfrozen water content in equation (2.11) by temperature and the coefficients  $a$  and  $b$  were estimated by regression analysis of the measured data of temperature and unfrozen water content. However, it could be the case that " $a$ " and " $b$ " might vary for different types of soils. In Zhang et al.'s model, the presence of unfrozen water content in the frozen part of the soil

was admitted. However, its mobility was considered doubtful and hence, such water mass transfer was not accounted, unless it had evaporated and was transported in a gas state.

4. Zhang et al. (2016) simulated the natural field impacts of precipitation, evaporation and heat fluxes from the net radiation, which was omitted in the current study.
5. In this work, detailed positioning of the soil structure was considered, based on the experimental data of the measured temperature, vertical linear volumetric change registered by testing time and the obtained moisture-density relation.

#### **5.4 Chemical mass transfer**

The results obtained for tests 2, 4 and 5 indicate chemical content redistribution over the entire column length when fed from the base with 11-22 g/L sodium chloride solution. Despite the contradictory testing results obtained by some scientists (Brouchkov, 2000; Vidyapin and Cheverev, 2008; Bing and He, 2011), all the samples measurements in the conducted tests confirmed secondary salinisation induced by the temperature gradient. According to Torrance and Schellekens' (2006) review, the known hydrodynamic models for mass transfer, which use simulation and prognosis modelling, were based on the empirical formulae of heat and water flow, whilst expressing the driving force as the difference of the 'free energy'. The authors thus pointed out that such models do not require the knowledge of the origin of the driving force, as expressed by the energy balance and the temperature gradient.

Consequently, in this study the chemical mass transfer was considered in terms of the driving forces and the system equilibrium. There are several reasons for explaining the migration phenomena of chemical content from the warm side to cold and from the saline water table to non-saline soil content:

- ❖ Firstly, according to thermodynamic theory, a substance always migrates from a higher chemical potential towards a lower one. Chemical diffusion was induced by the chemical potential gradient, by feeding the non-saline samples with brine, which subsequently strived to equilibrate the ion distribution in the pore water over the sample length. Similar to the moisture migration explained by Wu *et al.* (2015), the driving force of chemical mass transfer takes the form:

$$F_{m,chem} = -\nabla\mu_{chem} \quad (5.11)$$

where,  $F_{m,chem}$  – force per mole of chemical content (N/mol); and  $\nabla\mu_{chem}$  – chemical potential difference. The sign indicates the direction of the driving force.

So, the body force of chemical migration per unit volume  $f_{m,chem}$  is accordingly:

$$f_{m,chem} = -\frac{1}{V_{m,chem}}\nabla\mu_w \quad (5.12)$$

where,  $V_{m,chem}$  – molar volume of chemical here,  $m^3$   $V_{m,chem} = \frac{M}{\rho}$ .  $M$  - molar mass, for sodium chloride is  $M=58.5 \text{ g/mol}$ ,  $\rho$  - density of the solution,  $g/l$ .

The tested soils comprised kaolinite clay and sand particles, where the former is a mineral consisting of hydroxides of aluminium silicates:  $Al_2[Si_2O_5](OH)_4$ . According to Mengel (2011), the negatively charged clay particles attract positively charged ions, which in the current case were represented by exchangeable cations of soluble de-icing chemicals. The total number of cations that can be held by soil particles is called the cation exchange capacity and is equal to 3-15 meq/100 g in kaolinite soils (Robertson *et al.*, 1999). According to the Hofmeister series, the relative strength of the cations' adsorption to colloids increases in the sequence of:  $Al^{3+} > H^+ > Ca^{2+} > Mg^{2+} > K^+ = NH_4^+ > Na^+$ . Notably, the soils' buffer capacity increases by increasing the dispersion and lowering the temperature (Robertson *et al.*, 1999). So, the upper part of the soil samples with non-saline pore water content and lower temperature obtained increased cation exchange capacity, while the lower part of the sample, conversely, being saline, possessed lower buffer capacity of ion content. The difference of the salinity potential over the sample length and the increased ion capacity in low temperature soils gives a rational explanation for the driving force of chemical transfer from a saline water table upwards to a non-saline freezing front.

- ❖ Secondly, according to Tschapek *et al.* (1978), the soil surface tension in dilute solutions is  $0.01-0.02 \cdot 10^{-7} \text{ J/cm}^2$  less than that in the soils with non-saline pore water. The only possible way to transport the positively charged ions of sodium chloride is for them to migrate with film water in a liquid soluble state. As the gravitational water might freeze in the sub-zero temperature of the soils (Figure 5.1a-d), the hygroscopic water can remain liquid due to the surface tension down to very low temperatures of  $-70 \text{ }^\circ\text{C}$  or even below (Koopsman and Miller, 1966). Eventually this

hygroscopic water becomes the main source of the chemical mass transport either in unsaturated or saturated soils.

- ❖ Lastly, the surface tension of the film water is also inversely related to the temperature (Figure 5.1d). So, the migration of film water is caused by a cryosuction force and partial transition of it further into the ice state. Consequently, the desiccation of the film water in the frozen zone induces its replenishment from the warm soil part. Concerning the dissolved ions of sodium chloride, they are transported together with the hygroscopic water like magnets over the charged surface (Figure 5.8).

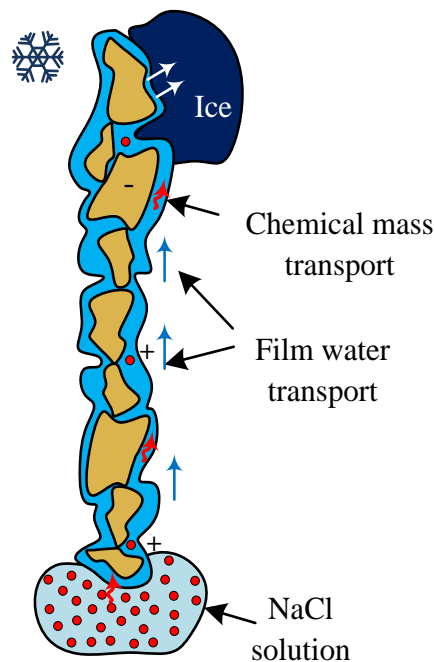


Figure 5.8 - Conceptual model of chemical mass transfer

Owing to chemical osmosis, which refers to the equilibration of moisture by the chemical potential, the moisture transport towards the freezing front was reduced. The moisture tended to equilibrate the chemical concentration in the pore water, which was higher at the base. While the cryosuction, with much greater force, tended to pull the moisture content upwards to the freezing front (Figure 5.9). As a result, the moisture mass transfer was reduced in the top layers during the secondary salinisation with sodium chloride solution supply.

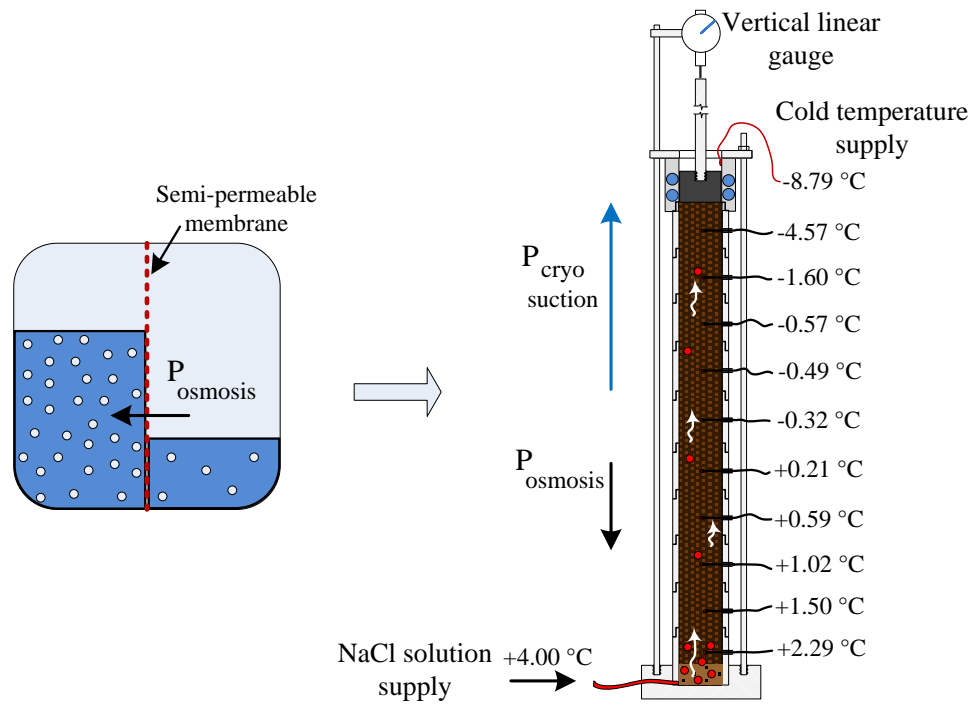


Figure 5.9 – Mass transfer and impact strength diagram

### 5.5 Summary

The modified testing method facilitated observation of the temperature distribution through the sample length when frozen from the top with a cooling rate of 2 °C/day. The maximum frost heave was observed when the movement speed of the freezing front was 2 cm/day. The considered conceptual model of mass transfer in unsaturated soils explained moisture migration during unidirectional freezing toward the freezing front as a flow of vapour. According to the phase equilibrium and thermodynamic relationship, assuming that all vapour in the pores was fully saturated, it was possible to calculate the heat and mass transfer in the freezing media. The amount of ice built up from vapour sublimation in 24 h during its passing through a section was calculated as the difference of the vapour rates passing with the obtained velocity over the cumulative air voids channel cross section.

The amount of ice built up in denser soils, like in the soil sample in column #5, was up to 10 times less than the loose soil sample in column #1. The waste heat in sample #5 was lower by 10 times, accordingly, since most of the energy was spent on the phase transfer, rather than for cooling. Whilst the speed of the vapour movement towards the freezing top remained the same, the reduced void ratio and small size of the cross section

of the air voids channels caused diminished moisture mass transfer in the gaseous condition.

Numerous studies have determined that the voids ratio, moisture content and freezing rate have a critical impact on moisture mass transfer and the frost heave rate. Substantial vapour mass transfer was achieved in the soils with moisture content sufficiently below the saturation moisture content  $W_{sat}$  and high voids ratio. The fact that the slow freezing rate contributes to frost heave supports the hypothesis that vapour transfer induces phase transformations within the temperature zones, which require some extra time. Time is also required to develop a sufficient pore pressure gradient in the soils with high voids ratio and to enable convection to occur in the form of moisture transfer in a gaseous condition under temperature change. As soon as the pores are filled with ice deposited from the vapour mass, further mass transfer could only continue by hygroscopic water, which in turn, depended on surface tension, chemical content and particles size of the soil.

Conducting freeze-thaw cycles with non-saline soil samples supplied with 11000-22000 mg/l brine from the base, facilitated observation of the chemical mass transfer. The chemical mass transfer to the frozen front was observed in various density and voids content samples all over the sample length. The driving force was explained as a cryosuction force, effected by the hygroscopic water in a liquid state with dissolved de-icing chemical ions in it, which migrated towards the freezing front. The surface tension forces and soil particles surface charge attracted the chemical ions to move to the freezing front. Ion exchange capacity in soils with low temperature and the reduced surface tension in saline pore water promoted chemical mass transfer. The concentration of de-icing chemicals in the pore water exceeded the supplied solution by 2-2.5 times.

The above described vapour transport model significantly modifies the moisture mass transfer determination approach and with knowledge of the volume of hygroscopic mass displacement, can help to solve the outstanding issues of cryosuction force required to overcome the surface tension for moisture transport implementation. The use of a dynamic component significantly intensifies the phase transitions of soils under the road and potentially accelerates the freezing-thawing processes. However, due to the defined secondary salinization, a detailed examination of heat-water mass transfer requires in highway subsoils when de-icing chemicals are used.

With concern to progressive chemical transfer caused by temperature reduction, and possible design solutions, it is recommended to consider some moisture isolation



layers under the subbase layer of the road, such as plastic film covering or silicone gel injections. Moisture isolation would also benefit the temperature field distribution during the frost heaving. These isolation layers in the road cross section should be installed with a gradient downward from the road centre to the roadside. Such an arrangement would benefit the drainage of subbase materials. The reasonable use of de-icing chemicals and avoidance of excessive chemical contamination of the roadside soil is also essential. Since the increased porosity of soils is a main source for the moisture mass transfer in a gaseous state, the filling of subsoils' pores with solidifying liquids would prolong the working time of highways and reduce the operating costs, although might effect of the subbase work performance – i.e. make it less elastic.

## 6 CONCLUSIONS AND RECOMMENDATIONS FOR FUTURE WORK

### 6.1 General overview

Against the backdrop of the ongoing global warming and the expansion of areas with periglacial soil formation (Harris *et al.*, 2009), the associated risk of seasonal freeze-thaw related damage to highway subsoils should not be ignored. Analysis of the contemporary problems of highways winter exploitation with de-icing chemicals in cold regions has indicated the necessity of more detailed study of the secondary salinisation impact on the roadside area and highway subsoils. Because of the potential complexity of soil conditions on site and the practical issues when implementing field research, a laboratory-based approach using non-saline soil samples in an “open system” was developed. The significantly modified experimental design not only benefited from clear observation of temperature distributions and de-icing chemical transport over the sample length with time, but also, delivered a better understanding of moisture mass transfer in a vapour state at sub-zero temperatures. The maximum frost heave was observed at the freezing front of 2 cm/day moving rate. Moreover, increased sample length signified the reduction of temperature drop near the transition zone next to the 0 °C isotherm. Such retardation of the freezing rate was necessary for the phase transition to occur and the heat balance to equilibrate or endeavour to so.

The moisture intake and its redistribution within the soil samples were also found to depend on the density and the chemical content of pore water. The total moisture intake in ice and unfrozen water, which was pulled up to the top 10 cm section, prevailed in a deionised water supply test. The moisture distribution over the sample length more fluctuated in soil samples with a deionised water supply than when there was a sodium chloride solution supply, but in the latter case there was a greater formation of ice lens.

Frost heave and density change in the soil samples emerged as depending on the moisture redistribution and chemical content of the pore water during the freeze-thaw cycles. The soils supplied with deionised water showed an increase in frost heave in the second freezing cycle, whereas the samples with de-icing chemicals supply exhibited a reduction. The samples with loose density were compacted during the freeze-thaw cycles, while dense soils became loosened. The density change of soils was inversely related to the moisture content, which in turn, inversely depended on the sodium chloride content in pore water. Specifically, the chemical component retarded the moisture transport to the

frozen and non-saline top section owing to chemical osmosis, which pertains to the tendency to equilibrate the moisture according to the chemical potential. Whilst the cryosuction forces induced the dissolved ions of sodium chloride to migrate within the hygroscopic water.

The engineering properties of the samples after freeze-thaw cycles signified a clear reduction in strength, mainly because of increased moisture content and lower dry density. No obvious impact of de-icing chemicals was noted in the thawed samples. It was shown that a shallow water table induced greater moisture intake to the soil samples and consequently, their reduction in strength.

As many road subsoils are designed to be exploited in unsaturated conditions or undergo an unsaturated transition stage, while being frozen (Figure 5.1), it is crucial to consider the moisture mass transfer in a gaseous state, accompanied by phase transitions. Building on the experimental results, the conceptual model for soil freezing was considered from the perspectives of moisture content, phase transfer and volume changes with temperature within the freezing soil. To determine the moisture mass transfer at different freezing stages, the degree of saturation and the voids ratio with time, were set as the input parameters. Moisture mass transfer in the unsaturated freezing soils with a significant voids ratio was implemented predominantly with vapour flow. The concept of the moisture flow in a gaseous state benefits from having a clear calculation algorithm, absence of empirical relations and compliance with the laws of physics. Vapour convection was naturally induced by the temperature gradient, where the driving force was presented by saturated vapour pressure difference with further energy release by the phase transfer in the frozen zone. This mode of moisture transfer is applicable for both saline and non-saline soils. Notably, the voids ratio and the moisture content have a significant impact on the mass transfer rate and ice growth. After the pore volume is filled with ice, primarily deposited from the vapour, further mass transfer has to be considered with hygroscopic water, which stays in a liquid state even at very low temperature. The migration of the hygroscopic water is explained as being driven to the frozen side by cryosuction forces owing to a difference in surface tension.

A similar theoretical approach was applied to the chemical mass transfer, which was observed in all the samples irrespective of their density and moisture content. The amount of sodium chloride measured by the electrical conductivity probe of the diluted dry sample and related to the volume of pore water after freeze-thaw cycles exceeded the supplied solution in concentration level by 2.0-2.5 times. The migration of sodium

chloride was driven by diffusion and the tendency to equilibrate the chemical potential of the soil system, while the dissolved ions of salt were transported within the hygroscopic water.

Consideration of the phenomenon of vapour mass transfer and the interphase equilibrium in freezing soils can help to explain many hitherto misunderstood problems of moisture mass transfer occurring where highway subsoils are exposed to temperature oscillations around freezing.

## **6.2 Key findings of the work**

Further outcomes have been concluded from the conducted research, as follows.

1. The significantly modified testing method, including the slow freezing techniques and longer samples lengths, is an effective way to evaluate the impact of freeze-thaw cycles on soils.
2. The chemical mass transfer induced by chemical potential and temperature gradient was established in all previously non-saline soil samples of various densities and sample length. The driving force for this was explained by chemical diffusion, while the chemical mass transport was implemented via dissolved ions moving within the hygroscopic water content.
3. The obtained results have improved understanding of the heat and mass transfer phenomenon during the unidirectional freezing of soils and their secondary salinisation with a de-icing chemical or deionised water supply.
4. The conceptual model for frost heave in soils was developed based on the vapour mass transfer. The algorithm of vapour flow calculation in unsaturated soils was presented using fundamental thermodynamic equations.

## **6.3 Key limitations**

It is unclear exactly which elements migrated (or the ratio between anions and cations) during the secondary salinisation in the freezing soils, as the electrical conductivity data simply indicate the presence of ions in the sample. A potential limitation in the data is due to the design of the experiment, particularly not being able to extract geotechnical samples below 0°C. However, as the focus was on the overall impact of freeze-thaw on moisture transport, the overall conclusions are considered to be sound. The total moisture distribution in ice and unfrozen water could not be monitored over the sample lengths with respect to the testing time. As a result, the conclusions are based on total net moisture transfer measured at the end of each test. It should be noted that these

limitations do not detract from the scientific contribution of the work, where vapour flow was identified as a key source for moisture mass transfer.

## **6.4 Further research**

### **6.4.1 Moisture mass transfer perspectives**

According to the findings of the research, the integrated moisture mass transfer in sub-zero temperatures includes moisture transport in a gaseous flow and hygroscopic water transfer in a liquid state, which in turn, depends on the surface tension and the cryosuction forces. Consequently, both vapour mass transfer and associated phase transitions need to be taken into account. That is, only after taking into consideration both components of moisture flow and understanding its driving forces, will it be possible to move to a new stage of the moisture mass transfer theory.

Further research could include vapour mass transfer in quantitative analysis for different types of soils, taking into account the freezing rates, volumetric-moisture characteristics and particle size scenarios. The available techniques need to be reviewed and expressed with formulae explaining the driving force of hygroscopic water transport and vapour transport capacity. Special attention should be given to vapour mass transfer under highways. Application of the dynamic load, causing repeated short-term pressure increases and accompanying phase transition, would have an effect on the volumetric variations and this need to be considered in conjunction with site observations.

Regarding laboratory experiments, installation of pore pressure probes and equipment sets for determining the voids ratio and moisture content, measured by sample length and recorded hourly, would benefit the calculations of the total flow of moisture with time. It is also important to consider the measurement and monitoring of hygroscopic moisture transport in relation to the testing time. The knowledge of the displacement of this component could entirely solve the problem of integrated moisture mass transfer in soils under sub-freezing temperatures.

The presented vapour flow model is suitable for implementation with numerical analysis, including the finite element method, finite volume method among others, where the mass of built ice can be calculated from the deposited vapour over time, according to the temperature in each mesh, separately and further integrated into the continuous flow. Determination of the hygroscopic moisture is feasible as the difference of the total mass transfer and vapour flow. Application of the presented method would benefit the accuracy

of frost heave prognosis by fostering understanding of soil degradation, in particular, in highway subsoils.

#### **6.4.2. De-icing chemicals mass transfer perspectives**

The obtained de-icing chemicals mass transfer involves a chemical process, first of all. However, it is important to conduct interdisciplinary laboratory research to consider the microscale analysis for driving forces and charges during the chemical diffusion in soils under the temperature gradient. Moreover, the confirmed chemicals migration results need to be determined with mass spectrometry methods for element identification. Further, the algorithm of chemical mass transfer calculation needs to be developed for the quantity simulation model. It is also important to assess the rate of salinisation so as to provide a long term prognosis regarding highway subsoils exploitation and its effect on the temperature field distribution in winter time. Consequently, the laboratory and in situ studies might be continued in terms of engineering properties and the bearing capacity of highway subsoils, both in frozen and thawed conditions.

## LIST OF REFERENCES

- Abzhalimov, R.S. (2007) 'Calculation of the negative-temperature distribution of soils over the depth of frost', *Soil mechanics and foundation engineering*, 44(1), pp. 31-37.
- Aksenov, V.I. (2008) *Saline frozen soils of Arctic shore as structure base*. Gevorkyan, S.G. edn. Moskow: Vse o mire stroitelstva, (in Russian).
- Arenson L.U. and Segó, D.C. (2006) 'The effect of salinity on the freezing of coarse-grained sands', *Canadian geotechnical journal*, 43(3), pp. 325-337.
- Arenson, L.U., Segó, D.C. and Newman, G. (2006) 'The use of a convective heat flow model in road designs for Northern regions', *IEEE*, pp. 1-8.
- Arenson, L.U., Xia, D., Segó, D.C. and Biggar, K. (2005) 'Brine and unfrozen water migration during the freezing of Devon silt', *Proceedings of the 4th Biennial Workshop on Assessment and Remediation of Contaminated Sites in Arctic and Cold Climates (ARCSACC)*. Edmonton, Canada, 8-10 May 2005, pp. 35-44.
- Arenson, L.U., Azmatch, T.F. and Segó, D.C. (2008) 'A new hypothesis of ice lens formation in frost-susceptible soils', *Ninth International Conference of Permafrost*, Fairbanks, Alaska, pp.59-65 .
- Azmatch, T.F., Segó, D.C., Arenson, L.U. and Biggar, K.W. (2012) 'Using soil freezing characteristic curve to estimate the hydraulic conductivity function of partially frozen soils', *Cold Regions Science and Technology*, 83-84, pp. 103.
- Baker, G.C. and Osterkamp, T.E. (1989) 'Salt redistribution during freezing of saline sand columns at constant rates', *Water Resources Research*, 25(8), pp. 1825-1831.
- Benson, C. and Othman, M. (1993) 'Hydraulic Conductivity of Compacted Clay Frozen and Thawed In Situ', *Journal of Geotechnical Engineering*, 119(2), pp. 276-294.
- Beskow, G. (1935) *Soil Freezing and frost heaving with special application to roads and railroads*. Swed. Geol. Soc.
- Bi, Guiquan (2012) 'Study on influence of freeze-thaw cycles on the physical-mechanical properties of loess', *Smart Materials and Intelligent Systems*, 442, pp. 286-290.
- Bing, H. and He, P. (2011) 'Experimental investigations on the influence of cyclical freezing and thawing on physical and mechanical properties of saline soil', *Environmental Earth Sciences*, 64(2), pp. 431-436.
- Bing, H. and He, P. (2008) 'Experimental study of water and salt redistribution of clay soil in an opening system with constant temperature', *Environmental Geology*, 55(4), pp. 717-721.
- Bing, H. and Ma, W. (2011) 'Laboratory investigation of the freezing point of saline soil', *Cold Regions Science and Technology*, 67(1-2), pp. 79-88.

- Bockheim, J., Vieira, G., Ramos, M., Lopez-Martinez, J., Serrano, E., Guglielmin, M., Wilhekm, K., Nieuwendam, A. (2013) 'Climate warming and permafrost dynamics in the Antarctic Peninsula region', *Global and Planetary Change*, 100, pp. 215-223.
- Blomqvist, G. and Johansson, E. (1999) 'Airborne spreading and deposition of de-icing salt — a case study', *Science of The Total Environment*, 235(1–3), pp. 161-168.
- Bronfenbrener, L. (2008) 'A non-instantaneous kinetic model for freezing in porous media', *Chemical Engineering and Processing: Process Intensification*, 47(9–10), pp. 1631-1646.
- Bronfenbrener, L. and Bronfenbrener, R. (2010) 'Modeling frost heave in freezing soils', *Cold Regions Science and Technology*, 61(1), pp. 43-64.
- Brouchkov, A.V. (2002) *Experimental study of water transfer in frozen saline soils under mechanical loads*.
- Brouchkov, A. (2000) 'Salt and water transfer in frozen soils induced by gradients of temperature and salt content', *Permafrost and Periglacial Processes*, 11(2), pp. 153-160.
- BS 1377-1: 1990: (1990) *Methods of test for soils for civil engineering purposes. General requirements and sample preparation* British Standards Institute.
- BS 1377-2:1990: (1990) *BS 1377-2:1990: Methods of test for soils for civil engineering purposes. Classification tests* British Standards Institute.
- BS 1377-3:1990: (1990) *BS 1377-3:1990: Methods of test for soils for civil engineering purposes. Chemical and electro-chemical tests* British Standards Institute.
- BS 1377-4:1990: (1990) *BS 1377-4:1990: Methods of test for soils for civil engineering purposes. Compaction-related tests* British Standards Institute.
- C. Michael Lee, P.E. (2017) *The Snow and Ice Control Operations Manual*. Manual Notice 2017-1 edn. USA: Texas Department of Transportation.
- Cary, J.W. (1987) 'A New Method for Calculating Frost Heave Including Solute Effects', *Water Resources Research*, 23(8), pp. 1620-1624.
- Chamberlain, E.J. and Gow, A.J. (1979) 'Effect of freezing and thawing on the permeability and structure of soils', *Engineering Geology*, 13(1–4), pp. 73-92.
- Cheverev, V.G., Ershov, E.D., Magomedgadzhieva M.A., Vidyapin, I.Y. (1998) 'Results of physical simulation of frost heaving in soils' *Proc. of the 7th Intern. Conf. on Permafrost*. Yellowknife, Canada, pp. 145–149.
- Chunpeng, H., Yanmin, J., Peifeng, Ch., Guibo, R. and Dongpo, H. (2010) 'Automatic Measurement of Highway Subgrade Temperature Fields in Cold Areas', *Intelligent System Design and Engineering Application (ISDEA), 2010 International Conference*, 409-412.



- Cui, Z., He, P., and Yang, W. (2014) 'Mechanical properties of a silty clay subjected to freezing-thawing', *Cold Regions Science and Technology*, 98, pp. 26-34.
- Cui, Z. and Zhang, Z. (2015) 'Comparison of dynamic characteristics of the silty clay before and after freezing and thawing under the subway vibration loading', *Cold Regions Science and Technology*, 119, pp. 29-36.
- Diolaiuti, G.A., Maragno, D., Agata C., Smiraglia, C., Bocchiola, D. (2011) 'Glacier retreat and climate change: Documenting the last 50 years of Alpine glacier history from area and geometry change of Dosde Piazzi glaciers (Lombardy Alps, Italy)', *Progress in Physical Geography*, 35(2), pp.161-182.
- Dirksen, C. and Miller, R.D. (1966) 'Closed-system freezing in unsaturated soils', *Soil Sciences Society of Am. Proc.*, 30, pp. 168.
- Dreving, V.P. (1954) *The phase rule*. Moscow: Moscow State University. (in Russian).
- Everett, D.H. (1961) 'The thermodynamics of frost damage to porous solids', *Transactions of the Faraday Society*, (57), pp. 1541-1551.
- Farifteh, J., Farshad, A. and George, R.J. (2006) 'Assessing salt-affected soils using remote sensing, solute modelling, and geophysics', *Geoderma*, 130(3-4), pp. 191-206.
- Feinberg, M. (1979) 'On Gibbs' phase rule', *Archive for rational mechanics and analysis*, 70(3), pp. 219; 219-234; 234.
- Feldman, G.M. (1967) 'Moisture migration and stratified texture in freezing soils', *Engineering Physics*, 13, pp. 425-429.
- Findlay, S.E.G. and Kelly, V.R. (2011) 'Emerging indirect and long-term road salt effects on ecosystems', *Annals of the New York Academy of Sciences*, 1223(1), pp. 58-68.
- Frolov, A.D. and Komarov, I.A. (1983) 'Characteristics of the thermophysical and electric property changes of saline frozen soils'. In *Proceedings, Fourth International Symposium of Thermal Engineering and Science for Cold Regions*. USA Cold Regions Research and Engineering Laboratory, Special Report 92-22, pp.282-287.
- Gardener, W.R. (1958) 'Some steady-state solutions of the unsaturated moisture flow equation with application to evaporation from water table', *Soil Sciences*, (85), pp. 223-232.
- Giakoumakis, S.G. (1994) 'A model for predicting coupled heat and mass transfers in unsaturated partially frozen soil', *International Journal of Heat and Fluid Flow*, 15(2), pp. 163-171.
- Giakoumakis, S.G. and Tsakiris, G.P. (1991) 'Eliminating the effect of temperature from unsaturated soil hydraulic function', *Journal of Hydrology*, 129(1-4), pp. 109-125.

- Gilpin, R.R. (1980) 'A model for the prediction of ice lensing and frost heave in soils', *Water Resources Research*, 16, pp. 918-930.
- Godwin, K.S., Hafner, S.D. and Buff, M.F. (2003) 'Long-term trends in sodium and chloride in the Mohawk River, New York: the effect of fifty years of road-salt application', *Environmental Pollution*, 124(2), pp. 273-281.
- Gorelik, Ya.B. and Kolunin V.S. (2001) 'Amazing permafrost', *Nature*, 10 pp.7-14.
- Grigoryev, B.V. and Shabarov, A.B. (2012) 'Experimental study of freezing and thawing of soils in non-equilibrium conditions', *Vestnik of Tyumen' state university*, (4), pp. 53-60.
- Harlan, R. (1973) 'Analysis of coupled heat-fluid transport in partially frozen soil.', *Water Resour Res*, (9(5)), pp. 1314-1323.
- Harris, Ch., Arenson, L.U., Chrisrtiansen, H.H., Etzelmuller, B., Frauenfelder, R., Gruber, S., Haeberli, W., Hauck, Ch., Holzle, M., Humlum, O., Isaksen, K., Kaab, A., Kern-Lutschg, M.A., Lehning M., Matsuoka, N., Murton, J.B., Notzli, J., Phillips, M., Seppala, M., Springman, S.M., Muhll, D.V. (2009), 'Permafrost and Climate in Europe: Monitoring and modelling thermal, geomorphological and geotechnical responses', *Earth Science Reviews*, 92, pp.117-171.
- Hart, B., Bailey, P., Edwards, R., Hortle, K., James, K. and McMahon, A. (1991) 'A review of the salt sensitivity of the Australian freshwater biota', *Hydrobiologia*, (210(1-2)), pp. 105-144.
- Hazirbaba, K., Zhang, Y. and Leroy Hulsey, J. (2011) 'Evaluation of temperature and freeze-thaw effects on excess pore pressure generation of fine-grained soils', *Soil Dynamics and Earthquake Engineering*, 31(3), pp. 372-384.
- Head, K.H. (2011) *Manual of soil laboratory testing*. 3rd edition, volume I edn. Boca Ration, USA: CRC.
- Head, K.H. and Epps, R. (2011) *Manual of soil laboratory testing*. 3rd edition, volume II edn. Boca Raton, USA: CRC.
- Henry, K.S. (2000) *A review of the thermodynamics of frost heave*. Hannover, New Hampshire: US Army Corps of Engineers.
- Hermansson, Å. (2004) 'Laboratory and field testing on rate of frost heave versus heat extraction', *Cold Regions Science and Technology*, 38(2-3), pp. 137-151.
- Hivon, E.G. and Segó, D.C. (1995) 'Strength of frozen saline soils', *Canadian Geotechnical Journal*, 32(2), pp. 336-354.
- Hoekstra, P. (1969a) 'Physics and chemistry of frozen soils', *Nat Acad Sciences-Nat Research Council-Highway Research Board-Special Report*, (103), pp. 78-90.

- Hoekstra, P. (1969b) 'Water movement and freezing pressures', *Soil Sciences Society of Am. Proc.*, 33, pp. 512-518.
- Hoekstra, P. (1966) 'Moisture movement in soils under temperature gradients with the cold-side temperature below freezing', *Water Resources Research*, 2(2), pp. 241-250.
- Horvath, Z., Micheli, E., Mindszenty, A., Berényi-Uveges, J. (2005) 'Soft-sediment deformation structures in Late Miocene–Pleistocene sediments on the pediment of the Mátra Hills (Visonta, Atkár, Verseg): Cryoturbation, load structures or seismites?' *Tectonophysics*, 410(1–4), pp. 81-95.
- Ishikawa, T. and Miura, S. (2011) 'Influence of freeze-thaw action on deformation-strength characteristics and particle crushability of volcanic coarse-grained soils', *Soils and Foundations*, 51(5), pp. 785-799.
- Ishikawa, T., Tokoro, T., Ito, K. and Miura, S. (2010) 'Testing Methods for Hydro-Mechanical Characteristics of Unsaturated Soils Subjected to One-Dimensional Freeze-Thaw Action', *Soils and Foundations*, 50(3), pp. 431-440.
- Iushkov, B.S. and Sergeev, A.S. (2015) 'Reserach of dependence of frost heaving clay soils to freezing speed', *Transport. Transport facilities.Ecology*, (4), pp. 130-139.
- Kweon, G. and Hwang, T. (2013) 'Deformational characteristics of subgrade soils and subbase materials with freeze-thaw', *KSCE Journal of Civil Engineering*, 17(6), pp. 1317-1322.
- Jame, Y.W. and Norum, D.I. (1980) 'Heat and mass transfer in a freezing unsaturated porous medium', *Water Resources Research*, 18(4), pp. 811-819.
- Ji, Z., Xu, X. and Yu, L. (2010) 'Macroscopic frost heave model based on segregation potential theory', *Transactions of Tianjin University*, 16(4), pp. 304-308.
- Junwei, Z., Jinping, L. and Xiaojuan, Q. (2013) 'Thermal stability analysis under embankment with asphalt pavement and cement pavement in permafrost regions', *TheScientificWorldJournal*, 2013, pp. 549623.
- Kay, B.D. and Groenevelt, P.H. (1974) 'On the interaction of water and heat transport in frozen and unfrozen soils, 1. Basic theory; the vapour phase', *Soil Science Society of America Journal*, 38, pp. 395-400.
- Kay, B.D. and Groenevelt, P.H. (1983) 'Redistribution of solutes in freezing soil: exclusion of solutes', *Proceedings - Permafrost, 4th International Conference*. Fairbanks, AK, USA, Washington, DC, USA: Natl Acad Press, 584-588.
- KazPravda (2016) 'Astana streets are going to be treated with de-icing chemicals of new generation', *Republic News "KazPravda"*, 3 November, p. <http://www.kazpravda.kz/news/tehnologii/reagentom-novogo-pokoleniyabudut-obrabativat-ulitsi-astani/>.

- Kelting, D.L., Laxson, C.L. and Yerger, E.C. (2012) 'Regional analysis of the effect of paved roads on sodium and chloride in lakes', *Water research*, 46(8), pp. 2749-2758.
- Kiyalbayev, A. (2003) *Environmental safety in the operation of highways and city streets*. Almaty: Gylym.
- Konovalov, A.A. (2007) 'Phase balance and steady strength of frozen ground', *Earth Cryosphere*, XI(3), pp. 51-62.
- Konrad, J.M. and Morgenstern, N.R. (1981) 'Segregation potential of a freezing soil', *Canadian Geotech Journal*, 18(4), pp. 482-491.
- Konrad, J.M. (1989) 'Physical processes during freeze-thaw cycles in clayey silts', *Cold Regions Science and Technology*, 16(3), pp. 291-303.
- Konrad, J.M. and Samson, M. (2000) 'Hydraulic conductivity of kaolinite-silt mixtures subjected to closed-system freezing and thaw consolidation', *Canadian Geotechnical Journal*, 37(4), pp. 857-869.
- Konrad, J. (2005) 'Estimation of the segregation potential of fine-grained soils using the frost heave response of two reference soils', *Canadian Geotechnical Journal*, 42(1), pp. 38-50.
- Koopsman, R.W.R. and Miller, R.D. (1966) 'Soil freezing and soil water characteristic curves', *Soil Science Society of America Journal*, (22), pp. 278-281.
- Kværnø, S.H. and Øygarden, L. (2006) 'The influence of freeze–thaw cycles and soil moisture on aggregate stability of three soils in Norway', *Catena*, 67(3), pp. 175-182.
- Kweon, G. and Hwang, T. (2013) 'Deformational characteristics of subgrade soils and subbase materials with freeze-thaw', *KSCE Journal of Civil Engineering*, 17(6), pp. 1317-1322.
- Lai, Y., Pei, W., Zhang, M. and Zhou, J. (2014) 'Study on theory model of hydro-thermal–mechanical interaction process in saturated freezing silty soil', *International Journal of Heat and Mass Transfer*, 78, pp. 805-819.
- Lee, W., Bohra, N.C., Altschaeffl, A.G., White, T.D. (1995) 'Resilient modulus of cohesive soils and the effect of freeze-thaw', *Canadian Geotechnical Journal*, 32(4), pp. 559-568.
- Loch, J.P.G. and Kay, B.D. (1978) 'Water redistribution in partially frozen, saturated silt under several temperature gradient and overburden loads', *Soil Science Society of America Journal*, 42(3), pp. 400-406.
- Loch, J.P.G. (1981) 'State-of-the-art report — frost action in soils', *Engineering Geology*, 18(1–4), pp. 213-224.

- Lundmark, A. and Jansson, P. (2008) 'Estimating the Fate of De-icing Salt in a Roadside Environment by Combining Modelling and Field Observations', *Water, Air and Soil Pollution*, 195(1-4), pp. 215-232.
- Lundmark, A. and Olofsson, B. (2007) 'Chloride Deposition and Distribution in Soils Along a Deiced Highway - Assessment Using Different Methods of Measurement', *Water, Air and Soil Pollution*, 182(1-4), pp. 173-185.
- Marion, G.M. (1995) *Freeze-Thaw Processes and Soil Chemistry. Special Report* Philadelphia: American Society for Testing and Materials.
- Matsumura, Shinji and Yamazaki, Koji (2012) 'A longer climate memory carried by soil freeze-thaw processes in Siberia', *Environmental Research Letters*, 7(4), pp. 045402.
- Matsuoka, N. (2011) 'Climate and material control on periglacial soil processes: Towards improving periglacial climate indicators', *Quaternary Research*, 75, pp. 356-365.
- Mengel, David D. (2011) 'Fundamental of Soil Cation Exchange Capacity' (CEF). Available at <https://www.extension.purdue.edu/extmedia/ay/ay-238.html>. (Accessed: 10<sup>th</sup> March 2017)
- Michalowski, R.L. and Zhu, M. (2006) 'Frost heave modelling using porosity rate function', *International Journal for Numerical and Analytical Methods in Geomechanics*, 30(8), pp. 703-722.
- Miller, R.D. (1972) 'Freezing and heaving of saturated and unsaturated soils', *Highw Res Rec*, (39), pp. 1-11.
- Ming, F. and Li, D. (2015) 'Experimental and Theoretical Investigations on Frost Heave in Porous Media', *Mathematical Problems in Engineering*, (Article ID 198986), pp. doi:10.1155/2015/19898.
- Mizoguchi, M. (1990) *Water, heat and salt transport in freezing soil* Ph.D thesis. University of Tokyo.
- Murton, J.B., Ozouf J.-C., Peterson, R. (2016), 'Heave settlement and fracture of chalk during physical modelling experiments with temperature cycling above and below 0 °C', *Geomorphology*, 270, pp. 71-87.
- Nagare, R., Schincariol, R., Quinton, W. and Hayashi, M. (2012) 'Effects of freezing on soil temperature, freezing front propagation and moisture redistribution in peat: laboratory investigations', *Hydrology and Earth System Sciences*, 16(2), pp. 501-515.
- Nguyen, A.D., Arenson, L.U., Sego, D.C. and Biggar, W.K. (2010) 'The dependence of strength and modulus of frozen saline sand on temperature, strain rate and salinity', *Proceedings of the 63rd Canadian Geotechnical Conference*. Calgary, AB, Canada, September 12-16, pp. 467-475.

- Norrström, A.C. and Jacks, G. (1998) 'Concentration and fractionation of heavy metals in roadside soils receiving de-icing salts', *Science of The Total Environment*, 218(2-3), pp. 161-174.
- O'Neill, K. (1983) 'The physics of mathematical frost heave models: A review', *Cold Regions Science and Technology*, 6(3), pp. 275-291.
- O'Neill, K. and Miller, R.D. (1985) 'Exploration of a Rigid Ice Model of Frost Heave', *Water Resources Research*, 21(3), pp. 281-296.
- Othman, M.A. and Benson, C.H. (1993) 'Effect of freeze-thaw on the hydraulic conductivity and morphology of compacted clay', *Canadian Geotechnical Journal*, 30(2), pp. 236-246.
- Oztaş, T. and Fayetorbay, F. (2003) 'Effect of freezing and thawing processes on soil aggregate stability', *Catena*, 52(1), pp. 1-8.
- Padilla, F. and Villeneuve, J. (1992) 'Modelling and experimental studies of frost heave including solute effects', *Cold Regions Science and Technology*, 20, pp. 183-194.
- Panday, S. and Corapcioglu, M.Y. (1991) 'Solute rejection in freezing soils', *Water Resources Research*, 27(1), pp. 99-108.
- Pedersen, L.B., Randrup, T.B. and Ingerslev, M. (2000) 'Effects of road distance and protective measures on deicing NaCl deposition and soil solution chemistry in planted median strips', *Journal of Arboriculture*, 26(5), pp. 238-245.
- Penner, E. (1970) 'Frost heaving forces in Leda clay', *Canadian Geotechnical Journal*, 7(1), pp. 8-16.
- Penner, E. (1967) 'Heaving Pressure in Soils During Unidirectional Freezing', *Canadian Geotechnical Journal*, 4(4), pp. 398-408.
- Penner, E. (1977) 'Fundamental aspects of soil action', *Frost Action in Soils*. Sweden, University Lulea: , 17-28.
- Philip, J.R. and de Vries, D.A. (1957) 'Moisture movement in porous materials under temperature gradients', *Trans. Am. Geophys.*, (38), pp. 222-231.
- Qi, J., Ma, W. and Song, C. (2008) 'Influence of freeze-thaw on engineering properties of a silty soil', *Cold Regions Science and Technology*, 53(3), pp. 397-404.
- Qi, J., Vermeer, P.A. and Cheng, G. (2006) 'A review of the influence of freeze-thaw cycles on soil geotechnical properties', *Permafrost and Periglacial Processes*, 17(3), pp. 245-252.
- Robertson, G.P., Sollins, P., Ellis, B.G. and Lajtha, K. Exchangeable ions, pH, and Cation Exchange Capacity. Available at: <http://andrewsforest.oregonstate.edu/pubs/pdf/pub2709.pdf> (Accessed 10<sup>th</sup> March 2017)

- Sakanov, D.K. (2007) *Regional specific features of temperature mode of the road constructions* Cand. in techn. sci. Kazakh academy of transport and communication named after M. Tynyshbayev.
- Samanta Lax Eric W. Peterson (2008) 'Characterization of chloride transport in the unsaturated zone near salted road', *Environmental Geology*, 58(5), pp. 1041-1049.
- Sarsembayeva, A.S. (2005) *Improvement of chemical method for liquidation the winter slipperiness on highways* Cand. in technical sciences. Kazakh Academy of Transport and Communication. (in Russian)
- Sarsembayeva, A. and Collins, P. (2015) 'A Modified Freeze-Thaw Laboratory Test for Pavement Sub Soils Affected by De-icing Chemicals', *IAEG XII Congress, Engineering Geology for Society and Territory - Volume 6*. Torino, September 15-19. Switzerland: Springer International Publishing, 243-247.
- Sarsembayeva, A. and Collins, P. (2015) 'Evaluation of frost heave and the temperature-moisture migration relationship using a modified laboratory method', *Proceedings of the XVI ECSMGE Geotechnical Engineering for Infrastructure and Development* Edinburgh, 13-17 September 2015. UK: Institution of Civil Engineers, 3341-3346.
- Sarsembayeva, A. and Collins, P. (2017) 'Evaluation of frost heave and moisture/chemical migration mechanisms in highway subsoil using a laboratory simulation method', *Cold Regions Science and Technology*, 133, pp. 26-35.
- Sheikin, I.V. (1990) 'Features of thermal properties of saline soils', *Nauka*, (Saline frozen soils as basements of buildings), pp. 20-24. (in Russian)
- Sheshukov, A.Y. and Nieber, J.L. (2011) 'One-dimensional freezing of nonheaving unsaturated soils: Model formulation and similarity solution', *Water Resources Research*, 47(11).
- Shoop, S.A. and Bigl, S.R. (1997) 'Moisture migration during freeze and thaw of unsaturated soils: Modeling and large scale experiments', *Cold Regions Science and Technology*, 25(1), pp. 33-45.
- Shoop, S., Affleck, R., Haehnel, R. and Janoo, V. (2008) 'Mechanical behavior modeling of thaw-weakened soil', *Cold Regions Science and Technology*, 52(2), pp. 191-206.
- Simonsen, E. and Isacsson, U. (2001) 'Soil behavior during freezing and thawing using variable and constant confining pressure triaxial tests', *Canadian Geotechnical Journal*, 38(4), pp. 863-875.
- Simonsen, E. and Isacsson, U. (1999) 'Thaw weakening of pavement structures in cold regions', *Cold Regions Science and Technology*, 29(2), pp. 135-151.
- Simonsen, E., Janoo, V.C. and Isacsson, U. (1997) 'Prediction of temperature and moisture changes in pavement structures', *Journal of Cold Regions Engineering*, 11(4), pp. 291.

- Sinitsyn, A. and Løset, S. (2011) 'Strength of frozen saline silt under triaxial compression with high strain rate', *Soil Mechanics & Foundation Engineering*, 48(5), pp. 196-202.
- SNIP RK 2.04-01-2010 (2010) *SNIP RK 2.04-01-2010 Building Climatology*, Almaty, Kazakhstan: RGP "Kazakh Research and Design Experimental Institute of Earthquake Engineering and Architecture."
- SNIP RK 3.03-09-2006 (2006). *SNIP RK 3.03-09-2006 Highways*, Almaty, KAZGOR.
- Starke, J.O. (1989) 'Effects of freeze-thaw weather conditions on compacted clay liners', *Proceedings of the 12th Annual Madison Waste Conference*. Wisconsin, University of Wisconsin-Madison, 412-420.
- Storme, M., Konrad, J. and Fortier, R. (2004) 'Assessment of thaw weakening in pavement stiffness using the spectral analysis of surface waves', *Canadian Geotechnical Journal*, 41(3), pp. 510-522.
- Sutherland, H.B. and Gaskin, P.N. (1973) 'Pore water and heaving pressures developed in partially frozen soils', *Proc.Int.Conf.Permafrost, 2nd*, pp. 409-419.
- Szymanski, W., Skiba, M., Wojtun, B., Drewnik, M. (2015) 'Soil properties, micromorphology, and mineralogy of Cryosols from sorted and unsorted patterned grounds in the Hornsund area, SW Spitsbergen' *Geoderma*, 253-254, pp. 1-11.
- Taber, S. (1930) 'The Mechanics of Frost Heaving', *The Journal of geology*, 38(4), pp. 303-317.
- Tang, Y. and Xu, J. (2016) 'Shield Tunneling in Rock–Soil Interface Composite Formations', *Geotechnical and Geological Engineering*, 34(6), pp. 1693-1705.
- Taylor, G.S. and Luthin, J.N. (1978) 'A model for coupled heat and moisture transfer during soil freezing', *Can.Geotech.J.*, (15), pp. 548-555.
- Teltayev, B.B. and Suppes, Y.A. (2014) 'A new map of road freezing depth in Kazakhstan', *KazdorNII Bulletin*, 3-4(43-44), pp. 35-52.
- Torrance, J.K. and Schellekens, F.J. (2006) 'Chemical factors in soil freezing and frost heave', *Polar Record*, 42(01), pp. 33-42.
- Tschapek, M., Scoppa, C.O. and Wasowski, C. (1978) 'The surface tension of soil water', *Journal of Soil Science*, 29(1), pp. 17-21.
- Tsytovtich, N.A., Kronik, Y.A., Markin, K.F., Aksenov, V.I. (1973) *II International Conference on Permafrost*, USSR, Yakutsk. Abstracts of papers. Publishing House Nauka, Moscow. (in Russian).
- Tulebekova, A.S., Zhusupbekov, A.Z., Shakhmov, Z.A. and Yenkebayev, S.B. (2012) 'Experience of testing according to international standard ASTM on problematical



- soil ground of Astana', *Bulletin of L.N. Gumilyov Eurasian National University*, (2), pp. 126-131.
- Vengosh, A. (2003) 'Salinization and Saline Environments', in Editors-in-chief: Heinrich D. Holland and Karl K. Turekian (eds.) *Treatise on Geochemistry*. Oxford: Pergamon, pp. 1-35.
- Vidyapin, I.Y. and Cheverev, V.G. (2008) 'The hydraulic of freezing saline soils', *Earth Cryosphere*, 12(4), pp. 43-45.
- Wagner, W., Saul, A., and Pruss, A., *J. Phys. Chem. Ref. Data*, 23, 515, 1994. Chemical mass transfer
- Wan, X., Lai, Y. and Wang, C. (2015) 'Experimental Study on the Freezing Temperatures of Saline Silty Soils', *Permafrost and Periglacial Processes*, pp. n/a-n/a.
- Wang, D., Ma, W., Niu, Y., Chang, X. and Wen, Z. (2007) 'Effects of cyclic freezing and thawing on mechanical properties of Qinghai–Tibet clay', *Cold Regions Science and Technology*, 48(1), pp. 34-43.
- Wang, E., Cruse, R.M., Chen, X. and Daigh, A. (2012) 'Effects of moisture condition and freeze/thaw cycles on surface soil aggregate size distribution and stability', *Canadian Journal of Soil Science*, 92(3), pp. 529-536.
- Williams, P.J. (1968) 'Properties and behavior of freezing soils ', *Norwegian Geotechnical Institute Paper*, pp. 72-120.
- Wu, D., Lai, Y. and Zhang, M. (2015) 'Heat and mass transfer effects of ice growth mechanisms in a fully saturated soil', *International Journal of Heat and Mass Transfer*, 86, pp. 699-709.
- Xu, X., Wang, J., Zhang, L., Deng, Y., Chuvilin, E., Yershov, E., Ishizaki, T. and Fukuda, M. (1997) 'Mechanism of frost heave by film water migration under temperature gradient', *Chinese Science Bulletin*, 42, pp. 1290-1294.
- Xu, X., Lai, Y., Dong, Y. and Qi, J. (2011) 'Laboratory investigation on strength and deformation characteristics of ice-saturated frozen sandy soil', *Cold Regions Science and Technology*, 69(1), pp. 98-104.
- Yariv, S. and Cross, H. (1979) *Geochemistry of colloid systems*. Berlin: Springer Verlag, Heidelberg, New York.
- Yarkin, A.N. (1990) 'Effect of salinity on the mechanical and rheological properties of frozen soil', *Nauka*, (Saline frozen soils as basement of buildings), pp. 103-107. (in Russian).
- Zhang, M., Wen, Z., Xue, K. and Chen, L. (2016) 'A coupled model for liquid water, water vapour and heat transport of saturated–unsaturated soil in cold regions: model formulation and verification', *Environmental earth sciences*, (75:701), pp. 1-19.

- Zhang, S., Lai, Y., Sun, Z. and Gao, Z. (2007) 'Volumetric strain and strength behavior of frozen soils under confinement', *Cold Regions Science and Technology*, 47(3), pp. 263-270.
- Zhang, S., Sun, Z., Xu, X. and Du, H. (2013) 'Volumetric calculation method and temperature characteristics of frozen soil in mechanical testing', *Cold Regions Science and Technology*, 85(0), pp. 225-231.
- Zhang, Y. and Michalowski, R.L. (2015) 'Thermal-Hydro-Mechanical Analysis of Frost Heave and Thaw Settlement', *Journal of Geotechnical and Geoenvironmental Engineering*, 141(7), pp. 4015027.
- Zheng, L. and Shen, Y. (2014) *Theoretical model of moisture migration in frost soil material*.
- Zhou, J., Wei, C., Wei, H. and Tan, L. (2014) 'Experimental and theoretical characterization of frost heave and ice lenses', *Cold Regions Science and Technology*, 104–105, pp. 76-87.
- Zhussupbekov, A., Zh., Omarov, A.R., Zhukenova, G.A. and Tanyrbergenova, G.K. (2016) 'Geotechnical Infrastructures of New Capital Astana on Problematical Soil Ground', *Proceedings of the 17th Nordic Geotechnical Meeting. Challenges in Nordic Geotechnic*. Reykjavik, Iceland, 25 – 28 May 2016, pp. 923-930.

## Appendix A

### A.1 Particle Size Analysis Results

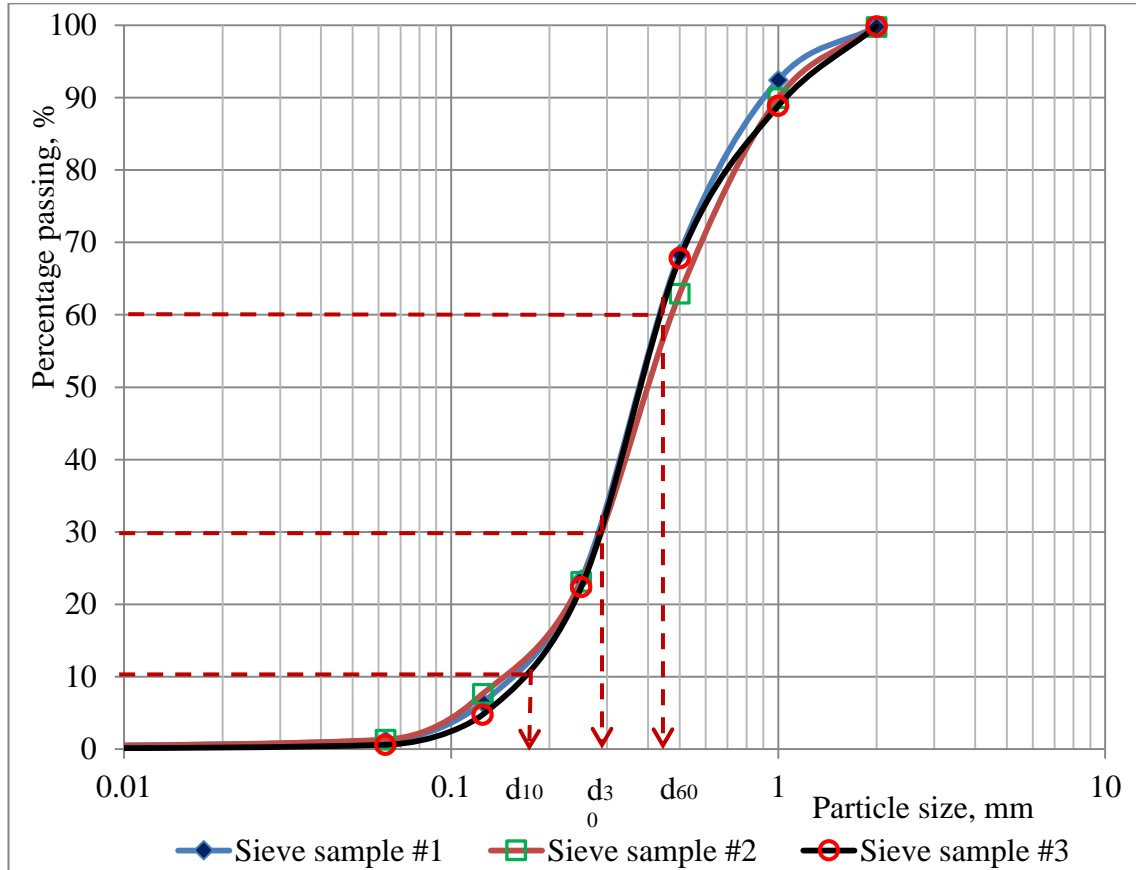


Figure A.1 – Particle size analysis of the sand part in the modelled soils, determined by dry sieving

Sieve No Mesh size, mm	Percentage passing, %		
	Sieve sample #1	Sieve sample #2	Sieve sample #3
2	99.81	99.78	<b>99.83</b>
1	92.42	89.93	<b>88.85</b>
0.5	68.41	62.92	<b>67.81</b>
0.25	23.47	23.12	<b>22.41</b>
0.125	6.47	7.68	<b>4.79</b>
0.063	1.26	1.33	<b>0.62</b>
0.0001	0.01	0.01	<b>0.01</b>

$$C_u = \frac{d_{60}}{d_{10}} = \frac{0.44}{0.18} = 2.4 \quad \text{Uniformly-graded sand}$$

$$C_c = \frac{(d_{30})^2}{d_{10} \cdot d_{60}} = \frac{0.44^2}{0.18 \cdot 0.295} = 3.65 \quad \text{Both of criteria for sand } C_u \geq 6 \text{ and } 1 < C_c < 3 \text{ are not met, therefore the sand part of the soil was classified as SP or poorly graded sand.}$$

**A.2 Plasticity Limits tests**

Date of the test: 09.09.2019

Plastic limit test was in accordance with BS 1377: Part2: 1990: 4.2.3. Sample fraction passed through 0.425mm sieve being used.

Table A.2 – Atterberg limits tests – Plastic limit

Plastic Limit	test	1	2	3	4	Average
Container no.		702	712	728	720	
Mass of wet soil & container	g	45.36	44.81	42.04	41.64	
Mass of dry soil & container	g	42.89	42.49	40.31	40.19	
Mass of container	g	32.79	32.91	32.84	33.95	
Mass of moisture	g	2.47	2.32	1.73	1.45	
Mass of dry soil	g	10.10	9.58	7.47	6.24	
Moisture content	%	24.46	24.22	23.16	23.24	23.77%

Cone penetrometer method, according with BS 1377: Part2: 1990: 4.3. Sample passed through 0.425mm sieve.

Table A.3 - Atterberg Limits – Cone test

Liquid Limit	est	1	2	3	4	5	Average
Initial dial gauge reading	mm	0	0	0	0	0	
Final dial gauge reading	mm	19.68	17.92	23.06	20.07	17.04	
		20.52	18.63	22.83	19.42	17.52	
		19.76	18.1	23.42	19.59	17.72	
Average penetration	mm	19.99	18.22	23.10	19.69	17.43	
Container no.		727	704	711	706	726	
Mass of wet soil & container	g	58.53	58.03	58.53	60.62	60.35	
Mass of dry soil & container	g	51.63	51.43	51.26	53.37	52.96	
Mass of container	g	33	33.56	32.66	33.26	32.88	
Mass of moisture	g	6.9	6.6	7.27	7.25	7.39	
Mass of dry soil	g	18.63	17.87	18.60	20.11	20.08	
Moisture content	%	37.04	36.93	39.09	36.05	36.80	37.18%

### A.3 Particle density test results

- kaolinite  $\rho_s = 2.501 \text{ g/cm}^3$
- sand  $\rho_s = 2.646 \text{ g/cm}^3$
- sandy clay including 50% sand by mass & 50% clay by mass  $\rho_s = 2.615 \text{ g/cm}^3$

### A.4 Compaction test results

Table A.4 - Proctor test results

Moisture content W, %	Dry density, Mg/m <sup>3</sup>	Air voids, %			Bulk density, Mg/m <sup>3</sup>	95% of maximum dry density, Mg/m <sup>3</sup>
		0%	5%	10%		
11.77	1.86	2.00	1.9	1.80	2.08	1.80
13.09	1.89	1.95	1.85	1.75	2.14	1.80
14.39	1.90	1.90	1.81	1.71	2.17	1.80
15.47	1.86	1.86	1.77	1.68	2.14	1.80
18.38	1.74	1.77	1.68	1.59	2.07	1.80
19.84	1.70	1.72	1.64	1.55	2.04	1.80
20.92	1.66	1.69	1.61	1.52	2.01	1.80
23.23	1.60	1.63	1.55	1.46	1.98	1.80

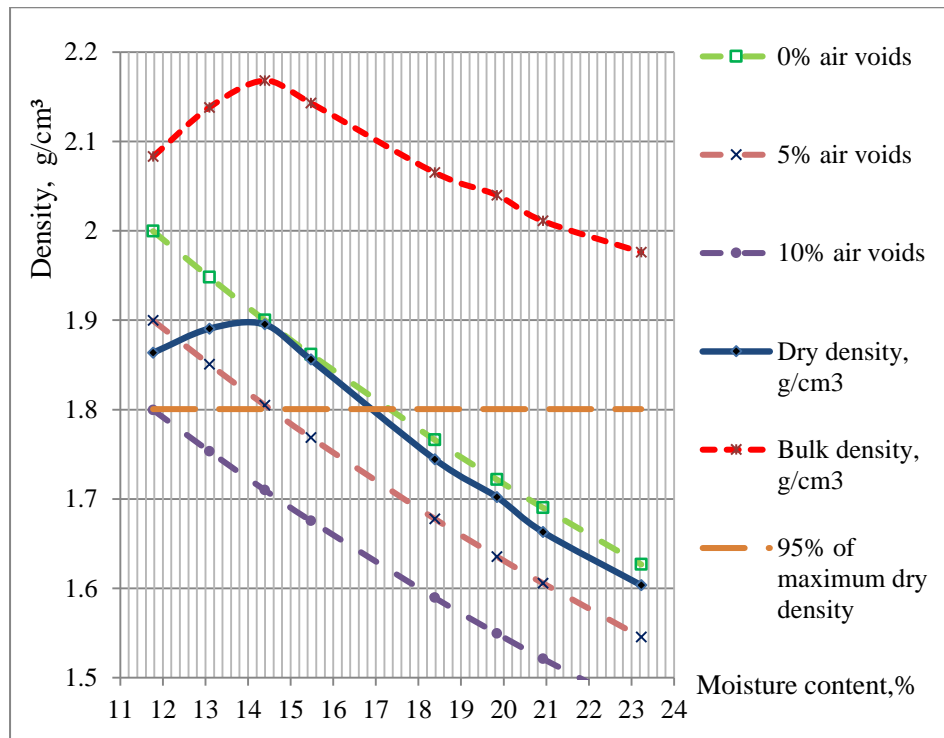


Figure A.2 – Proctor tests results with 2.5 kg rammer ('light' compaction)

Table A.5 – Compaction of soil samples in Test 3 with changing density between the columns

N	Achieved dry density before the test, Mg/m <sup>3</sup>	Soil portion	Compaction pressure applied per each portion of soil
#1	1.178	2.5 scoops of soils	1 push with 15 kg full cap pressure
#2	1.302	2 scoop of soils	2 pushes with 15 kg full cap pressure
#3	1.345	1 scoop of soils	1 push with 15 kg full cap pressure
#4	1.471	2.5 scoops of soil	2 blows with 2.5 kg rammer and 2 times with 15 kg full cap pressure
#5	1.527	2.5 scoops of soil	3 blows with 2.5 kg rammer
#6	1.607	2.5 scoops of soil	5 blows with 2.5 kg rammer
#7	1.651	2.5 scoops of soil	8 blows with 2.5 kg rammer
#8	1.795	2.5 scoops of soil	15 blows with 2.5 kg rammer
#9	1.798	2.5 scoops of soil	31/32 blows with 2.5 kg rammer

Table A.6 – Compaction of soil samples in Test 4 with changing density between the columns

N	Achieved dry density before the test, Mg/m <sup>3</sup>	Soil portion	Compaction pressure applied per each portion of soil
#1	1.285	2.5 scoop of soils	2 pushes with 15 kg full cap pressure
#2	1.310	1 scoop of soils	1 push with 15 kg full cap pressure
#3	1.503	2 scoops of soil	3 pushes with 15 kg full cap pressure
#4	1.375	2.5 scoop of soil	8 pushes with 15 kg full cap pressure
#5	1.452	1 scoop of soil	4 pushes with 15 kg full cap pressure
#6	1.531	2.5 scoops of soil	4 blows with 2.5 kg rammer
#7	1.645	2.5 scoops of soil	8 blows with 2.5 kg rammer
#8	1.684	2.5 scoops of soil	12 blows with 2.5 kg rammer
#9	1.779	2.5 scoops of soil	31/32 blows with 2.5 kg rammer

Table A.7 – Compaction of soil samples in Test 5 with changing density between the columns

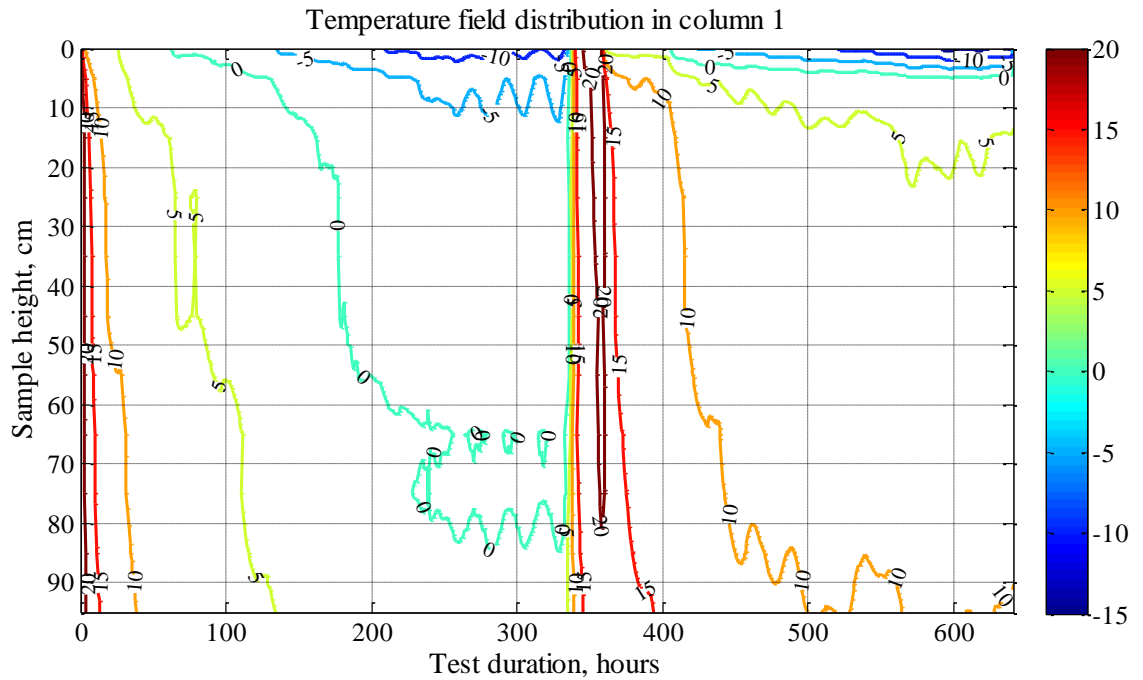
N	Achieved dry density before the test, Mg/m <sup>3</sup>	Soil portion	Compaction pressure applied per each portion of soil
#1	1.339	2.5 scoops of soil	2 times with 15 kg full cap pressure
#2	1.367	1 scoop of soil	1 push with 15 kg full cap pressure
#3	1.430	1 scoop of soil	1 blow with 2.5 kg rammer and 1 push with 15 kg full cap pressure
#4	1.508	2 scoops of soil	2 blows with 2.5 kg rammer and 1 push with 15 kg full cap pressure
#5	1.530	1 scoop of soil	2 blows with 2.5 kg rammer and 1 push with 15 kg full cap pressure
#6	1.541	2.5 scoops of soil	4 blows with 2.5 kg rammer
#7	1.674	2.5 scoops of soil	8 blows with 2.5 kg rammer
#8	1.780	2.5 scoops of soil	14 blows with 2.5 kg rammer
#9	1.801	2.5 scoops of soil	31/32 blows with 2.5 kg rammer

## Appendix B

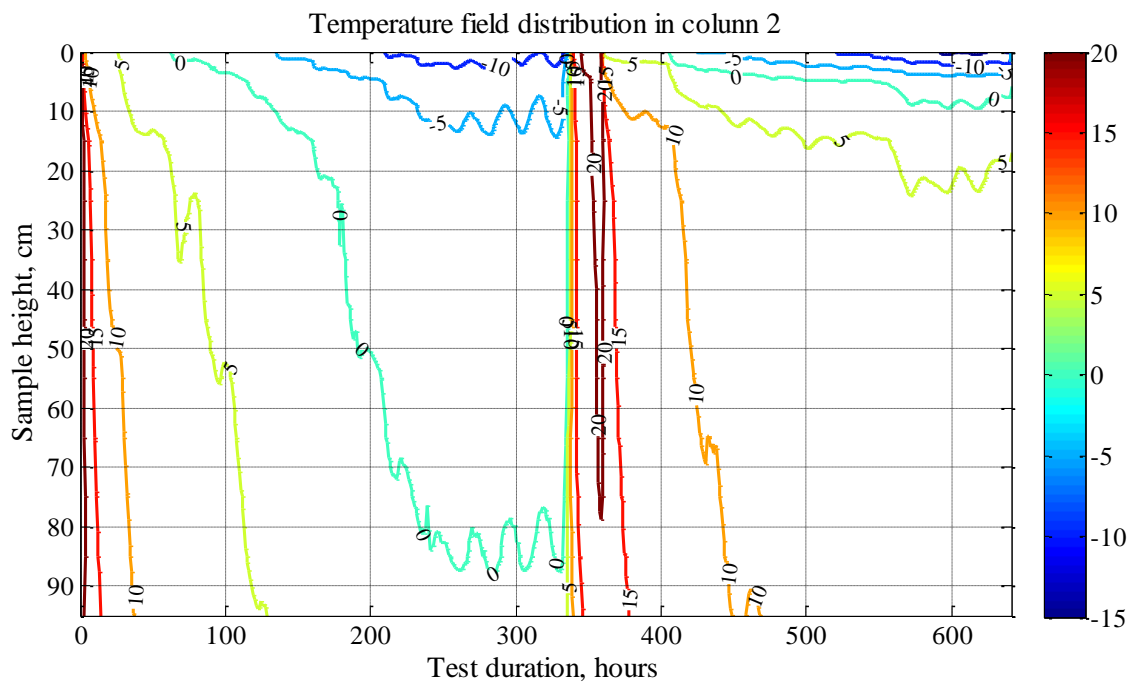
### Temperature field distribution counterplot graphs

Temperature field distribution in Test 1 with deionised water supply. The samples were packed with maximum dry density and 100 cm length.

a)

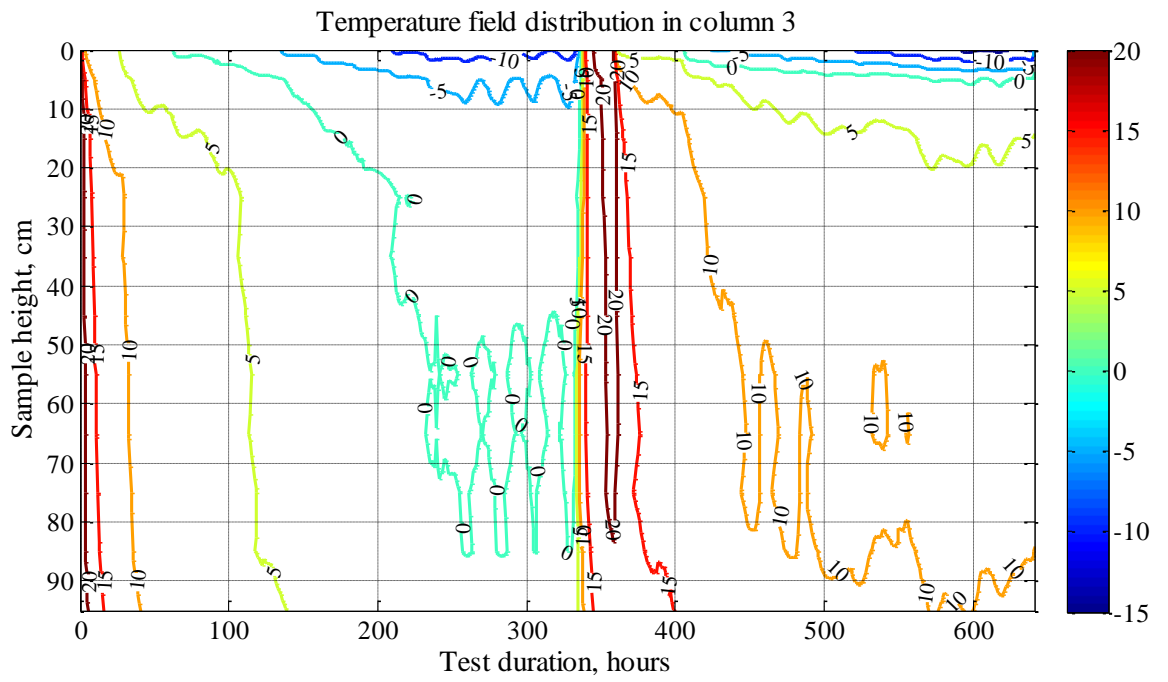


b)

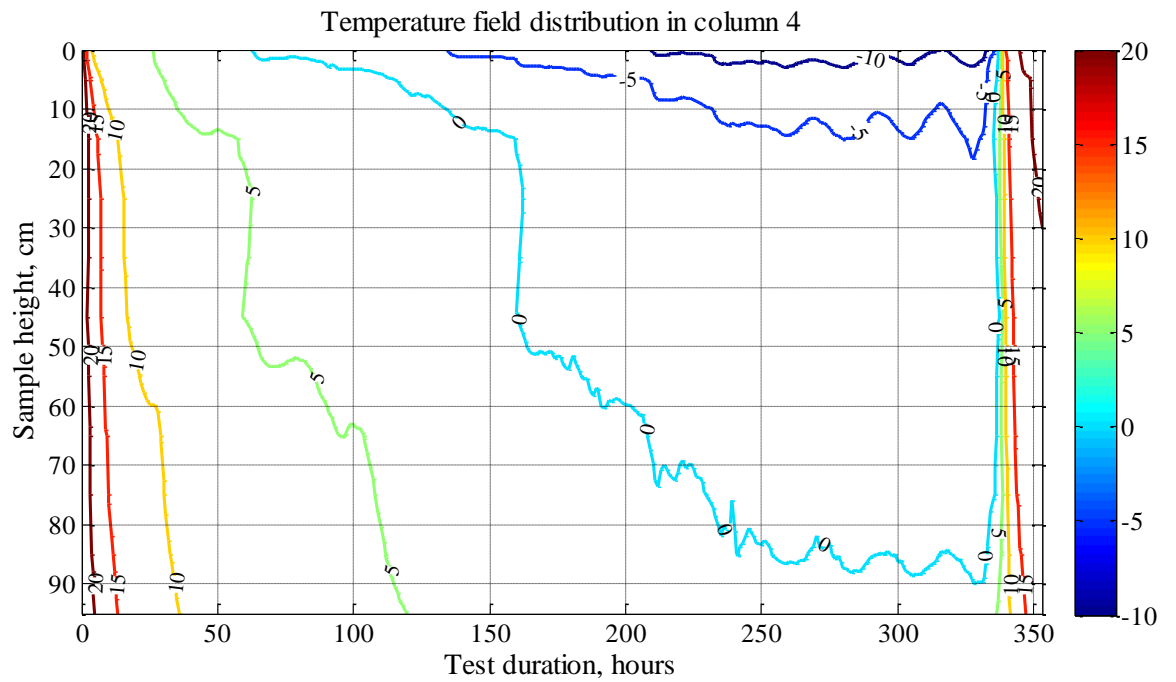




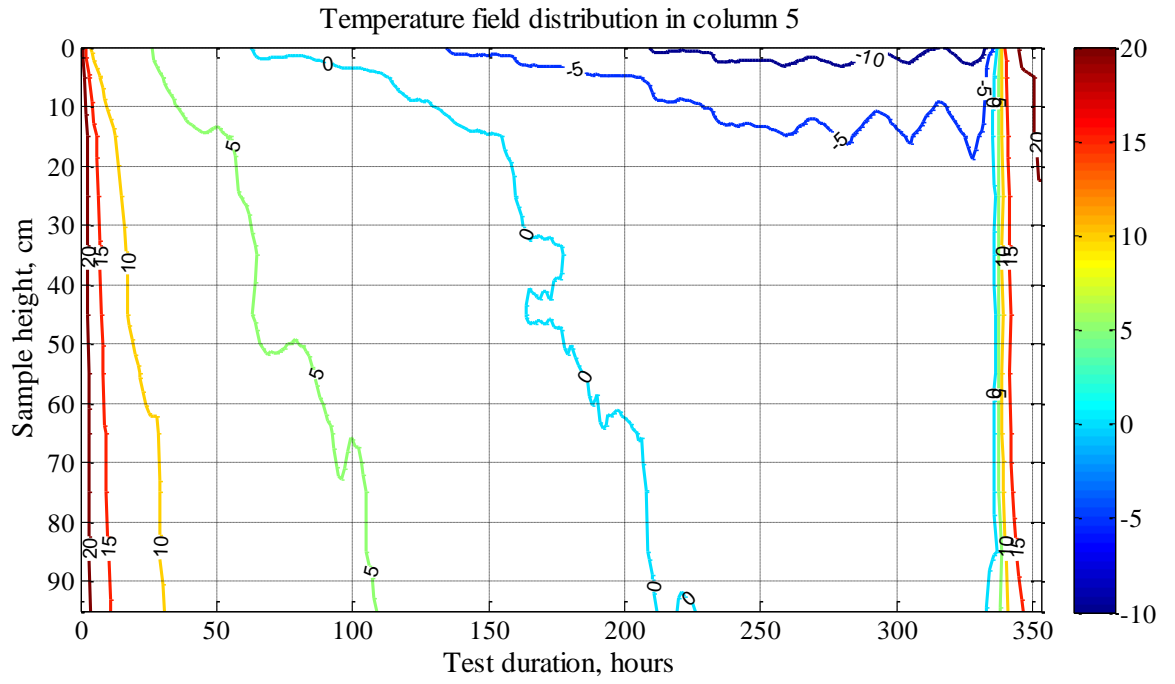
c)



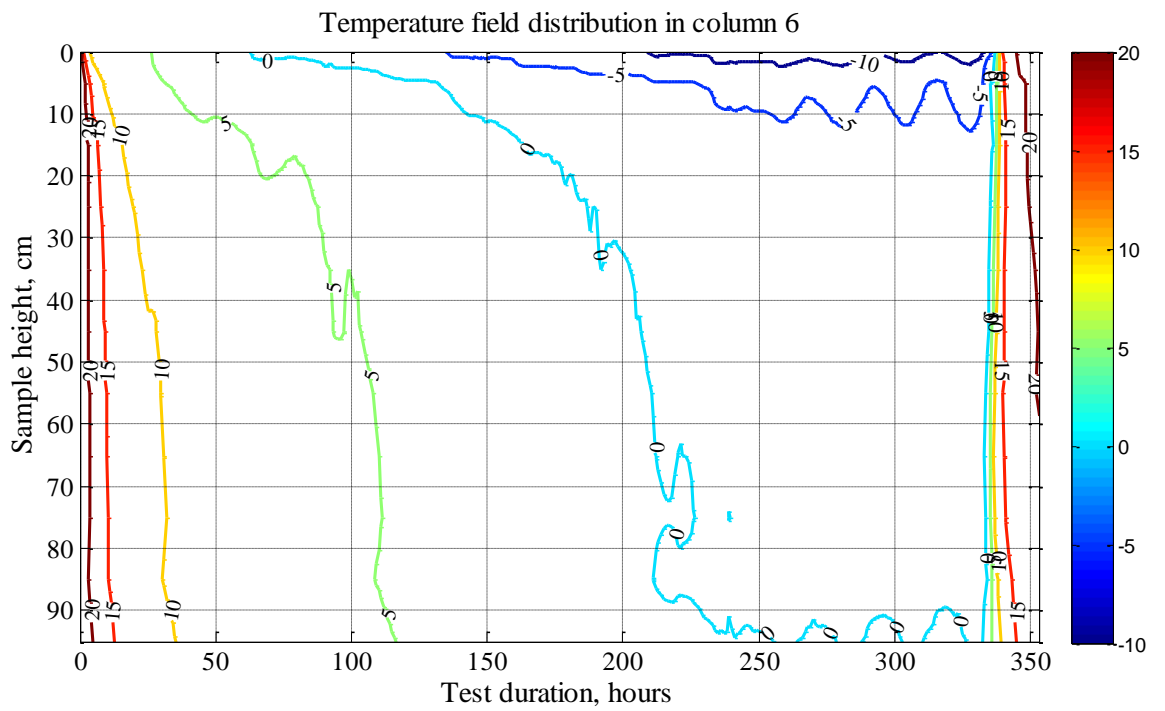
d)



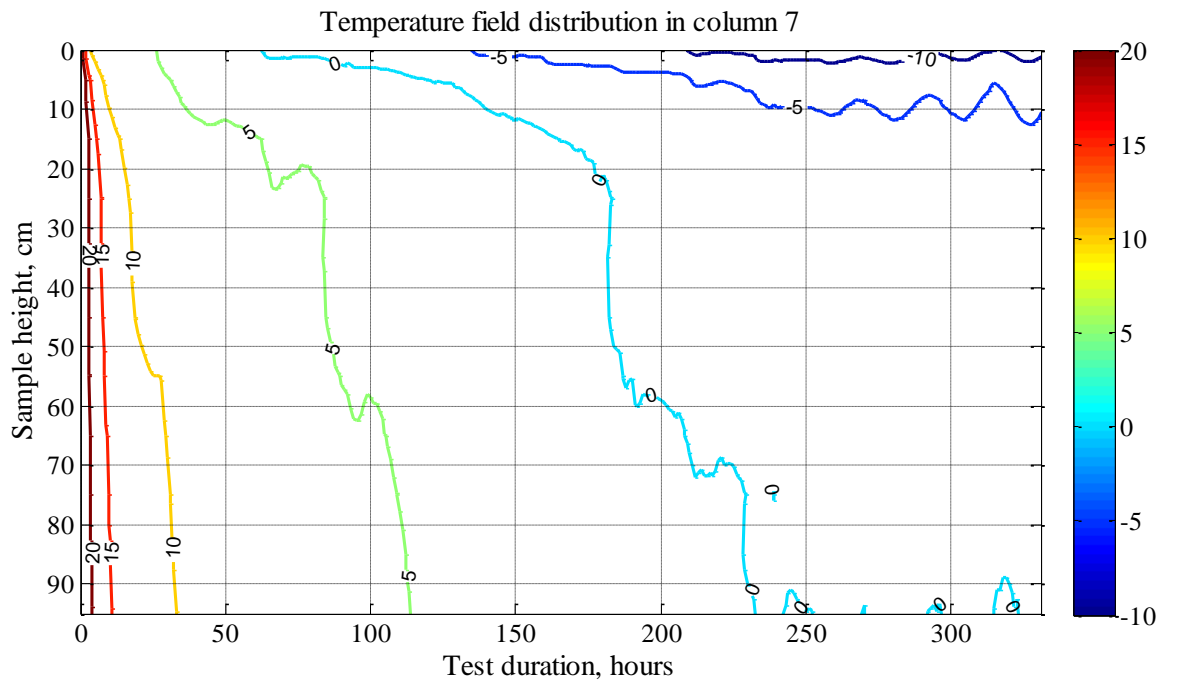
e)



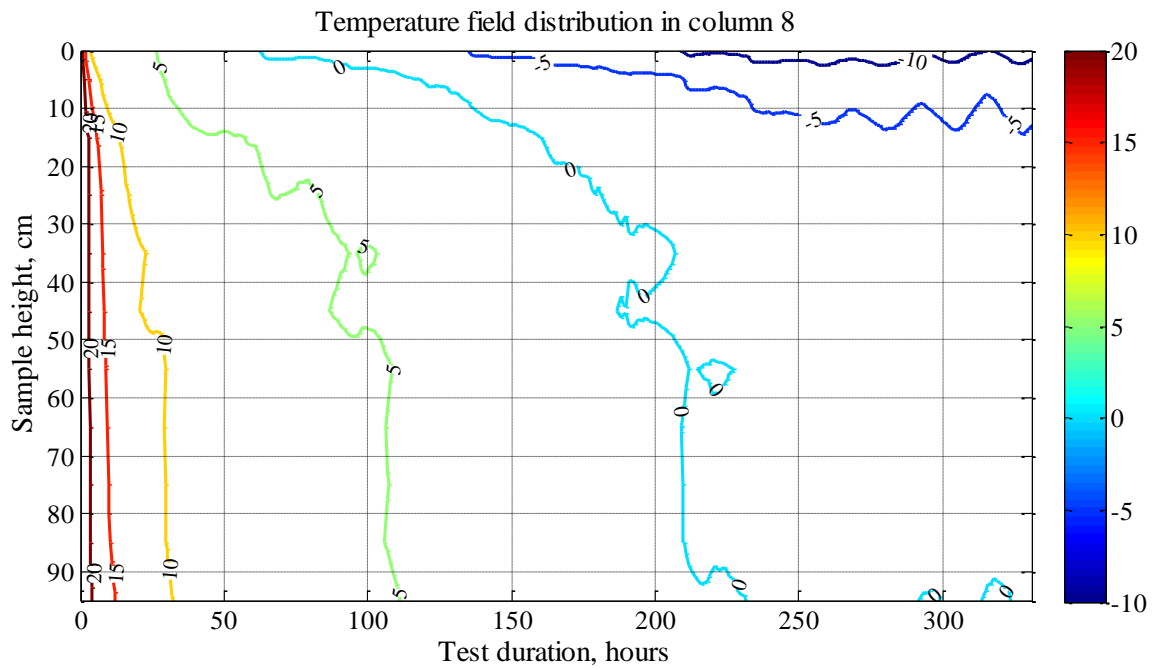
f)



g)



h)



i)

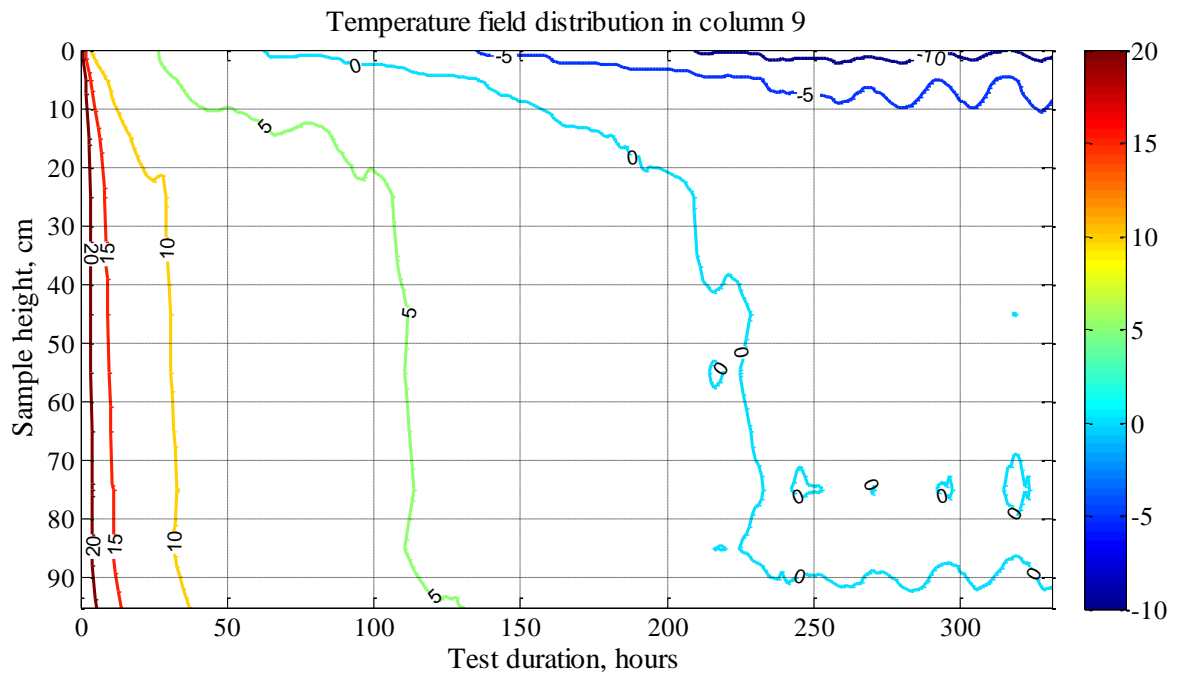


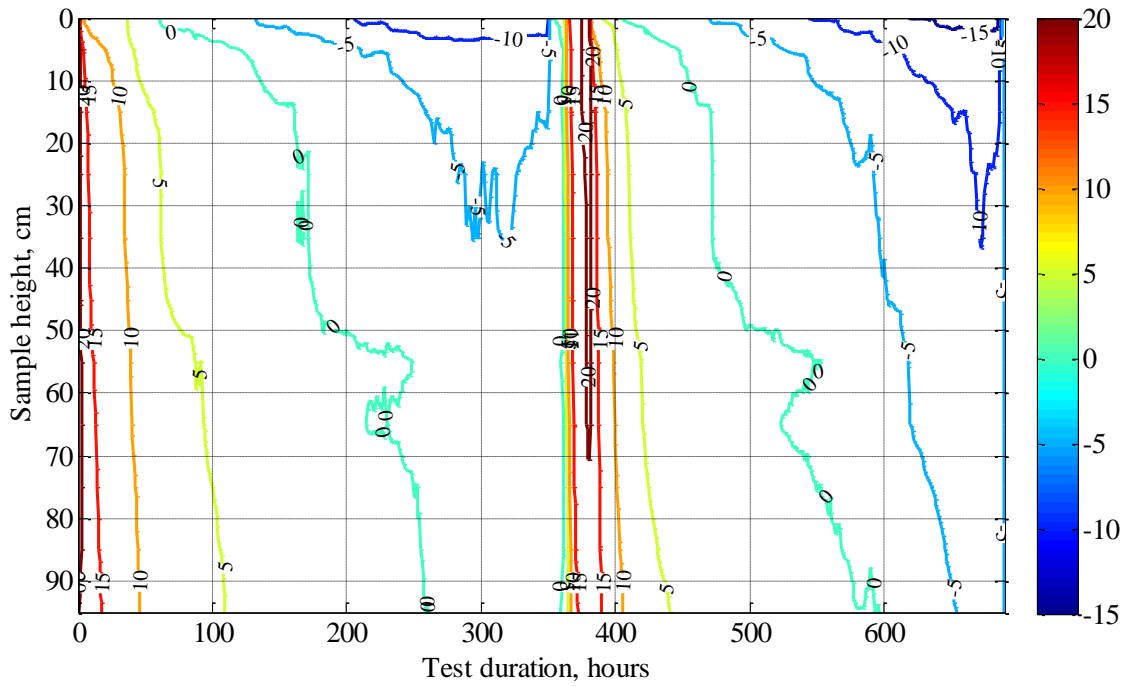
Figure B.3 – Temperature field distribution during in Test 1: a-c - columns #1-#3 terminated after 2 freeze-thaw cycles, d-f - columns #4-#6 terminated after the first freeze-thaw cycle, g-i - columns #7-#9 terminated after the first freezing cycle.

## Temperature field distribution in Test 2

The soil samples were packed with maximum dry density and supplied with 11,000 mg/litre sodium chloride solution from the base.

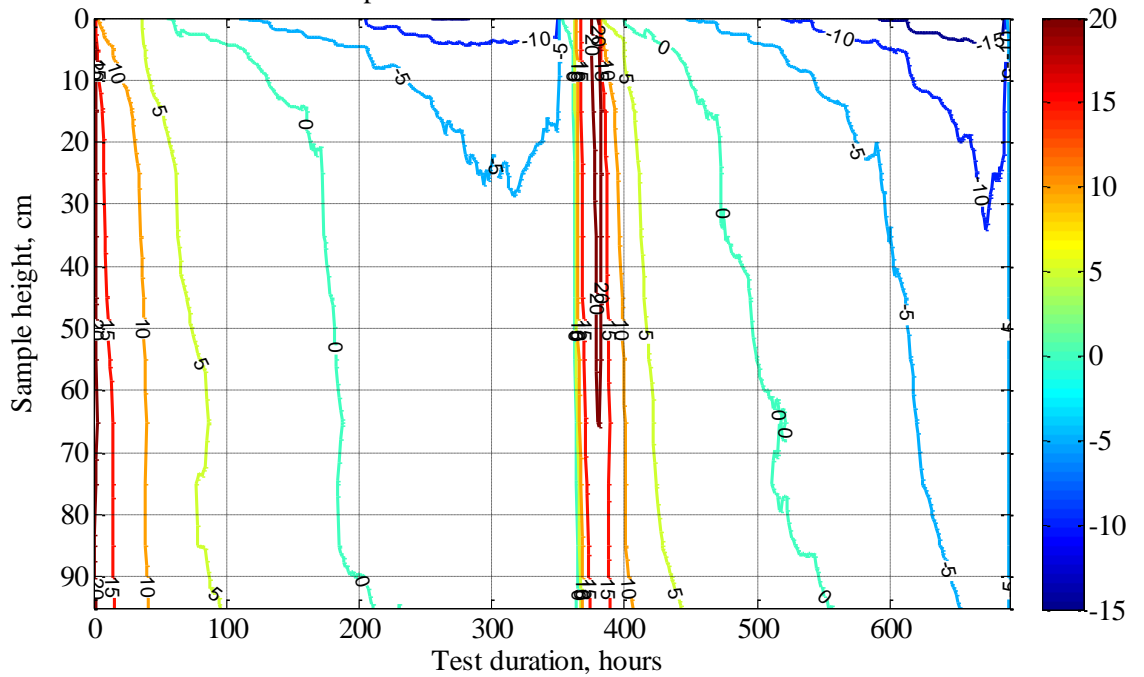
a)

Temperature field distribution in column 1

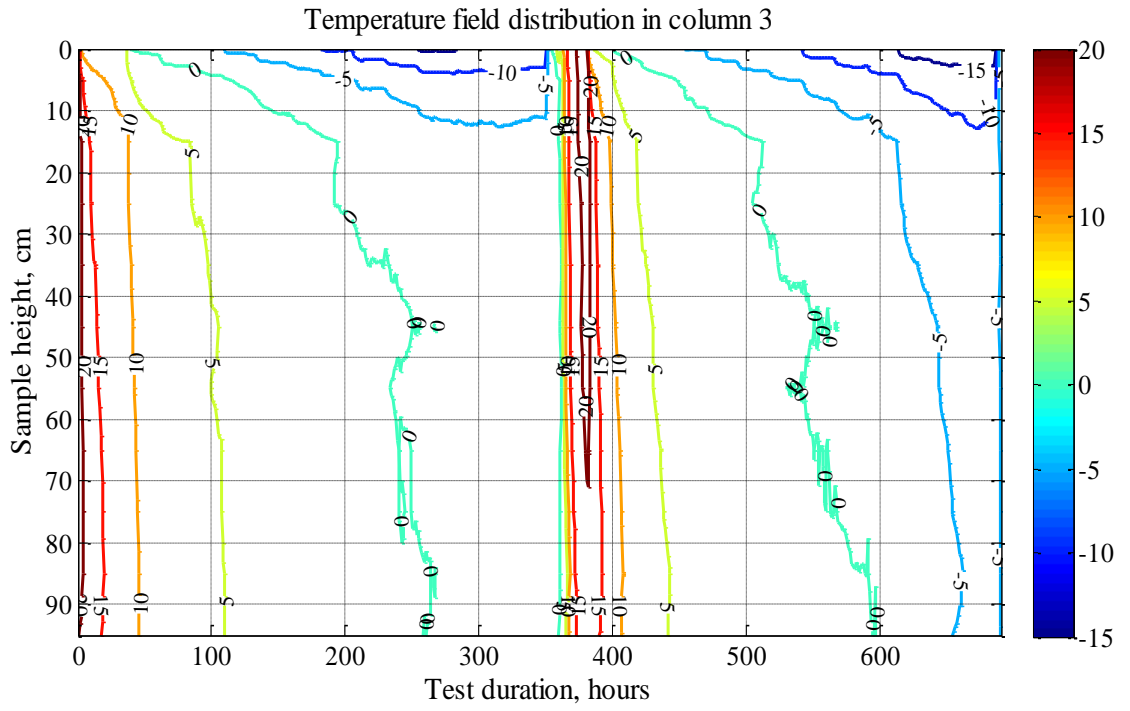


b)

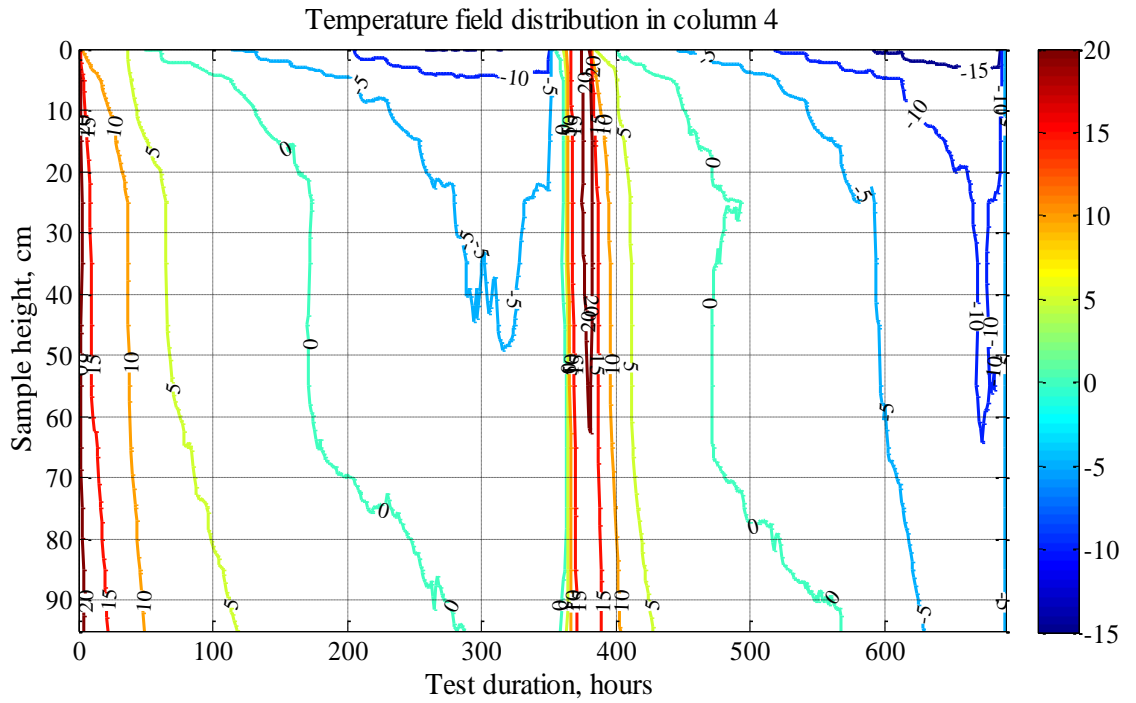
Temperature field distribution in column 2



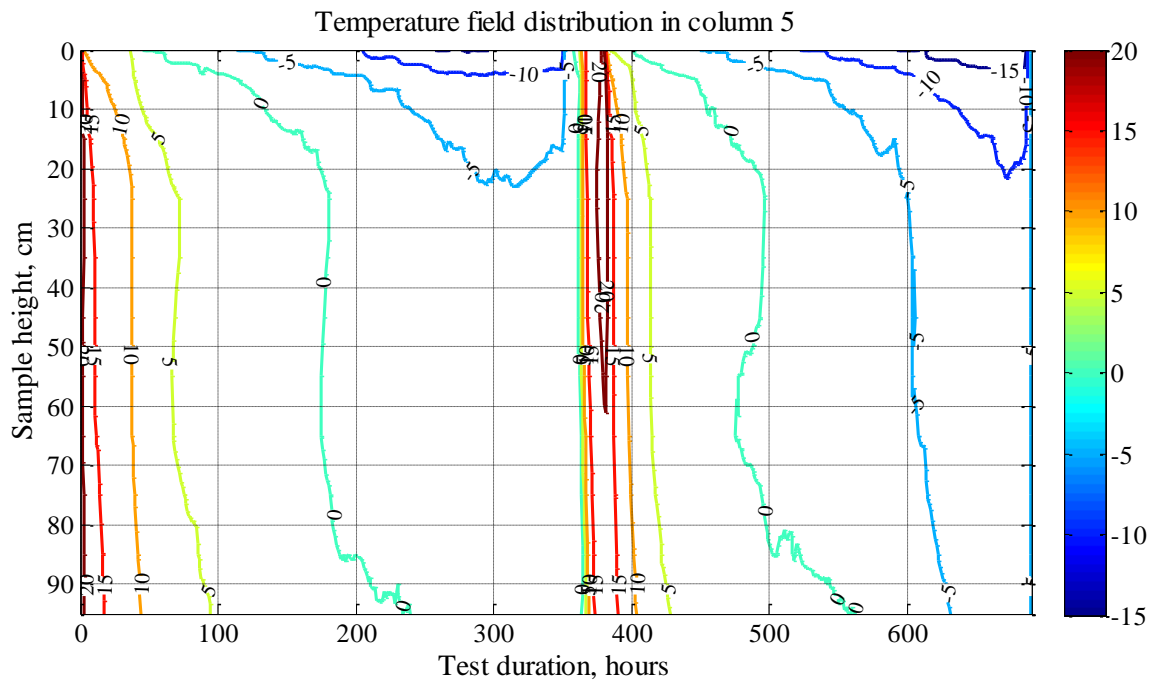
c)



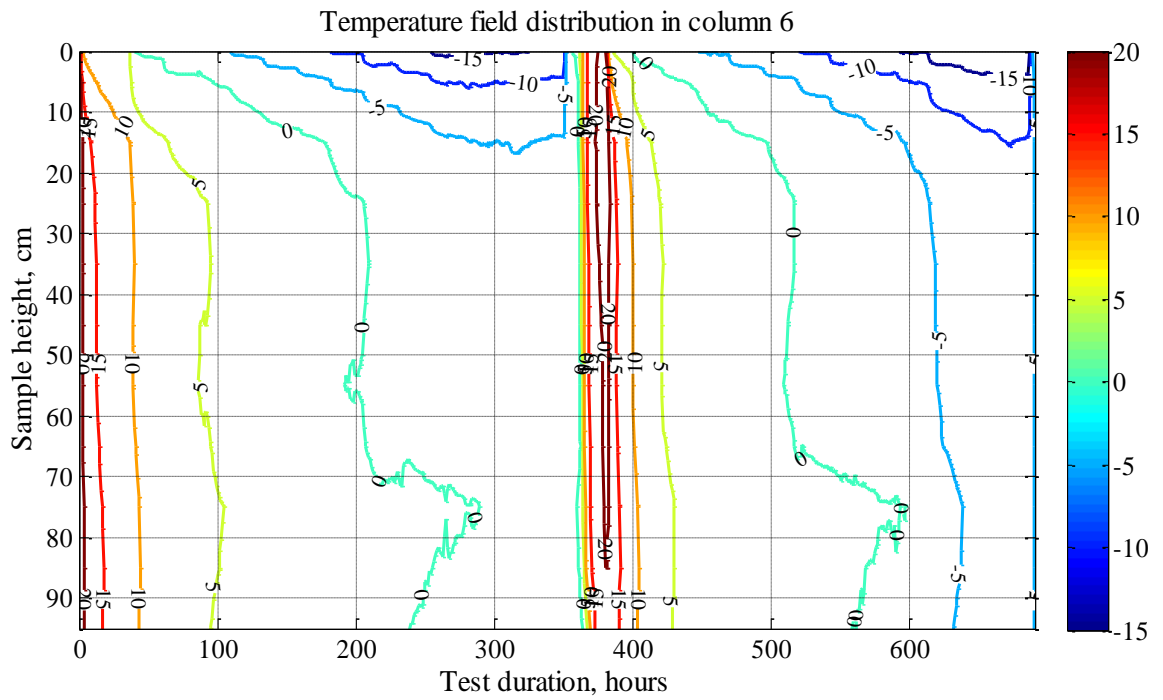
d)



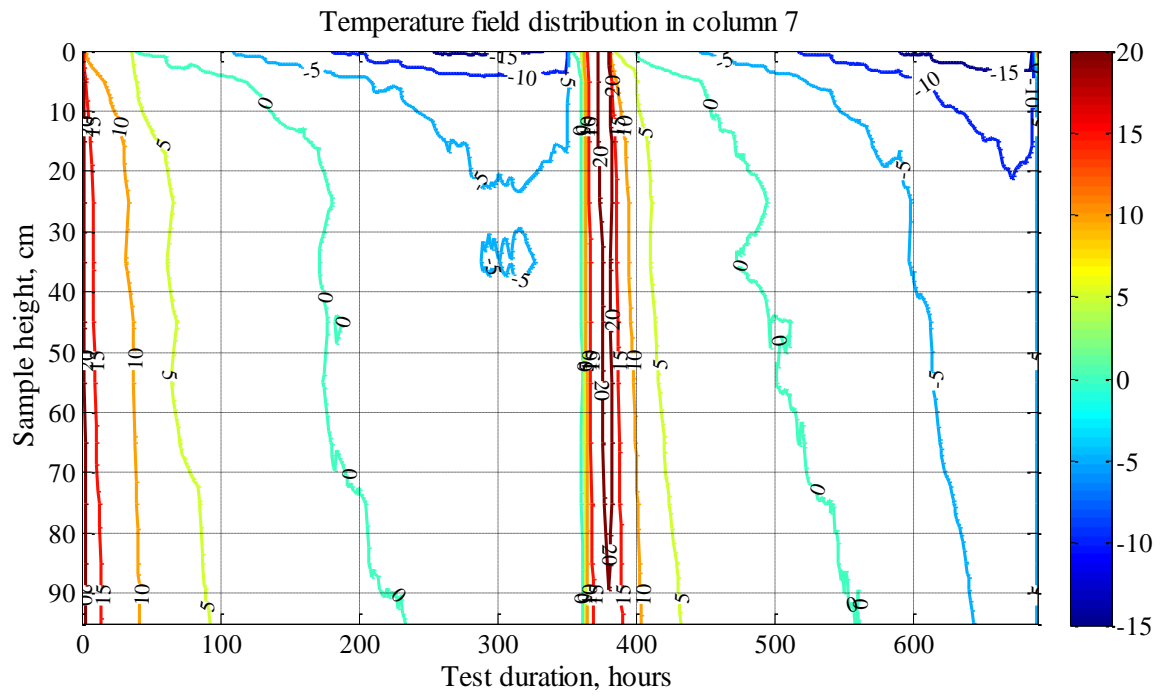
e)



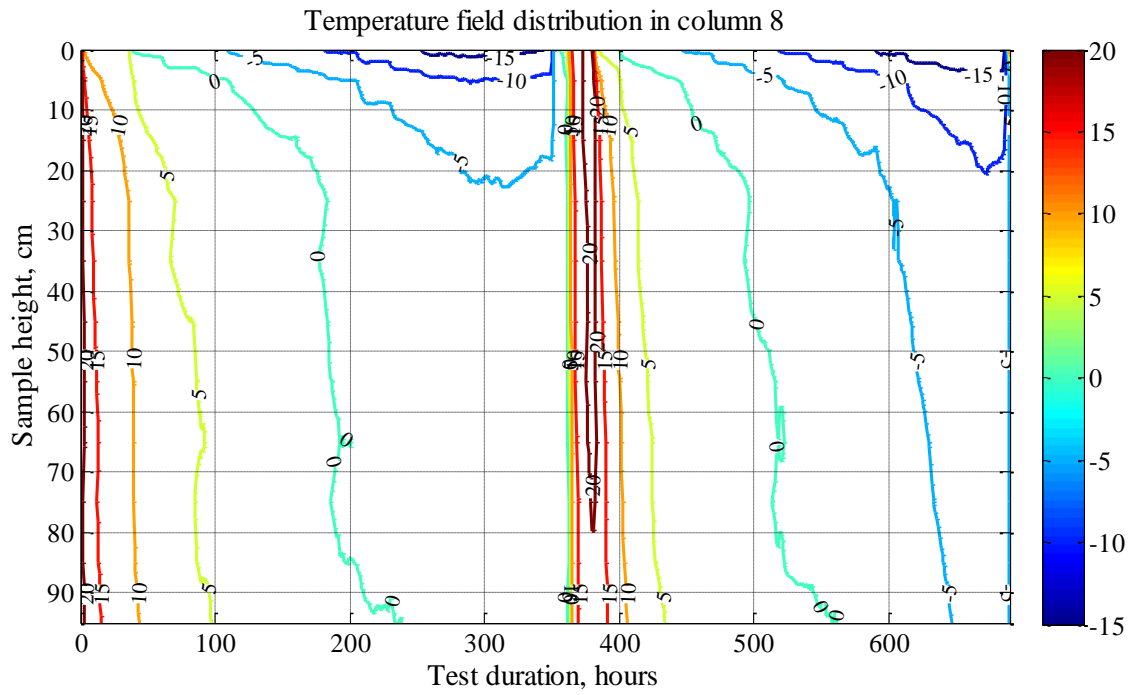
f)



g)



h)





i)

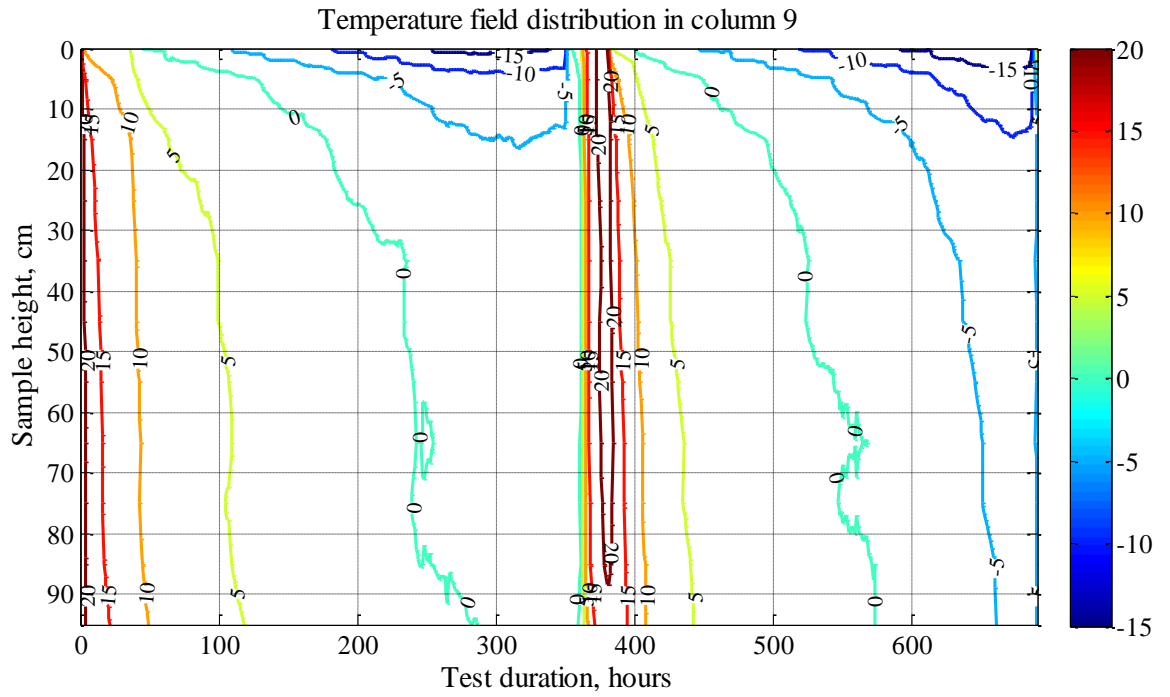
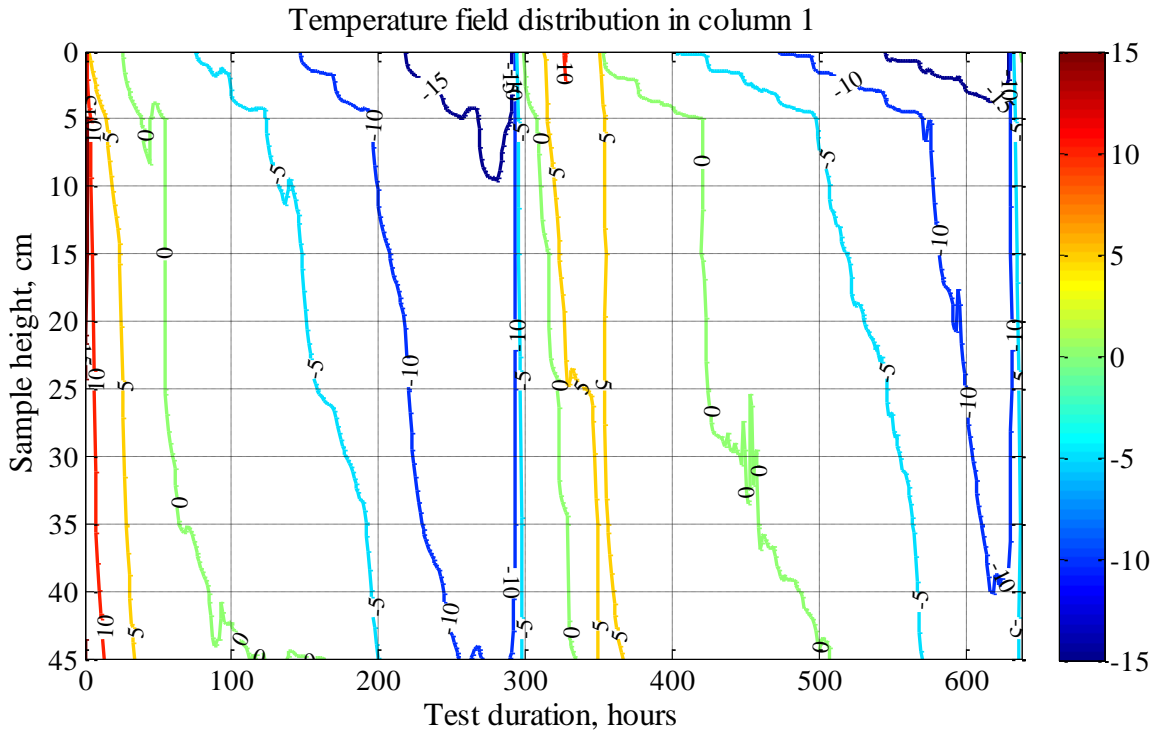


Figure B.2 a-i – Temperature field distribution in columns #1-#9 within 2 freeze-thaw cycles in Test 2.

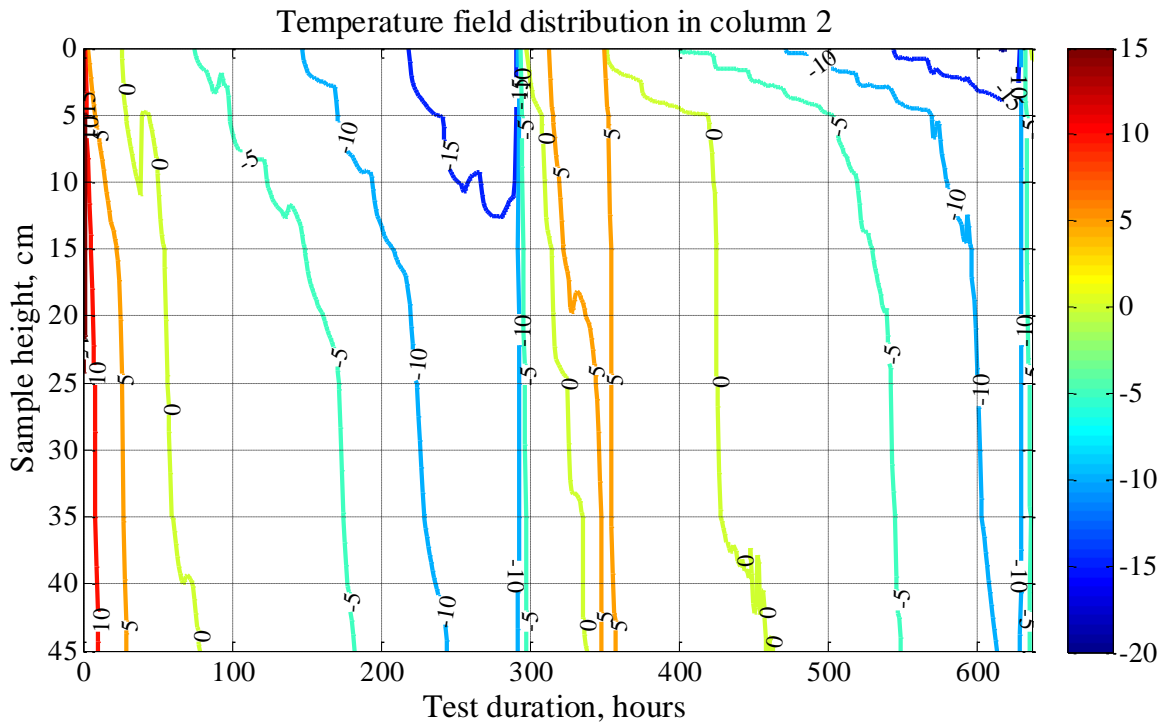
### Temperature field distribution in Test 3

Samples with varied dry density and deionised water supply from the base. The length of the soil sample 50 cm.

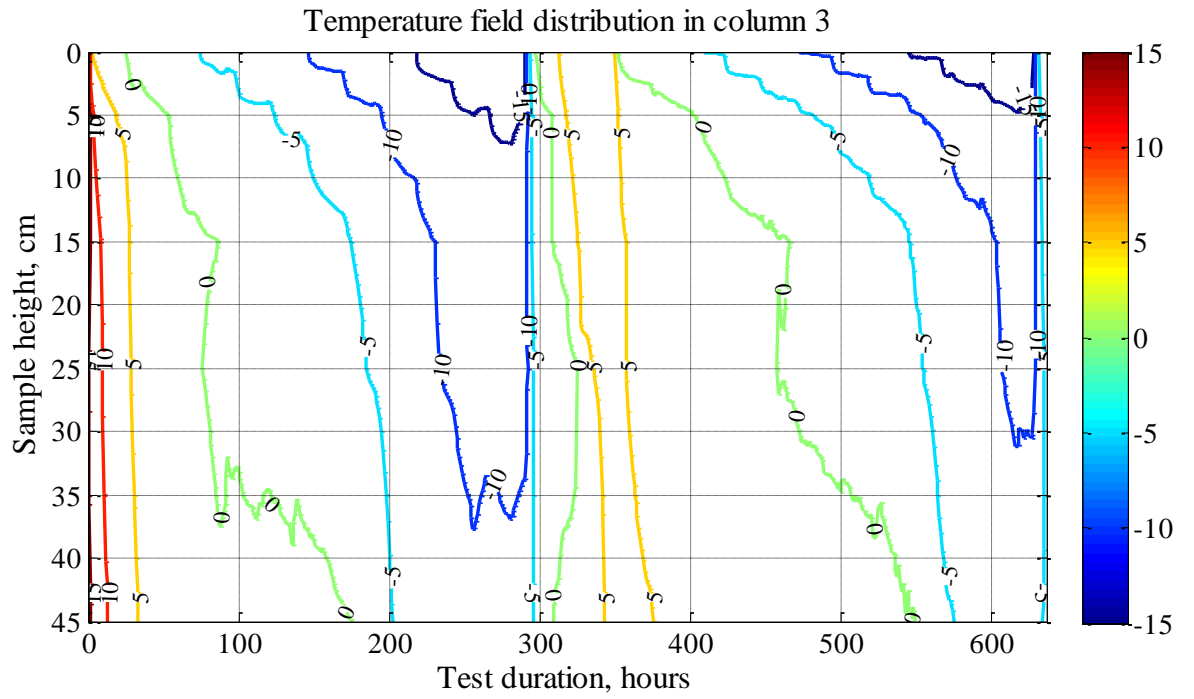
a)



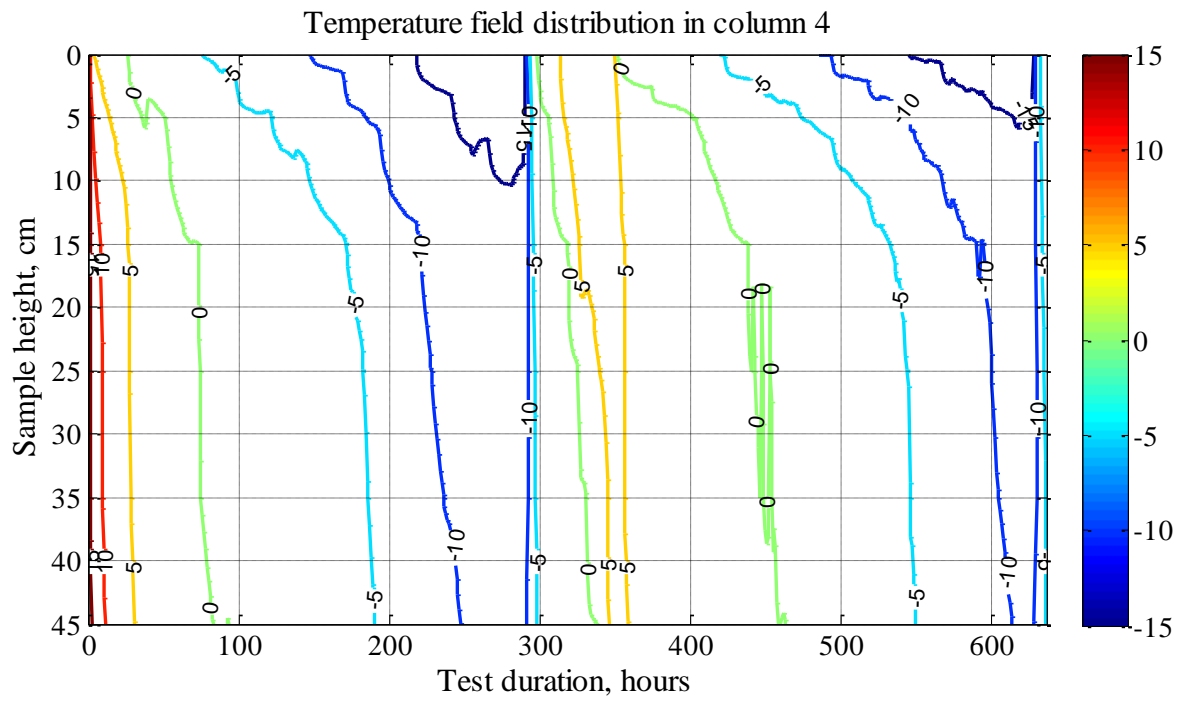
b)



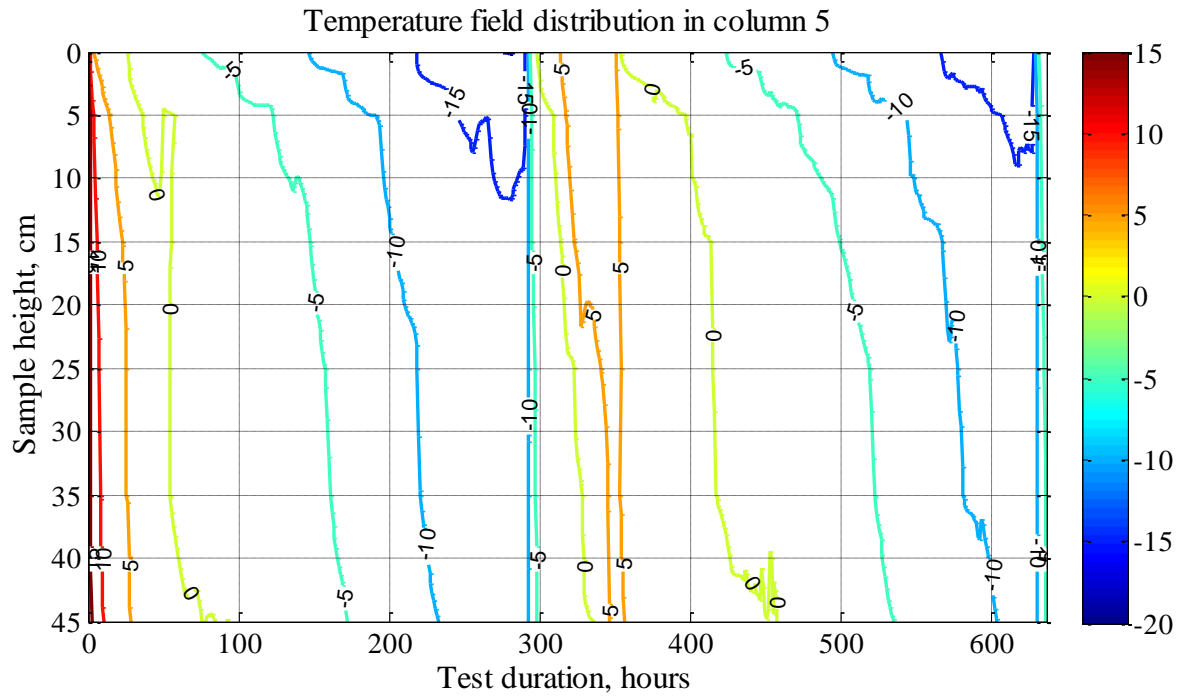
c)



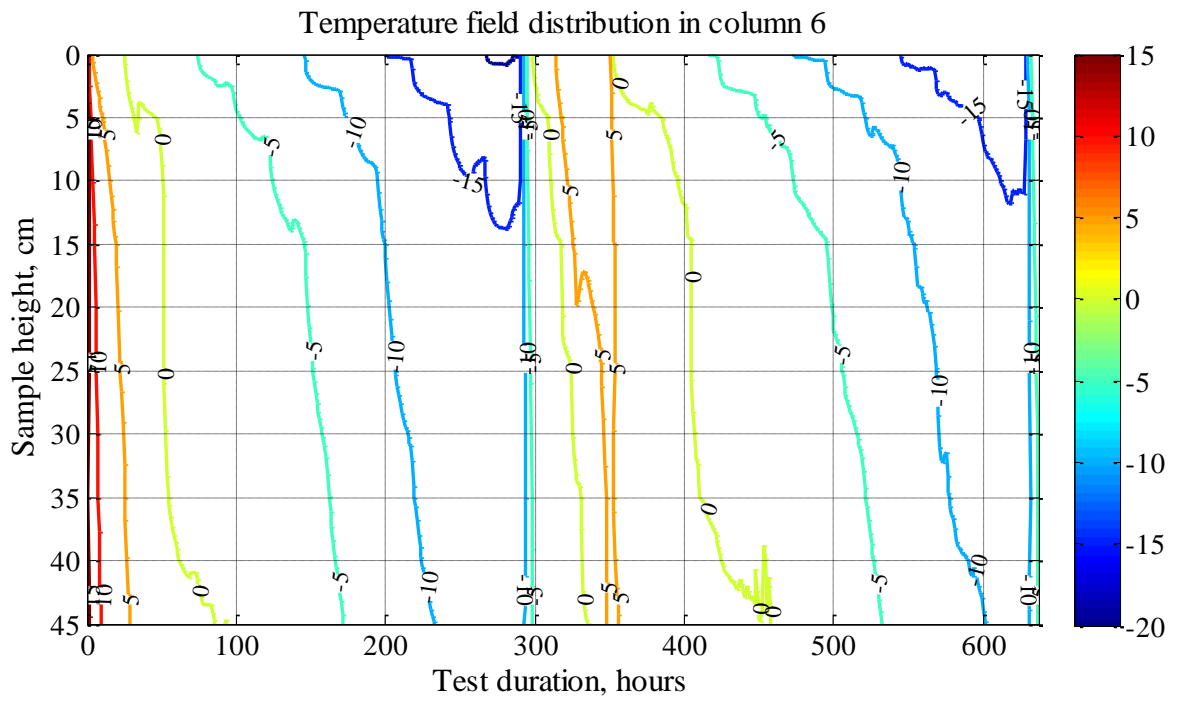
d)



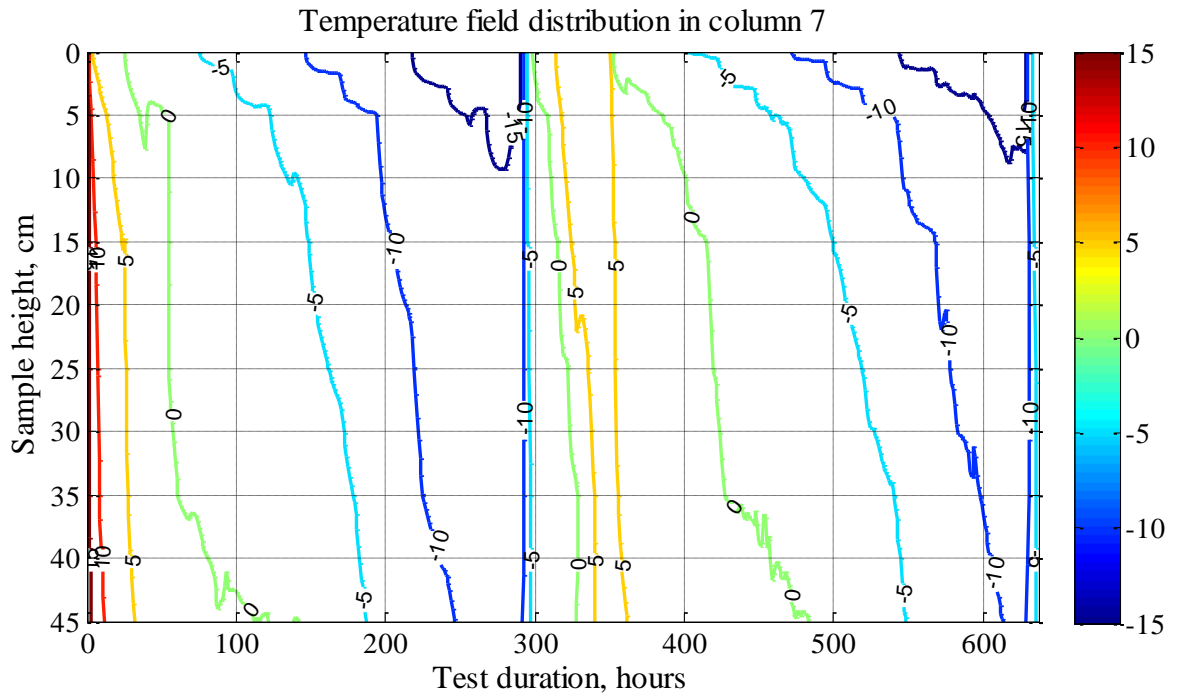
e)



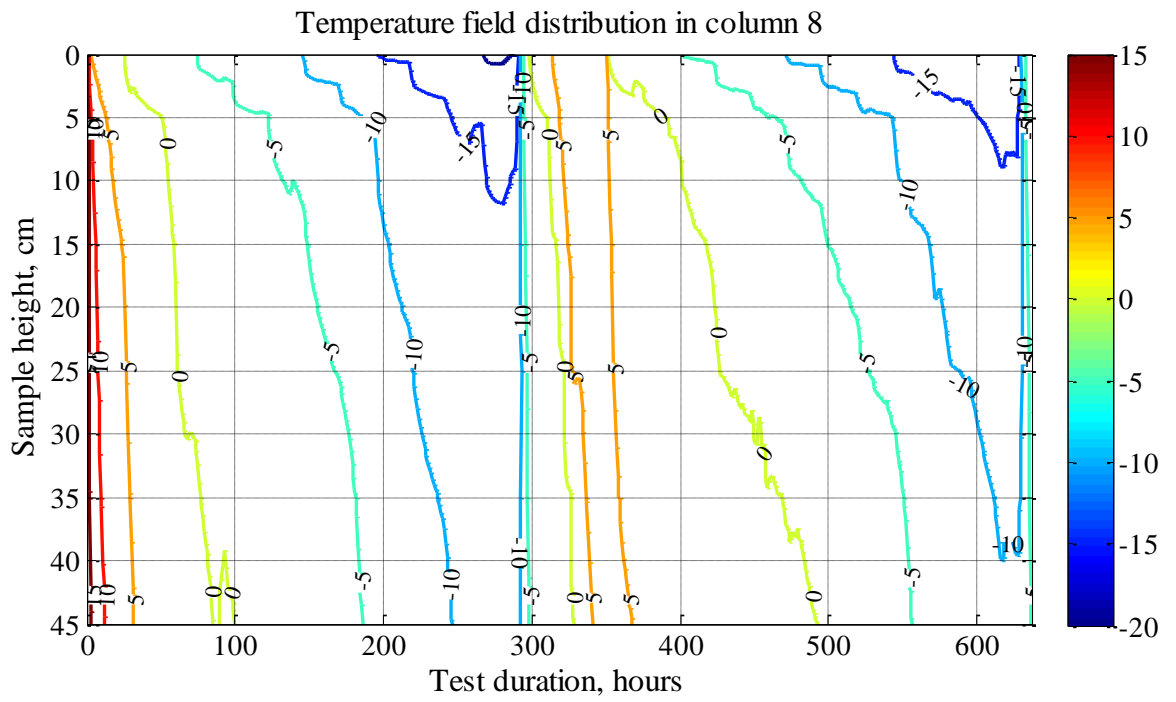
f)



g)



h)



i)

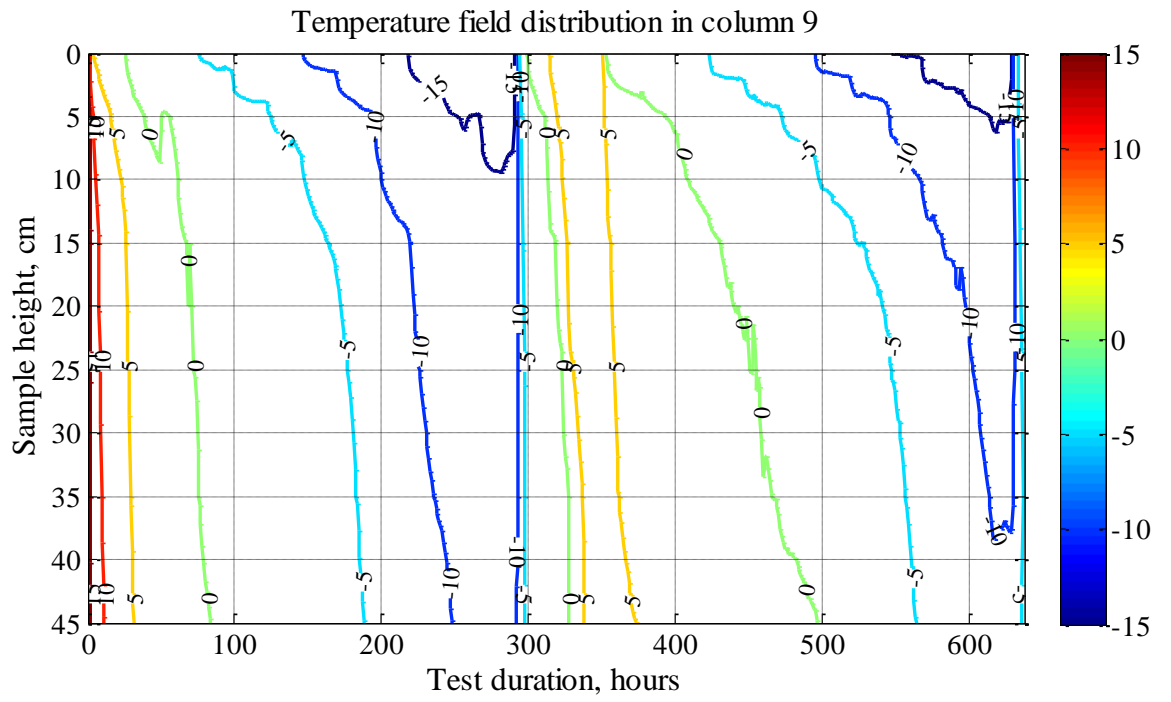
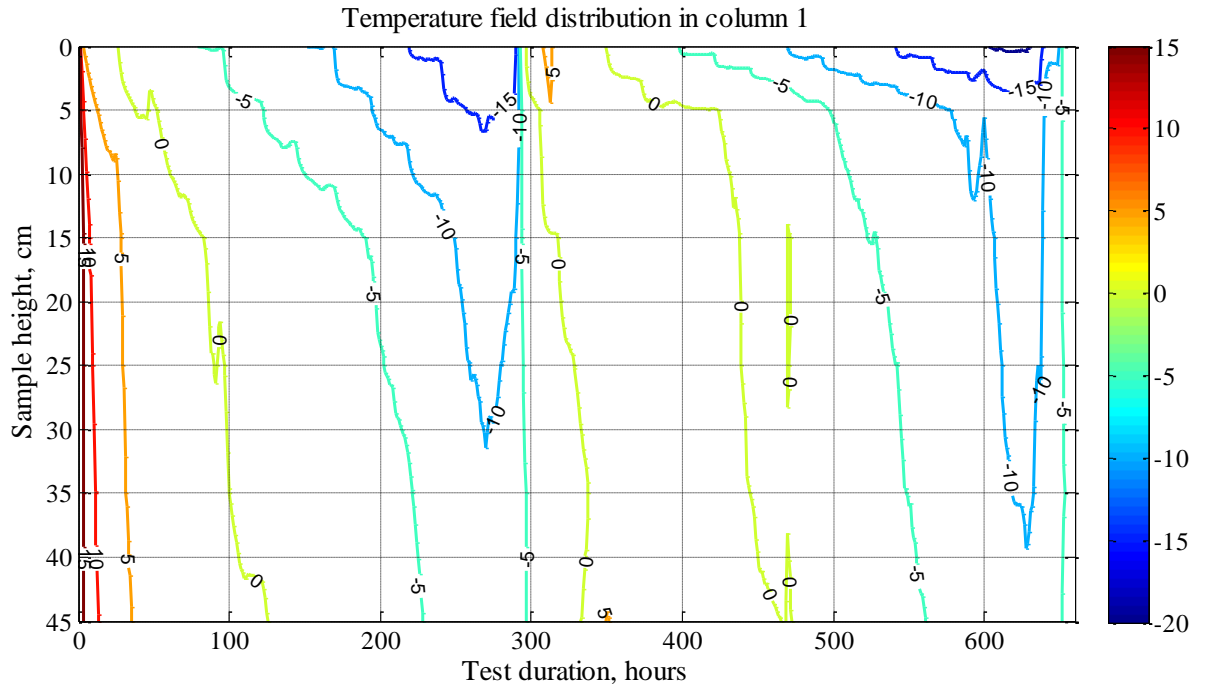


Figure B.3 a-i – Temperature field distribution in Test 3 in soil columns #1-#9 within two freeze-thaw cycles

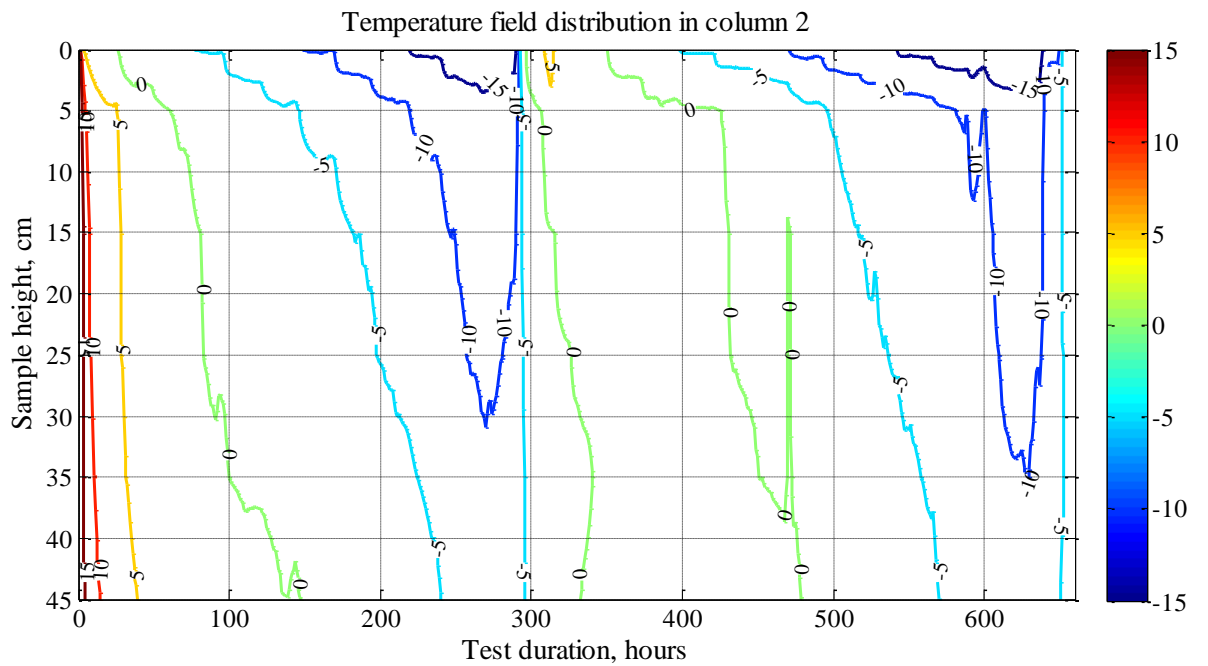
## Temperature field distribution in Test 4

Samples were compacted with varied dry density and 11,000 mg/litre sodium chloride solution supply from the base. The length of the soil samples 50 cm.

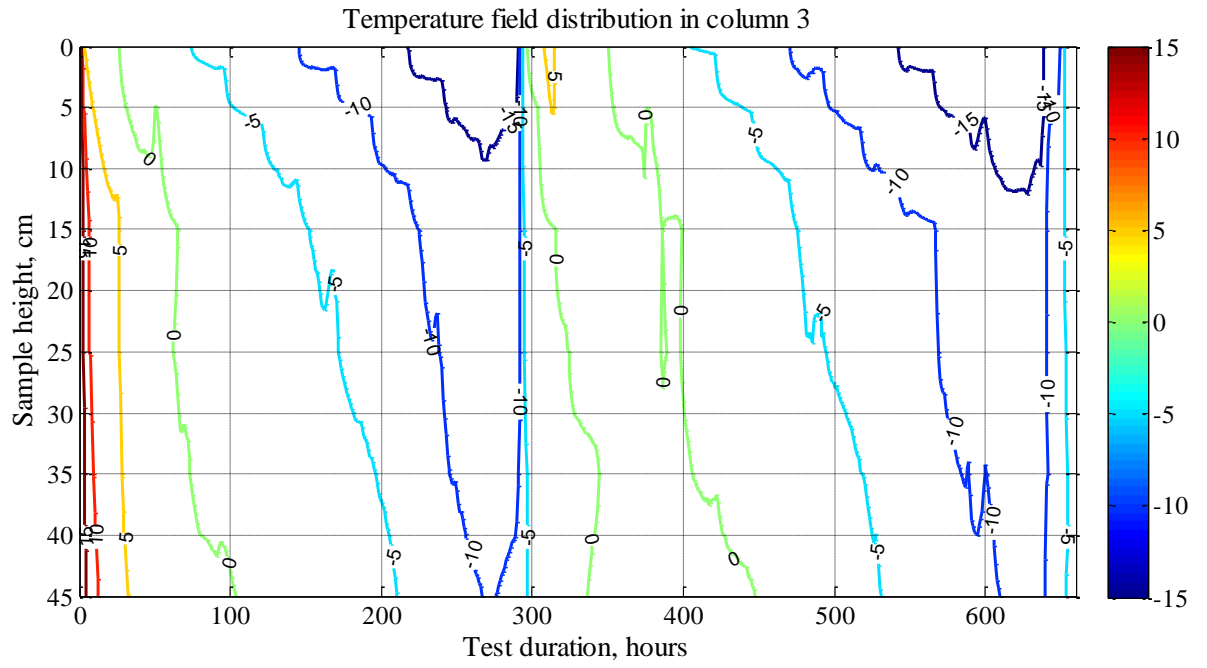
a)



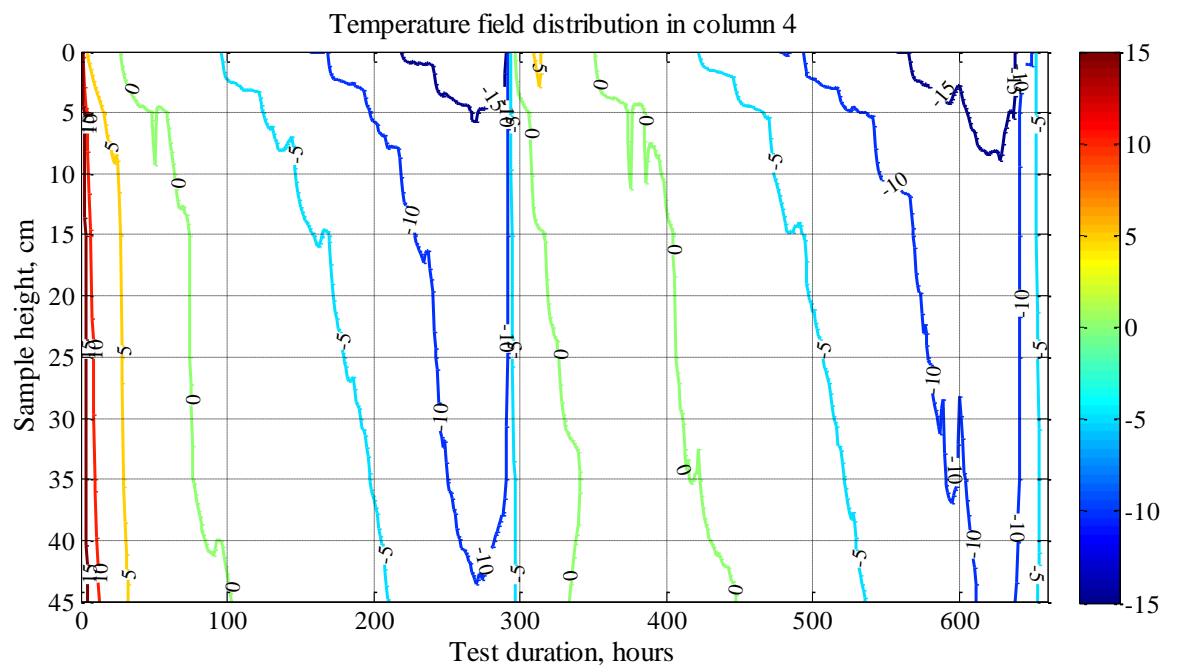
b)



c)

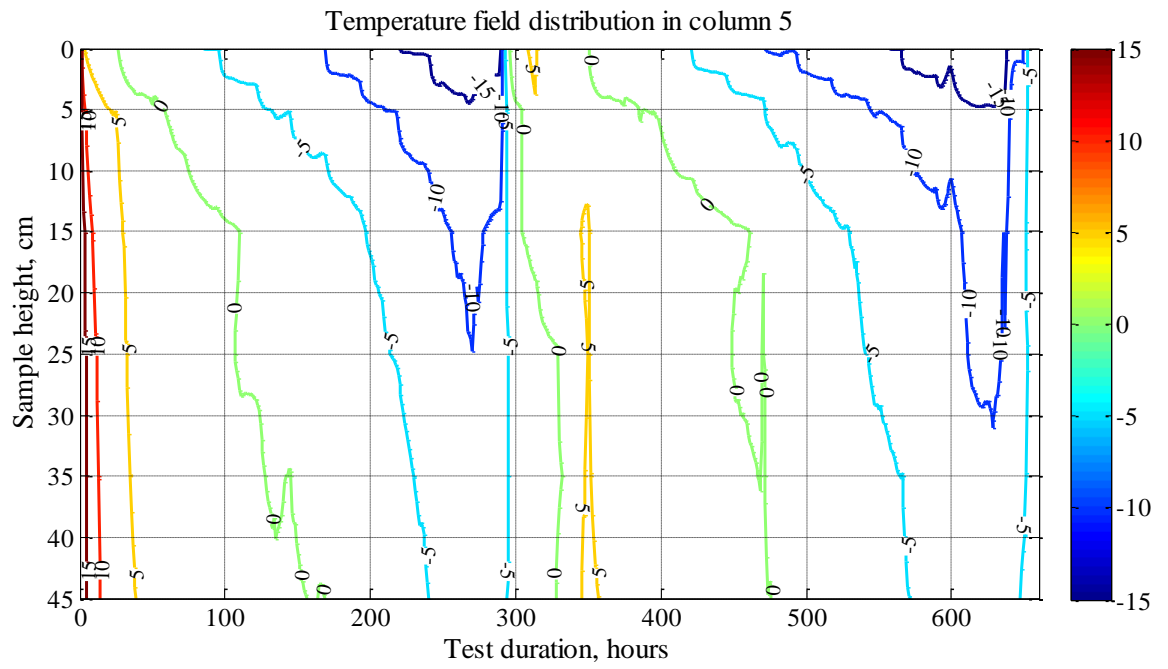


d)

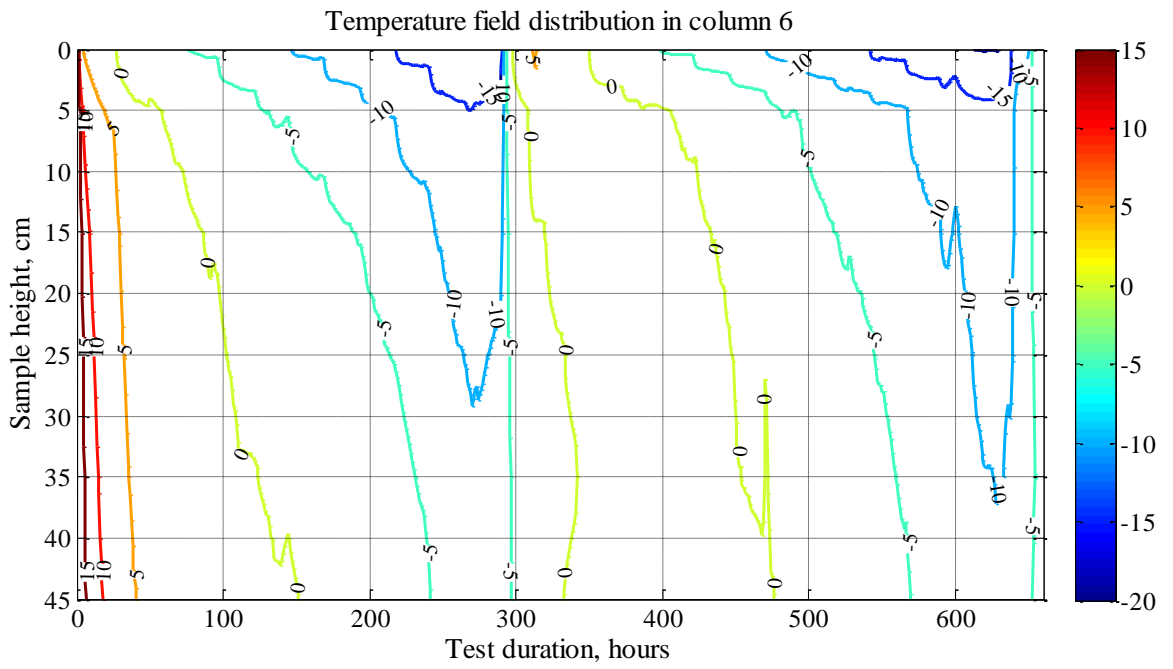




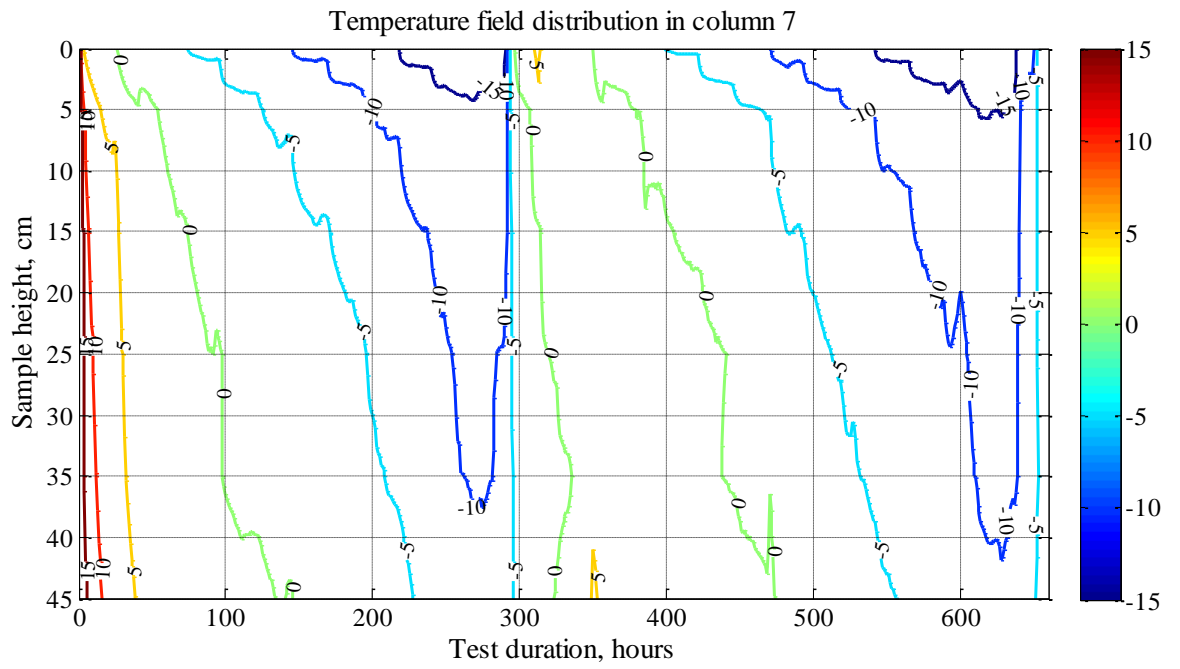
e)



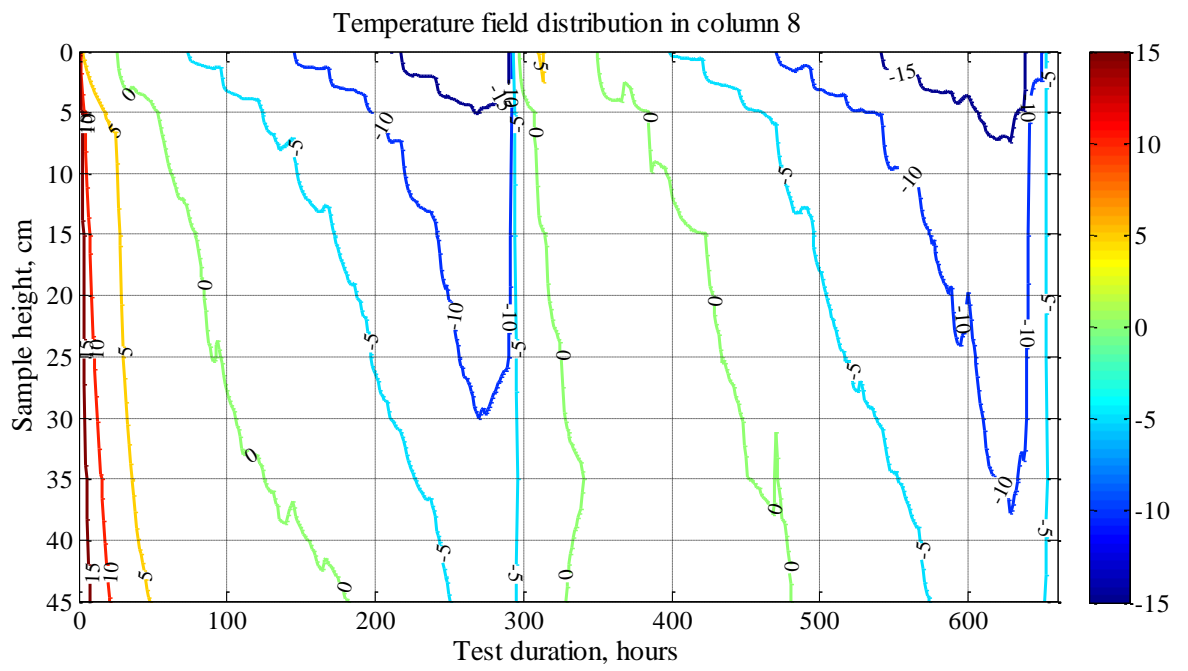
f)



g)



h)



i)

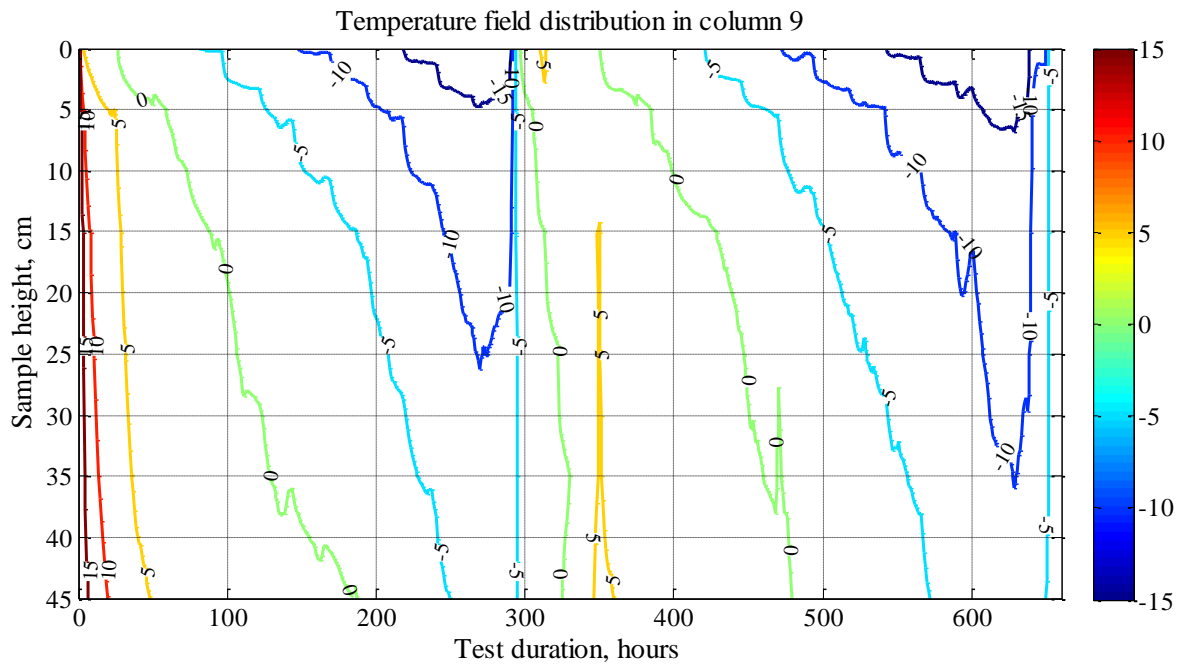
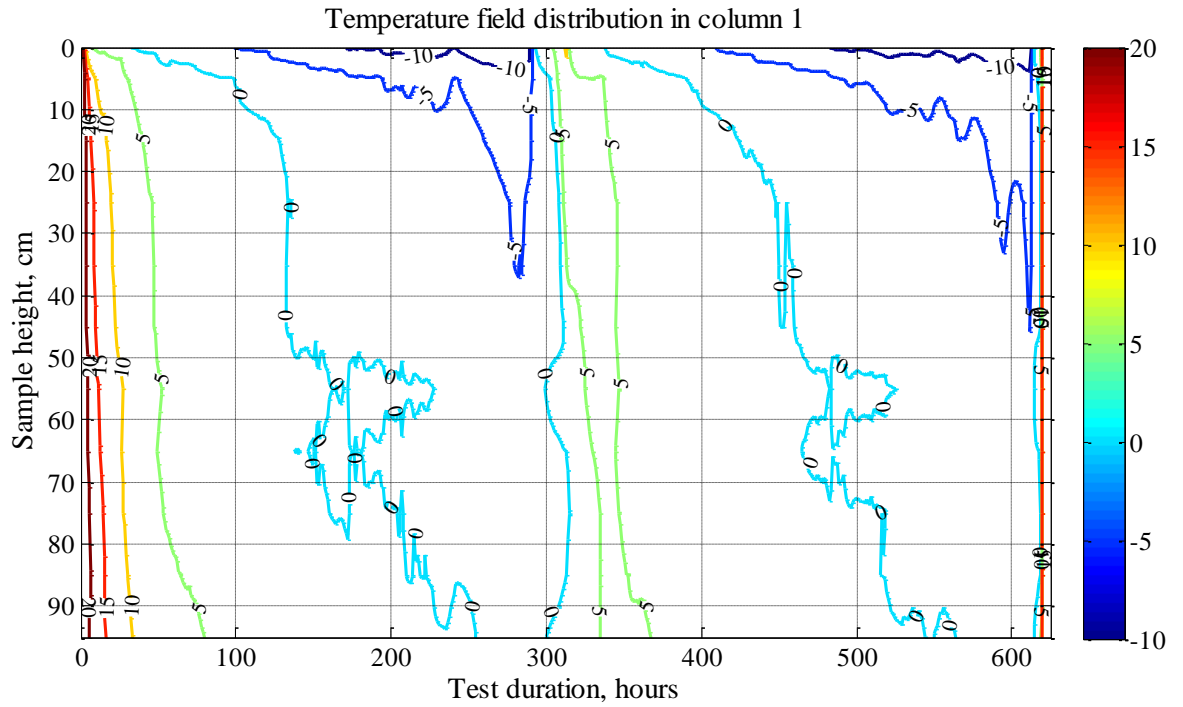


Figure B.4 a-i – Temperature field distribution in Test 4 in soil columns #1-#9 within two freeze-thaw cycles.

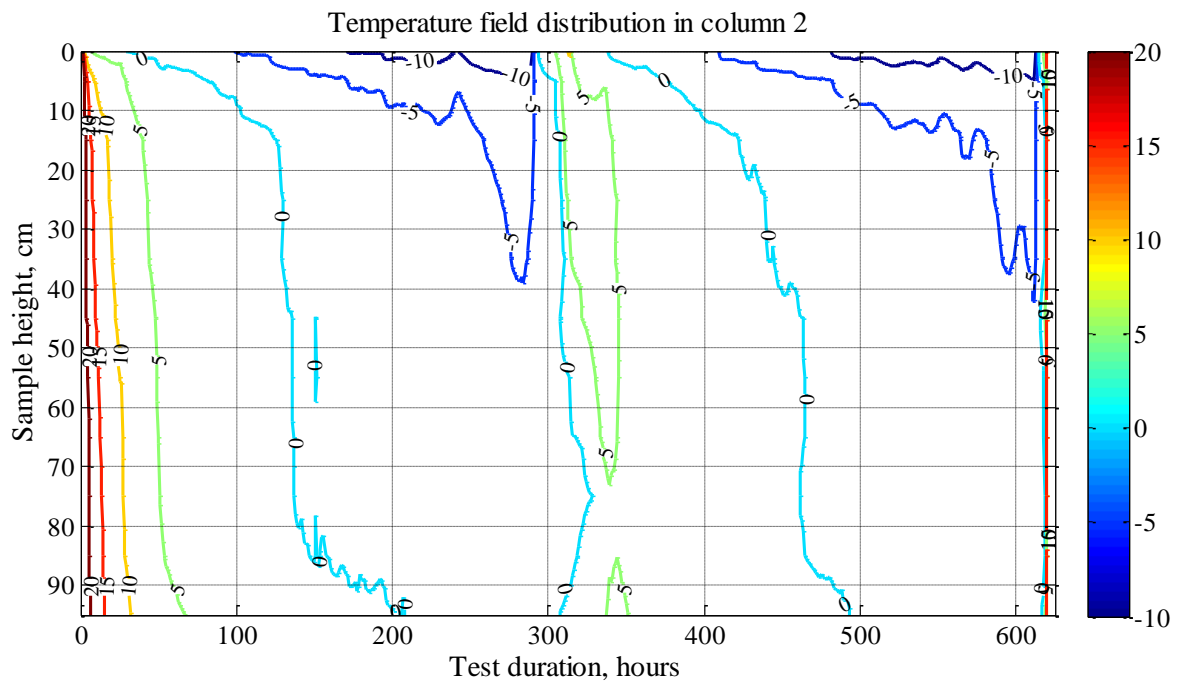
## Temperature field distribution in Test 5

Samples with varied dry density and 22,000 mg/litre sodium chloride solution supply from the base. The length of the soil samples 100 cm.

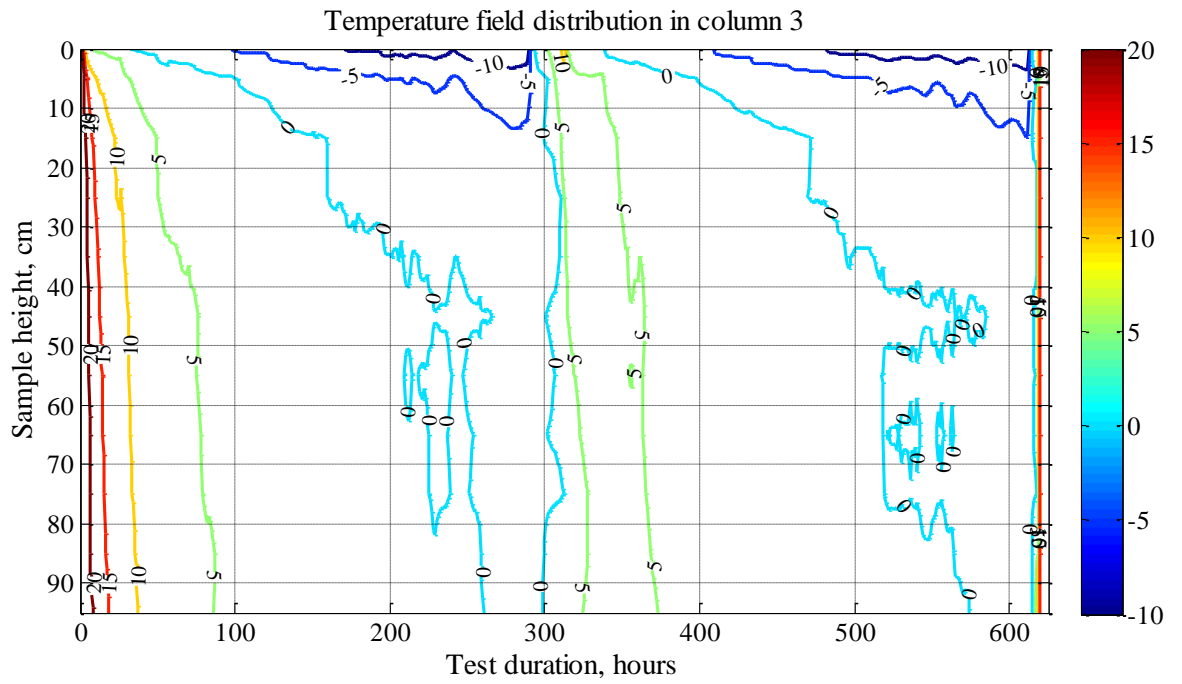
a)



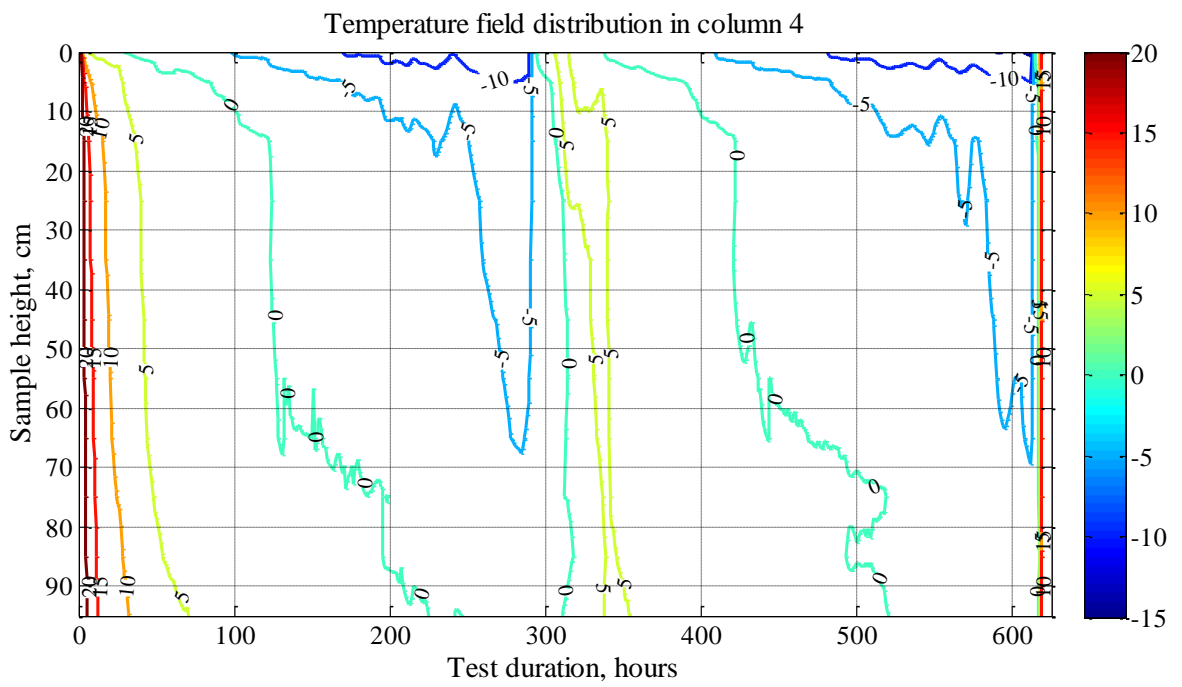
b)



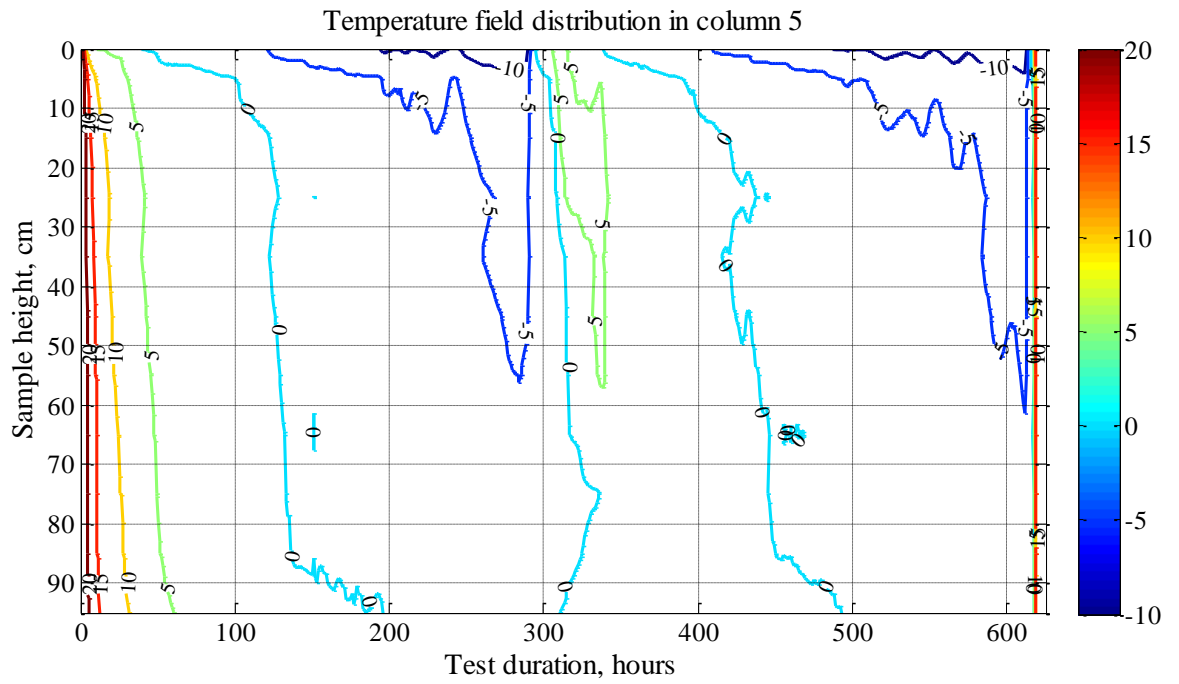
c)



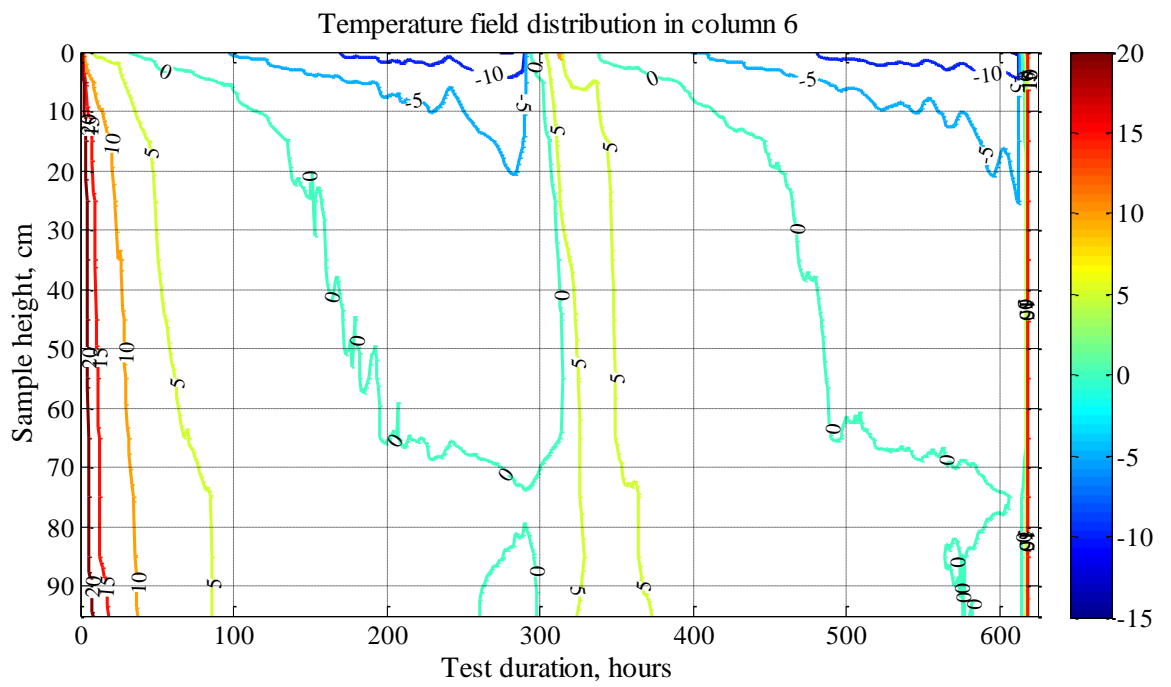
d)



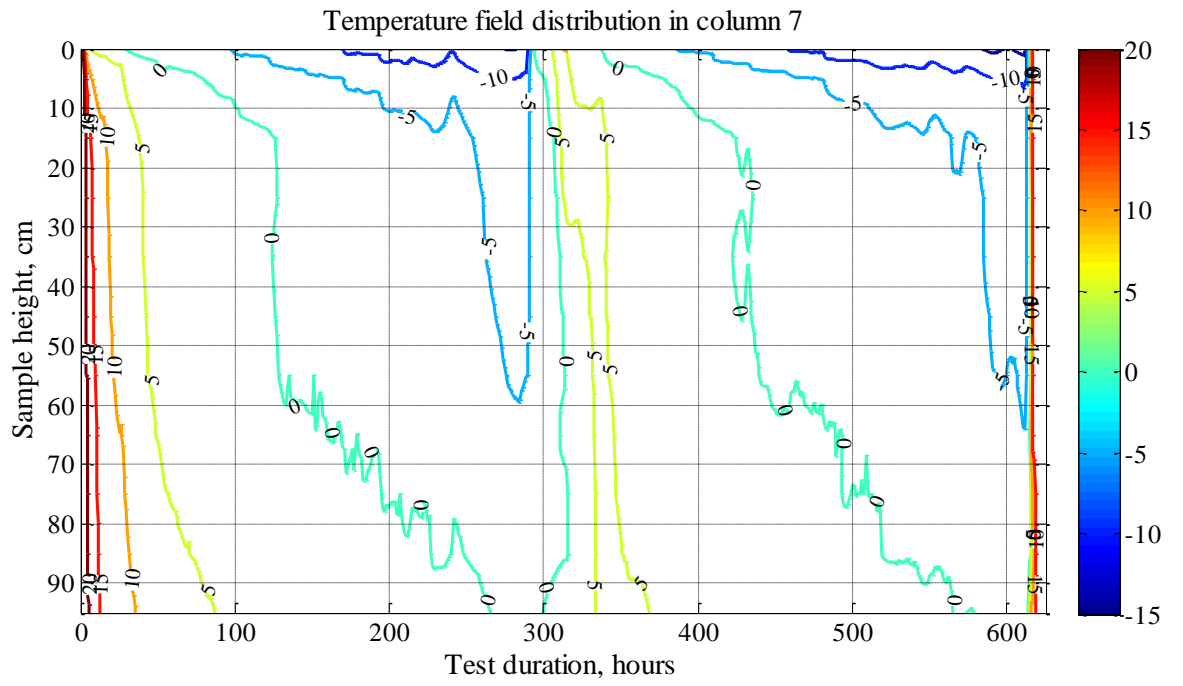
e)



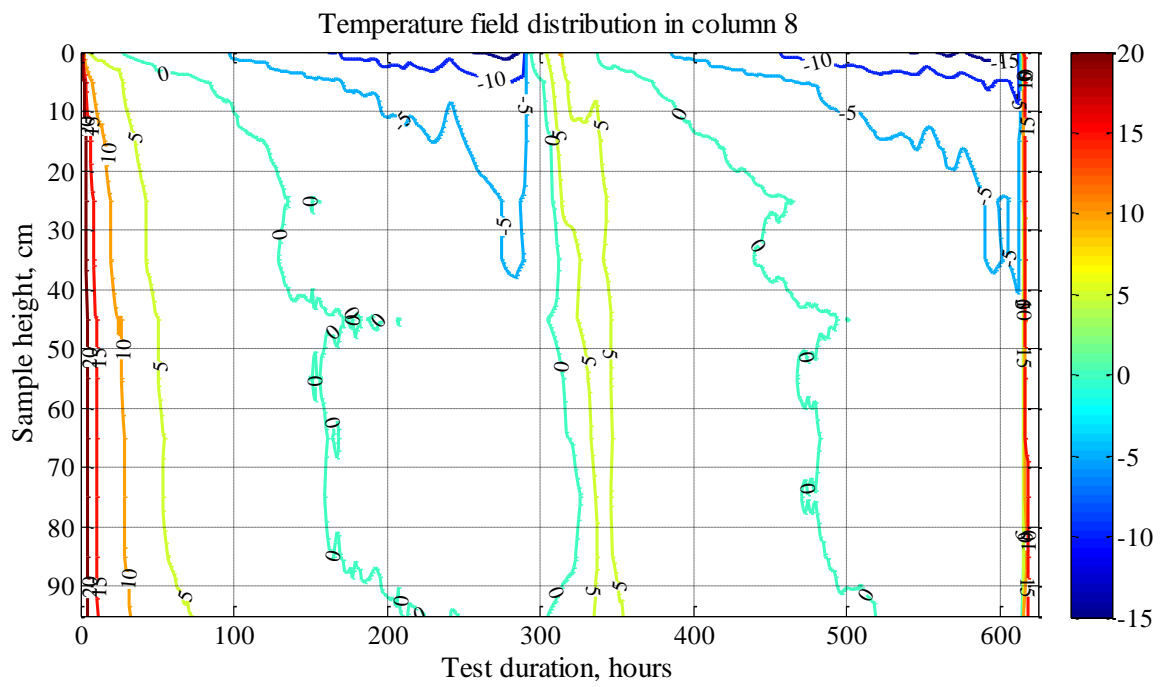
f)



g)



h)



i)

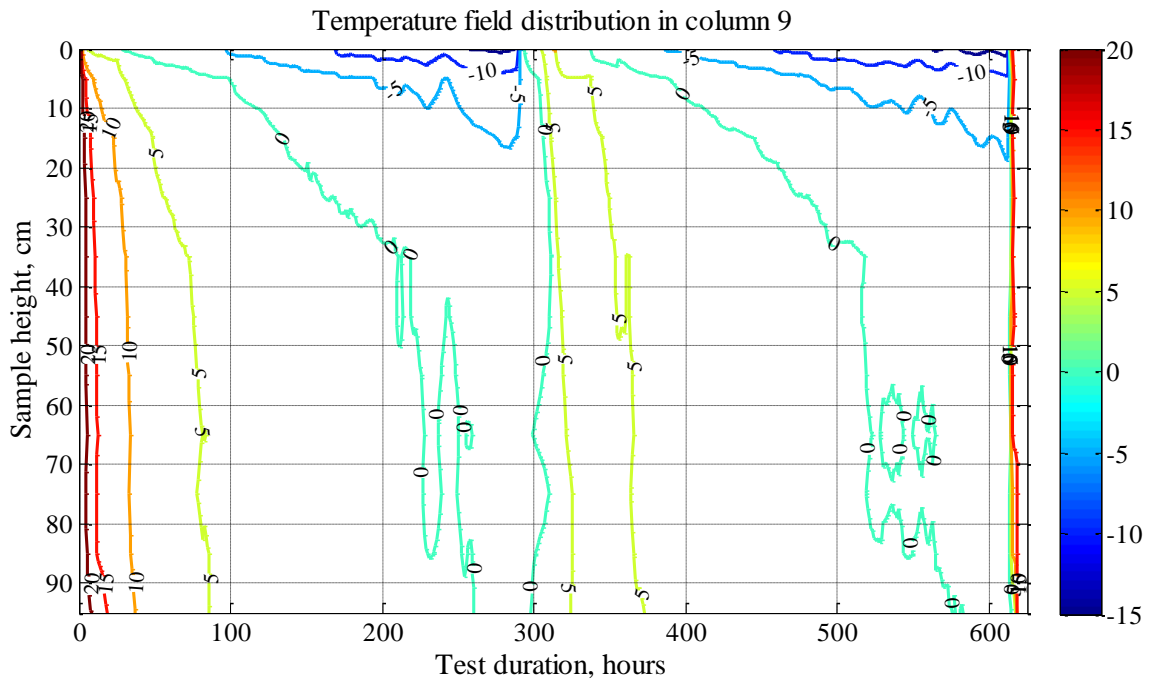


Figure B.5 a-i – Temperature field distribution in Test 5 in soil columns #1-#9 within two freeze-thaw cycles



## Appendix C

### Electrical conductivity measurements for chemical content determination

Table C.1 – Electrical conductivity readings after two freeze-thaw cycles in Test 2,  $\mu\text{S}$

Sample length, 10cm	Electrical conductivity, $\mu\text{S}$									Average for 9 columns
	#1	#2	#3	#4	#5	#6	#7	#8	#9	
0.1					0.29	0.22	0.26	0.21	0.22	0.24
0.9					0.33	0.21	0.22	0.36	0.31	0.29
1.9		0.28	0.3	0.32	0.34	0.31	0.21	0.09	0.3	0.27
2.9	0.3	0.33	0.3	0.33	0.34	0.26	0.3	0.1	0.33	0.29
3.9	0.32	0.35	0.32	0.31	0.35	0.31	0.26	0.1	0.3	0.29
4.9	0.29	0.37	0.31	0.32	0.38	0.25	0.27	0.09	0.29	0.29
5.9	0.29	0.35	0.29	0.36	0.41	0.33	0.28	0.09	0.28	0.30
6.9	0.3	0.33	0.32	0.33	0.39	0.34	0.28	0.09	0.29	0.30
7.9	0.27	0.23	0.24	0.3	0.22	0.25	0.26	0.11	0.24	0.24
8.9	0.42	0.42	0.29	0.35	0.34	0.33	0.4	0.36	0.28	0.35
9.1	0.46	0.5	0.34	0.41	0.37	0.42	0.57	0.53	0.42	0.45
9.2	0.81	0.75	1.03	0.57	0.64	0.91	0.88	0.58	0.85	0.78
9.3	0.81	0.77	1.32	0.62	0.46	0.73	0.8	0.62	0.89	0.78
9.4	0.95	0.74	0.86	0.57	0.69	0.74	0.9	0.61	0.84	0.77
9.5	0.89	0.85	1.08	0.66	0.51	0.84	0.93	0.62	0.94	0.81
9.6	0.88	0.87	0.99	0.79	0.72	0.91	1.04	0.8	0.99	0.89
9.7	1.02	0.77	1.1	0.85	0.86	0.87	1.14	0.92	1.25	0.98
9.8	1.05	0.9	1.02	0.9	0.82	1.01	1.19	0.9	1.31	1.01
9.9	1.07	0.95	1.01	0.89	0.76	1.04	0.9	0.98	1.24	0.98
10	1.13	1.14	1.05	0.99	0.99	1.2	1.13	1.06	1.59	1.14

Table C.2 - Electrical conductivity readings after to freeze-thaw cycles in Test 4,  $\mu\text{S}$

Sample length, cm	Electrical conductivity, $\mu\text{S}$									Average for 9 columns
	#1	#2	#3	#4	#5	#6	#7	#8	#9	
1	0.21	0.19	0.17	0.21	0.16	0.38	0.2	0.22	0.17	0.21
5	0.12	0.13	0.12	0.1	0.11	0.21	0.13	0.13	0.11	0.13
9	0.17	0.13	0.15	0.15	0.15	0.28	0.19	0.19	0.16	0.17
19	0.23	0.2	0.14	0.15	0.17	0.4	0.2	0.23	0.14	0.21
29	1.43	0.61	0.82	1.3	0.95	1.24	0.3	0.21	0.17	0.78
39	1.28	1.71	1.95	2.4	2.41	1.9	1.45	1.4	0.43	1.66
45	1.79	1.47	1.48	1.58	1.16	1.6	1.55	1.43	0.89	1.44
50	1.24	2.13	2.51	3.3	1.84	3.51	2.56	1.86	1.66	2.29

Table C.3 – Electrical conductivity readings after two freeze-thaw cycles in Test 5,  $\mu\text{S}$

Sample length, 10cm	Electrical conductivity, $\mu\text{S}$									Average for 9 columns
	#1	#2	#3	#4	#5	#6	#7	#8	#9	
0.1	0.2	0.17	0.39	0.28	0.2	0.09	0.28	0.29	0.23	0.24
0.5	0.18	0.18	0.29	0.21	0.19	0.09	0.22	0.29	0.23	0.21
0.9	0.23	0.25	0.25	0.23	0.20	0.09	0.22	0.19	0.22	0.21
1.9	0.17	0.25	0.31	0.15	0.14	0.15	0.22	0.26	0.21	0.21
2.9	0.17	0.19	0.18	0.14	0.12	0.13	0.30	0.20	0.19	0.18
3.9	0.19	0.19	0.16	0.15	0.17	0.09	0.25	0.26	0.2	0.18
4.9	0.21	0.18	0.18	0.23	0.15	0.08	0.22	0.21	0.21	0.19
5.9	0.36	0.17	0.16	0.24	0.13	0.08	0.25	0.2	0.21	0.20
6.9	0.34	0.35	0.37	0.24	0.33	0.13	0.22	0.21	0.2	0.27
7.9	0.89	1.07	0.93	1.25	1.78	0.43	0.3	0.24	0.14	0.78
8.9	1.70	1.42	3.09	2.82	1.95	1.25	0.78	0.67	0.31	1.55
9.0	2.71	2.98	1.59	2.30	2.29	2.10	1.77	1.08	0.38	1.91
9.5	3.07	3.15	1.90	1.59	2.78	2.72	1.89	1.45	0.95	2.17
10.0	1.82	3.41	2.70	2.01	2.83	2.74	3.7	2.21	1.89	2.59

Table C.4 – Chemical content after freeze-thaw cycles in % to oven dried soil weight in Test 5

Sample length, 10cm	Chemical content ratio to oven dried soil weight, %									Average for 9 columns
	#1	#2	#3	#4	#5	#6	#7	#8	#9	
0.1	0.06	0.05	0.15	0.10	0.06	0.01	0.10	0.10	0.07	0.08
0.5	0.05	0.05	0.10	0.06	0.05	0.01	0.07	0.10	0.07	0.06
0.9	0.07	0.08	0.08	0.07	0.06	0.01	0.07	0.05	0.07	0.06
1.9	0.05	0.08	0.11	0.04	0.03	0.04	0.07	0.09	0.06	0.06
2.9	0.05	0.05	0.05	0.03	0.02	0.03	0.11	0.06	0.05	0.05
3.9	0.05	0.05	0.04	0.04	0.05	0.01	0.08	0.09	0.06	0.05
4.9	0.06	0.05	0.05	0.07	0.04	0.00	0.07	0.06	0.06	0.05
5.9	0.14	0.05	0.04	0.08	0.03	0.00	0.08	0.06	0.06	0.06
6.9	0.13	0.13	0.14	0.08	0.12	0.03	0.07	0.06	0.06	0.09
7.9	0.39	0.48	0.41	0.57	0.83	0.17	0.11	0.08	0.03	0.34
8.9	0.79	0.65	1.46	1.33	0.91	0.57	0.34	0.29	0.11	1.55
9.0	1.28	1.41	0.74	1.08	1.08	0.98	0.82	0.49	0.15	1.91
9.5	1.45	1.49	0.89	0.74	1.31	1.28	0.88	0.67	0.42	2.17
10.0	0.85	1.62	1.27	0.94	1.34	1.29	1.76	1.04	0.88	2.59

## Appendix D

### Direct Shear Test Results

A direct shear test was conducted, according to BS 1377-7:1990, with 60x60mm sample preliminary consolidated with 5, 10 and 15kg load, which corresponds to 136, 272 and 409kN/m<sup>2</sup> pressure on the sample. The beam ratio was 1:10. A machine displacement speed of 0.5mm/min was applied, which is less than the recommended maximum displacement rate by BS 1377-7:1990. The minimum time to failure  $t_f$  was found by the equation:

$$t_f = 12.7 \cdot t_{100} = 12.7 \cdot 2.05 = 26.04 \text{ min} \quad (3.1)$$

where,  $t_{100}$  – is the final point on primary consolidation by square-root time plot in mm.  $t_{100} = 2.05 \text{ mm}$  (Appendix D, Figure D.2).

The likely horizontal shear formation was taken as 15min. The maximum displacement rate was found by the formula:  $\frac{t_f}{t_{horiz}} = \frac{15 \text{ mm}}{26.04 \text{ min}} = 0.57 \text{ mm/min}$ .

The maximum obtained shear stress  $\tau$  was found for all loading sets by the equation:

$$\tau = \frac{C_R \cdot R}{L^2} \cdot 1000 \text{ kPa} \quad (3.2)$$

where,  $L$  – length of the side of the shear box, 60mm here and the continual change in the area of contact is not formally taken into account (BS 1377-7:1990);

$C_R$  – the load ring calibration  $C_R = 2162.5 \text{ N}$  per 1mm of division on the loading ring dial gauge;

$R$  – reading of the loading ring in mm.

The normal stress  $\sigma_n$  corresponding to the maximum value of shear stress was found by the formula:

$$\sigma_n = \frac{9.81 \cdot W}{L^2} \cdot 1000 \text{ kN/m}^2 \quad (3.3)$$

where,  $W$  – total load applied to the specimen in kg.

According to consolidated drained direct shear test for the sample with moisture content  $W=17.2\%$  and dry density  $\rho_{dry} = 1.80 \text{ Mg/m}^3$ , the angle of internal friction obtained was  $\varphi = 24^\circ$  and the cohesion  $C = 10 \text{ kN/m}^2$  (Figure 3.8). Initial bulk density of

the specimen  $\rho = 2.11 \text{ Mg/m}^3$ , void ratio  $e_0 = 0.45$  and the degree of saturation  $S_0 = 99.4\%$ .

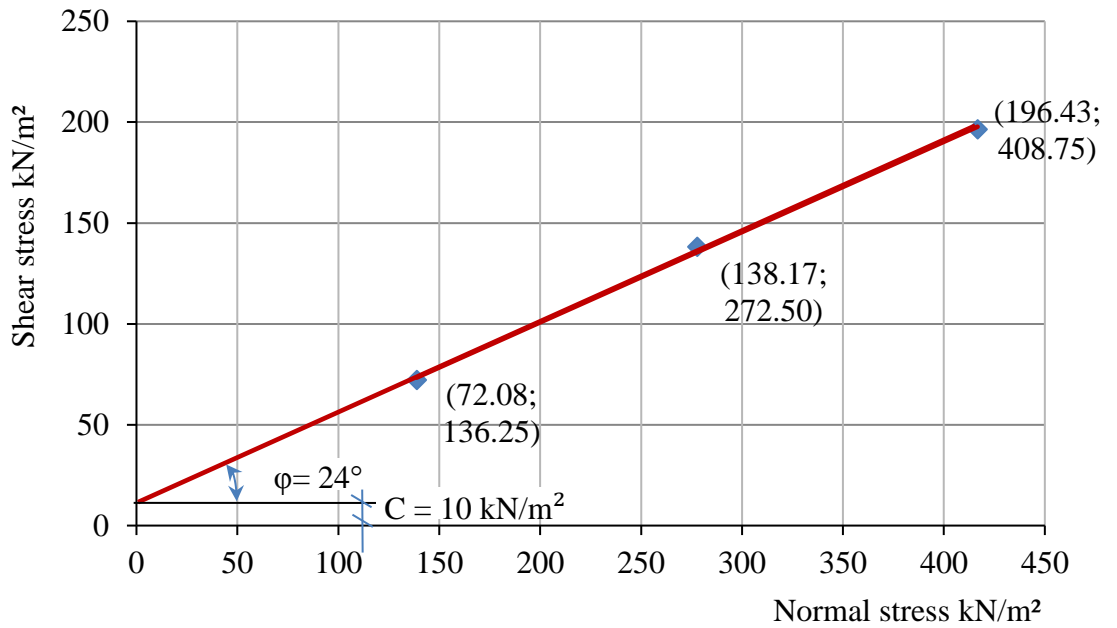


Figure D.1 – Direct shear results for 17.2% sandy clay soils with particle size less than 2mm

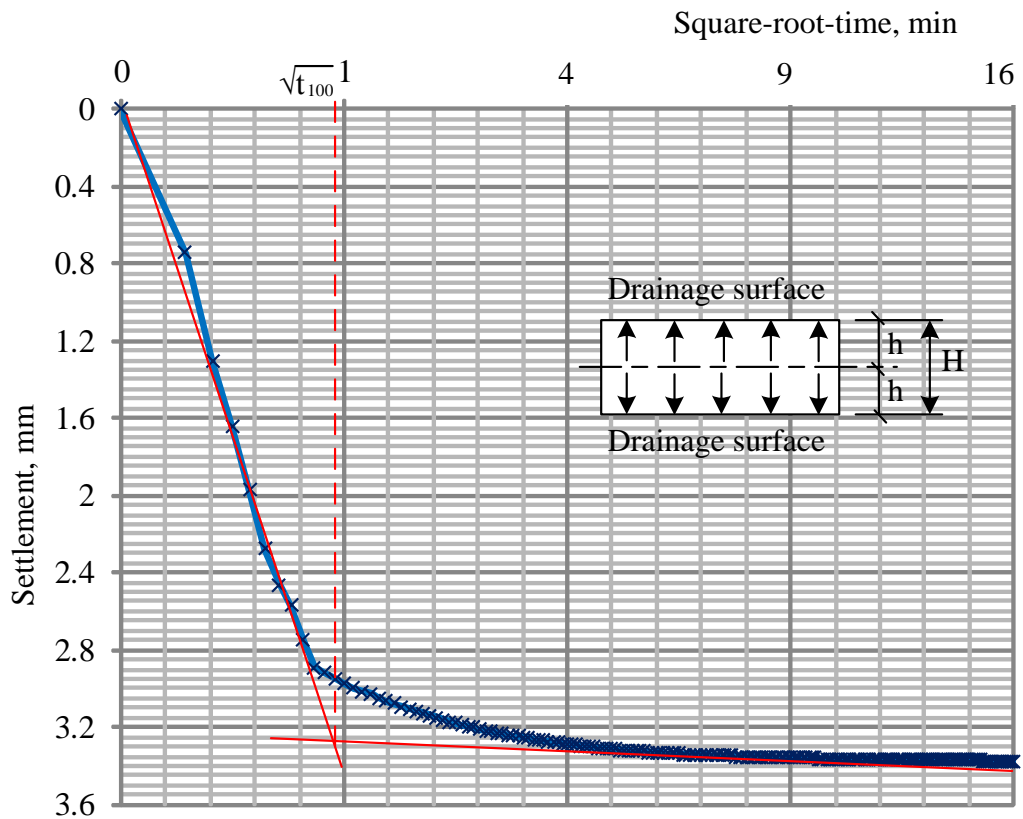


Figure D.2 – Determination of time of failure from consolidation curve in direct shear test

Drained shear test on sandy clay soils was carried out under the selection of normal pressure: 136, 272 and 408 kN/m<sup>2</sup>.

If  $\sqrt{t_{100}} = 0.98$  min, then  $t_{100} = 1$  min.

The coefficient of consolidation can be calculated by empirical formula:

$$c_v = \frac{0.103H^2}{t_{100}} = \frac{0.103 \cdot 20}{1} = 2.06 \text{ m}^2/\text{year}$$

where,  $H=20\text{mm}$  is a standard specimen height.

## Appendix E

### Post-test results

The bulk density distribution by the column length

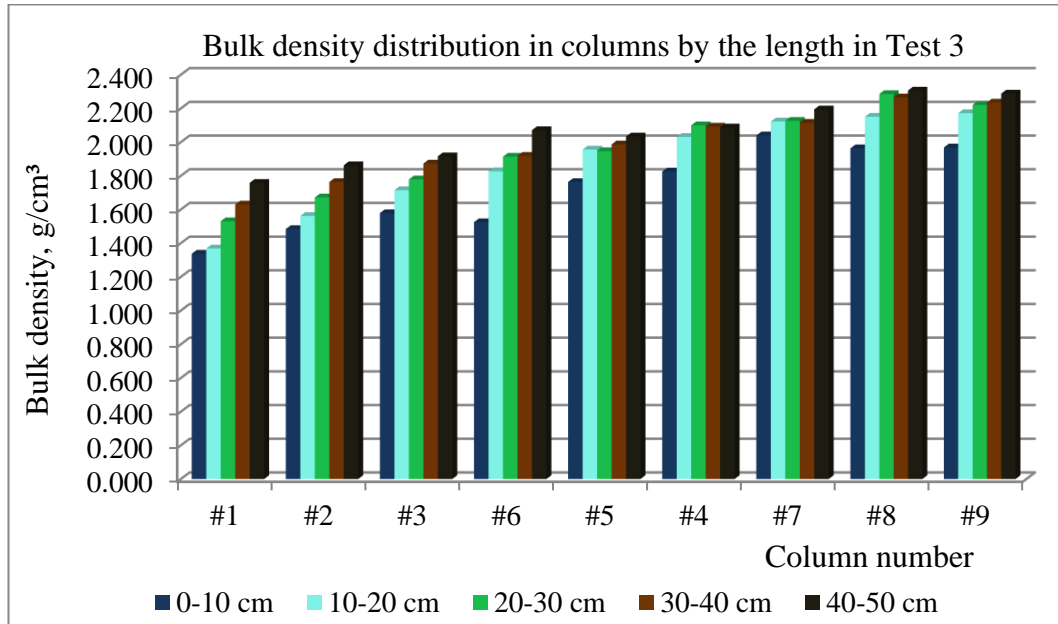


Figure E.1 – Bulk density distribution by the sample rings in Test 3

### Elastic modulus

A Pundit ultrasound machine was used to determine the elastic modulus. To obtain a better surface, contact a gel was applied on the locators' surfaces and to the samples' sides. As the moisture content did not affect the measurements, the elasticity modulus was determined for either wet or dried samples. The obtained results did not show a steady trend in the top sections, although this suggests that the elasticity modulus had reduced values in the top 20 cm layer owing to increased porosity, loose soil structure and intensified ice lens formation. The measurements have revealed that despite all the effort made to reduce the disruption of post-test structure of soil samples there was an intervention to the soil structure of either voids ratio or the packing state of soil particles during the melting and the extrusion from acrylic rings.

The obtained results of the elasticity modulus measurements are presented in the example of Test 2 in Figure E.2. Based on the average values, the outcomes reveal some reduction of the elasticity modulus in increased with moisture zones: in the heaved zone, due to intensive ice segregation; and in the capillary rise zone above the water table, due

to an increase in the volume voids. As the measurements were taken at the end of the test, after the complete thawing and drying in the oven, the samples structure might have been affected by some disruption during the thawing settlement and/or extrusion from the mould. Consequently, the obtained results for the elasticity modulus cannot be considered as the original soil characteristics, although they might be useful as an additional supporting data.

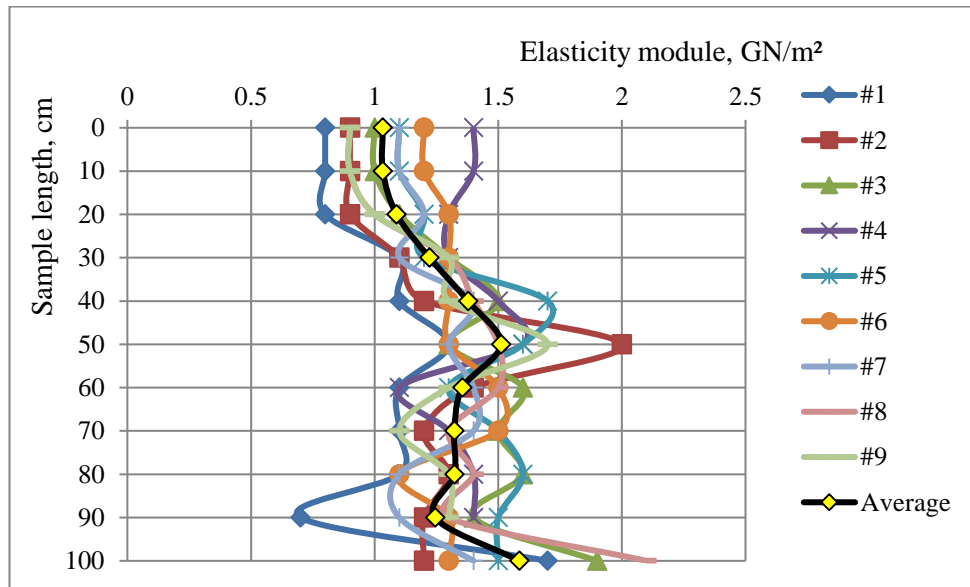


Figure 4.28- Elasticity module on example of Test 2